



---

**EVALUATION OF TRANSCRIPTION FACTOR  
ACTIVITY USING *IN VITRO* AND *IN VIVO* MODELS  
OF CHRONIC CHOLESTATIC LIVER DISEASE**

---

**Juliette Margaret Kathleen Maria Delhove**

A thesis submitted to the Faculty of Health Sciences, University of the Witwatersrand,  
Johannesburg, in fulfilment of the requirements for the degree of

**DOCTOR OF PHILOSOPHY**

---

## DECLARATION

I, Juliette Margaret Kathleen Maria Delhove, declare that this thesis is my own work and is submitted in fulfilment of the requirements for award of Doctor of Philosophy at the University of the Witwatersrand, Johannesburg. I hereby declare that it is an original work, representing my own academic effort and that all sources have been fully acknowledged.



---

Juliette M.K.M. Delhove

26/07/2016

---

Date

## ACKNOWLEDGEMENTS

Firstly, I would like to express my sincerest gratitude to my principal advisor, Professor Tristan McKay, for his continuous guidance and input. Thank you for giving me the motivation to pursue things that I never thought I could. You have been an amazing advisor and mentor to me during my time in your lab and have been instrumental in forming the scientist that I am today.

Also, to my supervisor at University College London, Dr Simon Waddington, a heartfelt thank you. Your creative ways to solving solutions always inspires me to do the same. I will always be grateful for your encouragement and advice during my time within the SomaBio group. Sincerest thanks for all the help with the animal work presented in this thesis, and for your “statistical” guidance. I cannot thank you enough for the opportunities that you have given me during the last 5 years.

To my supervisor Professor Patrick Arbuthnot, I have such appreciation for the opportunity that you have given to me, and for accepting me as part of your group. Your constant support, valuable suggestions, and willingness to help me through to the completion of my PhD shall never be forgotten, and I am proud to soon become a Witsie graduate.

To the McKay group, past and present, I am so grateful to have met so many good people who have made me laugh and kept me sane during these last few years. I will never forget the times that you messed with the organisation of my tips, pipettes, and keyboards amongst many other things. I probably deserved all of it. In particular, to Lorna, Kate, and Matt, a special thanks for not only being the great colleagues, but for becoming my friends along the way.

To other members of the Waddington and Arbuthnot group, particularly Dr Suzy Buckley, Rajvinder Karda, Dany Perocheau, Dr Marco Weinberg, Dr Tristan Scott, Dr Samantha Nicholson, and Dr Buhle Moyo, for all the assistance that you have given in various aspects of this project and for the great conference memories.

To my wonderful family, Gaëtan, Nicole, Florence, Sebastien, Christy, Lucas, and Dominique, you always give me strength through all of your kind and supportive words. Thank you for believing in me as I fulfil my potential.

Finally, to Marc, who has been a constant source of encouragement and good food during the writing up of this thesis. You are always so supportive and I couldn't have asked for a better partner to join me on this journey; it wouldn't have been the same without you as part of it.

## ABSTRACT

Biliary obstruction results in cholestasis characterised by progressive fibrosis, cholangiocyte hyperplasia and cirrhosis ultimately leading to liver failure. Underlying molecular mechanisms remain unclear but likely involve deregulation of signalling pathways within bipotent progenitor cells. Transduction of cell lines with vectors containing serial transcription factor (TF) binding sequences upstream of a minimal promoter driving luciferase expression have been widely used to study TF activity *in vitro*. The presented data expands upon this technology both *in vitro* and *in vivo* to enable quantification of bioluminescent output in living cell cultures and animals. A library of lentiviral vectors expressing either firefly luciferase or secreted NanoLuc luciferase was generated. Validation was performed by agonist-mediated activation and subsequent luciferase readout. Human hepatocellular HepaRG cells can be cultured as bipotent progenitors capable of differentiating into cholangiocytes or hepatocytes, and are a valuable tool for understanding cholangiocyte hyperplasia. HepaRGs transduced with WNT, Notch, or alpha-1 antitrypsin ( $\alpha$ 1AT) NanoLuc reporters were temporally assayed from culture media during differentiation. Two alternative differentiation procedures were performed based on previously published protocols predicted to enrich for either hepatocytes or cholangiocytes. The effect of Notch signalling on differentiation potential was determined through Notch signalling modulation. Data indicate that constitutive expression of JAGGED-1 results in a predisposition toward the cholangiocyte lineage. Conversely, the percentage of hepatocyte-like cells increased with the suppression of Notch signalling by NUMB. This enrichment is synergistic when used in conjunction with the 3-component differentiation protocol. For *in vivo* experiments, various high-titer VSV-G pseudotyped lentiviruses containing the reporters were administered by intravascular injection to P0 neonatal mice. This resulted in liver-restricted transduction and lifelong tolerance of the transgene. After establishing a bioimaging baseline, adult mice were subjected to partial bile duct ligation to induce a cholestatic phenotype, followed by serial bioimaging. This permitted the evaluation and comparison of temporal activities of a number of candidate signalling pathways involved in the differentiation of hepatic progenitor cells *in vitro* and the response to cholestatic injury *in vivo*. These methods of longitudinal assessment are an improvement on current methodologies and can be used as tools to obtain mechanistic insight or as drug-screening platforms.

# PUBLICATIONS ARISING FROM THIS WORK

## Peer-reviewed Journals

1. Buckley, S.M., **Delhove, J.M.K.M.**, Perocheau, D.P., Karda, R., Rahim, A.A., Howe, S.J., Ward, N.J., Arbuthnot, P., Johnson, M.R., Waddington, S.N. , McKay, T.R. 2015. In vivo bioimaging with tissue-specific transcription factor activated luciferase reporters. *Scientific Reports* (5), 11842
2. Hawkins, K., Joy, S., **Delhove, J.M.K.M.**, Kotiadis, V., Fernandez, E., Fitzpatrick, L., Whiteford, J., King, P., Bolanos, J., Duchen, M. 2016. NRF2 Orchestrates the Metabolic Shift during Induced Pluripotent Stem Cell Reprogramming. *Cell Reports* 4(8), pp. 1883-1891

## Publications arising from affiliated studies

1. Trivellin, G., Butz, H., **Delhove, J.**, Igreja, S., Chahal, H.S., Zivkovic, V., McKay, T., Patocs, A., Grossman, A.B., Korbonits, M. (2012). MicroRNA miR-107 is overexpressed in pituitary adenomas and *in vitro* inhibits the expression of aryl hydrocarbon receptor-interacting protein (AIP). *Am. J. Physiol. Endocrinol. Metab.*

## Book chapters

1. **Delhove, J.M.**, Rahim, A.A., McKay, T.R., Waddington, S.N., Buckley, S.M. (2012). Choice of surrogate and physiological markers for prenatal gene therapy. *Methods Mol. Biol.* 891, 273-290.
2. **Delhove, J.M.**, Hawkins, K.E., Waddington, S.N., McKay, T.R. (2016). Monitoring Transcription Factor Activated Luciferase Cassettes *In Vitro*. *Methods Mol. Biol.*

# CONFERENCE PROCEEDINGS

## Oral presentations

1. British Society of Gene and Cell Therapy, Fairbairn Award presentations: “Somatotransgenic bioimaging: A Novel Biosensing Platform for *In Vivo* Bioimaging.” Royal Holloway, University of London, 2013.

## Poster presentations

1. **Delhove, J.M.**, Waddington, S.N., Ward, N.J., Jathoul, A.P., Pule, M.A., McKay, T.R., Buckley, S.M. (2012). Development of bicistronic lentiviral vectors for continual in vivo and endpoint analysis of gene and stem cell transfer. (*British Society of Gene and Cell Therapy Conference*).
2. **Delhove, J.M.**, Waddington, S.N., McKay, T.R. (2013). Somatotransgenic bioimaging: a novel biosensing platform for *in vivo* bioimaging. (*European Society of Gene and Cell Therapy Conference*).
3. Buckley, S.M., **Delhove, J.M.**, Karda, R., Perocheau, D., Rahim, A.A., Waddington, S.N., McKay, T.R. (2014). Somatotransgenic Bioimaging: Modelling Disease Progression or Therapeutic Amelioration By Continued Tissue-Specific Bioluminescence Imaging in Living Small Animals. (*British Society of Gene and Cell Therapy Conference*).
4. Karda, R., **Delhove, J.M.**, Buckley, S.M., Ward, N.J., Rahim, A.A., Herbert, B., Mckay, T.R., Hagberg, H.E., Waddington, S.N., Johnson, M.R. (2014). Somatic Transgenesis of the Central Nervous System for Disease Modelling and Treatment. *Reproductive Sciences* 21, 276A-277A. (*Biochemical Society / British Neuroscience Association Meeting*).
5. **Delhove, J.M.**, Perocheau, D., Buckley, S.M., Karda, R., Waddington, S.N., McKay, T.R. (2015). Real-Time Monitoring of Transcription Factor Activity Using In Vitro and In Vivo Models of Cholestasis. 23, S72-S72. (*American Society of Gene and Cell Therapy Conference*).
6. Perocheau, D.P., Buckley, S.M., **Delhove, J.M.**, Karda, R., Mckay, T.R., Waddington, S.N. (2015). Use of Somatotransgenic Bioimaging as a Platform for Studying NF- $\kappa$ B Pathway in a Tissue-Specific Manner in Two Mouse Models of Inflammation: Rheumatoid Arthritis and Contact Dermatitis. 23, S151-S151. (*American Society of Gene and Cell Therapy Conference*).
7. Karda, R., **Delhove, J.M.**, Buckley, S.M., Perocheau, D.P., Rahim, A.A., Rocha-Ferreira, E., Ng, J., Suff, N., Mckay, T.R., Hagberg, H.H. (2015). Conscious whole body bioluminescence in somatic-transgenic rodents can be used to quantify and predict brain damage in a mouse model of Cerebral Palsy. 26, A8-A8. (*British Society of Gene and Cell Therapy Conference*).
8. Karda, R., **Delhove, J.M.**, Buckley, S.M., Rahim, A.A., Rocha-Ferreira, E., Perocheau, D., Ng, J., Mckay, T.R., Hagberg, H.H., Waddington, S.N. (2015). Generation of Light-Emitting Somatic-Transgenic Mice for Disease Modelling of Hypoxic Ischaemic Encephalopathy. *Reproductive Sciences* 22, 174A-174A. (*Society for Reproductive Investigation Annual Meeting*).

# TABLE OF CONTENTS

<b>LIST OF APPENDICES .....</b>	<b>xiv</b>
<b>LIST OF ABBREVIATIONS .....</b>	<b>xv</b>
<b>I) Liver architecture and physiology .....</b>	<b>1</b>
a) Structure and cell types of the liver	1
b) General functions of the liver	3
c) Bile function, production, and circulation	4
<b>II) Signalling pathways involved in hepatic development .....</b>	<b>6</b>
a) Developmental signalling pathways	6
i) <i>Transforming growth factor-<math>\beta</math> superfamily signalling pathways.....</i>	<i>7</i>
ii) <i>WNT signalling .....</i>	<i>8</i>
iii) <i>Canonical Notch signalling .....</i>	<i>10</i>
b) Overview of liver development	12
c) Development of the biliary tree	13
<b>III) Mortality and economic burden of liver disease .....</b>	<b>17</b>
<b>IV) Instigators of inflammatory activation, ECM remodelling and fibrotic resolution .....</b>	<b>18</b>
a) Role of NF- $\kappa$ B in liver tolerogenic responses and hepatic injury	18
b) Kupffer cell activation	19
c) Hepatic stellate cell activation	20
d) TGF- $\beta$ -mediated ECM production and perpetuation of the fibrotic response	21
e) Fibrotic resolution	22
<b>V) Mechanisms of regeneration .....</b>	<b>22</b>
a) The ductular reaction	22
b) The role of Sox9 during chronic liver injury	24
c) Osteopontin as a pro-fibrotic mediator	25
d) Role of WNT and Notch signalling in the regenerative response	26
<b>VI) Types of biliary diseases .....</b>	<b>27</b>
a) Primary sclerosing cholangitis and inflammatory responses	28
b) Primary biliary cirrhosis	28
c) Biliary atresia	29
d) Alagille syndrome	29

<b>VII) Animal model systems to study liver disease.....</b>	<b>30</b>
a) Spontaneous mutation models of hepatic fibrosis	30
b) Chemically induced models of cholestasis	30
c) Genetic models of hepatic fibrosis	31
d) Surgical models of hepatic fibrosis	31
<b>VIII) <i>In vitro</i> model systems of hepatic differentiation, disease, and pathway activation.....</b>	<b>32</b>
a) HepaRG cells	32
b) Genetic reporters	33
i) <i>Properties and reaction of firefly luciferase.....</i>	<i>34</i>
ii) <i>Genetically engineered luciferases.....</i>	<i>35</i>
<b>Hypothesis .....</b>	<b>38</b>
<b>Aims and Objectives: .....</b>	<b>38</b>
<b>2.0 Introduction to disease modelling using genetic reporters.....</b>	<b>40</b>
2.0.1 Conventional analysis of disease	40
2.0.2 The principle of the 3Rs of animal research	40
2.0.3 Whole-body, light-emitting transgenic animals for continual bioimaging of disease	41
2.0.4 Somatotransgenic Bioimaging (SomaBio)	43
<b>2.1 Results of luciferase reporter development .....</b>	<b>45</b>
2.1.1 Overlap-extension PCR and lentiviral cloning of novel luciferase constructs	45
2.1.2 Flow cytometry for presence of luciferase and eGFP	47
2.1.3 Cleavage efficiency of 2A polypeptide sequence by Western Blot	49
2.1.4 Spectral analysis of pLNT-SFFV-JDG	49
2.1.5 Virus production and transduction validation of pLNT-SFFV-JDG	50
2.1.6 Development of a rapid cloning system, the construction of pLNT-GW-JDG	51
2.1.7 Development of NanoLuc® and Vargula parental cloning vectors.	52
2.1.8 <i>In vitro</i> validation of constitutively driven JDG, RLuc2, VLuc2, and NLuc2	54
<b>3.0 Investigating signalling activity using transcription factor binding elements.....</b>	<b>57</b>
<b>3.1 Results of reporter validations <i>in vitro</i> .....</b>	<b>58</b>
3.1.1 <i>In vitro</i> validation of the pLNT-NF-κB-JDG construct	58
3.1.2 Time course and dose response of activin A activation of LNT-SBE-JDG <i>in vitro</i>	59
3.1.3 <i>In vitro</i> validation of WNT-JDG using LiCl	60
3.1.4 <i>In vitro</i> validation of Notch using co-culture with Jagged-1 overexpressing cells	61
<b>4.1 Results of reporter validations <i>in vivo</i>.....</b>	<b>63</b>
4.1.1 Monitoring of LPS-mediated inflammatory responses <i>in vivo</i> using a NF-κB reporter	63

4.1.2	Antagonistic abrogation of inflammatory NF- $\kappa$ B responses by dexamethasone	64
4.1.3	Exogenous activation of the LNT-SBE-JDG construct <i>in vivo</i> using activin A	65
<b>4.2</b>	<b>Molecular analysis of fibrosis and virus cell-type targeting</b>	<b>66</b>
4.2.1	Haematoxylin and eosin and Lilly's trichrome staining for liver morphology and fibrosis	66
4.2.2	Immunohistochemical analysis of lentiviral targeting of hepatic cell types	68
<b>4.3</b>	<b>Analysis of critical pathways involved in chronic liver injury</b>	<b>72</b>
4.3.1	SFFV-mediated luciferase expression is unaffected by pBDL surgical procedure	72
4.3.2	NF- $\kappa$ B activity monitoring during the acute phase of cholestasis	73
4.3.3	Smad 2/3 activation <i>in vivo</i> using fibrosis-inducing partial bile duct ligation	73
4.3.4	<i>In vivo</i> assessment of GFAP expression in response to biliary injury	75
4.3.5	<i>In vivo</i> evaluation of WNT signalling during chronic cholestasis	75
4.3.6	<i>In vivo</i> assessment of pLNT-Notch-JDG using BDL	77
<b>5.1</b>	<b>Results of HepaRG differentiation through media composition and genetic modulation</b>	<b>79</b>
5.1.1	Temporal reporter gene expression during alternative differentiation protocols	79
5.1.2	Phenotypic, qualitative, and quantitative assessment of differentiation protocols	81
5.1.3	Assessing the modulation of Notch signalling on differentiation potential	82
<b>6.0</b>	<b>Introduction to RNA-guided CRISPR/Cas9 genome editing</b>	<b>90</b>
<b>6.1</b>	<b>Results of genome editing of HepaRG cells</b>	<b>91</b>
6.1.1	Cloning of guides into the px330 CRISPR/Cas9 vector	91
6.1.2	HepaRG knockout of Sox9 using CRISPR/Cas9 technology	92
6.1.3	Analysis of Sox9 knockout clones	96
<b>7.0</b>	<b>Discussion</b>	<b>98</b>
<b>7.1</b>	<b>Dual reporter vectors can be successfully used within <i>in vitro</i> and <i>in vivo</i> model systems</b>	<b>98</b>
7.1.1	Development of a bicistronic firefly luciferase / GFP lentiviral construct	98
7.1.2	Validation of the pLNT-SFFV-JDG vector	99
7.1.3	Development of a library of reporters using Gateway cloning	99
7.1.4	Dual secreted luciferase platform permits longitudinal <i>in vitro</i> analysis of signalling	100
7.1.5	Constitutively expressed luciferases confirm substrate specificity	101
<b>7.2</b>	<b>Biosensing reporters as monitors of transcription factor activity</b>	<b>101</b>
7.2.1	NF- $\kappa$ B reporter cell lines respond significantly to agonist administration <i>in vitro</i>	101
7.2.2	Activin A induces a temporal and dose-dependent increase in Smad2/3 signalling <i>in vitro</i>	102
7.2.3	LiCl activates Wnt signalling and increases WNT-JDG reporter activity <i>in vitro</i>	103
7.2.4	Jagged-1 overexpression induces Notch signalling in an <i>in vitro</i> co-culture assay	104
7.2.5	Intravenous injection of VSV-g lentivirus predominantly targets hepatocytes <i>in vivo</i>	105

7.2.6	<i>In vivo</i> NF- $\kappa$ B signalling following ultrapure LPS treatment is TLR4 mediated	107
7.2.7	Dexamethasone-induced abrogation of NF- $\kappa$ B signalling	108
7.2.8	Activin A induces upregulation of SBE-mediated luciferase expression <i>in vivo</i>	110
7.2.9	Increases in NF- $\kappa$ B signalling are observed during the acute phases of pBDL	111
7.2.10	Novel Smad2/3 expression profiles are observed using SBE somatotransgenic animals	113
7.2.11	Induction of cholestatic liver injury results in a significant increase in GFAP expression	114
<b>7.3</b>	<b>The role of WNT signalling in cholestatic liver disease</b>	<b>116</b>
7.3.1	Hepatic $\beta$ -catenin localisation is not changed <i>in vivo</i> during BDL	116
<b>7.4</b>	<b>The role of Notch signalling in cholestatic liver disease</b>	<b>117</b>
7.4.1	Notch signalling displays a trend in decreased expression during acute phase of pBDL	117
<b>7.5</b>	<b>Modulation of media composition and Notch signalling results in differential capacities of hepatic progenitors to differentiate into hepatocytes and cholangiocytes <i>in vitro</i></b>	<b>119</b>
7.5.1	Notch, WNT, and $\alpha$ 1AT reporters show increased activity in response to protocol 2	119
7.5.2	Verification of increased hepatic and biliary markers using protocol 2	120
7.5.3	<i>JAGGED-1</i> overexpression increases cholangiocyte differentiation while <i>Numb</i> overexpression results in increased hepatocyte differentiation using protocol 2	121
<b>7.6</b>	<b>HepaRG knockout of Sox9 using CRISPR/Cas9 technology</b>	<b>125</b>
7.6.1	Sox9 site-specific genome editing using a cas9-expressing vector	125
7.6.2	Bi-allelic Sox9 knockout results in a mesenchymal phenotype that is non-viable	125
<b>7.7</b>	<b>Conclusions</b>	<b>126</b>
<b>8.0</b>	<b>Materials and Methods</b>	<b>129</b>
<b>8.1</b>	<b>Cloning of the constitutive SFFV- and GW-JDG parental vectors</b>	<b>129</b>
8.1.1	Primary PCR reagents and cycling parameters	129
8.1.2	Secondary PCR to create the 3XFLAG-FLuc-2A-eGFP bicistronic cassette	130
8.1.3	Restriction digest and ligation to produce pLNT-SFFV-JDG	131
8.1.4	Transformation and positive clone selection of pLNT-SFFV-JDG	132
8.1.5	Cloning to create the parental pLNT-GW-JDG vector	133
<b>8.2</b>	<b>Cloning of pLNT-GW-NanoLuc<sup>®</sup>-2A-eGFP and pLNT-SFFV-VLuc</b>	<b>134</b>
<b>8.3</b>	<b>Recombination reactions to produce lentiviral reporters</b>	<b>136</b>
<b>8.4</b>	<b>Validation of the pLNT-SFFV-JDG vector</b>	<b>137</b>
8.4.1	Fluorescence-Activated Cell Sorting for 3xFLAG tag and eGFP	137
8.4.2	Western blot for 3xFLAG and eGFP	137

<b>8.5 Bradford assay for total protein quantification .....</b>	<b>138</b>
<b>8.6 Luciferase assay for the assessment of luciferase reporter activity .....</b>	<b>139</b>
<b>8.7 General cell culture.....</b>	<b>139</b>
<b>8.8 Isolation and culturing of CD1 and <i>tlr4</i><sup>-/-</sup> MEFs.....</b>	<b>139</b>
<b>8.9 Lentivirus production and titering.....</b>	<b>140</b>
<b>8.10 Reporter assays .....</b>	<b>141</b>
<b>8.11 Development of the px330-Sox9 knockout CRISPR-Cas9 vector.....</b>	<b>141</b>
8.11.1 Cloning of the Sox9 guide-RNA into the px330 backbone	141
8.11.2 Ligation of phosphorylated, annealed oligos into <i>BbsI</i> digested px330	142
8.11.3 Nucleofection of genome editing plasmids and clonal amplification of HepaRG cells	142
8.11.4 Genomic DNA isolation from clonally amplified cells and PCR of Sox9 target region.	143
8.11.5 <i>SmaI</i> digest and T7 endonuclease I assay to determine occurrence of genome editing	144
8.11.6 Clonal amplification and knockout validation using PCR and restriction digestion	144
8.11.7 Sequencing of Sox9 homozygous knockout clones	145
<b>8.12 Tissue fixation, embedding, and sectioning .....</b>	<b>145</b>
<b>8.13 Hematoxylin and eosin staining .....</b>	<b>146</b>
<b>8.14 Lilley’s trichrome staining .....</b>	<b>146</b>
<b>8.15 Immunohistochemistry of liver sections .....</b>	<b>146</b>
<b>8.16 Hepatocyte and cholangiocyte differentiation utilising the HepaRG cell line .....</b>	<b>147</b>
<b>8.17 Generation and differentiation of Numb and Jagged overexpressing HepaRG lines.....</b>	<b>148</b>
8.17.1 Immunocytochemistry of modified and unmodified differentiated HepaRG cells	148
8.17.2 qPCR for expression of markers of progenitors, hepatocytes, and cholangiocytes	149
8.17.2.1 <i>RNA extraction</i> .....	149
8.17.2.2 <i>First-Strand cDNA synthesis</i> .....	149
8.17.2.3 <i>qPCR to quantitate hepatocytes and cholangiocytes from differentiation protocols</i> .....	150
8.17.3 Notch, Wnt and $\alpha$ 1AT reporter expression during differentiation	151
<b>8.18 Statistical analysis .....</b>	<b>152</b>
<b>8.19 <i>In vivo</i> work .....</b>	<b>152</b>
8.19.1 Animals	152
8.19.2 Bioluminescence imaging	152

8.19.3 <i>In vivo</i> reporter analysis	153
8.19.3.1 <i>NF-κB</i> activation using <i>LPS</i> .....	153
8.19.3.2 Dexamethasone-mediated abrogation of <i>NF-κB</i> signalling.....	153
8.19.3.3 Bile duct ligation model of cholestasis.....	153
8.19.4 Statistical analysis of <i>in vivo</i> experiment results	153
<b>Appendix A – Plasmid Maps.....</b>	<b>I</b>
Appendix A.i Plasmid map of pSEW-Asp-eGFP	I
Appendix A.ii Plasmid map of pLNT-SFFV-JDG	II
Appendix A.iii Plasmid map of pZs-Green-JDG	II
Appendix A.iv Plasmid map of pLNT-GW-MCS	III
Appendix A.v Plasmid map of pLNT-GW-JDG	III
Appendix A.vi Plasmid map of pLNT-GW-NLuc2	IV
Appendix A.vii Plasmid map of pLNT-SFFV-Vluc	IV
Appendix A.viii Plasmid map of pENTR-1A	V
Appendix A.ix Plasmid map of px330 with <i>BbsI</i> restriction sites for target sequence cloning	V
<b>Appendix B – Predicted sequence of the 3xFLAG-FLuc-2A-eGFP insert .....</b>	<b>VI</b>
<b>Appendix C – Home Office Animals (Scientific Procedures) Act 1986 Project Licence .....</b>	<b>VII</b>
<b>Appendix D – Turnitin Plagiarism report .....</b>	<b>VIII</b>

## TABLE OF FIGURES

Figure 1. Schematic diagram depicting the structure of the liver lobule. ....	1
Figure 2. Overview of hepatic cell types. ....	2
Figure 3. Hepatic metabolic zonation. ....	3
Figure 4. Bile flow from the gall bladder to the duodenum. ....	5
Figure 5. Induction of bile secretion from the gallbladder. ....	6
Figure 6. Branches of TGF- $\beta$ signalling. ....	7
Figure 7. Regulation of canonical Wnt signalling. ....	9
Figure 8. Representation of canonical Notch signalling through cell-to-cell interactions. ....	11
Figure 9. Transcriptional regulation of hepatoblast differentiation. ....	12
Figure 10. Endodermal budding of the liver. ....	13
Figure 11. Bile duct development. ....	14
Figure 12. TGF- $\beta$ -gradient mediated restriction of hepatobiliary lineages. ....	16
Figure 13. Markers of biliary and hepatocyte differentiation. ....	17
Figure 14. Illustration of canonical NF- $\kappa$ B signalling in response to TLR agonists. ....	19
Figure 15. Cellular changes arising during liver injury. ....	21
Figure 16. Regulators of ECM homeostasis. ....	22
Figure 17. Modes of liver regeneration in response to acute and chronic injury. ....	23
Figure 18. Regulation and downstream targets of Sox9. ....	25
Figure 19. Role of osteopontin in regulation of the ductular reaction. ....	26
Figure 20. Activation of WNT and Notch signalling in HPCs induces hepatocyte and cholangiocyte differentiation respectively. ....	27
Figure 21. Schematic of ligation point for partial bile duct ligation disease modelling. ....	32
Figure 22. D-luciferin oxidation reaction mediated by firefly luciferase. ....	34
Figure 23. Experimental design of conventional disease model with terminal analysis. ....	40
Figure 24. Illustration of germline transgenic concept. ....	41
Figure 25. Germline transgenic animal models used in whole-body bioluminescent imaging. ....	43
Figure 26. Illustration of the concept of somatotransgenic bioimaging. ....	44
Figure 27. Gel electrophoresis of primary and secondary PCR, and restriction digest of pLNT-SFFV-JDG clones. ....	47
Figure 28. Functional validation of GFP and luciferase expression. ....	48
Figure 29. Functional validation of pLNT-SFFV-JDG. ....	50
Figure 30. Schematic of Gateway recombination cloning using the pENTR shuttle vector and the pLNT-GW-JDG lentiviral vector. ....	51
Figure 31. Cloning to generate the Gateway-FLuc-2A-GFP (pLNT-GW-JDG) parental vector. ....	52
Figure 32. Restriction digest checks of pLNT-GW-NLuc2 and pLNT-SFFV-Vluc cloning. ....	54
Figure 33. Substrate specificity assay for JDG, RLuc2, VLuc2 and NLuc2. ....	55
Figure 34. LNT-NF- $\kappa$ B-JDG activation in response to LPS. ....	58

Figure 35. Validation of pLNT-SBE-JDG using the agonist, activin A, in ascending doses and in various cell lines.....	59
Figure 36. <i>In vitro</i> validation of LNT-WNT-JDG vector in various cell lines. ....	60
Figure 37. <i>In vitro</i> validation of pLNT-Notch-JDG using Jagged-1 dose response curve and time course. ..	61
Figure 38. Validation of NF- $\kappa$ B using CD1 and <i>tlr4</i> <sup>-/-</sup> mice. ....	64
Figure 39. Response of NF- $\kappa$ B signalling when challenged with the glucocorticoid, dexamethasone. ....	65
Figure 40. Activation of pLNT-SBE-JDG <i>in vivo</i> using exogenous activin A.....	65
Figure 41. H&E and trichrome staining of sham operated and pBDL livers.....	67
Figure 42. GFP colocalisation with hepatic cell types using cell-type specific markers. ....	72
Figure 43. Mean luminescence intensity of LNT-SFFV-JDG transduced mice with or without BDL surgery. ....	72
Figure 44. NF- $\kappa$ B reporter activation in response to partial bile duct ligation model of cholestasis. ....	73
Figure 45. Activation of pLNT-SBE-JDG <i>in vivo</i> following pBDL surgery.....	74
Figure 46. GFAP activation in response to pBDL. ....	75
Figure 47. Effect of pBDL on $\beta$ -catenin signalling <i>in vivo</i> .....	76
Figure 48. Mean fluorescence intensity and immunofluorescence of LNT-Notch-JDG transduced mice with or without BDL surgery.....	77
Figure 49. Reporter gene analysis during protocol 1 and protocol 2 differentiation. ....	80
Figure 50. Microscopic phase images of HepaRG cells using protocol 1 and 2.....	81
Figure 51. Immunohistochemical and qPCR analysis of protocol 1 and protocol 2.....	82
Figure 52. Differentiation potentials of HepaJag and HepaNumb cell lines in response to variable differentiation protocols. ....	83
Figure 53. Immunohistochemical and qPCR analysis of HepaJag and HepaNumb cell lines in response to protocol 1 and 2.....	87
Figure 54. Genome editing using CRISPR/Cas9. ....	90
Figure 55. Sox9 knockout genomic location and Cas9 cleavage site. ....	92
Figure 56. Cloning and validation of the px330-Sox9 genome editing vector. ....	94
Figure 57. Sequencing of 2 clones following CRISPR-Cas genome editing of the Sox9 locus. ....	95
Figure 58. Phenotypic differences in wildtype and Sox9 knockout HepaRG cells. ....	96
Figure 59. Dual mechanism of anti-inflammatory activity of glucocorticoids. ....	109
Figure 60. NF- $\kappa$ B-mediated enhancement of TGF- $\beta$ signalling in HSCs via BAMBI downregulation. ....	111
Figure 61. Overlap extension concept and cloning of pLNT-SFFV-JDG. ....	129

## LIST OF TABLES

Table 1. Table of the major functions of the liver. ....	3
Table 2. Features of the firefly, red-shifted renilla, vargula and NanoLuc luciferases. ....	37
Table 3. Primers used to generate primary products for 3xFLAG-FLuc-2A-eGFP construction. ....	130
Table 4. Reaction parameters to generate primary products for 3xFLAG-FLuc-2A-eGFP construction. ....	130
Table 5. Reagents and concentrations for secondary overlap-extension PCR. ....	131
Table 6. Restriction enzyme digests of JDG insert and pSEW-Asp-eGFP backbone. ....	132
Table 7. Reagents and volumes for quick ligation of pLNT-SFFV-JDG. ....	132
Table 8. Restriction digest reagents and volumes for the detection of positive recombinant clones. ....	133
Table 9. Primary and Secondary PCR for the generation of NLuc-2A-GFP and VLuc. ....	135
Table 10. Primers oligonucleotides for amplification of NanoLuc®, 2A-eGFP and vargula. ....	136
Table 11. Sequence of adenoviral E1A minimal promoter oligos. ....	137
Table 12. Table of reporters, agonists, and activation parameters. ....	141
Table 13. Oligos used to develop guide RNAs and amplify Sox9 target region. ....	142
Table 14. Phosphorylation reaction using T4 polynucleotide kinase. ....	142
Table 15. PCR reaction for amplification of Sox9 genomic region containing CRISPR/Cas9 target site. ....	143
Table 16. T7 endonuclease assay hybridisation mix. ....	144
Table 17. Primary and secondary antibodies used for immunohistochemistry. ....	147
Table 18. Primary and secondary antibody information used for immunocytochemistry. ....	148
Table 19. First-strand cDNA synthesis reaction. ....	149
Table 20. qPCR reaction for Sox9, OPN, HNF-1 $\beta$ , and Hey1. ....	150
Table 21. qPCR reaction for ALB and $\beta$ -actin. ....	150
Table 22. Cycling parameters for qPCR using Sybr Select qPCR mix. ....	150
Table 23. Cycling parameters for qPCR using Sybr® greenER™ qPCR mix Sybr Select qPCR mix. ....	151
Table 24. Primers used in differentiation experiment qPCR reactions. ....	151

# **LIST OF APPENDICES**

## **Appendix A – Plasmid Maps**

Appendix A.i Plasmid map of pSEW-Asp-eGFP

Appendix A.ii Plasmid map of pLNT-SFFV-JDG

Appendix A.iii Plasmid map of pZs-Green-JDG

Appendix A.iv Plasmid map of pLNT-GW-MCS

Appendix A.v Plasmid map of pLNT-GW-JDG

Appendix A.vi Plasmid map of pLNT-GW-NLuc2

Appendix A.vii Plasmid map of pLNT-GW-VLuc

Appendix A.viii Plasmid map of pENTR-1A

**Appendix B – Predicted sequence and primer binding sites of the 3xFLAG-FLuc-2A-eGFP insert**

**Appendix C – Home Office Animals (Scientific Procedures) Act 1986 Project Licence**

**Appendix D – Turnitin plagiarism report**

## LIST OF ABBREVIATIONS

<b><math>\alpha</math>1AT</b>	alpha-1 antitrypsin	<b>CFTR</b>	cystic fibrosis transmembrane conductance regulator
<b>AAV</b>	adeno-associated virus	<b>CO<sub>2</sub></b>	carbon dioxide
<b>AFP</b>	alpha-fetoprotein	<b>cPPT</b>	central polypurine tract
<b>ALK</b>	activin-like kinases	<b>CRISPR</b>	clustered regularly interspaced short palindromic repeats
<b>APC</b>	adenomatosis polyposis coli	<b>CSL</b>	CBF1, Suppressor of Hairless, Lag-1
<b>ALB</b>	albumin	<b>DAPI</b>	4',6-diamidino-2-phenylindole
<b>AMP</b>	adenosine monophosphate	<b>DAB</b>	3, 3'-diaminobenzidine
<b>ANOVA</b>	analysis of variance	<b>DDC</b>	3,5-diethoxycarbonyl-1,4-dihydrocollidine
<b>APC</b>	antigen presenting cell	<b>dH<sub>2</sub>O</b>	distilled water
<b>APES</b>	3-aminopropyltriethoxysilane	<b>DKK</b>	Dickkopf
<b>ATP</b>	adenosine triphosphate	<b>DMEM</b>	Dulbecco's modified Eagle's medium
<b>BDL</b>	bile duct ligation	<b>DNA</b>	deoxyribonucleic acid
<b>BEC</b>	biliary epithelial cells	<b>dNTP</b>	deoxyribonucleotide triphosphate
<b>bp</b>	base pair	<b>DSL</b>	Delta, Serrate, Lag2
<b>bGHpA</b>	bovine growth hormone polyadenylation signal	<b>DTT</b>	dithiothreitol
<b>BMP</b>	bone morphogenetic protein	<b>E</b>	embryonic day
<b>BSA</b>	bovine serum albumin	<b>EDTA</b>	ethylenediaminetetraacetic acid
<b>cAMP</b>	cyclic adenosine monophosphate	<b>eGFP</b>	enhanced green fluorescent protein
<b>Cas</b>	CRISPR-associated	<b>EHBD</b>	extrahepatic bile duct
<b>CCCD</b>	cooled charge-coupled device camera		
<b>CK</b>	cytokeratin		
<b>CK1<math>\alpha</math></b>	casein kinase 1 $\alpha$		

<b>ELISA</b>	enzyme-linked immunosorbant assay	<b>HSV-Tk</b>	herpes simplex virus-thymidine kinase
<b>EMT</b>	epithelial-to-mesenchymal transition	<b>ICAM-1</b>	intracellular adhesion molecule 1
<b>EtOH</b>	ethanol	<b>IGF-1</b>	insulin-like growth factor-1
<b>FBS</b>	fetal bovine serum	<b>IHBD</b>	intrahepatic bile duct
<b>FCS</b>	fetal calf serum	<b>Indel</b>	insertions/deletions
<b>FGF</b>	fibroblast growth factor	<b>IL-1<math>\beta</math></b>	interleukin-1 $\beta$
<b>FLuc</b>	firefly luciferase	<b>IL-6</b>	interleukin-6
<b>FMDV</b>	foot and mouth disease virus	<b>IMS</b>	industrial methylated spirits
<b>GFAP</b>	glial fibrillary acid protein	<b>IRDye</b>	infrared dye
<b>GR</b>	glucocorticoid receptor	<b>JDG</b>	Juliette Delhove Green
<b>GSK-3<math>\beta</math></b>	glycogen synthase kinase-3beta	<b>LAP</b>	latency-associated protein
<b>GW</b>	Gateway <sup>®</sup>	<b>LPS</b>	lipopolysaccharide
<b>HCl</b>	hydrochloric acid	<b>LRP5/6</b>	low-density-lipoprotein-related protein5/6
<b>HDF</b>	human dermal fibroblasts	<b>LTBP</b>	latent TGF- $\beta$ binding protein
<b>H&amp;E</b>	haematoxylin and eosin	<b>LB</b>	Luria-Bertani
<b>Hes-1</b>	hairy/enhancer-of-split 1	<b>LiCl</b>	lithium chloride
<b>Hey-1</b>	Hes-related family bHLH transcription factor with YRPW motif protein 1	<b>LTR</b>	long terminal repeats
<b>HF</b>	high fidelity	<b><math>\mu</math></b>	micro ( $10^{-6}$ )
<b>HGF</b>	hepatocyte growth factor	<b>m</b>	milli ( $10^{-3}$ )
<b>HIV-1</b>	human immunodeficiency virus-1	<b>M</b>	molar
<b>HPC</b>	hepatic progenitor cells	<b>MAML-1</b>	Mastermind-like-1
		<b>MAPK</b>	mitogen-activated protein kinase
		<b>MEFs</b>	mouse embryonic fibroblasts
		<b>MgCl<sub>2</sub></b>	magnesium chloride

<b>MMP</b>	matrix metalloproteinase	<b>PDGF</b>	platelet-derived growth factor
<b>MOI</b>	multiplicity of infection	<b>PEI</b>	polyethylenimine
<b>MoMLV</b>	Moloney murine leukemia virus	<b>PEST</b>	proline-glutamic acid-serine-threonine
<b>MOPS</b>	3-(N-morpholino) propanesulfonic acid	<b>PFA</b>	paraformaldehyde
<b>MP</b>	minimal promoter	<b>PKA</b>	protein kinase C
<b>NHEJ</b>	non-homologous end joining	<b>PKM2</b>	pyruvate kinase M2 splice isoform
<b>NICD</b>	Notch intracellular domain	<b>pLNT-JDG</b>	lentivirus containing Juliette Delhove Green insert
<b>NF-<math>\kappa</math>B</b>	nuclear factor- $\kappa$ B	<b>PPAR</b>	peroxisome proliferator-activated receptor
<b>nm</b>	nanometres	<b>ppi</b>	inorganic phosphate
<b>NLuc</b>	NanoLuc®	<b>PVDF</b>	polyvinylidene fluoride
<b>NRR</b>	negative regulatory region	<b>qPCR</b>	quantitative real time PCR
<b>OC</b>	Onecut	<b>rATP</b>	ribo-adenosine-5'-triphosphate
<b>OD</b>	optical density	<b>Rbp-J<math>\kappa</math></b>	retinol binding protein
<b>OE-PCR</b>	overlap extension polymerase chain reaction	<b>RLU</b>	relative light units
<b><math>\Psi</math></b>	psi packaging signal	<b>ROI</b>	region of interest
<b>P24<sup>Gag</sup></b>	HIV-1 p24 gag capsid protein	<b>RS-RLuc</b>	red-shifted renilla luciferase
<b>PAI-1</b>	plasminogen activator inhibitor-1	<b>SA-<math>\beta</math>-gal</b>	Senescence-associated $\beta$ -galactosidase
<b>PAGE</b>	polyacrylamide gel electrophoresis	<b>SIN</b>	self-inactivating
<b>PAMPS</b>	Pathogen associated molecular patterns	<b>siRNA</b>	short interfering RNA
<b>PI3K</b>	phosphatidylinositol 3-kinase	<b>shRNA</b>	short hairpin RNA
<b>pBDL</b>	partial bile duct ligation	<b>SFFV</b>	spleen focus-forming virus
<b>PBS</b>	phosphate buffered saline		
<b>PCR</b>	polymerase chain reaction		

<b>SOC</b>	super optimal broth with catabolite repression	<b>TTR</b>	transthyretin
<b>Sox9</b>	Sex determining region Y-box 9	<b>Tween-20</b>	polysorbate-20
<b>T7EN1</b>	T7 endonuclease I	<b>uPA</b>	urokinase plasminogen activator
<b>TAD</b>	transcriptional activation domain	<b>V</b>	volts
<b>TAE</b>	tris-acetate-EDTA	<b>VEGF</b>	vascular endothelial growth factor
<b>TAK1</b>	TGF- $\beta$ -activated kinase	<b>Vluc</b>	vargula luciferase
<b>TALEN</b>	transcription activator-like effector nucleases	<b>vp/ml</b>	virus particles per millilitre
<b>tBDL</b>	total bile duct ligation	<b>VSV-g</b>	vesicular stomatitis virus glycoprotein
<b>T<math>\beta</math>RI</b>	TGF- $\beta$ receptor type I	<b>v/v</b>	volume per volume
<b>T<math>\beta</math>RII</b>	TGF- $\beta$ receptor type II	<b>WPRE</b>	Woodchuck Hepatitis Virus (WHV) Posttranscriptional Regulatory Element
<b>T<math>\beta</math>RIII</b>	TGF- $\beta$ receptor type III	<b>WHV</b>	Woodchuck Hepatitis Virus
<b>TBS-T</b>	tris-buffered saline-Triton-X-100	<b>WIF</b>	WNT inhibitory protein
<b>TCF/LEF</b>	T cell-specific transcription factor / lymphoid enhancer-binding factor-1	<b>w/v</b>	weight per volume
<b>TCR</b>	T cell receptor	<b>w/w</b>	weight per weight
<b>TDO</b>	tryptophan 2,3 dioxygenase	<b>ZFN</b>	zinc finger nuclease
<b>TLE</b>	transducin-like enhancer protein 1		
<b>TLR4</b>	toll-like receptor 4		
<b>TNF-<math>\alpha</math></b>	tumour necrosis factor- $\alpha$		
<b>TNFR-1</b>	tumour necrosis factor receptor 1		
<b>tPA</b>	tissue plasminogen activator		
<b>Tris</b>	tris(hydroxymethyl)-aminomethane		

---

**CHAPTER 1**

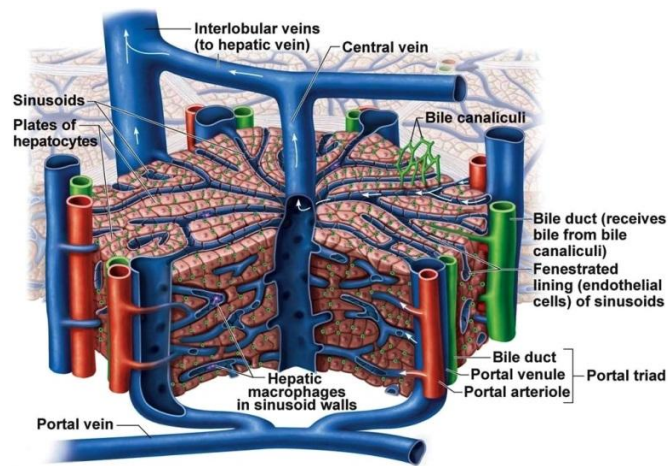
**GENERAL INTRODUCTION**

---

## I) Liver architecture and physiology

### a) Structure and cell types of the liver

The liver is a dynamic organ which plays an integral role in the homeostatic maintenance of the entire body. It functions in a range of metabolic processes, acting as a store for a host of vitamins and enzymes, and also plays a crucial role in detoxifying the body of xenobiotic compounds. The liver is composed of liver lobules composed of both parenchymal and mesenchymal cells, depicted in **Figure 1**, which at a histological scale are small hexagonal subdivisions consisting of plates of hepatocytes radiating from the central vein. Around the perimeter of the lobule is a distinctive cluster known as the portal triad composed of the hepatic artery, portal vein, and bile duct, all bound together by a perivascular fibrous capsule.



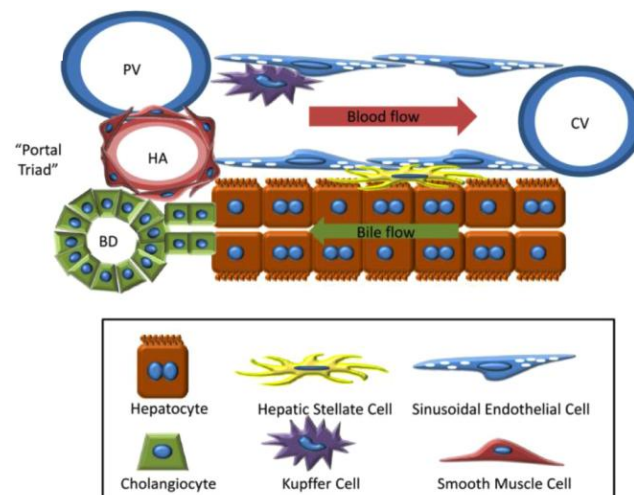
[https://cms.webstudy.com/WebstudyFileSystem/testovaci/GetFile/293875/Ch%2022/Ch22b/figure\\_22\\_25c\\_labeled.jpg](https://cms.webstudy.com/WebstudyFileSystem/testovaci/GetFile/293875/Ch%2022/Ch22b/figure_22_25c_labeled.jpg)

#### **Figure 1. Schematic diagram depicting the structure of the liver lobule.**

Each liver lobule consists of radiating hepatocytes emanating from the central vein. The portal vein, hepatic artery, and bile duct constitute the portal triad. Sinusoids act as hepatic capillaries to transport blood towards the central vein, while also acting as the residence for macrophagic Kupffer cells.

The liver is composed of both parenchymal and mesenchymal cells that are responsible for the functions within the liver (**Figure 2**). The most abundant hepatic cell type is the parenchymal hepatocyte, which accounts for over 80% of the total liver mass and whose basolateral membranes contain microvilli utilised in nutrient intake. Hepatocytes are hexagonally shaped, highly polarised epithelial cells and have an endodermal embryological origin<sup>1</sup>. The plates of hepatocytes are separated from each other by the sinusoids, which serve as the primary capillaries in the liver involved in the transport of blood<sup>2</sup>. Resident within the sinusoidal lumen are the hepatic immune macrophages, the Kupffer cells. These cells are believed to be replenished in the liver through extrahepatic recruitment of bone-marrow derived monocytes that are macrophage precursors, or alternatively through local proliferation of mature resident Kupffer cells<sup>3</sup>. As a critical component of the innate

immune system, their role is to phagocytose microorganisms and other particulate matter, which are brought into the liver through the portal vein. They also process and present antigens, and respond to such invasions through the secretion of pro-inflammatory mediators including, cytokines, nitric oxide and reactive oxygen intermediates<sup>4</sup>. Between the basal surface of the hepatocytes and the sinusoidal endothelial cells is the peri-sinusoidal space of Disse which contains blood plasma from which the hepatocytes receive their nutrients. The space of Disse also contains the hepatic stellate cells (HSCs), previously termed lipocytes, which amongst other roles, act as fat-storage cells and reservoirs of vitamin A within the healthy liver. They also demonstrate the capacity to synthesise collagens and other extracellular matrix proteins involved in hepatic fibrosis<sup>5</sup>. The region known as the canal of Hering has the primary role of draining bile out of the liver, and is also the site of hepatic progenitor cells. More recently however, CD133<sup>+</sup> hepatic stellate cells (HSCs) within the space of Disse have been demonstrated to contribute to the stem cell population. CD133 is a cell surface protein which has been used as a characteristic marker of stem/progenitor cells of hematopoietic origins. Kordes *et al.* demonstrated that these CD133<sup>+</sup> HSCs have the ability to differentiate into myofibroblast-, endothelial- and hepatocyte-like cells *in vitro*<sup>6</sup>. They also exhibit properties of progenitor cells in that they are able to grow clonally in culture and yet maintain their ability to differentiate, indicating their self-renewal potential<sup>7</sup>. Other parenchymal cells within the liver are the biliary epithelial cells, termed cholangiocytes, which line the biliary tree. The primary function of these cells is to alkalinise the canalicular bile prior to its entry into the duodenum through the secretion of HCO<sub>3</sub><sup>-</sup> which exerts a protective effect against bile-acid induced cholangiocyte injury<sup>8</sup>.



<http://www.mdpi.com/2073-4409/1/4/1261/htm>

### Figure 2. Overview of hepatic cell types.

The liver is organised into rows of hepatocytes with the bile flowing through the sinusoids leading to the bile ducts. The bile duct (BD), hepatic artery (HA), and portal vein (PV) form the portal triad. Blood flows from the portal vein to the central vein (CV). A number of cells are also resident within the liver, each playing a fundamental role in hepatic homeostasis<sup>9</sup>.

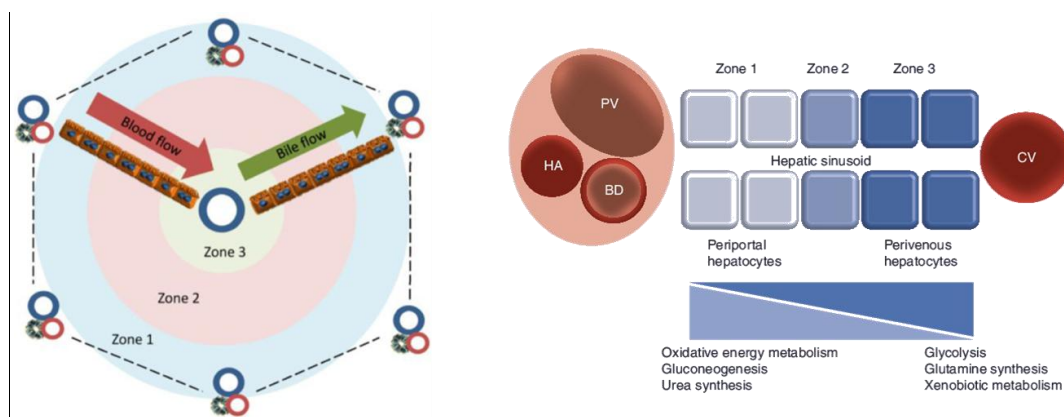
**b) General functions of the liver**

The liver is the largest organ in the body and is responsible for a wide range of roles including metabolic, endocrine, and secretory functions (**Table 1**)<sup>10</sup>.

**Table 1. Table of the major functions of the liver.**

1) Carbohydrate metabolism	Gluconeogenesis Glycogen synthesis and metabolism
2) Fat metabolism	Fatty acid and lipoprotein synthesis Cholesterol synthesis and excretion Ketogenesis
3) Protein metabolism	Synthesis of plasma proteins Urea synthesis
4) Hormone metabolism	Metabolism, conjugation and excretion of both steroidal and polypeptide hormones
5) Xenobiotic metabolism	Drug and foreign compound metabolism and excretion
6) Storage	Glycogen, vitamin A, vitamin B12, iron
7) Bilirubin metabolism	Metabolism and secretion of bilirubin

Metabolic processing is one critical component of liver function. The liver lobule is organised in metabolic zones such that gradients of metabolism are formed. Periportal hepatocytes form part of zone 1, mainly involved in gluconeogenesis, cholesterol biosynthesis, and urea synthesis. This is in contrast to the hepatocytes located perivenously that form part of zone 3 and are part of xenobiotic metabolism, glycolysis, bile acid biosynthesis and glutamine synthesis. The region between these zones has intermediate functions between the two zones and is classified as zone 2 (**Figure 3**)<sup>11</sup>.



<http://www.mdpi.com/2073-4409/1/4/1261/htm>

**Figure 3. Hepatic metabolic zonation.**

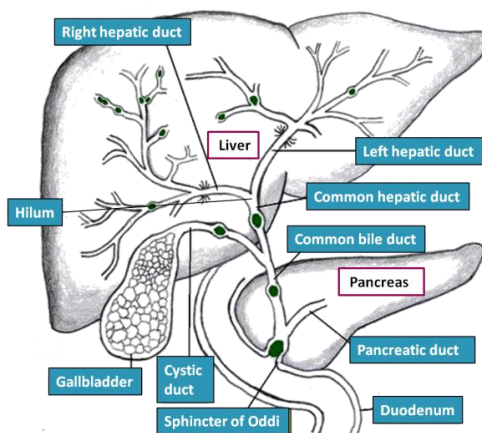
Metabolites are processed in different regions of the liver dependent upon their location in zones 1, 2, or 3. Zones are concentric regions from the central vein and out towards the portal triads. Blood flows toward the central vein, whilst bile flows down the sinusoids and into the bile ducts, countercurrent to the flow of blood. Each of the zones is responsible for specific biological functions.

Another function of the liver is the production of proteins, with up to 50% of total protein synthesised being albumin. Albumin is essential for maintaining oncotic pressure within the capillaries. This osmotic pressure is exerted by the presence of proteins within the plasma that subsequently pull water into the circulatory system, thereby maintaining the balance of water between the capillaries and the circulatory system. Another integral role of albumin is the binding and transportation of hormones<sup>12</sup>. Proteins involved in the immune response are also synthesised in the liver and include the c-reactive protein which activates the complement cascade and complement proteins involved in the clearance of pathogens<sup>13</sup>. Carrier proteins involved in transporting of molecules from the liver to other parts of the body are also hepatically synthesised. An example of this is transferrin, a potent chelator involved in cellular iron homeostasis which maintains  $Fe^{3+}$  in a redox-inert state, thereby preventing the production of damaging free radicals<sup>14</sup>. Tight regulation of iron through hepatic iron-sensing is vital, as low levels of iron result in the development of iron deficiency anaemia. Red blood cells contain iron-containing haemoglobin which binds, carries, and releases oxygen to tissues throughout the body, a requirement for aerobic cellular respiration. Contrastingly, iron overload in the liver results in the generation of excess reactive oxygen species and causes hepatic injury, particularly fibrosis, cirrhosis, steatohepatitis, and hepatocellular carcinoma<sup>15</sup>.

### **c) Bile function, production, and circulation**

Bile is the dark green fluid that is made in the liver and stored in the gallbladder. It plays a crucial role in digestive processes, as it contains bile acids and pigments, phospholipids, cholesterol, and bicarbonates. Firstly, the function of bile is to facilitate emulsification of fats and aid absorption of the fat-soluble vitamins, A, D, E, and K<sup>16</sup>. It is also essential for the absorption of metals such as copper and nickel which are essential factors for haemoglobin synthesis<sup>17</sup>. Lastly, it plays a critical role in the excretion of waste products, particularly end products of haem metabolism<sup>18</sup>. Haemoglobin originating from the destruction of senescent red blood cells is broken down by monocyte macrophages of the spleen, bone marrow, and the hepatic Kupffer cells to produce water-insoluble, unconjugated bilirubin<sup>19</sup>. This lipid-soluble form is then bound to serum albumin and transported to the liver. Dissociation of bilirubin from albumin occurs at the sinusoidal interface of the hepatocytes<sup>20</sup> where the bilirubin enters the hepatocyte through facilitated diffusion<sup>18</sup>. Within the liver, the albumin is removed and the bilirubin is conjugated to glucuronic acid, making it water soluble. The conjugated bilirubin subsequently combines with bile which is synthesised by the hepatocytes from the products of cholesterol metabolism to form bile salts. In the absence of disease, the bile flows into the bile canaliculi and subsequently flows, countercurrent to the hepatic circulation, towards the outside of the liver lobule where it drains from the canals of Hering and into the bile duct.

The bile is subsequently concentrated and stored within the gall bladder<sup>21</sup>. **Figure 4** shows the bile flow of the biliary tree from the liver and down into the duodenum.

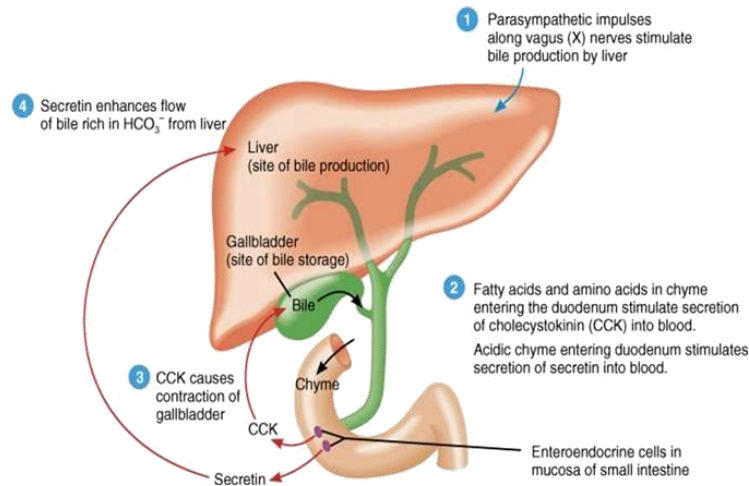


<http://gallstoneflush.com/images/biliary%20tract.JPG>

**Figure 4. Bile flow from the gall bladder to the duodenum.**

Hepatocytes synthesise bile which flows through the bile canaliculi towards the hepatic bile ducts through the canals of Hering. The bile is routed through the common hepatic duct towards the gallbladder where it is stored until required. Hormonally-induced contraction of the gallbladder causes bile to enter the common bile duct.

The semifluid, partially digested food formed after passing through the stomach and the small intestine is known as chyme. It contains a host of digestive enzymes and hydrochloric acid from the stomach, creating the ideal niche for the breakdown of food by protein-digesting enzymes<sup>22</sup>. As the acid chyme enters the duodenum, inactive prosecretin is activated to yield the active hormone, secretin, which is absorbed via the hepatic portal system<sup>23</sup>. Secretin subsequently binds G-protein coupled receptors of large cholangiocytes<sup>24</sup>, and activates adenyl cyclase to produce cAMP<sup>25</sup>. An essential step in the extrusion of bicarbonate is the phosphorylation of the cystic fibrosis transmembrane conductance regulator (CFTR), a chloride channel, by protein kinase A (PKA)<sup>26</sup>. Dysfunction of the CFTR ion channel, as seen in cystic fibrosis, results in the insidious development of biliary fibrosis and periportal inflammation, characteristics also seen in individuals afflicted with primary sclerosing cholangitis, a highly inflammatory biliary disease<sup>27</sup>. Secretin is responsible for the secretion of high concentrations of bicarbonate ions into the duodenum to neutralise the acid contents of the stomach<sup>28</sup>, as well as to provide the optimal, slightly alkaline or neutral pH, in which the pancreatic digestive enzymes are functional<sup>29</sup>. A second hormone, cholecystokinin, is released from the cells in the duodenum in the presence of peptones and proteases, partial products of digestion, as well as long-chain fatty acids. Cholecystokinin stimulates the secretion of pancreatic enzymes and causes the gall bladder to contract and release bile through the cystic duct into the common bile duct, and finally into the intestine through the sphincter of Oddi<sup>30</sup> (**Figure 5**). Through the portal venous system, approximately 95% of biliary secretions are returned to the liver to be reused<sup>21</sup>.



<http://1.bp.blogspot.com/-b3xImFaEdwU/UNeuUlbjZI/AAAAAAAAAnw/W2Os993QaFQ/s1600/digestive12.jpg>

**Figure 5. Induction of bile secretion from the gallbladder.**

The presence of acid chyme triggers the release of the hormones cholecystokinin and secretin. Cholecystokinin stimulates the release of enzymes from the pancreas and causes contraction of the gallbladder to facilitate the release of bile, while secretin induces neutralisation of the acid bile.

## II) Signalling pathways involved in hepatic development

All of the processes within the liver are regulated at the molecular level by signalling pathways which are tightly regulated. These pathways have temporal activities which may be specific to the developmental process, while others are recapitulated during the process of regeneration and repair. Novel methods of monitoring pathway activity, particularly in an *in vivo* context, are ongoing as better technologies are being developed and exploited.

### a) Developmental signalling pathways

Many diseases of the liver occur as a result of deregulation of cell signalling during developmental processes. Understanding developmental pathways is relevant to acquired liver diseases in adults as signalling expression profiles observed during embryogenesis are exploited as a mechanism of liver repair and the deregulation of such pathways is causative in the development of disease. Some of the main cell signalling pathways involved during development, hepatobiliary disease, and regeneration are TGF- $\beta$ , WNT, Notch, and NF- $\kappa$ B signalling, all of which will be discussed both in their developmental and disease-specific contexts.

### i) Transforming growth factor- $\beta$ superfamily signalling pathways

One of the key pathways in endoderm formation involves the transforming growth factor (TGF- $\beta$ ) superfamily of transcription factors. The TGF- $\beta$  superfamily members can be divided into two branches, with TGF- $\beta$ I, myostatin, Nodal, Inhibin and Lefty 1,2 activating the TGF- $\beta$  signalling branch, while the bone morphogenetic proteins (BMPs) are responsible for the BMP signalling branch, each of which phosphorylate specific R-SMAD proteins<sup>31</sup> (**Figure 6**). TGF- $\beta$  receptors are classified into 3 different classes, with type I (T $\beta$ RI) alternatively termed activin-like kinases (ALK), Type II (T $\beta$ RII), and type III (T $\beta$ RIII). Ligand binding leads to the formation of a hetero-tetrameric complex of two T $\beta$ RI and two T $\beta$ RII receptors<sup>32</sup>. This catalytically favourable orientation permits T $\beta$ RII to phosphorylate T $\beta$ RI which subsequently activates the cytoplasmic Ser/Thr kinase domain within the cytoplasm<sup>32</sup>. There are five receptor-regulated SMAD proteins (R-SMADS), namely SMAD1, SMAD2, SMAD3, SMAD5, and SMAD8. Receptor-mediated phosphorylation of the R-SMADS induces a conformational change within the protein, resulting in its dissociation from the receptor complex. The R-SMADS subsequently form transcriptional complexes, which, when phosphorylated, have a high affinity for the coSMAD, SMAD4, and bind to it<sup>33</sup>. This R-SMAD/coSMAD complex subsequently translocates into the nucleus where it binds to specific response elements. These response elements are short sequences of DNA within the promoter regions of genes which are able to bind specific transcription factors to regulate gene expression of DNA targets<sup>34</sup>.

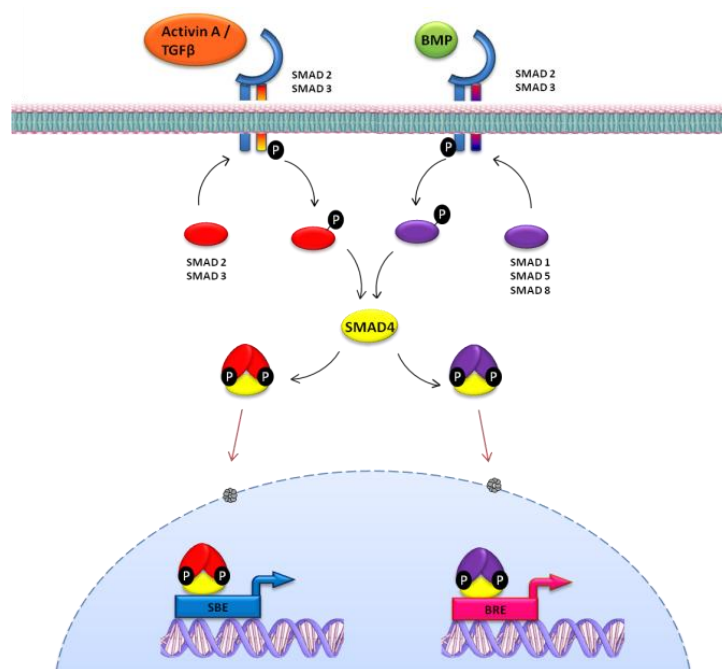


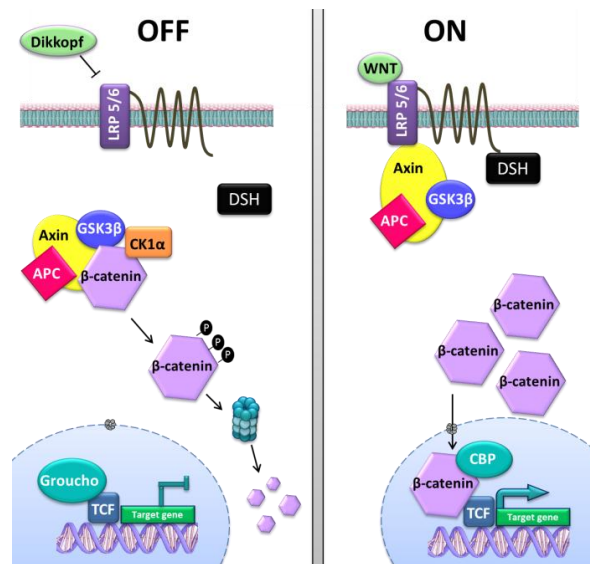
**Figure 6. Branches of TGF- $\beta$  signalling.**

TGF- $\beta$  signalling is activated through binding of an agonist to the receptor. This induces intracellular phosphorylation of the receptor and subsequent R-SMADs, making them conformationally receptive to binding to coSMAD4. The complexes subsequently translocate into the nucleus where they bind to their respective response elements depending on whether the TGF- $\beta$  or BMP part of the pathway was ligand activated.

## ii) WNT signalling

Another critical pathway involved in both development and disease is the Wnt signalling pathway. In the 1980s, Christiane Nusslein-Volhard and Eric Wieschaus performed large-scale mutant screens in *Drosophila melanogaster* and found that many Wnt genes, a family of genes, were required for axis determination during embryonic development<sup>35</sup>. Wnt proteins have emerged as critical regulators of stem cell self-renewal and cancer, with aberrant signalling leading to tumorigenesis in a number of cellular contexts<sup>36</sup>. This complex pathway is characterised by canonical WNT signalling, non-canonical planar cell polarity pathway, and non-canonical Wnt/Calcium pathway, all of which have distinct ligands and downstream targets. Wnt signalling is highly conserved across species, and is involved in the regulation of cell polarity<sup>37</sup>, axis determination<sup>38</sup>, cell fate determination<sup>39, 40</sup> and a range of other functions during embryogenesis.

The best characterised of these Wnt signalling pathways is canonical Wnt signalling which is  $\beta$ -catenin mediated. This pathway is highly regulated both spatially and temporally and is activated upon the binding of secreted Wnt proteins to the N-terminal domain of the seven-transmembrane-spanning Frizzled (Fz) family of receptors<sup>41</sup>. Wnt-bound Fz then forms a co-receptor complex with low-density-lipoprotein-related protein5/6 (LRP5/6)<sup>42</sup>. In the absence of Wnt ligand stimulation,  $\beta$ -catenin is held in a destruction complex with axin, adenomatosis polyposis coli (APC), casein kinase 1 $\alpha$  (CK-1 $\alpha$ ) and glycogen synthase kinase-3beta (GSK-3 $\beta$ ). Poly-ubiquitination of  $\beta$ -catenin by GSK-3 $\beta$  targets it for proteasomal degradation, causing cessation of any subsequent downstream signalling<sup>43</sup>. In conjunction with proteasomal modulation, Wnt target genes are kept in a repressed state through the association of TCF with transcriptional co-repressor complex, Groucho/transducin-like enhancer protein 1 (TLE), a transcriptional repressor which interacts with histone deacetylases, thereby maintaining transcriptional inactivation<sup>44,45</sup>. However, addition of Wnt ligand sequesters the negative Wnt regulator, Axin, to the cell membrane. Binding of axin to the cytoplasmic tail of LRP-5/6<sup>46</sup> is mediated through phosphorylation by either CK1 $\gamma$  or GSK-3 $\beta$ <sup>47</sup>. Following LRP-5/6 activation, Dishevelled is recruited to Fz, becomes phosphorylated, and antagonises the kinase activity of GSK-3 $\beta$ <sup>48</sup>. The downstream effects include inhibition of phosphorylation of axin by GSK-3 $\beta$ , leading to its decreased stability and cytoplasmic levels<sup>49</sup>, as well as the inhibition of GSK-3 $\beta$ -mediated phosphorylation of  $\beta$ -catenin, which liberates  $\beta$ -catenin from the destruction complex and halts subsequent degradation<sup>50</sup>. The stabilisation and accumulation of  $\beta$ -catenin causes its translocation into the nucleus where it displaces groucho/TLE repressors from the TCF/LEF DNA binding motif and associates with CREB-binding protein (CBP)/300, a histone acetyltransferase involved in chromatin activation<sup>51</sup> (**Figure 7**).



[http://www.wormbook.org/chapters/www\\_wntsignaling/wntfig1.jpg](http://www.wormbook.org/chapters/www_wntsignaling/wntfig1.jpg)

**Figure 7. Regulation of canonical Wnt signalling.**

In the absence of ligand binding to the Wnt receptor,  $\beta$ -catenin is prevented from nuclear translocation through its interaction with the destruction complex consisting of Axin, APC, CK1 $\alpha$ , and GSK-3 $\beta$ . Upon ligand binding, Axin binds to the LRP receptor, while Dishevelled is recruited to the Frizzled receptor and is phosphorylated. This releases  $\beta$ -catenin from the repressive hold of the destruction complex, allowing its cytoplasmic accumulation and subsequent translocation into the nucleus where it activates downstream target genes.

$\beta$ -catenin also has an important role in cell-cell adhesions by complexing with E-cadherin to bridge it to the actin cytoskeleton at the adherens junctions. The loss of either  $\beta$ -catenin or E-cadherin is associated with a loss of intercellular junction integrity and increased invasiveness of tumors<sup>52</sup>. Maintenance of these tight junctions is required for correct formation of the bile canaliculi, with the liver-specific loss of  $\beta$ -catenin resulting in intrahepatic cholestasis<sup>53</sup>. This mobilisation of E-cadherin to  $\beta$ -catenin is regulated by the IL-6 family cytokine, oncostatin M (OSM) and is a key regulator for the formation of adherens junctions during liver development<sup>54</sup>. Alternatively,  $\beta$ -catenin can act as a modifier of gene expression in a Wnt-independent manner through its association with c-Met, the receptor for hepatocyte growth factor (HGF). Binding of HGF to c-Met dissociates the c-MET/ $\beta$ -catenin complex in a dose-dependent manner, and allows phosphorylation and the nuclear translocation of  $\beta$ -catenin independent of canonical Wnt signalling<sup>55</sup>.

Antagonists of the Wnt pathway are crucial for Wnt temporospatial signal modulation. A number of secreted proteins have been identified which prevent the interaction of Fz or LRP5/6 with their Wnt agonist. These include Dickkopf (Dkk)<sup>56</sup>, soluble Frizzled-related proteins<sup>57</sup>, Frzb<sup>58</sup>, Wnt-inhibitor protein (WIF)<sup>59</sup>, and the Wnt inhibitor Wise<sup>60</sup>. These inhibitors act to tightly regulate signalling and are able to do so in a dose-dependent manner to allow the production of a morphogenic gradient during embryogenesis which is imperative for precise pattern formation.

### iii) Canonical Notch signalling

Notch signalling between cells is carried out through direct cell-cell ligand-receptor interactions. This permits signal transduction to induce transcriptional activation of genes which are involved in a multitude of biological activities during both embryogenesis<sup>61</sup> and adult life<sup>62,63</sup>. Some of the downstream effects include proliferation, stem cell maintenance, and cell fate determination. Notch receptors comprise a large, single-pass Type I transmembrane receptor which contains both a large extracellular domain, and a small intracellular domain. Following translation, the Notch receptor undergoes crucial modifications, glycosylation and fucosylation, to become fully functional<sup>64</sup>. In mammals, there are four known Notch receptors (Notch 1-4) which have distinct transcriptional activities and have both redundant and unique functions<sup>65</sup>. There are five canonical Notch signalling ligands belonging to either the Jagged/Serrate (Jagged 1,2) family of proteins, or the Delta-like (Dll 1, 3, and 4) family.

Notch signalling is one of the few pathways whose signalling is dependent upon a series of proteolysis events, with the final cleavage resulting in signal transduction without the need of a secondary messenger or signal amplification cascade. Following post-translational modification, the first of 4 cleavage events takes place at the S1 site by a furin like-convertase, producing a mature receptor which is then targeted to the cell surface<sup>66</sup>. This cleavage converts the Notch polypeptide into a Notch extracellular domain and a Notch transmembrane and intracellular domain, with heterodimer formation retained through noncovalent interactions<sup>67</sup>. Binding of the ligand causes a conformational change and exposes the S2 cleavage site to the ADAM-family metalloproteinases, Tumour (TACE)<sup>68</sup> resulting in ectodomain shedding. The remaining membrane-tethered transmembrane domain containing the S3 and S4 cleavage sites then becomes the substrate for  $\gamma$ -secretase, with cleavage resulting in the liberation of the Notch intracellular domain (NICD) and its subsequent translocation into the nucleus<sup>69</sup>. In the absence of NICD, the transcription factor CSL (CBF1, Suppressor of Hairless, Lag-1) associates with DNA-binding recombination signal binding protein (RBP)- $\text{J}\kappa$ , co-repressor proteins and deacetylases, exerting a repressive signal upon target genes<sup>70</sup>. Nuclear accumulation of NICD and its interaction with CSL triggers an allosteric change which displaces the transcriptional repressors and converts the repressive signal of (RBP)- $\text{J}\kappa$  into an activation signal through its association with a transcriptional activation complex which includes Mastermind-like-1 (MAML-1) and the histone acetyltransferase, p300<sup>71</sup>. Recruitment of activators to the promoter triggers the transcription of Notch target genes such as *Hes1* and *Hes5* which are critically involved in differentiation<sup>70</sup>. Termination of signalling is carried out through hyperphosphorylation of NICD on its proline-glutamic acid-serine-threonine (PEST) and transcription activation domain (TAD) domains by kinases such as CDK8, thereby targeting it for proteasomal degradation by the E3 ubiquitin ligase<sup>72</sup> (**Figure 8**). Notch signalling is exquisitely context

dependent, with the timing, length, and intensity of expression all intricately controlled to provide the diverse array of Notch expression profiles observed within varying niches.

### Numb inhibition of Notch signalling

Numb is a membrane-associated phosphotyrosine binding protein involved in regulating fate determination. Its primary role within cellular differentiation is to inhibit Notch signalling which is a necessary component of self-renewal in stem and progenitor cells<sup>73</sup>. Two downstream targets of Notch signalling are hairy and enhancer-of-split 1 (HES1) and Hes-related family bHLH transcription factor with YRPW motif protein 1 (HEY1), which function as transcriptional repressors of tissue-specific transcription factors, thereby increasing the capacity for self-renewal<sup>74</sup>. Numb biologically antagonises Notch signalling through association with  $\alpha$ -adaptin, a component of clathrin-coated pits involved in endocytosis<sup>75</sup>. Receptor-mediated internalisation of Notch via numb is thus capable of repressing further Notch signal transduction. Numb also exerts its inhibitory effects by promoting ubiquitination of the membrane-bound Notch1 receptor. The E3 ubiquitin ligase, Itch, and Numb act cooperatively to promote the degradation of NICD, leading to a loss of Notch signalling<sup>76</sup>. A more in-depth understanding of how the above-mentioned pathways are regulated during development and induce disease is highlighted below.

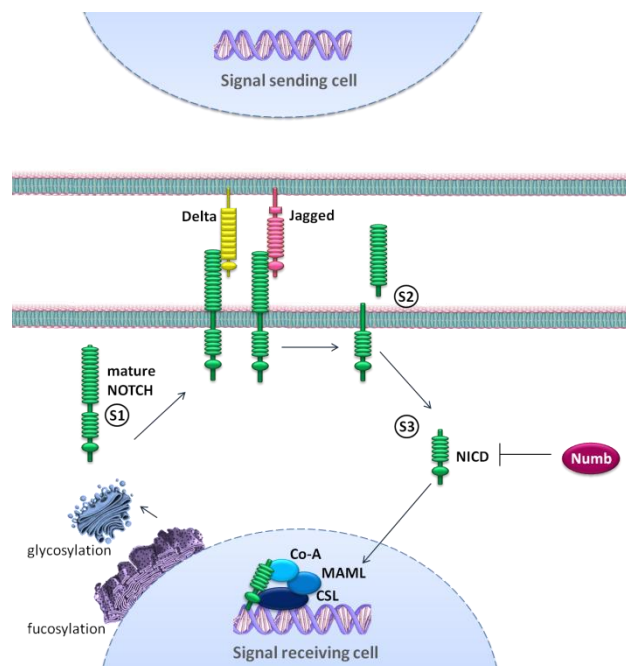
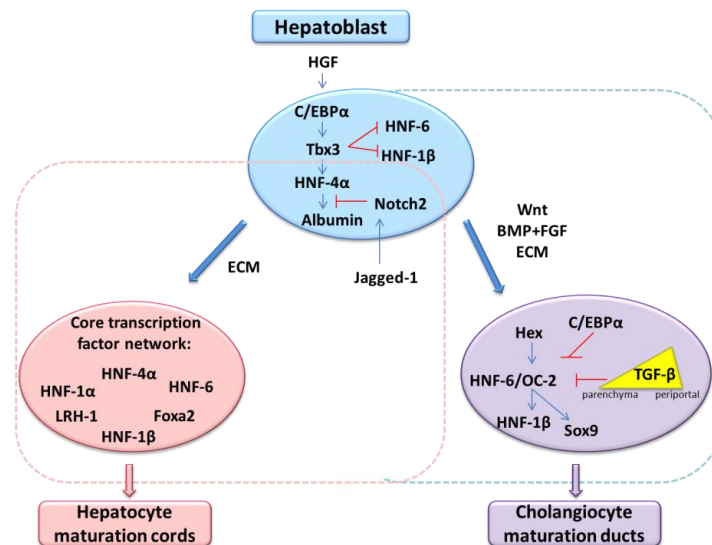


**Figure 8. Representation of canonical Notch signalling through cell-to-cell interactions.**

Following posttranslational modifications, the mature Notch receptor resides as a single transmembrane receptor within the plasma membrane of the signal receiving cell. Following binding by one of the Notch ligands, a series of proteolytic cleavage events results in the formation of NICD, the Notch receptor domain capable of binding directly to DNA binding motifs, recruiting other co-activators, and causing transcription of Notch target genes.

## b) Overview of liver development

Over the last decade, much research has been done to further the understanding of the mechanisms of hepatic development. This has led to key genes and molecular pathways being identified and used to produce hepatic-like cells that have therapeutic potential for a range of diseases. Many of these pathways are synonymous with those involved during the process of tissue repair and regeneration. An overview of some of the core transcription factors involved in the differentiation of hepatoblasts toward hepatocytes and cholangiocytes that will be further discussed are illustrated in **Figure 9**.



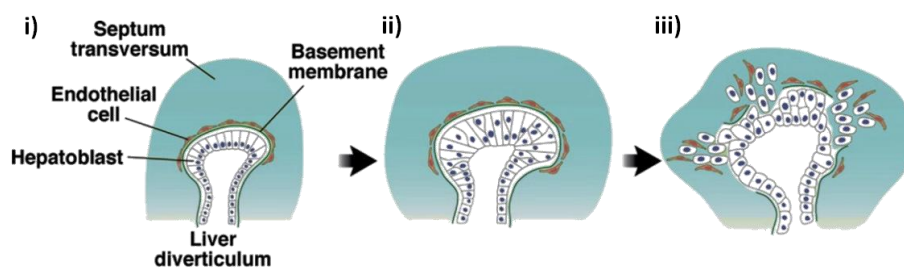
[http://www.tankonyvtar.hu/en/tartalom/tamop425/0011\\_1A\\_Transzdifferentiation\\_en\\_book/ch01s07.html](http://www.tankonyvtar.hu/en/tartalom/tamop425/0011_1A_Transzdifferentiation_en_book/ch01s07.html)

### Figure 9. Transcriptional regulation of hepatoblast differentiation.

The differentiation of hepatoblasts to hepatocytes and cholangiocytes is dependent upon a core circuit of transcription factors and signalling pathways. The temporal expression of these core transcription factors is crucial to their determination of cell fate.

Key stages of hepatic development include competence, induction, specification, proliferation, and migration. The concept of developmental “competence” is characterised by cells which have not yet been specified to become a particular cell type, but have the capacity to respond to molecular specification-inducing signals. It has been hypothesised that the endoderm must enter a stage of competence prior to hepatic specification. Mediators of hepatic competence include forkhead box protein (FoxA) and GATA4, both of which affect the transcriptional activity of one the earliest and best characterised hepatocyte markers, albumin (ALB). The next stage of liver development is termed “specification”, and refers to the commitment of cells towards a specific differentiated state. The position of the ventral endoderm relative to the cardiac mesoderm is critical to hepatic cell fate, as FGF-mediated specification is concentration-dependent. Lower concentrations induce hepatic specification, while higher concentrations specify lung tissue<sup>77</sup>. Mesodermal Wnt expression promotes hindgut development, and its inhibition by the endoderm through the secretion of Wnt

antagonists is required for subsequent liver development<sup>78</sup>. By E8.5 the liver bud is formed with early molecular evidence of hepatic specification seen by expression of *transferrin*<sup>79</sup>, *ALB*, *AFP*<sup>80</sup>, and *HNF4a*<sup>81</sup> in a region of the ventral endoderm. Following specification at E9.5 or day 22 of human embryonic development, the liver diverticulum is formed from the primitive gut and is surrounded by a basement membrane composed of laminin, collagen IV, fibronectin, and heparin sulphate proteoglycan<sup>82</sup>. It is here that the hepatoblasts begin to proliferate<sup>83</sup>, mediated by *Hex* signalling<sup>84</sup>. Expression of metalloproteinases (MMPs) by the hepatoblasts is required for the breakdown of the basement membrane, with inhibition of MMP activity resulting in the failure of the hepatoblasts to migrate into the septum transversum<sup>85</sup>. By E10-15, the liver bud undergoes rapid growth and is vascularised and colonised by hematopoietic cells<sup>86</sup>. From E13, the bipotent hepatoblasts begin to differentiate into either biliary epithelial cells (alternatively termed cholangiocytes), if in close proximity to the portal veins, or into hepatocytes<sup>86</sup>.



[http://www.stembook.org/sites/default/files/pubnode/1eb96f61005e0c07df780954b6df2580a1c71d6d/Liver\\_development/Zorn10.jpg](http://www.stembook.org/sites/default/files/pubnode/1eb96f61005e0c07df780954b6df2580a1c71d6d/Liver_development/Zorn10.jpg)

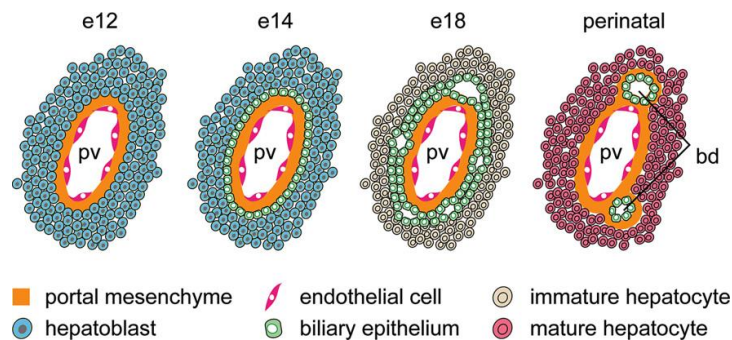
**Figure 10. Endodermal budding of the liver.**

i) Liver bud formation begins with the formation of the liver diverticulum containing pseudostratified hepatoblasts. ii) The hepatoblasts undergo proliferation and iii) subsequently undergo EMT and migrate through the basement membrane and invade the adjacent septum transversum.

### c) Development of the biliary tree

The extrahepatic and intrahepatic regions of the biliary tree have discrete developmental origins. Genetic knockout experiments have highlighted the importance of several key transcription factors required for biliary development, including *Hhex*<sup>87</sup>, *HNF6*<sup>88</sup>, and *HNF1β*<sup>89</sup>. Hepatoblast differentiation into cholangiocytes occurs around E13.5 in the mouse, with intrahepatic bile duct (IHBD) development highly conserved in humans, rats, and mice. The first step in bile duct morphogenesis is the formation of the ductal plate consisting of SOX9-positive cells. SOX9 is a temporally fundamental transcription factor in bile duct development and will be discussed later in more detail. The ductal plate is formed from the periportal hepatoblasts which are located at the interface between the hepatic parenchyma and the portal mesenchyme. This continuous, single layer of cholangiocytes duplicates around E16.5 and undergoes dramatic remodelling to form the bile ducts. Biliary differentiation occurs in a sequential but asymmetrical manner, with the cells on the portal

side of the ductal plate beginning differentiation earlier than the hepatoblasts on the parenchymal side. This differentiation asymmetry resolves with subsequent maturation of the bile duct<sup>90</sup>. At the time of birth, the remainder of the ductal plate progressively regresses while the mature ducts migrate and integrate into the portal mesenchyme<sup>88</sup> (**Figure 11**). This process is temporally coordinated with the formation of hepatic portal arteries through stage-specific communication of angiogenic factors with developing biliary structures<sup>91</sup>. The cholangiocytes are responsible for the development of a vascular endothelial growth factor (VEGF) gradient, which subsequently determines arterial vasculogenesis within their vicinity<sup>91</sup>. Progressive development of the IHBD begins from the hilum of the liver out towards the periphery of the liver lobes, with the ducts progressively connecting to form an interconnected network into which the bile can drain into the extrahepatic bile ducts<sup>92</sup>. This means that neonatally, mature ducts which already possess radial symmetry can be seen near the hilum, while asymmetric structures are still seen at the periphery. This is in contrast to adults which display mature bile ducts throughout the lobes.



<http://www.sciencedirect.com/science/article/pii/S0016508509004636>

**Figure 11. Bile duct development.**

At E13, hepatoblasts in direct contact with the portal vein mesenchyme begin to attain a cuboidal shape and are fated to become biliary epithelia. From E17, this initial layer, or ductal plate, duplicates to form a bilayer. This bilayer forms focal dilations which eventually give rise to the bile ducts, while the remainder of the ductal plate regresses over time. Parenchymal hepatoblasts differentiate into hepatocytes.

**Transcription factor modulation of cholangiocyte differentiation**

Numerous signalling pathways are known to have a significant impact on determining the lineage of the hepatoblasts. Wnt/ $\beta$ -catenin signalling has been shown to promote the differentiation of cholangiocytes through inducing expression of EGF<sup>93</sup>, which in combination with HGF, are able to form biliary structures from cultured hepatocytes *in vitro*<sup>94</sup>. Definitive experiments have been performed to show the requirement of Wnt signalling in biliary differentiation. Using embryonic liver explants cultured with antisense morpholino oligos to  $\beta$ -catenin resulted in the loss of cells positive for CK19, a cholangiocyte-specific marker. Monga *et al.* also noted an increase in C-KIT expression, a marker of liver stem cells, within the  $\beta$ -catenin inhibited hepatocytes<sup>95</sup>. Moreover, the treatment of liver explants with conditioned medium containing the well-characterised Wnt agonist, Wnt3a, was

able to induce biliary differentiation characterised by CK19<sup>+</sup> staining<sup>96</sup>. These results were further validated *in vivo* by Tan *et al.* who demonstrated that inactivation of  $\beta$ -catenin results in bile duct paucity. Histologically the  $\beta$ -catenin knockout mice showed a reduction in overall hepatocyte numbers due to 1) increased apoptosis due to oxidative stress, and 2) diminished expansion capacity due to a decrease in cyclin-D1<sup>97</sup>. Taken together, this data shows that  $\beta$ -catenin plays a critical role in the proliferation, survival, and differentiation of the hepatoblasts and is integral to survival.

Furthermore, recent studies have elucidated the contribution of the periportal TGF- $\beta$  concentration gradient to biliary cell differentiation. This activin/TGF- $\beta$  gradient is regulated through the expression of the Onecut (OC) transcription factors, HNF-6 (OC-1) and OC-2, which inhibit TGF- $\beta$  signalling within the hepatic parenchyma to allow hepatocyte differentiation. High levels of TGF- $\beta$  signalling around the portal vein, however, support the differentiation of hepatoblasts towards cholangiocytes<sup>98</sup> with multiple signalling pathways acting to suppress pro-hepatocyte transcription factors, HNF4 $\alpha$ <sup>99</sup>, Tbx3<sup>100</sup>, and C/EBP<sup>101, 102</sup>. Following differentiation of the hepatoblasts to mature cholangiocytes, T $\beta$ RII expression is repressed in a negative feedback loop of TGF- $\beta$ . Confirmation of the necessity of the OC transcription factors in cholangiocyte specification has been determined through knockout of the OC genes. This results in a perturbation of the TGF- $\beta$  gradient and the creation of hybrid hepato-biliary cells that exhibit characteristics of, and stain for markers of both biliary and hepatocyte cell lineages<sup>88</sup>. A critical clue in deciphering the regulation of the TGF- $\beta$  gradient is seen in the *Hnf6* and *Oc2* knockout mice. It is known that these transcription factors modulate the expression of the TGF- $\beta$  antagonists, follistatin and  $\alpha$ -2-macroglobulin, and repress the expression of the TGF- $\beta$ -receptor II gene. The knockout mice see a strong downregulation in antagonist expression, while increasing the expression of the TGF- $\beta$  type II receptor, leading to an increase in TGF- $\beta$  signalling within these transgenic animals compared to their wildtype littermates<sup>98</sup> (**Figure 12**). The model proposed by Antaniou *et al.* is that the TGF- $\beta$  signalling gradient induces sequential differentiation of the cells on the portal side, followed by those on the parenchymal side of the duct<sup>90</sup>. Further mechanistic evidence of TGF- $\beta$  signalling in the development of the ductal plate is seen in the increased expression of SMAD5, a component of TGF- $\beta$ /BMP signalling, within BECs that form the ductal plate. This is in contrast to the expression of chordin, a TGF- $\beta$ /BMP pathway antagonist, whose expression is seen throughout the liver. This gives corroborative evidence that TGF- $\beta$ /BMP expression is limited to hepatoblasts that are in contact with the portal mesenchyme, and that its expression is regulated by chordin in those hepatoblasts that do not contribute to formation of the ductal plate<sup>103</sup>.

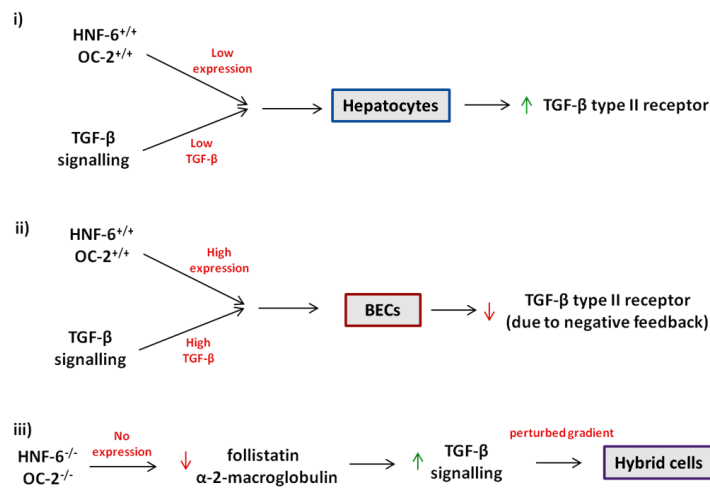


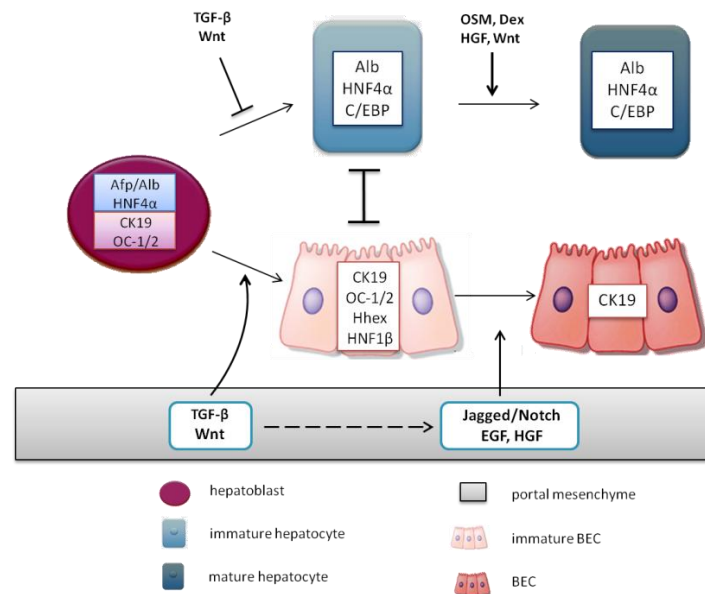
**Figure 12. TGF- $\beta$ -gradient mediated restriction of hepatobiliary lineages.**

A radial gradient of TGF- $\beta$  signalling is observed with high periportal expression that is gradually reduced towards the parenchyma. High levels of Onecut factors and TGF- $\beta$  signalling induce biliary epithelial cell differentiation. Following maturation, there is a repression of T $\beta$ RII expression due to TGF- $\beta$  negative feedback. Parenchymal hepatoblasts express low levels of the Onecut factors and are exposed to the lower levels of the TGF- $\beta$  gradient, leading to their differentiation into hepatocytes. Double knockout of HNF6 and OC-2 results in perturbation of their respective gradients leading to the generation of hybrid cells.

In parallel to its modulation of the TGF- $\beta$  signalling gradient, the cholangiocyte-specific transcription factor HNF6 has also been shown to regulate the expression of *Hnf1 $\beta$*  within cholangiocytes<sup>88</sup>. HNF1- $\beta$  is required for cholangiocyte function, as its deficiency results in the paucity or absence of normal primary cilia used in cell sensory functions<sup>104</sup>. Heterozygous mutations have been found to result in ductal plate malformations and cholestasis in humans<sup>105</sup>, while homozygous deletions result in ductopenia and bile duct dysplasia<sup>105</sup>. *Hnf6*<sup>-/-</sup> mice showed the presence of hepatic bile deposits and increased levels of bilirubin, indicators of cholestatic syndrome induced by disrupted IHBD morphogenesis<sup>88</sup>. Both HEX<sup>87</sup> and HNF-6<sup>88</sup> also play integral roles later in development as they regulate HNF1- $\beta$  during the process of remodelling of the ductal plate. Furthermore, the BMP receptor-regulated SMAD5 has also been found to be highly expressed in those cells that form the ductal plate, whereas the expression of chordin, a TGF- $\beta$ /BMP antagonist is highly expressed in cells that do not contribute to the formation of the ductal plate<sup>103</sup>.

Another critical signalling pathway involved in the formation of the biliary tree is the Notch pathway. It is required for bile duct morphogenesis with biliary differentiation and tubule formation requiring dose-dependent signalling<sup>90</sup>. Notch has also been found to have a definitive role in the development of biliary tubules as a lack of biliary tubule formation is seen in *Hes1* null mice at birth. During liver development, expression of JAGGED-1 is restricted within the portal mesenchyme within the neonatal mouse, while NOTCH2 and HES1 expression is observed in cholangiocytes which reside adjacent to the JAGGED-1-positive cells<sup>106</sup>. Taken together, these experiments have highlighted the role for several key signalling pathways in the initiation and maturation of hepatocytes and

cholangiocytes. These factors and their temporal activation are tightly controlled and require activators, inhibitors, and the formation of periportal and perivenous gradients for normal development (**Figure 13**).



Adapted from: <http://www.stembook.org/node/512>

**Figure 13. Markers of biliary and hepatocyte differentiation.**

Bipotent progenitors express both hepatocytes and BEC markers. TGF- $\beta$  and Wnt signalling from the portal mesenchyme are suggested as promoting the expression of BEC-associated transcription factors, while suppressing hepatocyte-specific transcription factors. Subsequent Notch, EGF and HGF signalling then reinforce the BEC lineage segregation. Hepatoblasts within the parenchyma that are not exposed to periportal signalling are able to upregulate genes involved in hepatocytes differentiation. Mature hepatocytes are derived through subsequent exposure to OSM, Dex, HGF, and Wnt.

### III) Mortality and economic burden of liver disease

For the body to maintain homeostasis, hepatic pathways and processes must be carefully controlled at the molecular level. The continual loss of homeostasis can result in the development of disease. According to the European Association for the Study of the Liver (EASL), approximately 0.1% of the European population is affected by cirrhosis, with 170,000 deaths per year, while the WHO attributes approximately 47,000 deaths per year in the EU to hepatocellular carcinoma. The leading causes of cirrhosis and hepatic cancers are excessive alcohol consumption, hepatitis B & C, and metabolic syndromes consistent with obesity<sup>107</sup>. On a global level, liver disease on the whole is on the rise. Therefore, distinctions at a molecular level between healthy and pathological states may give insight for novel pharmacological targets. The aim would therefore be to rectify aberrant signalling pathways and return hepatic homeostasis. Both *in vitro* and *in vivo* models have been generated to assess and target relevant pathways involved in hepatic diseases. These include the use of reporters which express a quantifiable marker in response to pathway activation such as  $\beta$ -galactosidase,

chloramphenicol acetyltransferase, or light-emitting luciferases. *In vivo*, transgenic models have been invaluable in elucidating the pathogenic effects of particular genes, with more recent light-emitting luciferase transgenics used to study transcriptional regulation of pathways within a living organism. Interrogation and further investigation of these signalling pathways *in vivo* is important for drug targeting strategies for liver disease as appropriate modulation of these pathological signals may offer therapeutic benefit. There is particular emphasis on increased predictability of *in vitro* assays prior to *in vivo* experimentation and decreasing the number of animals used within academic and industrial research in studies of liver disease.

#### **IV) Instigators of inflammatory activation, ECM remodelling and fibrotic resolution**

##### **a) Role of NF- $\kappa$ B in liver tolerogenic responses and hepatic injury**

While particular transcription factors are required for the precise development of the liver, others are activated in response to various insults and are crucial to regain liver homeostasis and repair. The nuclear factor- $\kappa$ B (NF- $\kappa$ B) signalling pathway is most frequently associated for its role in inflammation where, in the short term, it is immensely beneficial in wound-healing processes in response to acute injury by promoting regeneration. Contrastingly, failed cessation of these inflammatory responses leads to chronic, long-term inflammation which has a negative impact upon the liver's regenerative potential and results in an increased fibrotic phenotype. The liver is unique in that it has a dual blood supply and not only receives blood from the hepatic arteries, but also receives a continuous supply of blood from the gastrointestinal tract via the portal vein. Blood originating from the portal vein is therefore enriched for potential antigens<sup>108</sup>. The liver is a central immunological organ involved in the clearance of systemic bacterial infection as it hosts approximately 80% of the body's macrophages. NF- $\kappa$ B inducers include pathogen-derived molecules such as lipopolysaccharide (LPS), which originate from Gram-negative bacteria, and also exogenous DNA/RNA that stimulate Toll-like receptors (TLRs)<sup>109</sup>. Inflammatory cytokines, tumour necrosis factor- $\alpha$  (TNF- $\alpha$ ), and interleukin (IL-1)<sup>110</sup>, also have the capacity to activate NF- $\kappa$ B signalling and in turn initiate the transcription of a host of genes involved in the regulation of inflammation, cell survival, and immune responses.

NF- $\kappa$ B functions as a heterodimeric transcription factor controlling genes involved in immunity, inflammation, proliferation and the prevention of apoptosis. The NF- $\kappa$ B family of transcription factors include RelA (p65), NF- $\kappa$ B1 (p50 and its precursor p105), NF- $\kappa$ B2 (p52 and p100), c-Rel and RelB<sup>111</sup>. These transcription factors are sequestered within the cytoplasm in an inactive state by an inhibitor of  $\kappa$ B (I $\kappa$ B $\alpha$ ) through the masking of nuclear localisation signals found on the NF- $\kappa$ B proteins. Site-specific phosphorylation of I $\kappa$ B $\alpha$  by IKK results in I $\kappa$ B $\alpha$  proteasomal degradation and its dissociation from NF- $\kappa$ B. Unmasking of the nuclear localisation signal allows NF- $\kappa$ B to

translocate into the nucleus, bind to NF- $\kappa$ B enhancer elements in gene promoters, and induce transcriptional expression of target genes<sup>112</sup> (**Figure 14**).

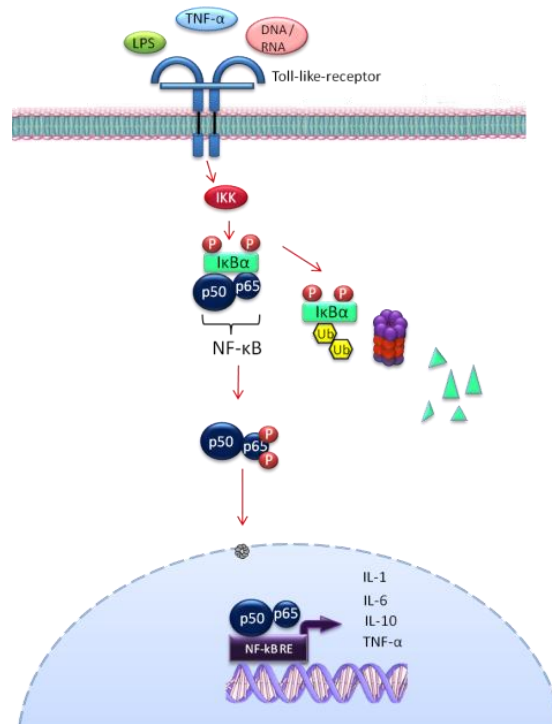


**Figure 14. Illustration of canonical NF- $\kappa$ B signalling in response to TLR agonists.**

Upon agonist binding to the TLR receptor, inhibitor of  $\kappa$ B kinase phosphorylates I $\kappa$ B on conserved residues, thereby promoting I $\kappa$ B $\alpha$  proteasomal degradation. This exposes the nuclear localisation signal on the NF- $\kappa$ B heterodimer allowing its translocation into the nucleus and subsequent binding to its response element and activation of transcription of pro-inflammatory/anti-inflammatory genes.

NF- $\kappa$ B has non-immune related roles in the maintenance of tissue homeostasis, but has also been implicated in the pathogenesis of many inflammatory diseases. Dual-functioning NF- $\kappa$ B signalling not only leads to the expression of pro-inflammatory molecules, but is also capable of modulating anti-inflammatory signalling processes. Kupffer cells exposed to normal physiological doses of LPS showed that NF- $\kappa$ B induces the expression of its direct target interleukin-10 (IL-10), an anti-inflammatory cytokine, that subsequently downregulates the release of pro-inflammatory cytokine, IL-6 and TNF $\alpha$  and modulates the liver’s response to low antigenic levels<sup>113</sup>.

### **b) Kupffer cell activation**

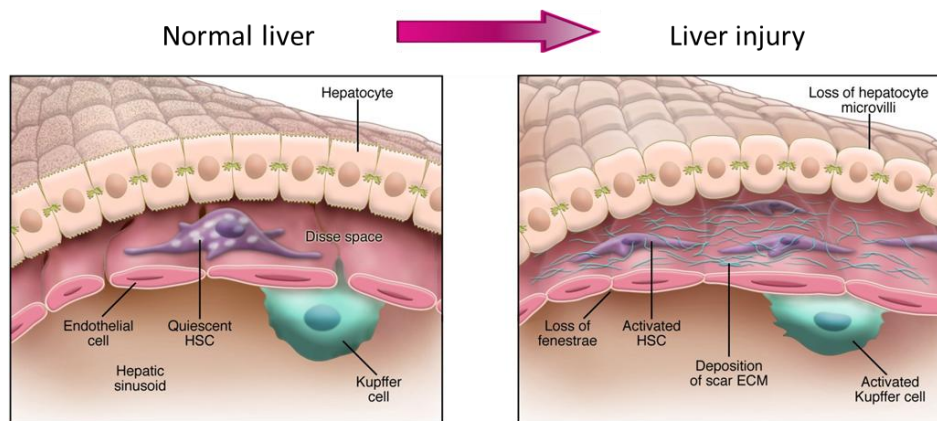
Strong inflammatory responses may be beneficial in the short term to eradicate pathogens, however, long term activation of inflammatory signals may have deleterious effects. In the context of low “physiological” level of LPS, Kupffer cells release anti-inflammatory cytokines such as IL-10<sup>113</sup>. TNF- $\alpha$ , IL-10, nitric oxide, and reactive intermediates all work to suppress T cell activation, which may contribute to necessary hepatic immune tolerance since low levels of LPS exposure in the liver is ongoing<sup>114</sup>. Inactivation of LPS is through deacylation by a lipase that removes the secondary fatty

acyl of LPS that is required for its recognition by the TLR4 receptor, thus preventing prolonged inflammatory responses in the liver<sup>115</sup>. This state of tolerance can then be reversed by increasing stimulatory signalling through exposure to a sufficiently strong, pathogen-specific signal<sup>116</sup>. In other contexts, such as high levels of LPS, Kupffer cells are able to secrete proinflammatory cytokines such as TNF- $\alpha$ , IL-6, IL-1 $\beta$ , or leukotrienes<sup>117</sup>. These inflammatory mediators are involved in liver injury, since it has been shown that LPS alone does not harm hepatocytes<sup>118</sup>. This leads to the induction of hepatocyte apoptosis, activation of fibrogenic hepatic stellate cells, and the TNF-mediated activation of T-cells<sup>119</sup>. Chronically activated Kupffer cells also produce the profibrogenic cytokines, TGF- $\beta$  and monocyte chemoattractant protein 1 (MCP-1), which critically have the capacity to recruit inflammatory infiltrate in regenerating bile ducts<sup>120</sup> and can activate quiescent HSCs and aid in their transdifferentiation to myofibroblasts<sup>121</sup>. Seki *et al.* demonstrated using Kupffer-cell depleted mice, that Kupffer cells are required for HSC activation through their expression of TGF- $\beta$ <sup>121</sup>. Additionally, Kupffer cells produce platelet-derived growth factor (PDGF), TNF- $\alpha$ , IL-1 $\beta$ , and a host of other pro-inflammatory and pro-fibrotic chemokines used to perpetuate the fibrotic response<sup>122</sup>.

Kupffer cells and leukocytes have been shown to interact through intracellular adhesion molecule 1 (ICAM-1), with ICAM-1 deficient mice having a reduced ability to regenerate after partial hepatectomy. It is therefore proposed that the interaction of the Kupffer cells with leukocytes triggers a local inflammatory response, which subsequently leads to the Kupffer cell-dependent release of TNF- $\alpha$  and IL-6 which participate in the regenerative process<sup>123</sup>. Gadolinium chloride is a metal salt known to depress the phagocytic activity of Kupffer cells through defective surface attachment and engulfment of debris<sup>124</sup>. The use of gadolinium chloride to inhibit Kupffer cells was shown to prevent cholestasis, oxidative stress, necrosis, and fibrosis induced by the carbon tetrachloride induced model of hepatic injury<sup>125</sup>.

### c) Hepatic stellate cell activation

Within hepatic stellate cells, LPS causes the activation of I $\kappa$ B kinase (IKK), a crucial kinase involved within the NF- $\kappa$ B pathway that activates NF- $\kappa$ B signalling<sup>4</sup>. It has been shown that LPS-mediated activation of the NF- $\kappa$ B signalling pathway within quiescent HSCs occurs specifically through TLR4, and not TLR2, to promote fibrogenesis. The mechanism of fibrogenesis is two-fold. Firstly, NF- $\kappa$ B signalling upregulates chemokine production and induces chemotaxis of Kupffer cells. Secondly, LPS stimulation causes the downregulation of the pseudoreceptor, Bambi, which functions as a negative regulator of TGF- $\beta$  signalling. This in turn sensitises the HSCs to further TGF- $\beta$  signalling and allows unrestricted activation of the Kupffer cells<sup>121</sup>. Cellular comparisons between the various cell types in healthy and injured livers are diagrammatically represented in **Figure 15**.



<http://image.slidesharecdn.com/liverhistology-140827080532-phppapp01/95/histology-of-normal-liver-60-638.jpg?cb=1409126763>

**Figure 15. Cellular changes arising during liver injury.**

Within the normal liver, the quiescent stellate cells reside in the Space of Disse, however, in response to injury, they become activated and are the primary mediators in the deposition of extracellular matrix and the formation of fibrosis. There is also a marked loss of fenestration between the sinusoidal endothelial cells<sup>126</sup>.

**d) TGF- $\beta$ -mediated ECM production and perpetuation of the fibrotic response**

The hallmark of liver disease is the excessive deposition of extracellular matrix proteins (ECM), such as collagen, in response to liver injury. Recurrent/chronic injury results in deregulated wound healing leading to the accumulation of fibrotic tissue<sup>127</sup>. One of the two cell types that contributes to ECM deposition are activated HSCs which produce the main source of matrix<sup>128</sup>, matrix metalloproteinases (MMPs) which are the zinc-dependent endopeptidases responsible for degradation of the ECM, and MMP inhibitors responsible for regulating matrix degradation<sup>129</sup>. Upon activation, HSCs are able to transdifferentiate from a vitamin A-storing cell to a more mesenchymal myofibroblastic cell whose phenotypic characteristics include increased cell migration, adhesion, and proliferation, expression of  $\alpha$ -SMA, contractibility, increased rough endoplasmic reticulum, and the ability to secrete ECM<sup>130</sup>

The cytokine TGF- $\beta$ I is largely responsible for the transformation of hepatic stellate cells into myofibroblasts and is the main regulator of ECM synthesis and deposition during hepatic injury<sup>22</sup>. It is synthesised as an inactive precursor that is unable to bind to its cognate receptor. Once TGF- $\beta$  is released from the cells, it associates with the protein, latency-associated protein (LAP), to form a small inactive complex. This complex is subsequently bound to latent TGF- $\beta$  binding protein (LTBP), a component of the ECM, which together then serve as a tissue reservoir of TGF- $\beta$ <sup>131</sup>. In response to injury, latent TGF- $\beta$  is activated through the enzymatic processes involving plasmin<sup>132</sup>, integrin<sup>133,134</sup>, thrombin<sup>135</sup>, or conformational changes, thereby liberating TGF- $\beta$ <sup>136</sup>.

### e) Fibrotic resolution

During the resolution phase of fibrosis however, the scar-associated macrophages become the primary source of MMP-13, which mediate the degradation of matrix, and a subsequent regression of fibrosis<sup>137</sup>, while also secreting TNF-related apoptosis-inducing ligand (TRAIL) which induces caspase 9-mediated HSC apoptosis<sup>138</sup>. The remodelling of the liver matrix is reliant upon a fine balance of proteases and their inhibitors. Efficient wound healing requires the generation of plasmin from its precursor, plasminogen, by urokinase/tissue plasminogen activator (uPA). The activity of uPA is regulated by the inhibitor, plasminogen activator inhibitor-1 (PAI-1). These enzymes play a fundamental role in the proteolytic degradation of ECM and maintenance of organ homeostasis. It has been demonstrated that TGF- $\beta$  tightly regulates and increases the expression of plasminogen activator inhibitor-1 (PAI-1). During the process of wound healing, PAI-1 is found to be elevated, leading to a decrease in uPA/tPA and plasmin-dependent MMPs. In pathological conditions, PAI-1 is found to be massively increased in fibrotic tissues, while the lack of PAI-1 has been found to be protective against fibrosis<sup>131</sup>.

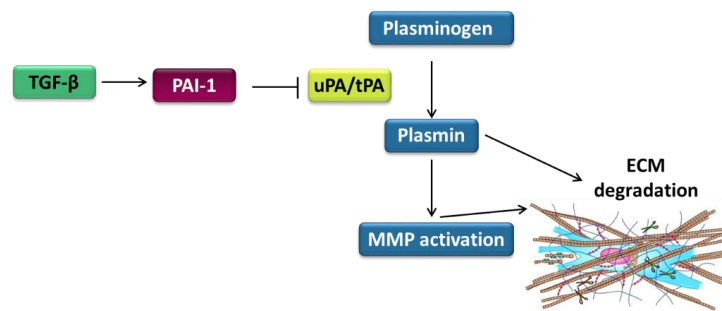


**Figure 16. Regulators of ECM homeostasis.**

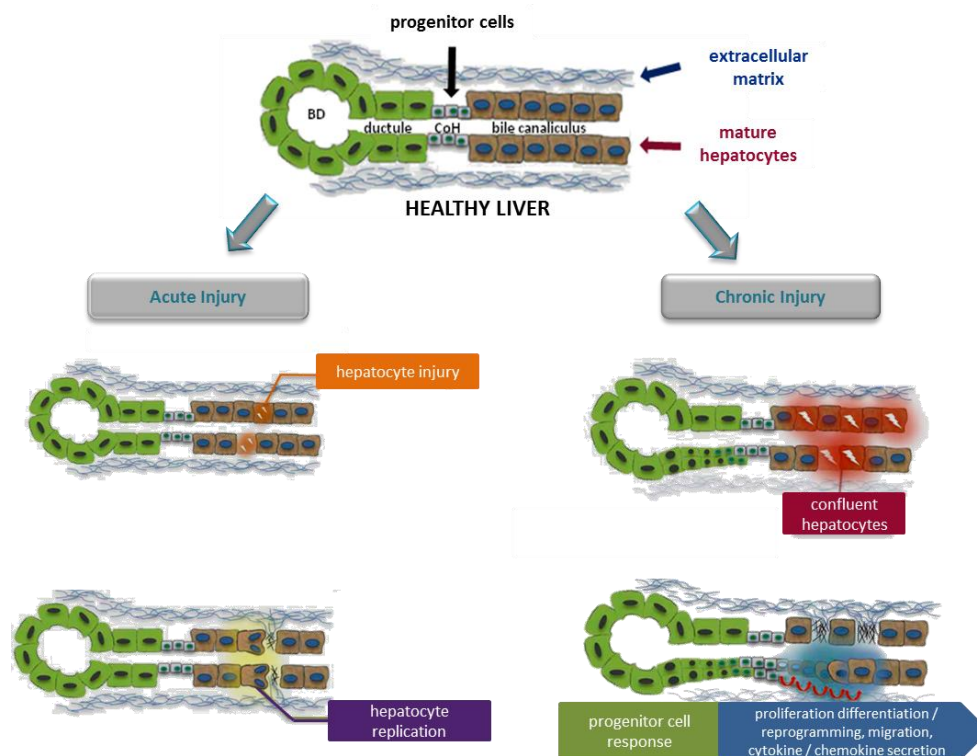
Degradation of ECM is regulated by plasmin and MMPs. Inactive plasminogen, the precursor of plasmin, is activated by the serine proteases, uPA/tPA. These proteases are negatively regulated by PAI-1 which in turn is positively regulated by TGF- $\beta$ .

## V) Mechanisms of regeneration

### a) The ductular reaction

Following initial insult and the liver's attempt to reduce the accumulation of ECM, a number of other processes are initiated which are dependent on the type of injury. For instance, in several *in vivo* models, the liver has been shown to possess immense regenerative potential following partial hepatectomy. It has been demonstrated that the liver returns to exactly pre-partial hepatectomy size after a 2/3 partial hepatectomy, after which liver growth and cell proliferation are subsequently halted<sup>139</sup>. During fulminant hepatic damage, a vast degree of regeneration occurs through the mitotic activity of the hepatocytes. However, upon chronic injury, the proliferative ability of hepatocytes and cholangiocytes is halted by replicative senescence and the liver is no longer able to be reliant upon its potential to self-renew through cell division. Instead, it relies on the capacity of a population of

bipotent hepatic progenitor cells (HPCs) to differentiate into either cholangiocytes or hepatocytes according to whether the hepatocellular or biliary compartment is predominantly damaged (**Figure 17**). This population of progenitor cells is found as a very small percentage of total liver mass within the normal liver; however, impaired replication of the liver parenchymal cells triggers a substantial activation and expansion of the HPCs as a compensatory mechanism to sustain the pace of regeneration that is required<sup>140</sup>. Depending of the type of disease setting, the bipotent progenitors amplify to become cells which morphologically resemble cholangiocytes, hepatocytes, or intermediates of the two. In general however, the hepatocyte-like cells predominantly reside along the parenchymal border, while the cholangiocyte-like-cells are more portally situated<sup>141</sup>. Chronic activation of the HPC compartment in the liver leads to the presence of lesions, characterised by the presence of ductular epithelial cells along the margins of the portal tract observed histologically as ductular reactions (DR). The cells found within these reactions are in close contact with mesenchymal and inflammatory cells as well as a complex of ECM. During the reactive process, the cells within the DR acquire novel functions including the ability to secrete growth factors, chemokines and cytokines<sup>142</sup>, which allow for integrated paracrine signalling between various cells within the reaction in an attempt to repair the damaged tissue.



[http://www.frontiersin.org/files/Articles/62272/fphys-04-00258-r2/image\\_m/fphys-04-00258-g001.jpg](http://www.frontiersin.org/files/Articles/62272/fphys-04-00258-r2/image_m/fphys-04-00258-g001.jpg)

**Figure 17. Modes of liver regeneration in response to acute and chronic injury.**

During acute injury, hepatocytes or cholangiocytes are able to divide through mitosis to repair the damage. The ability to proliferate through mitotic events is lost during chronic liver injury. Within the healthy liver, the hepatic progenitor cells reside in the canal of Hering. During the process of chronic injury, these bipotent cells begin to proliferate and differentiate according to the hepatic compartment that is damaged, thereby regenerating the liver.

## b) The role of Sox9 during chronic liver injury

Sex determining region Y-box 9 (Sox9) is a transcription factor known to be highly expressed within hepatic progenitors, with its expression seen to increase in differentiating cholangiocytes, while decreasing when directed down the hepatocyte lineage. Embryonically, homozygous mutations in Sox9 result in early lethality while heterozygosity for loss-of-function mutations result in haploinsufficiency. The lack of SOX9 expression results in campomelic dysplasia, an autosomal-dominant disease characterised by skeletal malformation, XY sex reversal, and neonatal lethality, indicating a dosage requirement for Sox9 during organogenesis<sup>143</sup>.

Sox9 has also been found to have a fundamental role in the development of the bile duct. Duct formation begins with a primitive ductal structure which contains Sox9<sup>+</sup> cholangiocytes on the portal side and Sox9<sup>-</sup> hepatoblasts on the parenchymal side. Following a TGF- $\beta$ -mediated maturation step, the biliary tube is composed exclusively of Sox9<sup>+</sup> cholangiocytes. Liver-specific inactivation of Sox9 in mice results in delayed duct formation and an abnormal persistence of T $\beta$ RII expression within the portal side of ductal plate, highlighting the temporal role of Sox9 in biliary morphogenesis<sup>90</sup>. Lineage tracing following multiple models of hepatic injury have shown the contribution of Sox9<sup>+</sup> precursors in liver regeneration by producing a transgenic model which permanently labelled Sox9-expressing cells and their progeny through LacZ expression following tamoxifen induction. In response to either carbon tetrachloride (CCl<sub>4</sub>) or bile duct ligation the number of X-gal lineage-labelled hepatocytes increased, spreading from the portal field to the central vein, as depicted in the streaming liver hypothesis. Induction of either hepatic injury did not induce SOX9 expression within hepatocytes or endothelial cells, but rather was restricted to those cells which positively stained for cytokeratin, indicating their ductal cell origin. SOX9-expressing cells were also detected in proliferating duct cells. The data presented by Furuyama *et al.* indicates that Sox9<sup>+</sup> precursor cells contribute to hepatocyte differentiation during the regenerative process in response to these models of hepatic disease<sup>144</sup>. Within human fetal hepatocytes, Hanley *et al.* illustrated aberrant expression of SOX9 increased the expression of several genes that encode ECM components, including *COL2a1*, and *COMP1*. Inappropriate ECM deposition results in fibrosis and the role of Sox9 within the fibrotic environment were further interrogated. The same authors showed that *in vitro*, hepatic stellate cells transdifferentiated to myofibroblasts in response to increased TGF- $\beta$  signalling. This led to an increase in Sox9 expression and caused the production of the major ECM component, Type I collagen, the predominant collagen type seen in organ fibrosis. Lastly, they demonstrated that Sox9 expression is increased during the activation of hepatic stellate cells in response to TGF- $\beta$  signals<sup>145</sup>. More recently, *in vivo* models of fibrosis and *in vitro* experiments utilising culture-activated HSCs have shown that SOX9 colocalises with Osteopontin (OPN), an important component of the ECM used as a biomarker of fibrosis severity. SOX9 was shown by Pritchett *et al.* to bind to a conserved

region, upstream of OPN and regulate its expression. This study also suggested that Hedgehog signalling lies upstream of Sox9 and that the loss of SOX9 resulted in a significant decrease in downstream OPN production<sup>146</sup>.

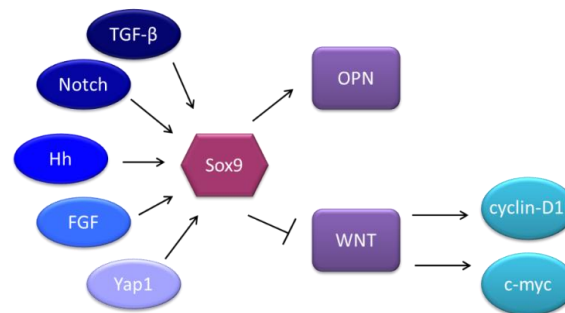
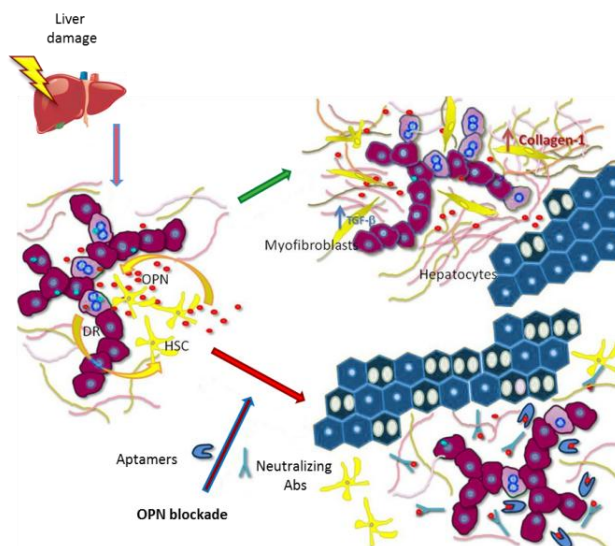


**Figure 18. Regulation and downstream targets of Sox9.**

Sox9 has been found to be regulated by a number of molecular pathways. Subsequently, it is able to induce expression of the pro-fibrotic cytokine, osteopontin. Furthermore, it is also able to negatively regulate the Wnt signalling pathway and Wnt downstream targets, such as cyclin-D1 and c-myc.

### c) Osteopontin as a pro-fibrotic mediator

OPN has increasingly been of interest in the development of fibrogenic events. It is a pleiotropic cytokine able to both induce cell motility and also cause persistent inflammation<sup>147</sup>. Within recent years, OPN has been implicated in the pathogenesis and progression of multiple liver diseases<sup>148</sup>, with marked induction observed in various biliary fibrosis models including BDL<sup>149, 150</sup>. This glycoposphoprotein acts as a neutrophil chemoattractant by binding to integrin receptors, and is also involved in the generation of the ductular reaction. It does this through stimulation of HPC proliferation and migration, while also decreasing the ability of hepatocytes to proliferate. The cells within the DR, including HPCs, produce OPN and mediate the recruitment and activation of the hepatic stellate cells. Evidence shows that OPN is expressed in hepatic stellate cells and is involved in the upregulation of collagen I production which, synergistically with activated TGF- $\beta$  signalling, causes increased collagen deposition<sup>151</sup>. Corroborative evidence for the involvement of OPN in the increased severity of DR and fibrogenesis has been shown by Coombes *et al.* They demonstrated, through administration of OPN-neutralising antibodies, that there was a significant attenuation of the liver progenitor cell response, a reversal of EMT within Sox9<sup>+</sup> cells, and a reduction in severity of hepatic fibrosis<sup>152</sup> (**Figure 19**). Further understanding and modulation of osteopontin and its regulators has the potential to be utilised as an antifibrotic therapy, and thus continues to be a topic of active investigation in liver fibrosis research.



Strazzabosco M et al. Gut 2014;63:1693-1694

**Figure 19. Role of osteopontin in regulation of the ductular reaction.**

Chronic injury causes cells within the ductular reaction to produce OPN. This stimulates the recruitment of the HSCs and their transdifferentiation to myofibroblasts which induces TGF-β signalling and subsequent matrix deposition. OPN also blocks proliferation of hepatocytes. Addition of aptamers or neutralising antibodies causes cessation of crosstalk between the cells in the ductular reaction and increases hepatocyte proliferation.

**d) Role of WNT and Notch signalling in the regenerative response**

As the liver attempts to regain homeostasis, a number of cells and signalling pathways are activated in order to obtain fibrotic resolution and regenerate damaged hepatic compartments. The cells responsible for the regeneration of the parenchymal cell types are the bipotent hepatic progenitor cells. According to Boulter *et al.* who published a defining paper on the role of Wnt and Notch signalling during hepatic regeneration, differentiation of these hepatic progenitors is directly specified through their interaction with either myofibroblasts or macrophages. HPCs have been shown to differentiate into cholangiocytes through their direct interaction with activated myofibroblasts expressing JAGGED-1, a Notch signalling ligand. Alternatively, to facilitate hepatocyte regeneration, phagocytosis of hepatocyte debris after injury induces expression of Wnt3a, which subsequently elicits canonical Wnt signalling within the HPCs. This signalling results in the maintained expression of Numb, a cell fate determinant, and promotes the differentiation of the bipotent HPCs into hepatocytes<sup>40</sup>. Spee *et al.* have also shown in human specimens, strong activation of the Wnt pathway in microdissected HPCs isolated from livers which had undergone parenchymal liver disease, either acute necrotising hepatitis or chronic hepatitis C induced cirrhosis. They suggest that increased WNT signalling is required for the activation/expansion of the progenitor cell niche. In contrast, those HPCs isolated from livers which had primary biliary cirrhosis were found to have high levels of Notch signalling, proposed to drive the HPC cell fate towards the cholangiocyte lineage<sup>153</sup> (**Figure 20**). As an alternative to orthotopic liver transplantation, liver gene therapy and *ex vivo* differentiation of stem and progenitor cells is the focus of many cell and gene therapies for a host of hepatic diseases.

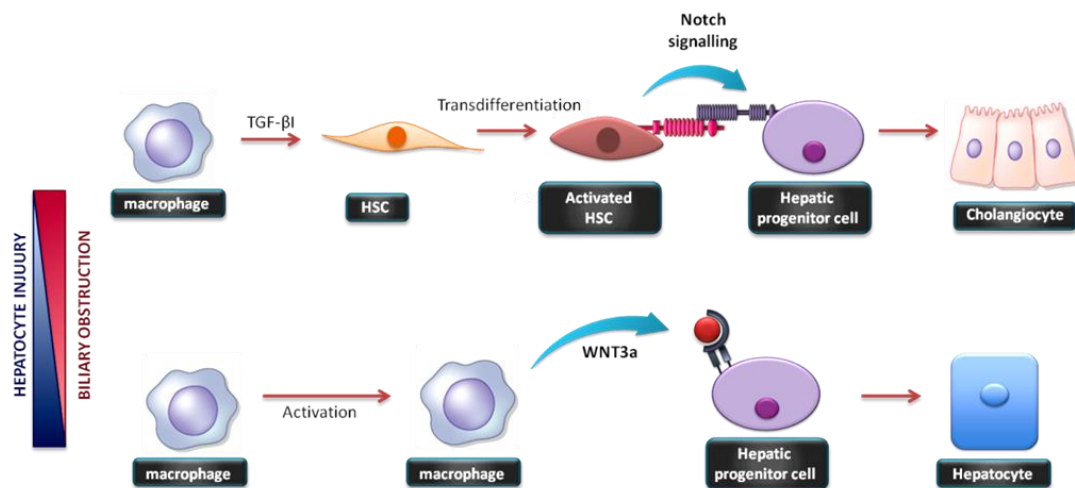


**Figure 20. Activation of WNT and Notch signalling in HPCs induces hepatocyte and cholangiocyte differentiation respectively.**

TGF- $\beta$ 1 induces stellate cell transdifferentiation and the expression of the Notch activator, Jagged-1. Through cell-to-cell interactions of the HPC with the activated HSC, notch signalling is activated and the cells are fated to become cholangiocytes. If however, the HPCs are exposed to exogenous macrophage-secreted Wnt3a, the cells undergo differentiation towards hepatocytes.

## VI) Types of biliary diseases

Although there are a number of liver diseases, the focus of this thesis is specifically on those involving the biliary tract, more specifically, those that exhibit a cholestatic phenotype. The term cholestasis is derived from Greek where it literally means “a standing still of bile”. Rupturing of the biliary canaliculi may result in the presence of histological “bile lakes” seen amongst the liver parenchyma. Disruption of bile flow can occur through impaired secretion of bile by the hepatocytes, or by obstruction in the intra- or extrahepatic bile ducts<sup>154</sup>. Due to its amphipathic properties, the accumulation of bile within the liver due to bile duct dysfunction causes hepatocyte apoptosis and necrosis due to its highly cytotoxic nature when present at high concentrations, leading to fibrosis and eventually cirrhosis<sup>16</sup>. Serum concentrations of conjugated bilirubin and the two liver enzymes, alkaline phosphatase and gamma-glutamyl transpeptidase (GGT), are typically elevated and used as biochemical markers of cholestatic pathology<sup>155</sup>. Clinical manifestations of cholestasis include jaundice, pruritus (itching), malabsorption, pale stools, dark urine, and abdominal pain. Jaundice is the yellowish pigmentation affecting the skin, sclera, and mucous membranes. Failure of bilirubin removal from the body leads to excess bilirubin in the blood (hyperbilirubinaemia)<sup>156</sup>. The development of conjugated hyperbilirubinaemia occurs during the development of biliary obstruction<sup>157</sup>, while unconjugated hyperbilirubinaemia is caused by a number of diseases such as hemolysis, Crigler-Najjar syndrome, and Gilbert syndrome<sup>158</sup>. In both cases, however, evidence of jaundice is present. Conjugated bilirubin has a lower binding affinity for albumin, and during obstructive cholestasis may overflow from the liver. The kidney becomes the predominant mode of excretion through the urine and, due to its pigment, makes the urine dark in colour<sup>20</sup>. Other than

surgical intervention, one of the most common modes of treatment for cholestatic disease is bile salt therapy using ursodeoxycholic acid (UDCA) which prevents or delays the progression of the disease<sup>159</sup>. Evidence indicates the mechanism of action to be three-fold through 1) cytotoxic protection of cholangiocytes from hydrophobic bile acids, 2) stimulation of hepatobiliary secretion to remove excess bile salt through upregulation of transporter proteins, 3) anti-apoptotic and survival pathway activation in hepatocytes<sup>160</sup>. Clinical management of cholestasis also includes vitamin supplementation to counteract fat-soluble vitamin deficiency due to fat malabsorption<sup>161</sup>. Although many of the clinical symptoms and management of cholestatic diseases is largely uniform, the aetiology, comorbidities, and histopathology of these diseases varies greatly, with examples of intrahepatic, extrahepatic, and genetic causes of cholestasis highlighted below.

#### **a) Primary sclerosing cholangitis and inflammatory responses**

Primary sclerosing cholangitis (PSC) is a progressive cholestatic disease resulting from chronic inflammation. Inflammation of the ducts leads to obliterative fibrosis and cirrhosis ultimately ensues. Both the intrahepatic and extrahepatic bile ducts can be affected. Histologically, PSC presents with typical periductal sclerosis seen as concentric fibrosis around the small interlobular bile ducts. The layered “onion-skin” fibrosis progressively narrows and obliterates the ductal lumen. A reduction or absence of bile ducts can also be accompanied by biliary hyperplasia and destruction of the limiting plate. Other features include the presence of ductular reaction and mononuclear cell infiltrate<sup>162</sup>.

#### **b) Primary biliary cirrhosis**

Primary biliary cirrhosis (PBC) is a progressive cholestatic disease with a prevalence of 40-400 per 1,000,000, and peak incidence within the fifth decade of life<sup>163</sup>. Interestingly, approximately 90% of those afflicted with the disease are woman, believed to be linked to the increased presence of oestrogen<sup>164</sup>. PBC is characterised by the presence of anti-mitochondrial antibodies (AMA)<sup>165</sup>. The presence of inflammatory granulomas<sup>166</sup> and damaged interlobular bile ducts is termed florid duct lesions, which are the sites of cholangiocyte proliferation<sup>167</sup>. The destruction of the bile ducts is immune mediated, with cells of the immune system attacking and destroying the bile ducts, resulting in progressive ductopenia. This causes scarring and subsequent obstruction of bile flow out of the liver. The bile thus accumulates within the liver and causes liver fibrosis which, if not resolved, may lead to cirrhosis<sup>168</sup>. In contrast to PSC, however, there is no indication of bile duct dilatation or beaded appearance.

### c) Biliary atresia

Biliary atresia (BA), also known as extrahepatic ductopenia and progressive obliterative cholangiopathy, is a congenital disease which only occurs in infants. Clinical presentation occurs within the first few weeks after birth without any gender predilection. It is characterised by the discontinuity of the extrahepatic biliary system leading to biliary obstruction and end-stage liver disease. BA is the most common cause of neonatal cholestasis and accounts for around 40-50% of all paediatric liver transplantations<sup>169</sup>. The mean survival time without treatment is around 18 months; however the prognosis is substantially better in those with early diagnosis and treatment, with a survival rate of 90%<sup>170</sup>. Complete atresia is reliant upon liver transplantation as a definitive treatment.

Although the aetiology of the disease is unknown, it has been hypothesised that an initiating event, induces apoptosis of the cholangiocytes. In genetically susceptible individuals, exaggerated inflammatory response ensues, followed by an autoimmune response targeted against the cholangiocytes resulting in progressive injury of the bile ducts<sup>169</sup>. The most plausible candidates of the initiating event, due to elevated antibody titers, appear to be reovirus type 3<sup>171</sup>, rotavirus<sup>172</sup>, herpes virus<sup>173, 174</sup>, human papillomavirus<sup>175</sup>, Epstein Barr virus<sup>176</sup>, and cytomegalovirus<sup>173</sup>. Other causal candidates include exposure to toxins, autoimmunity, errors during liver development, or genetic mutations<sup>177-181</sup>.

### d) Alagille syndrome

Alagille syndrome (AGS) is an autosomal dominant disorder characterised by hepatic ductopenia, however there is comparatively reduced portal fibrosis, while progression to biliary cirrhosis is rare in contrast to most cholangiopathies<sup>182</sup>. The occurrence of clinical abnormalities arise in cardiac, vascular, renal, facial, ocular, and central nervous systems<sup>183, 184</sup>. Clinical features arising from hepatic disruption include cholestasis, jaundice, and pruritis. Approximately 80-90%<sup>185, 186</sup> of AGS patients have a mutation within *JAGGED1*, and less frequently a mutation in *NOTCH2*<sup>187</sup>. Notably, AGS is histopathologically distinctive from other cholangiopathies in its near complete lack of HPCs and reactive ductular cells (RDCs). Conversely, there is an increased presence of intermediate hepatobiliary cells<sup>182</sup>, which are cells that are phenotypically or morphologically intermediate between cholangiocytes and hepatocytes and may immunostain for markers of both<sup>188</sup>. These hepatobiliary cells do not express the Notch downstream target, HNF1 $\beta$ , a biliary-specific transcription factor, and are therefore unable to differentiate into mature cholangiocytes<sup>182</sup>. Given the role of the ductular reaction in the fibrogenic response, it is not surprising then that the lack of this response results in reduced fibrosis such as is seen in AGS.

## **VII) Animal model systems to study liver disease**

### **a) Spontaneous mutation models of hepatic fibrosis**

One method of understanding the origins and progression of liver disease is by using animal models which manifest a similar phenotype to the one being studied. The use of animal models has been instrumental in giving greater insight into disease pathogenesis, aiding the development of novel therapeutics. Of particular interest have been the use of small rodents, due to their small size, comparatively reduced maintenance costs compared to other larger animal models, the similarity of organ systems in comparison to humans, and the similarity of diseases which affect both small rodents and humans. Some diseases within these small animal models have arisen through spontaneous mutation, through normal cellular processes which generate DNA-damaging free radicals as a by-product of cellular respiration<sup>189</sup>, or through errors occurring during replication and repair. A naturally occurring spontaneous mutation arose within the *Cpk* gene of the C57BL/6J mouse strain and is now a well characterised model of congenital polycystic kidney disease, which expresses a comorbid phenotype of hepatic fibrosis<sup>190</sup>.

### **b) Chemically induced models of cholestasis**

Various different methodologies allow researchers to mimic and better comprehend the pathophysiological and compensatory mechanisms associated with aberrant bile flow. The cholestatic phenotype can be induced through dietary supplementation with compounds such as the porphyrinogenic substance 3,5-diethoxycarbonyl-1,4-dihydrocollidine (DDC)<sup>191</sup> or the xenobiotic, alpha-naphthylisothiocyanate (ANIT)<sup>192</sup>, which each have distinct phenotypes, but ultimately both lead to cholestasis. DDC diet induced fibrotic models are widely used in the study of Mallory bodies, which are histopathology-determined inclusions seen within hepatocytes. These damaged intermediate filaments are a feature typically seen in alcoholic liver disease. This model results in the presence of a strong ductular reaction within one week, and an increase in the cytokines, VCAM, osteopontin, and TNF- $\alpha$  all increased within the BECs. The presence of mononuclear cell infiltrate, pericholangitis, and biliary fibrosis are characteristics of this model that are also observed within human primary sclerosing cholangitis<sup>191</sup>. Another model of cholangitis is induced through the administration of the xenobiotic, ANIT, which is toxic and results in the loss of activity of biliary cells while also causes weakening of the tight junctions between hepatocytes<sup>193</sup>. Both models have been and continue to be extensively used to elucidate disease-associated mechanisms and possible therapeutic interventions.

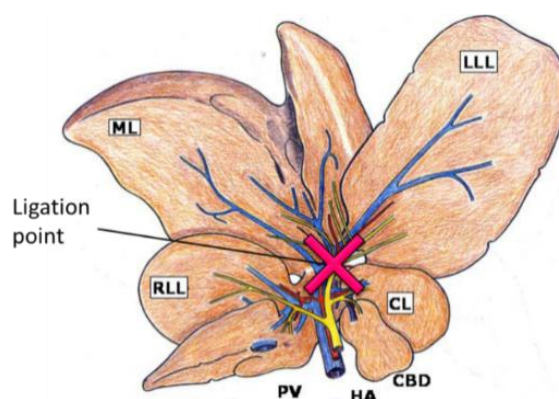
### c) Genetic models of hepatic fibrosis

Although chemical induction induces a disease phenotype, underlying genetic contributions would be beneficial for specific drug targeting of particular aberrant pathways due to abnormal gene expression. Genetic technologies have been driven forward by the need for targeted gene disruption or gene insertion, now attainable through the use of site-specific nucleases which are able to alter the genome from which a transgenic animal originates. Examples of these genome-editing nucleases include meganucleases<sup>194</sup>, zinc finger nucleases (ZFNs)<sup>195, 196</sup>, transcription activator-like effector nucleases (TALENs)<sup>197, 198</sup>, and most recently engineered clustered regularly interspaced short palindromic repeats (CRISPR) technology<sup>199</sup>. Genetically engineered rodents have been generated to model a huge diversity of human diseases including liver disease such as hepatic fibrosis<sup>200</sup>. One such transgenic is the *dnTGF-βRII* mouse which contains a dominant-negative form of the TGF-β receptor whose expression is CD4-promoter regulated, restricting its expression specifically to T cells<sup>201</sup>. This model strongly recapitulates the inflammatory biliary disease seen in human primary biliary cirrhosis as it mimics the spontaneous production of anti-mitochondrial antibodies which target and interfere with the correct function of the mitochondria. This phenotypic hallmark of primary biliary cirrhosis has also been noted within the IL2Rα knockout mouse<sup>202</sup>. A third model is the MDR2 model which has resulted from *Abcb4* gene knockout. This causes a decrease in the ability to excrete phosphatidylcholine into the bile and results in portal inflammation and the presence of ductular proliferation seen shortly after birth until end stage disease which occurs 3-6 months later. This model resembles phenotypic characteristics of sclerosing cholangitis and exhibits both biliary fibrosis and hepatocellular carcinoma<sup>203</sup>.

### d) Surgical models of hepatic fibrosis

Another method to induce rapid cholestatic liver injury is via surgical means. Bile duct ligation (BDL) is one of the most commonly performed experimental procedures used to induce obstructive cholestasis and fibrosis. The most frequently used version of this model is complete ligation of the common bile duct, which causes a significant fibrotic response to all 4 liver lobes approximately 21-28 days post-surgery<sup>204</sup>. The procedure induces cholangiocyte proliferation, along with portal inflammation, hypertension, and deposition of ECM by transdifferentiated myofibroblasts, morphological changes seen in human forms of biliary cirrhosis<sup>204</sup>. The drawback to using this technique is that it presents with a harsh phenotype and the mortality rate can be high due to infectious complications. The procedure also requires a high degree of technical accuracy. An alternative version of this technique, termed partial bile duct ligation (pBDL) has been described<sup>205</sup>. pBDL is performed by inserting a needle into the common bile duct, followed by ligation using a suture. The needle is subsequently removed, resulting in a constricted lumen in the bile duct, thereby

allowing limited bile flow. Heinrich *et al.* demonstrated histologically on 14-day post total bile duct ligation (tBDL) samples that there was significant portal-portal bridging fibrosis, inflammatory infiltrate, and ductular proliferation that was not seen in the pBDL model. The important distinction between tBDL and pBDL models is that the cholestatic indicators, bilirubin and alkaline phosphatase, decreased to normal levels within 10 days following pBDL, but remained elevated in tBDL animals. pBDL is therefore a superior model, specifically of acute forms of the disease, as it causes cholestasis, but does so with minimal histologically-assessed tissue injury, and importantly, does not progress to chronic cholestasis<sup>205</sup>. A third surgical model can be used to generate a chronic cholestatic phenotype, but with a less severe phenotype, is achievable through ligation of the common bile duct distal to the right and caudal lobe (**Figure 21**). This causes fibrosis in the median and left lobes, while mostly preserving the architecture and function of the right and caudate lobes<sup>206</sup>. Some changes within the parenchyma of non-obstructed lobes has also been noted and attributed to paracrine and/or endocrine signalling<sup>207, 206</sup>. This method improves the welfare of the animals, while still modelling the ductular reaction and proliferation of the progenitor cell niche in response to chronic injury.



<http://www.wjgnet.com/1948-5182/full/v4/i7/WJH-4-199-g004.htm>

**Figure 21. Schematic of ligation point for partial bile duct ligation disease modelling.**

Ligation of the common bile duct results in a severe phenotype. Partial bile duct ligation yields the same fibrotic phenotype, but in only 2 of the 4 lobes. The liver is ligated above the right and caudate lobes, obstructing bile flow only from the median and left liver lobes, which subsequently present with cholestasis and fibrosis<sup>208</sup>.

## VIII) *In vitro* model systems of hepatic differentiation, disease, and pathway activation

### a) HepaRG cells

Prior to proceeding to *in vivo* experimentation, thorough *in vitro* analyses should be conducted. For the data to be relevant, a suitable *in vitro* model is required. *In vitro* cell lines offer a valuable alternative to using animals as a first-line means of experimentation. They play a crucial role in elucidating molecular mechanisms of disease<sup>209</sup>, can be used in toxicity<sup>210</sup> and xenobiotic metabolism screens<sup>211</sup>, and give mechanistic insight into differentiation<sup>212-214</sup>. It is critical that the cell lines used

*in vitro* mimic the *in vivo* model inasmuch as possible. The scarcity, unpredictable availability, inter-individual variability, and limited life-span of primary hepatocytes makes their use limited when continuous cell-culture material is required for experimentation<sup>215</sup>. A vast majority of research involving hepatocytes has used the primary hepatocytes, HepG2 and Huh7 cell lines. The use of hepatocyte cell lines circumvents the issue of availability, however basal levels of metabolising enzymes in HepG2<sup>216, 215, 217</sup> and Huh7 cell lines<sup>217</sup> are significantly lower than in primary cell lines. As an alternative, the HepaRG cell line has been utilised as it maintains many of the functional characteristics of primary human hepatocytes. This cell line was isolated from a human hepatocarcinoma which developed secondary to chronic hepatitis C virus (HCV) infection in 2002<sup>218, 218</sup> and has since been used in studies of bioartificial livers<sup>219</sup>, drug metabolism and toxicology<sup>220, 221, 221</sup>, and HBV infection<sup>222, 223</sup>. A unique attribute of this cell line is its ability to exist as a culture of hepatic progenitor cells when seeded at low density. Upon confluence, these bipotent progenitors are able to terminally differentiate into hepatocyte-like cells which self-assemble into colonies<sup>222</sup>, or alternatively differentiate toward cholangiocytes<sup>224</sup>. Hepatic functionality can be enhanced when the cells are grown to confluence in the presence of dimethyl sulfoxide (DMSO)<sup>218</sup> and further induction of P450 activity is achieved through drug exposure, typically omeprazole, phenobarbital, and rifampicin<sup>225</sup>. More recently it has been shown that the proportion of cholangiocytes within the culture could be enriched by altering the culture media<sup>224</sup>. It is also known that HepaRG cells are capable of dedifferentiating and subsequently transdifferentiating into hepatocyte or biliary lineages via a bipotent progenitor<sup>226</sup>. Genetic manipulation of this cell line can thus be used to determine which pathways affect their differentiation potential and has been employed to generate data within this thesis. Using HepaRG cells could therefore be a valuable model for gaining insight into bile duct development, mechanistic elucidation of cellular processes, and the development of potential therapeutics for cholangiopathies.

## **b) Genetic reporters**

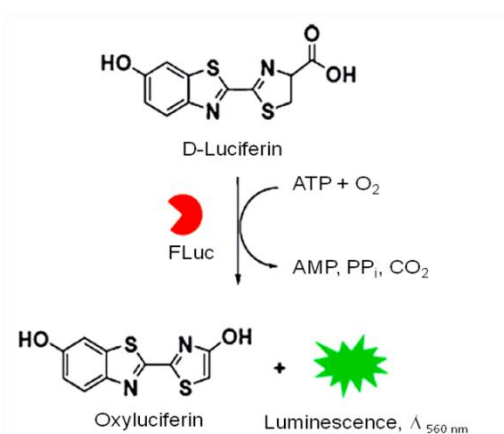
Once an appropriate cell line has been chosen, a quantitative method of functional output is required in order to study the molecular changes occurring within the cells. This can be in the form of secreted growth factors or chemokines, or in the case of gene regulation, luciferase expression. Luciferase is an ideal marker of transcriptional activity as it is highly sensitive and is not endogenously expressed within cell lines. The firefly luciferase (FLuc) from the North American firefly, *Photinus pyralis*, was the first to be cloned and characterised<sup>227</sup>. Since its induction into the world of molecular biology, it's broad-scale applicability has seen it become a powerful tool in studies ranging from investigating cancer<sup>228</sup>, cardiac regeneration<sup>229</sup>, neurodegeneration<sup>230</sup>, monitoring of infectious disease<sup>231</sup>, and tracking cell fate and function<sup>232</sup> to name but a few. Importantly, innovative design and diverse

applications utilising FLuc allow non-invasive, repeated, longitudinal collection of data that can also be applied to *in vivo* experiments.<sup>233</sup> The use of these reporters, combined with the use of DNA response elements which confer particular transcription factor binding and gene regulation, has shown increasing applicability within biological research. This is due to the non-invasive nature of data collection within animal models of disease. This concept shall be one of the main research focuses of this thesis, with novel developments and proof-of-concept work detailed in subsequent chapters, with particular emphasis within a cholestatic disease model.

### i) Properties and reaction of firefly luciferase

The use of luminescence as a quantitative measure of gene regulation is dependent upon the presence of the enzyme's substrate, D-luciferin. When D-luciferin is present, firefly luciferase is able to catalyse an oxidative reaction, provided there are a number of other exogenous cofactors available for the bioluminescent reaction to commence. These factors include adenosine triphosphate (ATP), Mg<sup>2+</sup>, as well as molecular oxygen. The first of this 2-step process involves the condensation of luciferin and ATP to produce luciferyl adenylate and inorganic pyrophosphate (PPi). Subsequently, the reactive luciferyl adenylate is oxidised and decarboxylated to form oxyluciferin with the production of an electronically excited product and the release of adenosine monophosphate<sup>234</sup> (**Figure 22**). When the excited oxyluciferin intermediate returns to its ground state, it releases a photon of light in the process to produce visible light<sup>235</sup>.

- (1) D-luciferin + ATP → luciferyl adenylate + PPi
- (2) luciferyl adenylate + O<sub>2</sub> → oxyluciferin + AMP + light



<http://pubs.rsc.org/services/images/RSCpubs.ePlatform.Service.FreeContent.ImageService.svc/ImageService/Articleimage/2009/CC/b908346d/b908346d-s1.gif>

**Figure 22. D-luciferin oxidation reaction mediated by firefly luciferase.**

The oxidation of D-luciferin leads to the production of oxyluciferin and a photon of light, mediated by the firefly luciferase.

FLuc in particular is a good biomarker as it does not require post-translational modifications, and its half-life both *in vitro* and *in vivo* is approximately 3 hours, allowing adequate timing for analysis<sup>236</sup>. The range of light emission from FLuc is in the range of approximately 530-640 nm, with a maximal peak occurring at 560 nm<sup>237</sup>. Its substrate, D-luciferin also has numerous advantages, not limited to having the option of several routes of administration, rapid diffusion through most tissues and cell types, and relative stability, all of which contribute to ease of image capture<sup>235</sup>. Due to the varying contexts in which luciferases are used, development of modified and alternative luciferases has been crucial in the evolution of bioluminescence imaging technology within the last decade.

## ii) Genetically engineered luciferases

### a) Firefly luciferase enhancements

Since molecular methods which employ luciferase as a tool occur outside of its natural firefly host, many luciferase constructs have been improved for mammalian expression by a process known as codon optimisation. The genetic code is degenerate in nature, and this feature makes it possible to produce an amino acid sequence which is identical, but producing this by tRNAs that are preferentially used within the recipient organism. Codon usage bias results in higher levels of translation efficiency and accuracy due to optimised translation processes related to the relative abundance of particular tRNA isoforms<sup>238</sup>. FLuc DNA has been further enhanced by removal of cryptic splice sites, sequence repeats, and local hairpin structures to increase mRNA stability<sup>233</sup>.

Furthermore, Tisi *et al.* have developed and performed *in vivo* screening of luciferase mutants and identified a superior FLuc mutant which has improved pH-tolerance and increased resistance to thermal inactivation up to 45°C. This mutant contains 5 non-synonymous mutations, substituting the bulky hydrophobic, solvent-exposed amino acids for hydrophilic ones, namely F14R, L35Q, V182R, I232K, and F465R without any accompanying loss of specific activity. These mutations are thought to exert a cumulative positive effect on pH and thermostability by stabilisation through electrostatic interactions. They were also shown to confer longer enzyme half-life compared to the wild-type luciferase<sup>239</sup>. These improved features offer significant advantages of the TISIX5 mutant luciferase over its wild-type predecessor, particularly for *in vivo* applications.

### b) Red-shifted Renilla luciferase

Luciferases originating from the sea pansy *Renilla reniformis* (Rluc), and numerous other ocean-derived organisms oxidise an imidazopyrazinone-based luciferin, coelenterazine, which releases light within the blue-green range of the spectrum at a wavelength of 480 nm<sup>240</sup>. The use of RLuc over

FLuc has been employed in experiments where the ATP-dependence of FLuc would be a limiting factor or where ATP stores are lacking, since RLuc is able to catalyse the oxidation of coelenterazine in an ATP-independent manner<sup>241</sup>.

The use of short-wavelength blue-green light emitted by RLuc within an *in vivo* environment is largely limited by the preferential absorption of this light by biological tissues. One of the issues occurring within bioimaging of deep tissues is that the pigmented molecules, such as haemoglobin, readily absorb and scatter the produced light within the blue to yellow ranges, which results in inadequate transmission of light through the tissues. This leads to decreased image sensitivity and spatial resolution<sup>242</sup>. There is approximately a 10-fold decrease in RLU per cm of tissue<sup>243</sup>, with the main sources of light absorption being haemoglobin and myoglobin<sup>242</sup>. Decreased absorption by these molecules occurs with light emitted at wavelengths >600 nm, in the red to infrared range of the spectrum. Light emitted in this range is able to penetrate through several centimetres of tissue, but with a peak spectral emission occurring at around 481 nm, only around 3% of the photons emitted from native RLuc are above wavelengths of 600 nm, making longer wavelength, red-shifted reporters an attractive alternative to unmodified renilla for use in *in vivo* bioluminescence imaging, particularly within deep or haemoglobin rich organs<sup>237, 242, 244</sup>. A particular red-shifted renilla (RS-RLuc) variant has been generated which has a 54 nm spectral redshift, allowing for an increased proportion of photons to be emitted over the critical 600 nm wavelength<sup>245</sup>.

### c) *Vargula* luciferase

*Vargula* luciferase is the luciferin found in the nocturnal sea ostracod *Vargula hilgendorffii* which naturally inhabits the waters of Japan where is more commonly known as “umi botaru” or the “sea firefly”. Historically, *vargula* has also been named *cypridina*, owing to the fact that it belongs in the family Cypridinidae<sup>246</sup>. In the presence of molecular oxygen, *vargulin*, its substrate, is able to be oxidised in the absence of ATP, and gives off light with a peak emission of around 452 nm. Interestingly, Thompson *et al.* showed through sequencing of the *vargula* gene, that it contains a signal sequence for secretion, and went on to show that *vargula* luciferase was secreted from mammalian cells into culture media and is well suited as a specific and highly sensitive reporter<sup>247</sup>. *Vargulas*' undoubted advantage over non-secreted luciferases is its ability to permit live cell monitoring and longitudinal collection of gene expression profiles without the need to lyse the cells.

### d) *Nanoluc* luciferase

NanoLuc® (NLuc) luciferase is a small luciferase of only 19 kDa, isolated from the deep sea shrimp *Oplophorus gracilirostris* where it is used as a defence mechanism against predation. The sequence has been isolated and cloned, with the aim of producing a luciferase capable of producing a sustained

signal with high sensitivity and low background interference. Following multiple rounds of mutagenesis, this enzyme was engineered to have improved luminescence and stability, and has been optimised for mammalian expression through codon-optimisation. Further optimisation was performed by nucleotide substitution to remove potential mRNA secondary structures, transcription factor binding sites, and also potential splice sites. NLuc utilises the substrate coelenterazine, or its more stable derivative furimazine, in an ATP-independent reaction. The reaction produces luminescence with an emission maximum at 454 nm and a signal half-life of >2h. In contrast to the flash luminescence produced by FLuc, RS-RLuc, and vargula, which occurs quickly within seconds or minutes and has a very short, intense signal, NLuc produces a glow-type luminescence which is not as bright, but can be sustained for hours. Using a secretion signal from the human IL-6 protein, a signal sequences was appended to the N-terminus of the reporter, allowing it to be secreted out of the cell. From a cell culture perspective, this allows for data collection without the necessity for cell lysis. The secreted NLuc has also been designed to have increased thermal stability, maintaining its enzymatic activity up to 55°C and for >15 hours at 37°C in culture media<sup>248</sup>. Below are the features for each of the 4 luciferases, firefly, red-shifted renilla, vargula, and NanoLuc (**Table 2**). The above mentioned reporters and models can be combined in order to generate a unique platform with which to perform continuous analysis of signalling pathway activity within cell culture and living animals. Improvement on current methodologies can therefore result in the generation of more robust data with a concurrent reduction of animals being used for each experiment.

**Table 2. Features of the firefly, red-shifted renilla, vargula and NanoLuc luciferases.**

FEATURES	LUCIFERASE			
	Firefly Luciferase	Red-shifted Renilla	Vargula Luciferase	NanoLuc Luciferase
<b>Substrate</b>	D-luciferin	Coelenterazine	Vargulin	Coelenterazine or furimazine
<b>Protein half-life</b>	3 hours	49 hours	60 hours	>15 hours (in culture)
<b>Half-life in flash assay</b>	Flash-type Luminescence; >30 minutes	Flash-type Luminescence; 5 minutes	Flash-type Luminescence; 30 minutes	Glow-type Luminescence; >2 hours
<b>Emission wavelength</b>	549 nm	535 nm	460 nm	454 nm

## Hypothesis

- 1) Tissue specific luciferase bioimaging can be used to quantify transcription factor activity *in vivo*.
- 2) Longitudinal liver specific luciferase bioimaging will provide new insights into the temporal activity of transcription factors following partial bile duct ligation.
- 3) Bipotent hepatic progenitor cell differentiation can be influenced by genetic manipulation of Notch signalling.

## Aims and Objectives:

- 1) Design novel bicistronic luciferase vectors for *in vitro* and *in vivo* use by generating a parental luciferase construct containing the Gateway™ cassette upstream of luciferase-2A-eGFP.
- 2) Validate biosensing reporter constructs *in vitro* by assessing luciferase expression over time in stably transduced cell lines in response to known agonists/inhibitors.
- 3) Perform proof of concept somatotransgenic bioimaging using CD1 and TLR4<sup>-/-</sup> mice transduced with the NF-κB reporter and challenged with LPS.
- 4) Investigate temporal signalling profiles of NF-κB, GFAP, TGF-β, Notch, and Wnt signalling in a mouse model of cholestasis induced by pBDL.
- 5) Assess the effects of Notch signalling on differentiation potential *in vitro* using the hepatic progenitor cell line, HepaRG. Cells constitutively expressing Jagged and Numb will be compared for their differentiation potential using qualitative and quantitative markers of hepatocytes and cholangiocytes.
- 6) Assess the effects of Sox9 ablation on differentiation potential utilising CRISPR/Cas genome editing technology to generate a homozygous knockout cell line and assessing differentiation potential using qualitative means.

---

**CHAPTER TWO**

**DEVELOPMENT OF BIOSENSING REPORTER**

**TECHNOLOGY**

---

## 2.0 Introduction to disease modelling using genetic reporters

### 2.0.1 Conventional analysis of disease

Even though the use of animal models has proved to be invaluable for gaining greater insight into disease processes, pathogenesis and potential therapeutic targets, the use of biochemical markers as the means of determining disease status has many shortcomings. One of the greatest drawbacks is the necessity of generating a large cohort of diseased mice to achieve statistical significance. Several animals would need to be culled at each of several time points in order to perform biochemical and histological analysis for determination of the extent of disease progression or regression. This process not only requires the use of a large number of animals for each experiment, but a substantial amount of time would be required to harvest and process each of the samples (**Figure 23**). Important to note is the discontinuous nature of such an experiment, with each data point being represented by a single animal. With the large amount of inherent inter-animal variation, this would decrease the probability of obtaining statistical significance. Continuous assessment of current protocols should be performed in line with the principles of humane animal research through improved methodologies, experimental design and appropriate statistical methods.

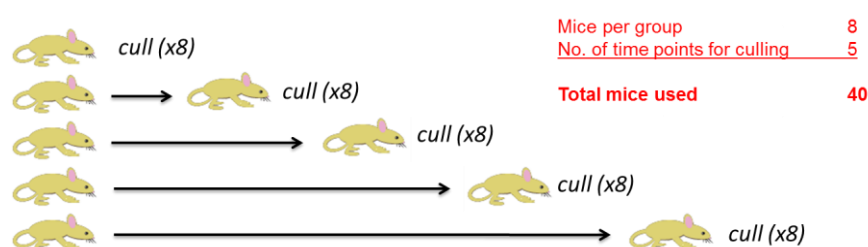


**Figure 23. Experimental design of conventional disease model with terminal analysis.**

A subset of the animal cohort is sacrificed at each time point to perform molecular analysis and determine disease progression/regression. Image courtesy of Dr. Simon Waddington.

### 2.0.2 The principle of the 3Rs of animal research

The concept of the three Rs is a set of principles which have been set out to diminish the number of animals used in scientific research. The principles were first introduced by Russell and Burch in 1959<sup>249</sup> and since then have become widely adopted. The three R's are reduction, refinement, and replacement. The aim when utilising animals for research purposes is to reduce the number of animals required by using methods which obtain the same amount of data from fewer animals, or obtaining more information from the same number of animals through improved experimental design, bioinformatics resources, or alternative techniques. Refinement refers to the altering of current methodologies to ones which inflict less suffering or distress upon the animals for example through using less invasive techniques, while replacement aims to substitute existing experiments involving

animals with alternatives in which animals are no longer required<sup>250</sup>. The use of luciferase as a reporter for gene expression is just one example in which the 3Rs can be implemented to reduce the number of animals required.

### 2.0.3 Whole-body, light-emitting transgenic animals for continual bioimaging of disease

To address the failings of terminal analysis, various models of light-emitting transgenics have been developed to facilitate non-invasive monitoring of disease states *in vivo*<sup>251-253</sup>. This is achieved through the addition of a synthetic construct within the animals which consists of a response element containing pathway-specific transcription factor binding sites upstream of the firefly luciferase gene. In response to particular disease stimuli, a specific biochemical pathway becomes activated, causing the recruitment and binding of nuclear transcription factors to their respective response elements, the region of the promoter which is able to bind specific transcription factors. This induces transcription factor-mediated expression of the downstream luciferase gene (**Figure 24**). Bioluminescence is captured by a highly-sensitive charge-coupled camera able to detect the visible light emitted from the organs of the animals. The bioluminescent image is then superimposed upon grey-scale photographic images of the animal to localise the emission signal. Therefore, quantifiable light emission can be used as a substitute marker of pathological molecular pathway activity without the need to cull the animal, a technology known as bioluminescence imaging.

Using this novel technology, it is possible to monitor, in a continual, non-invasive fashion, processes in numerous disease models including bacterial infections<sup>254</sup>, arthritis<sup>255</sup>, and LPS-induced liver<sup>256</sup> and brain inflammation<sup>257</sup>. Given that mammalian cells are devoid of endogenous light, even diminutive quantities of bioluminescence can be detected, making bioimaging an extremely sensitive investigative method during even the early stages of disease. These benefits make bioimaging a useful tool for investigating biological processes with the required sensitivity. It also makes temporal analysis within the same animal possible, even during the early stages of disease.

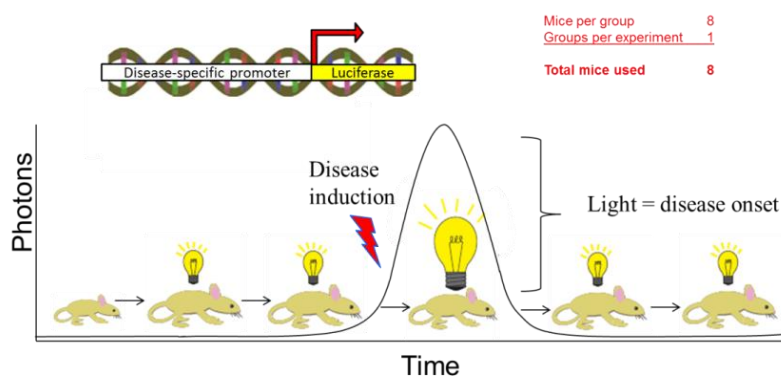


**Figure 24. Illustration of germline transgenic concept.**

Disease is induced in mice containing a luciferase driven by a disease-specific promoter. Promoter activation results in increased luciferase expression. Therefore, the amount of light generated is proportional to the amount of disease activation. Courtesy of Dr. Simon Waddington.

### **Benefits of bioluminescence imaging within germline transgenic animals**

There are many advantages of using bioluminescence imaging to analyse disease progression and potential therapeutics within animal models. Firstly, biological variation is substantially reduced since each animal is imaged at numerous different time points. This means that each animal acts as its own internal control and can be used to normalise its own luminescent signal<sup>237</sup>. This reduces the number of animals required to obtain statistical significance and is in line with upholding the principles of the 3Rs. This methodology is in contrast to studies in which terminal, post-mortem analysis is required, which limits the use of a single animal to one specific time point, resulting in the requirement for a large initial cohort of animals<sup>258</sup>. Secondly, there are economic benefits in the form of a reduction in animal usage. Thirdly, from a technical standpoint, the ease of analysis is beneficial. Conventional analysis requires a high level of expertise in a wide range of molecular biology techniques. In contrast, the process of bioluminescent imaging only requires the administration of substrate, D-luciferin, followed by the imaging of the animals within a light-tight imaging chamber, which requires relatively little technical knowledge. Data is captured (usually within less than 5 minutes), making this a rapid means of obtaining and processing data.

### **Disadvantages of bioluminescence imaging in germline transgenics**

Despite improved ability for deep-tissue analysis using germline transgenic rodents, several inherent drawbacks impede the broader-scale implementation of bioluminescent technology within research. One of the major factors is the time required to generate the desired light-emitting transgenic animal. For example, the generation of the line can take as much as 8-14 months to produce, while backcrossing of the animals onto the preferred background strain may increase this to up to 24 months, and is a very time consuming process. There is also a high degree of technical expertise that is required in order to perform the procedures<sup>259</sup>. The cost implications are also substantial as both interim and maintenance of the colony is required. One of the more inherent disadvantages is the lack of tissue-specific expression, due to the fact that the luciferase construct is ubiquitously expressed within every cell in the body. This can result in high background expression of the luciferase transgene, and may confound interpretation of the data (**Figure 25**).

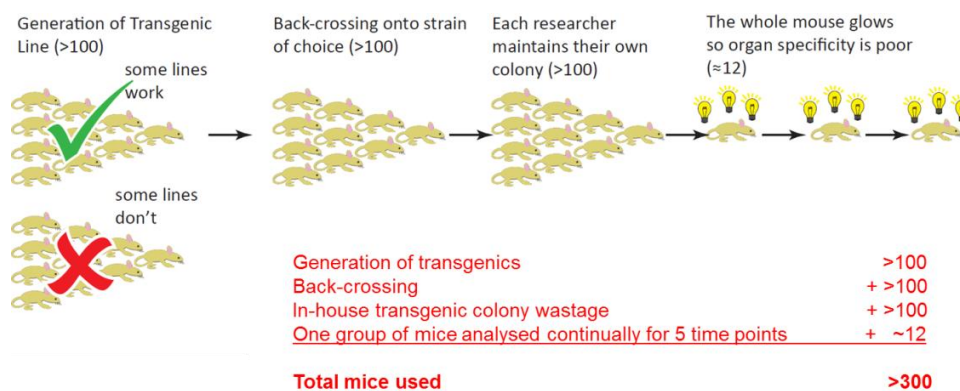


**Figure 25. Germline transgenic animal models used in whole-body bioluminescent imaging.**

The main disadvantages of light-emitting, germ-line transgenic animals is the time, cost, lack of sensitivity, and wastage of animals during the process of developing the desired transgenic. Illustration courtesy of Dr Simon Waddington.

#### 2.0.4 Somatransgenic Bioimaging (SomaBio)

As a means of addressing the lack of organ specificity while still maintaining the prior mentioned positive attributes of whole-body bioluminescent imaging, several modifications to the technology have been developed and are presented within this thesis. This has led to the generation of somatic transgenic animals which have many technical benefits over their whole-body transgenic predecessors. Generation of the somatic transgenic rodents relies on administration of an HIV-based lentiviral vector<sup>260</sup>. In recent years, lentiviral vectors have been developed and enhanced as gene delivery tools. Using lentiviruses results in the transduction and long-term expression of a desired gene, with targeting of these vectors already achieved in the lung<sup>261</sup>, neurons<sup>262</sup>, liver, muscle<sup>263</sup>, and heart<sup>264</sup>. In the context of somatransgenesis, lentiviral vectors are designed to specifically deliver a construct containing the luciferase reporter gene into the organ of interest particularly during the late fetal or early neonatal period of rodent development (**Figure 26**). The immune system of these animals is immature, facilitating tolerance towards the exogenous luciferase protein and enhancing transduction<sup>264</sup>. It should also be noted that due to the larger vector:body mass ratio, that a larger proportion of a specified organ can be transduced. Progeny of the transduced cells will give rise to cells which also contain the transgene, and so the initial transducing units used is able to have a greater transduction potential merely due to DNA replication and cell division compared to viral delivery performed directly in an adult animal. It would therefore be beneficial to target the expanding stem cell niche within neonatal / fetal animals.

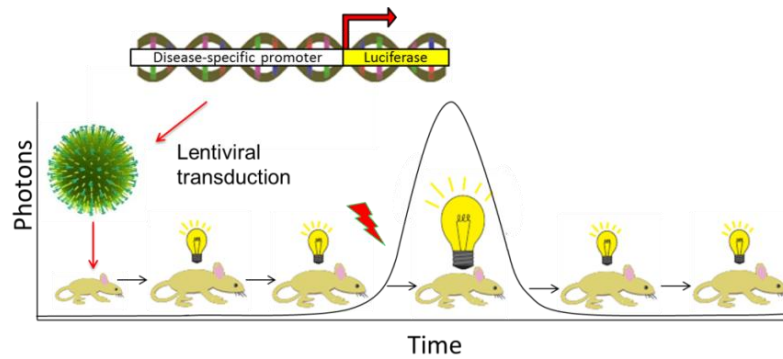


**Figure 26. Illustration of the concept of somatotropic bioimaging.**

Somatotropic bioimaging is achieved through viral transduction of the animal with the luciferase reporter gene during the neonatal period. Photonic output is measured over a series of time points to determine pathway-specific signalling activity. Illustration courtesy of Dr Simon Waddington.

### Advantages of Somatotropic technology

There are several advantages of using a technological platform such as somatotropic bioimaging, each of which addresses a particular drawback of prior methodologies or technologies. These benefits are summarised below:

#### i) Long-term expression

Compared to other gene transfer vectors, such as adeno-associated virus (AAV) and adenovirus, the lentivirus is a retrovirus that is able to reverse transcribe its RNA genome into a cDNA copy through the use of reverse transcriptase, the product of which then becomes stably integrated into the genome of the host<sup>265</sup>. In contrast to moloney leukemia virus<sup>266</sup>, it is able to do so in non-dividing cells<sup>267</sup>. This results in permanent expression of the transgene, a characteristic which has seen it become a popular choice of viral delivery.

#### ii) Organ and tissue specificity

Vector specificity for its target is a critical requirement for more reliable data and improved statistical power. Such specificity can be conferred via two means, the first biological and the second technical. Enhancing transduction can be achieved through substitution of the viral coat protein for an envelope containing surface glycoproteins derived from alternative viruses, a process known as pseudotyping. Viral pseudotyping is able to expand the range of potential targets, with those viruses capable of infecting a broad array of tissues being referred to as having broad tropism. One of the mechanisms in which tropism is conferred is through the interaction of the viral envelope protein with the cellular receptor on the target cell type<sup>268</sup>. The popularly used envelope, vesicular stomatitis virus glycoprotein (VSV-g), proved to be pantropic due to the ubiquitous nature of the receptor with which it interacts with. This receptor on the target cell is known as the low density lipoprotein receptor (LDLR)<sup>269</sup>. Amongst a host of alternative viral pseudotypes, the baculovirus envelope glycoprotein,

GP64, is of particular importance for gene transfer to the lungs. It has the ability to transduce the apical side of airway epithelia, making it a good candidate for gene therapy of cystic fibrosis<sup>261</sup>.

The technical means of organ targeting is achieved through delivery of virus through various routes of administration, which is a simple method employed to control the *in vivo* fate of the viral vectors each with their own advantages and disadvantages. These include oral, intravenous, intra-arterial, intra-portal, retrograde intravenous, direct injection, intraperitoneal, or organ surface methods of delivery<sup>270</sup>. It is vital to keep in mind that viruses have varying affinities to a cell due to cell polarity. The route of administration needs to permit viral access to the basal or apical side of the cell for efficient transduction<sup>270</sup>. Pseudotyping, changing of vector administration routes or a combination of these strategies can be immensely useful in gaining targeted expression of the transgenic construct.

### iii) Ease of tissue-specific transgenesis

In comparison to the production of a germline transgenic line, somatic transgenic animals are developed through neonatal or fetal administration of lentivirus. This is technically less demanding, less expensive, and much quicker to implement. The majority of time used to develop a somatic transgenic animal is spent on cloning of the pathway-specific response elements upstream of the chosen luciferase, which takes 1 to 8 weeks. Vector production and titering takes a further 2 weeks, and vector injection, integration and maturation of the mice approximately 8 more weeks. Since generation of somatic, light-emitting transgenic mice using fetal or neonatal administration of lentivirus is rapid and undemanding, it serves as the ideal system to assess novel biosensing constructs in a range of *in vivo* bioimaging applications.

This chapter focuses on the development of a library of transcription factor-specific response elements cloned upstream of a novel dual reporter. The aim is to develop lentiviral reporters that can be used to analyse molecular pathway activity in response to disease progression over time in a temporal manner, both *in vitro* and *in vivo*, and importantly, to obtain such data non-invasively from animals.

## 2.1 Results of luciferase reporter development

### 2.1.1 Overlap-extension PCR and lentiviral cloning of novel luciferase constructs

The desired constitutively expressing dual reporter vector contained the SFFV promoter upstream of a bicistronic firefly luciferase / GFP reporter cassette as depicted in **Figure 27a**. This vector contains all the relevant elements including a 5' long terminal repeat (LTR), central polypurine tract (cPPT), constitutive SFFV promoter, bicistronic luciferase-2A-GFP cassette, Woodchuck Hepatitis Virus (WHP) Posttranscriptional Regulatory element (WPRE), and 3' deleted LTR to produce functional lentiviral particles. To produce this vector, primary PCR products for each of the 3 desired fragments

were generated using their respective primer pairs and amplified from parental vectors, a kind gift from Dr Martin Pule, UCL. For each of the reactions, the expected product sizes of 125 bp, 1656 bp, and 907 bp were observed for 3xFLAG, FLuc, and 2A-eGFP respectively (**Figure 27b**). Subsequent to this, a secondary fusion PCR was performed to fuse the fragments and generate a single bicistronic cassette comprised of 3xFLAG-FLuc-2A-eGFP (**Figure 27c**). The plasmid pLNT-SEW-Asp-eGFP is a 2<sup>nd</sup> generation lentiviral vector containing a constitutive spleen focus-forming virus (SFFV) promoter which drives the expression of the *Aspergillus* antigen and eGFP to yield pLNT-SFFV-JDG. Following excision of the *Aspergillus* antigen- and eGFP-encoding DNA, the fused product was cloned into the destination lentiviral vector. Positive clones were selected based on a restriction digest pattern consisting of 3 fragments of 1317 bp, 2947 bp, and 7249 bp in length, of which there were 8 correct clones out of 12 (**Figure 27d**). The clones which were not correct contain various different banding patterns, and this is believed to be a result of recombination events that occur around the homologous lentiviral LTRs within RecA(-) bacteria and causes part of the plasmid to be excised<sup>271</sup>, resulting in alternative banding patterns in the restriction digest. The 3xFLAG-FLuc-2A-eGFP insert sequence and highlighted primer binding sites are shown in **Appendix A**.

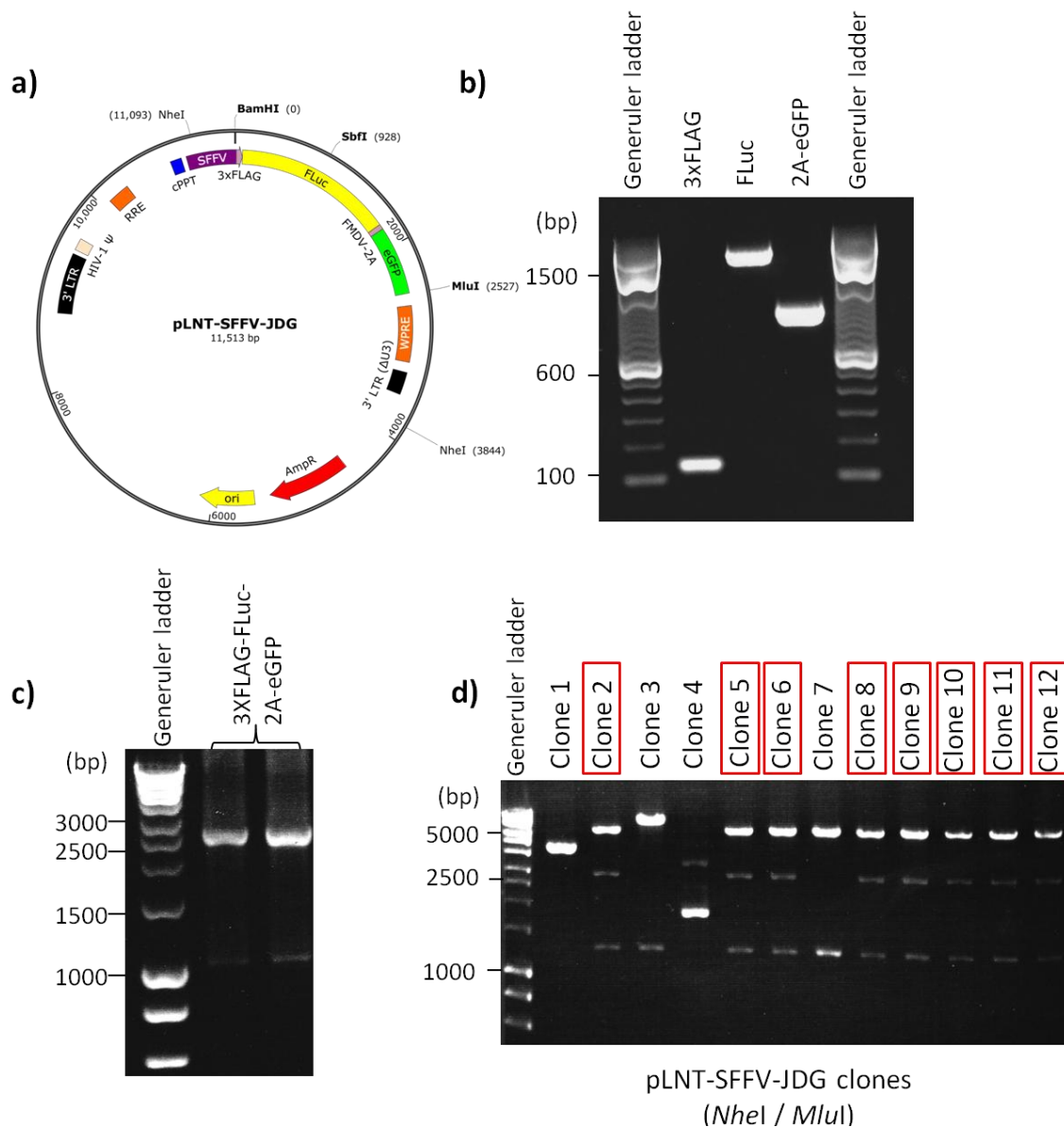


**Figure 27. Gel electrophoresis of primary and secondary PCR, and restriction digest of pLNT-SFFV-JDG clones.**

a) Schematic of pLNT-SFFV-JDG lentiviral vector. b) Primary PCR fragments amplified from respective parental vectors and electrophoresed to show 3xFLAG (125 bp), FLuc (1656 bp), and 2A-eGFP (907 bp) fragments. c) Gel demonstrating secondary overlap-extension PCR products fused to produce the 3XFLAG-FLuc-2A-eGFP insert (2614 bp). d) Double digested (*MluI* / *NheI*) pLNT-SFFV-JDG clones with correct clones (in red boxes) yielding DNA fragments of 1317, 2947, and 7249 bp, and empty backbone clones yielding fragments of 1686 and 7249 bp.

### 2.1.2 Flow cytometry for presence of luciferase and eGFP

To confirm the presence of the 3xFLAG and eGFP, flow cytometry was performed on cells which had been transfected with pLNT-SFFV-JDG. GFP can be detected through excitation of the fluorophore with a blue laser, however, since the 3xFLAG and the luciferase are not fluorophores, the addition of a fluorophore was required as an additional step. To determine the auto-fluorescence within the HEK293T cells, untransfected cells were used to set up “gates”. Using the forward scatter (cell size)

and side scatter (internal complexity) of the untransfected cells, the voltage was adjusted so that the untransfected cells (negative control) had an expression level of less than  $10^2$  on the 3xFLAG x-axis, and less than  $10^1$  on the GFP y-axis, corresponding to inherent auto-fluorescence of the cells. These negative control cells were restricted to quadrant R3 (**Figure 28ai**). Cells transfected with the positive control GFP construct were shown to be localised specifically to quadrant R1 (**Figure 28aii**). Another construct containing a well-characterised 3xFLAG tagged insert was used to transfect and used as the positive gating control for 3xFLAG, gated specifically to quadrant R4 (**Figure 28aiii**). HEK293T cells transfected with the novel pLNT-SFFV-JDG vector were shown to express both the 3xFLAG and eGFP, resulting in cells being present in quadrant R2 (**Figure 28aiv**). Using adequate gating controls resulted in less than 0.1% of non-transfected cells being seen in the GFP-positive quadrant, and 2.29% within the 3xFLAG-positive quadrant. Both GFP-positive and 3xFLAG positive controls showed less than 0.5% cells within the double detection R2 quadrant while pLNT-SFFV-JDG transfected cells showed 16.47% , significantly higher than the single 2.53% eGFP positive and single 1.52% 3xFLAG positive cells found within the sample.

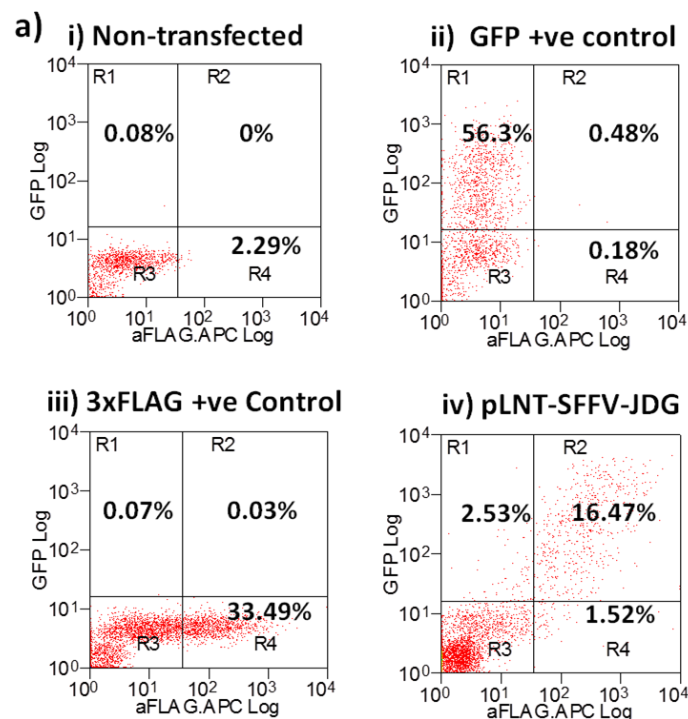


**Figure 28. Functional validation of GFP and luciferase expression.**

Flow cytometry on cells transfected with the pLNT-SFFV-JDG construct was performed to validate the expression of eGFP and 3xFLAG, which was used as a surrogate marker of the luciferase to which the FLAG-tag is fused. a) Untransfected HEK293T cells were used as the gating control, while cells transfected with either a b) well-characterised eGFP, or c) well-characterised FLAG-tag expressing vector were used as positive controls. d) The pLNT-SFFV-JDG construct was positive for both GFP and 3xFLAG, indicating dual expression of these proteins.

### 2.1.3 Cleavage efficiency of 2A polypeptide sequence by Western Blot

Using fluorophore-conjugated antibodies and the Li-Cor Odyssey Imaging System to quantify the relative amounts of fluorescence, the efficiency of FMDV-2A cleavage was determined. Using lysate from cells transfected with the pLNT-SFFV-JDG construct, polyacrylamide gel electrophoresis (PAGE) was performed. The Odyssey Western Blot detection system uses infrared dyes (IRDye) conjugated to the secondary antibody that produces near-infrared fluorescent signals that are able to be detected by the Odyssey fluorescence scanner. These IRDyes emit within the 800 channel (green) or the 680 channel (red) and these fluorescent signals are used as a means of visualisation. This is particularly beneficial in this context as the quantity of cleaved versus uncleaved product could be quantitatively determined.

By applying primary antibodies for either the 3XFLAG or the GFP followed by applying a green fluorophore-conjugated secondary antibody, 2A cleavage efficiency could be determined. The green band was used to detect the fusion protein consisting of the 3xFLAG peptide fused to the luciferase at 65 kDa, or the eGFP with an expected molecular weight of 27 kDa.  $\beta$ -actin was used as the loading control and probed with a red fluorophore-conjugated secondary antibody for signal detection of a band with an expected molecular weight of 47 kDa. The Western blot indicates the presence of cleaved products as both the 65 kDa and the 27 kDa can be seen, however, there is also the presence of a faint band around 92 kDa (**Figure 29a**).

### 2.1.4 Spectral analysis of pLNT-SFFV-JDG

Of the 12 clones selected, 8 clones were found to contain the insert. Individual spectral analyses were performed to determine which of the clones expressing luciferase had the highest enzymatic activity. Each of the clones was transfected onto HEK293T cells, lysed after 24 hours, and spectral emission determined through luminometry. An emission spectrum was generated by determining the light output at a series of wavelengths ranging from 450 to 750 nm. The greatest point of fluorescent intensity is known as the peak photonic output, which was empirically determined to be 549 nm for the pLNT-SFFV-JDG vector measured as relative light units. Analysis confirmed that luciferase expressed from clone 11 had the highest luciferase activity, with an output of 67293 relative light units (**Figure 29b**). The variation seen between clones may have been attributed to varying transfection efficiencies between wells. Ideally, a second reporter should be utilized to control for transfection efficiencies, or should be normalised to total protein content to account for cell numbers in each well. All subsequent measurements were controlled for via the latter method.

### 2.1.5 Virus production and transduction validation of pLNT-SFFV-JDG

Transient transfection of a gag-pol packaging plasmid, a VSV-g envelope plasmid, and the newly developed pLNT-SFFV-JDG vector, resulted in the production of virus particles that were concentrated using centrifugation. In order to determine the titer, a p24 ELISA was performed to yield the number of vector particles per  $\mu\text{l}$  of supernatant. This value was subsequently used to determine the multiplicity of infection (MOI), or the number of transducing viral particles per cell. HEK293T cells were transduced with the LNT-SFFV-JDG-containing virus and exhibited constitutive expression of the bicistronic cassette, clearly visualised microscopically using the GFP reporter (**Figure 29c**). Triplicate wells of LNT-SFFV-JDG transduced and untransduced cells were lysed and a luciferase assay performed. A significant ( $p = 3.48\text{E}^{-4}$ ) increase in luciferase expression was seen in the LNT-SFFV-JDG transduced versus untransduced cells, with a dramatic 2,367,160-fold increase in relative light units (**Figure 29d**).

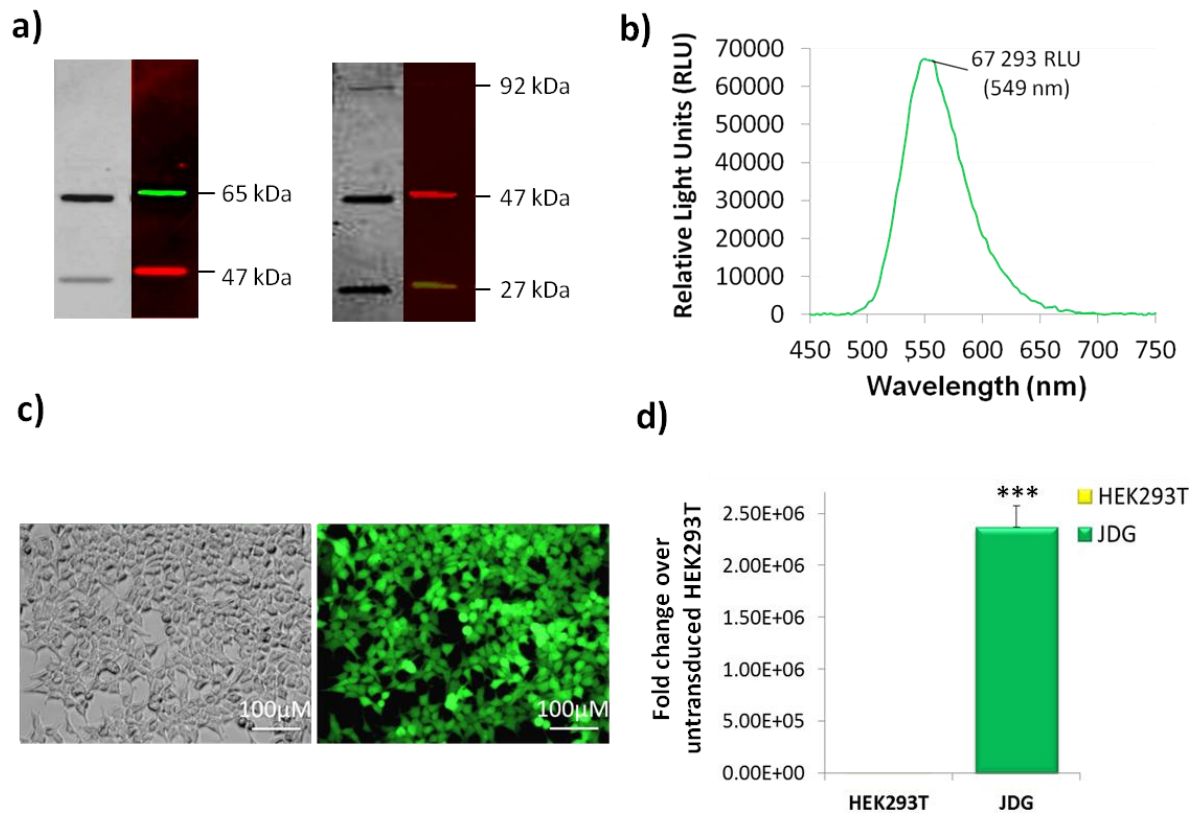


**Figure 29. Functional validation of pLNT-SFFV-JDG.**

a) Western blot showing protein products following 2A cleavage. The  $\beta$ -actin loading control (in red) is seen in both blots at 47 kDa, with the 65 kDa and 27 kDa fragments (in green) indicative of 3xFlag-FLuc and eGFP proteins respectively. The black-and-white version of the blot clearly shows a small proportion of uncleaved product at 92 kDa. b) Emission spectra of pLNT-SFFV-JDG transfected HEK293T cells between 450-750 nm, with peak emission at 549 nm. c) HEK293T cells transduced with LNT-SFFV-JDG lentivirus showing constitutive expression of GFP and d) luciferase.

### 2.1.6 Development of a rapid cloning system, the construction of pLNT-GW-JDG

Cloning each of the transcription factor binding sites (response elements) individually would be labour intensive and time consuming. Ideally, a method of rapid cloning would be employed to substitute the various transcription factor binding sites and generate a library of biosensing reporters. Gateway® cloning technology, developed by Invitrogen™, is a restriction-enzyme independent method of cloning. The Gateway® cassette (GW) is flanked by recombination sites and contains the *ccdB* toxicity gene which inactivates DNA gyrase and therefore acts as a potent inhibitor of bacterial cell proliferation<sup>272</sup>. This cassette is cloned into the destination vector, which in the case of the desired vector, was upstream of the bicistronic luciferase/GFP cassette. The accompanying recombination sites also flank the insert (in our case the response elements) cloned in the pENTR shuttle vector, and this region of homology between the recombination sites permits site-specific recombination to occur. This results in the Gateway® cassette being recombined out of the destination vector and into the pENTR vector, while the response element is recombined out of the pENTR vector and into the destination vector, upstream of the luciferase/GFP (Figure 30). The increased efficiency of obtaining the correct recombinant clone is due to dual selection. Only clones which contain the response element instead of Gateway containing the toxicity gene are able to grow in the bacteria, and a second layer of selection is conferred through antibiotic selection. The pENTR vector contains only kanamycin resistance, and bacteria transformed with this plasmid will therefore not grow on ampicillin-laden agar plates. Dual selection should theoretically result in the generation of only those clones which have the response element within the lentivirus backbone, grown in *ccdB*-sensitive bacteria, and plated onto ampicillin/carbenicillin agar plates.

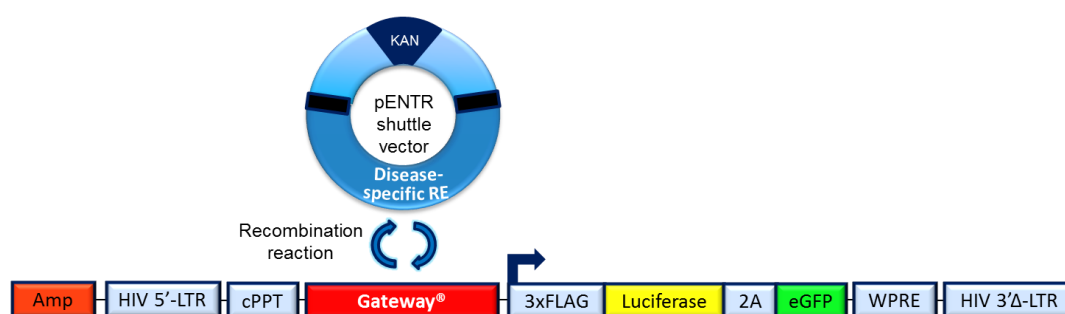


**Figure 30. Schematic of Gateway recombination cloning using the pENTR shuttle vector and the pLNT-GW-JDG lentiviral vector.**

The *ccdB*-containing Gateway® is cloned upstream of the luciferase cassette. During the recombination reaction, the pENTR vector, containing the disease-specific response elements undergoes site-specific recombination, resulting in a lentivirus containing the disease-specific response element upstream of the luciferase while the Gateway® cassette is shuttled into the pENTR vector.

In order to generate pLNT-GW-JDG for the rapid recombination of reporter elements upstream of the bicistronic luciferase/eGFP cassette, the JDG insert was initially subcloned into the expression plasmid, pZsGreen, and subsequently cloned into its final vector, pLNT-GW-MCS, as diagrammatically depicted in Figure 31a. Restriction enzyme digest of positive pZsGreen-JDG

clones yielded inserts of 209, 1123, 1457, and 4194 bp as is observed in clones 1-5 (**Figure 31b**). Following subcloning, the JDG cassette was cloned into the final pLNT-GW-MCS vector and screened for a correct clone (**Figure 31c**). The vector map of pZs-Green-JDG (**Appendix A.iii**) and pLNT-GW-JDG (**Appendix A.v**) vectors are given with relevant restriction sites.

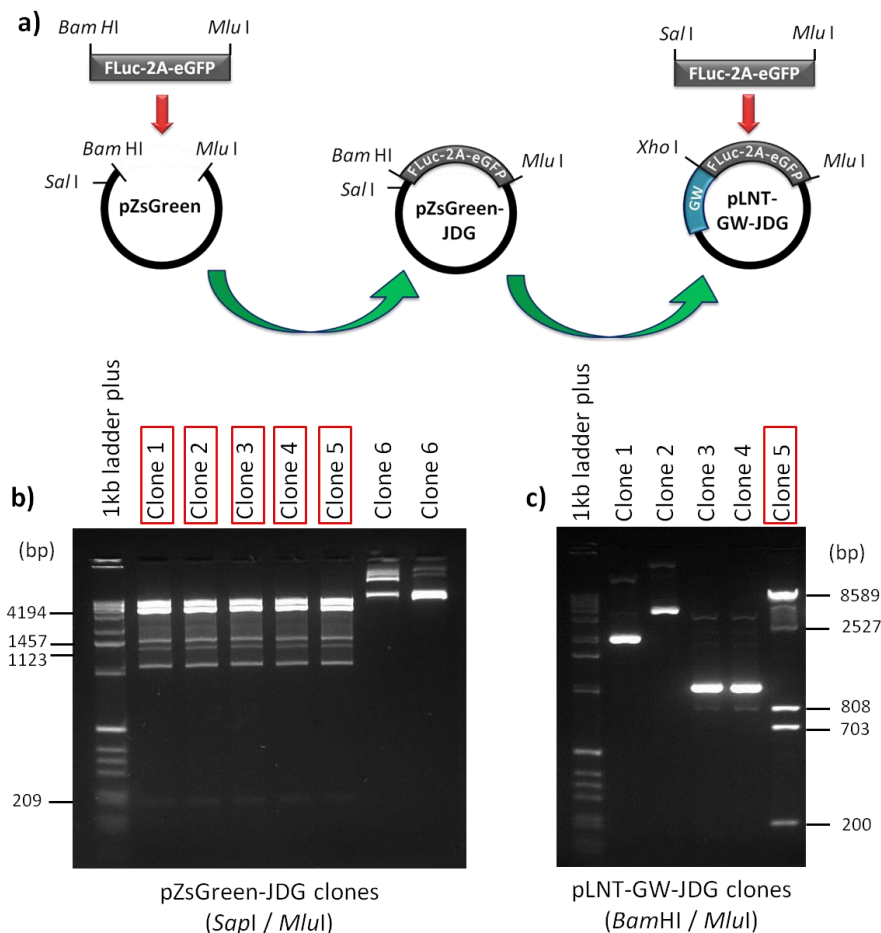


**Figure 31. Cloning to generate the Gateway-FLuc-2A-GFP (pLNT-GW-JDG) parental vector.**

a) Cloning strategy to produce the pLNT-GW-JDG vector. The bicistronic JDG cassette was primarily cloned into a subcloning vector before being cloned into the pLNT-GW backbone. b) Gel of pZsGreen-JDG clones double digested with *SapI* / *MluI* showed bands of the correct sizes. c) Gel of pLNT-GW-JDG clones digested with *BamHI* / *MluI* with clone 5 showing a clone with the correct size digest products to confirm the presence of the cloned JDG insert.

### 2.1.7 Development of NanoLuc® and Vargula parental cloning vectors.

While the use of firefly luciferase was the best candidate for longitudinal *in vivo* bioimaging due to its high signal intensity and stability, the necessity for cell lysis for luciferase quantification of *in vitro* assays made this vector less than desirable for temporal studies. The preferred luciferase for differentiation studies would allow the determination of luciferase activity from the same sample for the duration of the experiment, thus requiring that the luciferase is secreted instead of remaining intracellular. NanoLuc® is a newly developed luciferase that has been engineered for enhanced

luciferase performance and secretion of the luciferase into the media<sup>248</sup>. This feature negates the need for cell lysis and permits longitudinal studies *in vitro*. The use of a second secreted luciferase, such as vargula, under the control of a constitutive promoter, is then used to control for cell number within the model system.

The cloning strategy for cloning the fused NLuc-2A-GFP product into the lentiviral backbone is depicted in **Figure 32a**. Firstly, primary PCRs for NanoLuc and 2A-eGFP were performed and resulted in the expected 627 bp and 826 bp fragments respectively. Following overlap-extension PCR, a fusion product of 1403 bp was generated. This secondary fusion product was subcloned into the pENTR vector before being cloned into the lentiviral backbone. A screening restriction enzyme digest yielded a single clone which excised the fused PCR product insert and is seen as a 1389 bp fragment following gel electrophoresis (**Figure 32b**) with the map of pLNT-GW-NLuc2 shown in **Appendix A.vi**.

The vargula luciferase (Vluc) insert was amplified using a high-fidelity polymerase and resulted in the expected 1687 bp product. This product was subcloned into the pENTR-1A vector with the restriction enzyme digest check demonstrating that all 4 selected clones contained the insert. Recombination of Vluc into the pLNT-SFFV-GW vector was performed and clones screened for the presence or absence of the Vluc insert. Clone 1, 3, and 4 were positive for the insert of 1688 bp (**Figure 32c**). The vector map is shown in **Appendix A.vii**.

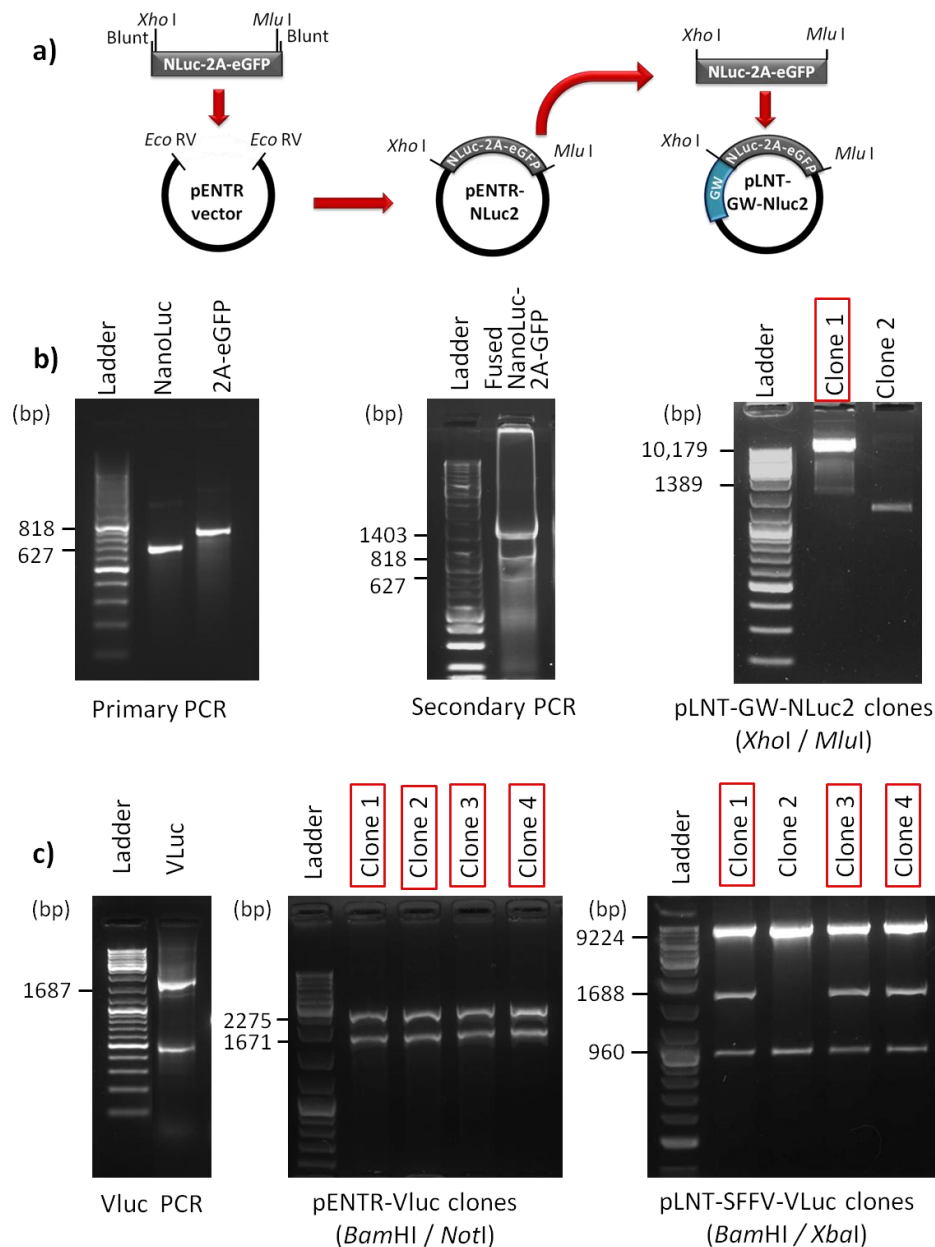


**Figure 32. Restriction digest checks of pLNT-GW-NLuc2 and pLNT-SFFV-Vluc cloning.**

a) Schematic of pLNT-GW-NLuc2 cloning strategy. b) Primary and secondary PCR of NanoLuc and 2A-eGFP to create a fused product. Clone screening digest with clone 1 shown to be positive for the NLuc2 insert. c) PCR of vargula luciferase and subsequent cloning into pENTR-1A. Positive clone selection of subcloning vector performed using restriction digestion. Following recombination, pLNT-GW-Vluc clones were screened to detect the Vluc insert with clones 1, 3, and 4 confirmed as positive.

### 2.1.8 *In vitro* validation of constitutively driven JDG, RLuc2, Vluc2, and NLuc2

An important point of consideration when utilising various luciferases within the same model system is the specificity of each of the luciferases for their particular substrate. To this end, virus was produced with constructs constitutively expressing either JDG (firefly), RLuc2 (renilla), Vluc2 (vargula), or NLuc2 (NanoLuc), which were used to transduce HEK293T cells. The lysate from these cells was used in a luciferase assay using each of the three luciferase substrates, namely D-luciferin, coelenterazine, and vargulin respectively. Renilla and NanoLuc luciferases are both able to produce

photonic outputs in the presence of coelenterazine. Data was normalised using a Bradford assay for total protein content, and untransduced HEK293T cells were used as the control to account for any background luminescence given by the substrates. All data are represented as fold-change over HEK293T cells alone, with statistical significance determined using a one-way ANOVA with Tukey's post-hoc test for significance. **Figure 33a** demonstrates that D-luciferin is highly specific for the firefly luciferase found within the pLNT-SFFV-JDG vector with a 2,367,160-fold increase in RLU over HEK293T lysate alone ( $p < 0.001$ ). Coelenterazine showed the greatest fold-change in luciferase expression in cells transduced with the pLNT-SFFV-RLuc2 vector with a fold change of 12,819 RLU ( $p < 0.001$ ) as seen in **Figure 33b**. Some cross reactivity was seen with the coelenterazine substrate in the sample containing the firefly luciferase (fold-change of 2716 RLU), vargula luciferase (fold change of 12 RLU), and nanoluc luciferase (fold change of 902 RLU), but this was not significant after Tukey's post-hoc testing. Vargulin showed highly specific activation of the vargula luciferase in the pLNT-SFFV-VLuc transduced cells with a fold change of 24,968 ( $p < 0.001$ )(**Figure 33c**). Relative GFP expression of each of the transduced cells lines was assessed microscopically using fluorescence imaging. High levels of GFP expression was detected for all constructs (**Figure 33d**).

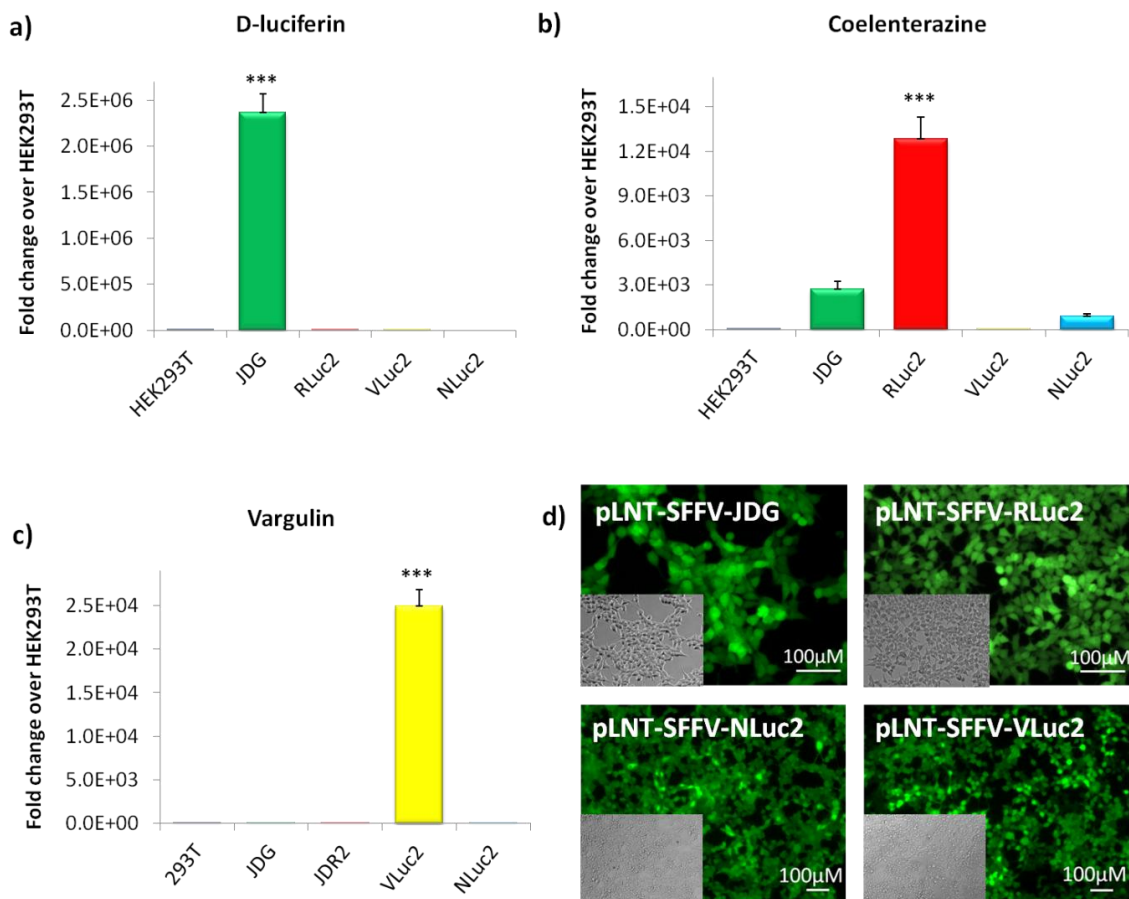


**Figure 33. Substrate specificity assay for JDG, RLuc2, VLuc2 and NLuc2.**

HEK293T cells transduced with JDG, RLuc2, VLuc2, or NLuc were subjected to luciferase assay using luciferase specific substrates, namely a) D-luciferin, b) coelenterazine, or c) vargulin. d) GFP expression of each of the constitutively expressing bicistronic vectors in HEK293T cells. Statistical significance determined by one-way ANOVA with Tukey's post-hoc test.

---

**CHAPTER THREE**

***IN VITRO* VALIDATION OF REPORTERS**

---

### **3.0 Investigating signalling activity using transcription factor binding elements**

Once the parental pLNT-GW-JDG vector had been generated, pENTR vectors containing the response elements to be recombined were required. pENTR vectors containing transcription factor activated response elements upstream of a minimal promoter were designed and *de novo* synthesised by Aldevron (Fargo, USA). The following step was to produce a biosensing vector which would be conditionally activated by pathway-specific agonists. Lentiviral delivery of vectors containing transcription factor binding elements upstream of a bicistronic reporter cassette would offer a unique method with which to interrogate biological pathways. In the context of this project, the reporters for NF- $\kappa$ B, SBE, Wnt and Notch were of particular interest as they are known to be fundamental in regenerative responses within the liver. Following cloning of these vectors, all constructs were subsequently validated *in vitro* prior to *in vivo* validation.

### 3.1 Results of reporter validations *in vitro*

#### 3.1.1 *In vitro* validation of the pLNT-NF- $\kappa$ B-JDG construct

Following recombination of pENTR-NF- $\kappa$ B with the parental pLNT-GW-JDG vector to yield pLNT-NF- $\kappa$ B-JDG, lentivirus was produced and a range of cell lines were transduced to produce multiple NF- $\kappa$ B stable reporter cell lines. The hepatic cell line, Huh7, was used to assess the effect of pro-inflammatory mediators upon NF- $\kappa$ B activation over several time points. Activation of the Huh7 NF- $\kappa$ B reporter line, followed by luciferase assay at 12, 24, 48, and 72 hours post activation was performed (**Figure 34a**). Data showing fold change over non-activated demonstrated a significant increase of luciferase expression at T = 12, 24, and 48 hours, with the highest fold change seen at 24 hours. Analysis of NF- $\kappa$ B activation in a broad range of cell lines was performed, and these included the use of 2 hepatic cell lines, HepG2 and Huh7, human fibroblasts, and fibroblasts isolated from TLR4 knockout mice. In all cases, significance was obtained, except for in the *tlr4*<sup>-/-</sup> MEFs which expectedly failed to reach significance ( $p = 0.2544$ ) (**Figure 34b**).

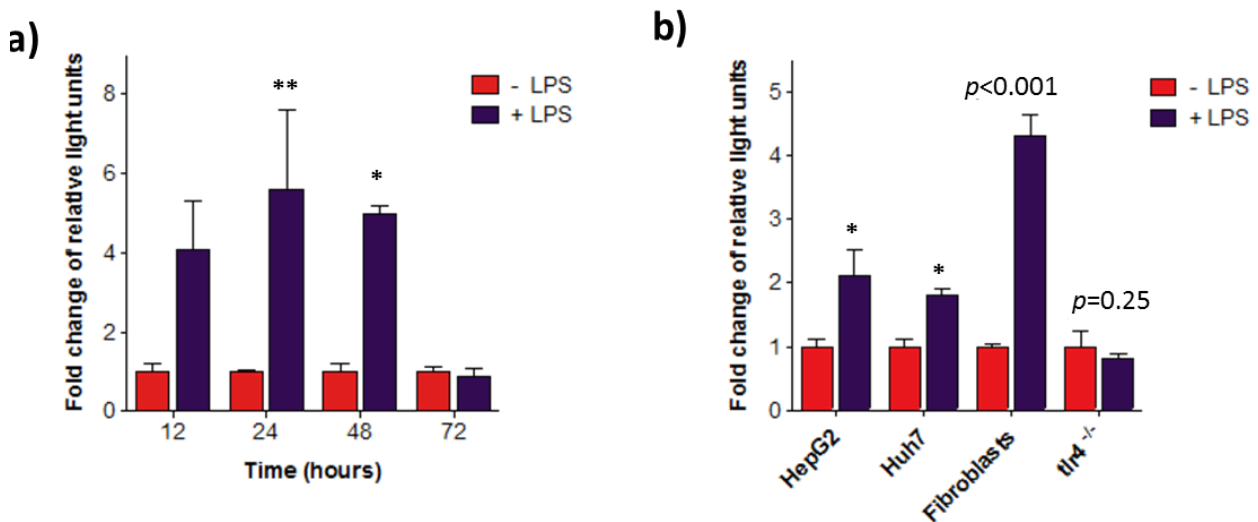


**Figure 34. LNT-NF- $\kappa$ B-JDG activation in response to LPS.**

a) Time course of activation in the Huh7 cell line following 4 hours of activation with LPS. Statistical significance ascertained by two way ANOVA b) Activation of two hepatic cell lines, HepG2 and Huh7, human fibroblasts, and *tlr4*<sup>-/-</sup> MEFs 48 hours post activation with LPS. Statistical significance was determined by Student's t-test. \*  $P < 0.05$ , \*\*  $P < 0.01$ , \*\*\*  $P < 0.001$ .

### 3.1.2 Time course and dose response of activin A activation of LNT-SBE-JDG *in vitro*

The next reporter to be validated was the vector containing the response element activated by TGF- $\beta$  signalling. Primary CD1 MEFs transduced with LNT-SBE-JDG were exposed to varying doses of activin A for a period of 48 hours prior to lysis and luciferase assay detection for relative pathway activation. The use of 1, 5, or 10 ng/ml of activin A resulted in no significant increase in luciferase expression in the activated versus their non-activated counterparts. However, the use of 50 and 100 ng/ml of activin A yielded a statistically significant difference between the activated and the non-activated samples ( $p = 0.027$  and  $0.045$  respectively) (**Figure 35a**).

Lentivirus containing the LNT-SBE-JDG construct was used to transduce a host of cell lines. These included 2 human stable cell lines, namely HEK293T and HeLa, human primary fetal fibroblasts isolated from the fetal portion of the placenta, and also mouse primary fibroblasts, from CD1 mice. Following viral integration, the cell lines were activated with the SMAD-2/3-specific agonist, activin A. Following 48 hours post-activation, a significant increase in luciferase expression was seen in all cell lines, with the HEK293T ( $p < 0.001$ ) and fetal fibroblasts ( $p = 0.001$ ) showing particularly high levels of statistical significance (**Figure 35b**).

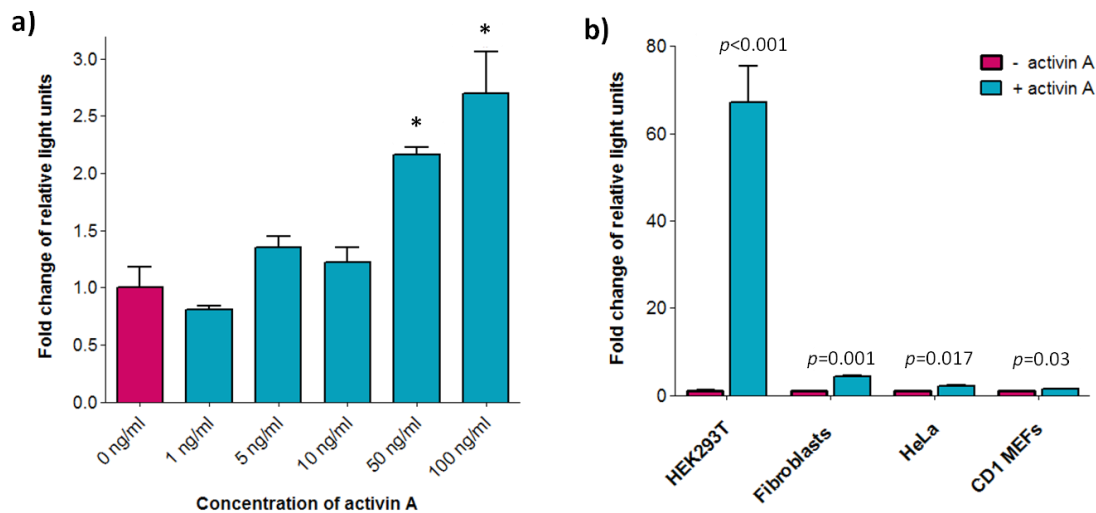


**Figure 35. Validation of pLNT-SBE-JDG using the agonist, activin A, in ascending doses and in various cell lines.**

a) Primary CD1 MEFs transduced with pLNT-SBE-JDG were activated with varying doses of activin A and the relative upregulation of luciferase expression ascertained through luciferase assay. b) HEK293T, human fetal fibroblasts, HeLas and CD1 MEFs were transduced with LNT-SBE-JDG and subsequently activated with activin A. Student's one-tailed t-test used for statistical significance. \*  $P < 0.05$ , \*\*  $P < 0.01$ , \*\*\*  $P < 0.001$ .

### 3.1.3 *In vitro* validation of WNT-JDG using LiCl

WNT signalling plays a crucial role in cell fate specification, proliferation, and migration. Within the context of liver regeneration, the role of WNT signalling in the lineage determination of bipotent hepatic progenitor cells following chronic liver damage requires further investigation. To this end, a WNT reporter construct containing conserved TCF/LEF transcription factor binding sites upstream of a luciferase cassette was generated. Three cell lines, namely HEK293T, NIH3T3, and HeLa were transduced with the LNT-WNT-JDG. Stimulation of canonical WNT signalling within the stable WNT reporter cell lines was achieved through the addition of lithium chloride (LiCl). Within all three cell lines, statistical significance was reached by 12 hours and remained elevated for the duration of the experiment. Data was plotted as fold change of LiCl-activated values over non-activated, baseline values. The greatest fold change was seen in HEK293T cells with a peak fold-change of 3129 noted at 72 hours and a significance value of  $p = 0.02$ . Although this was the point of greatest fold change, the point of greatest significance across the experiment was found at the 48 hour time point in NIH3T3s with a significance of  $p = 9.6E^{-8}$  (Figure 36).

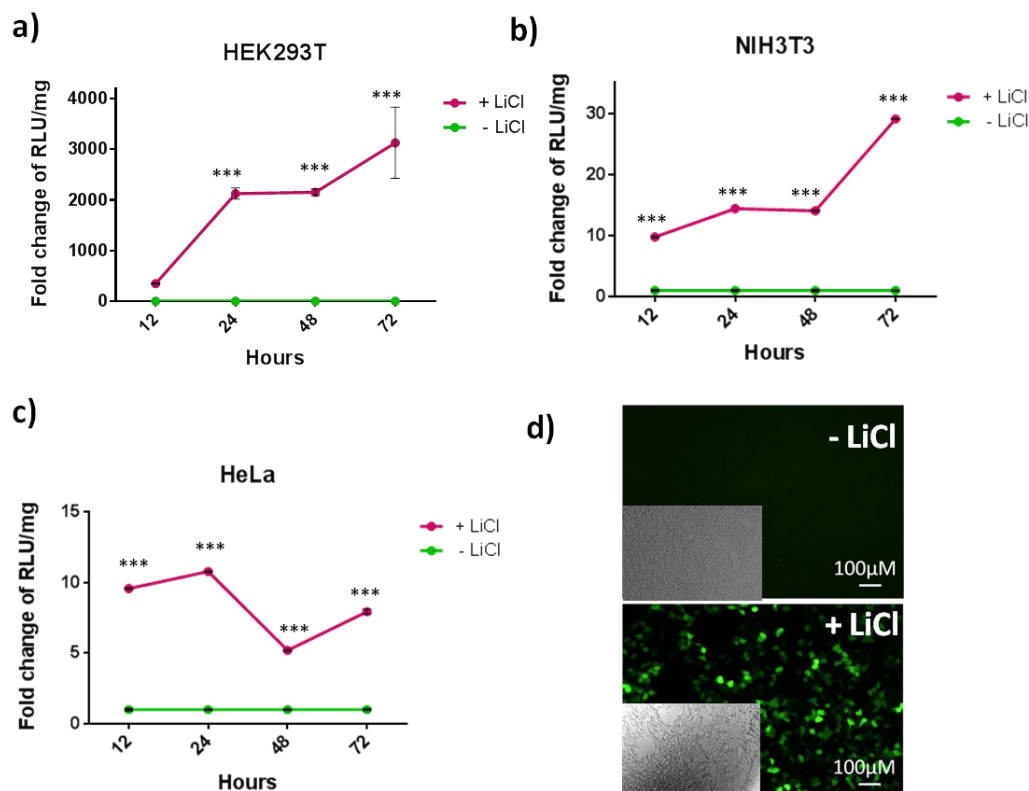


**Figure 36. *In vitro* validation of LNT-WNT-JDG vector in various cell lines.**

HEK293T (a), NIH3T3 (b) and HeLa (c & d) cells were transduced with LNT-WNT-JDG at an MOI of 10. The addition of LiCl was shown to upregulate WNT signalling in all cell lines, seen microscopically as the increase in GFP expression, and statistically as enhanced luciferase expression. Data analysed using two-way ANOVA with Bonferroni post-hoc test for significance. \*  $P < 0.05$ , \*\*  $P < 0.01$ , \*\*\*  $P < 0.001$ .

### 3.1.4 *In vitro* validation of Notch using co-culture with Jagged-1 overexpressing cells

Notch signalling uses juxtacrine signalling for signals to be transduced from one cell to the signal-receiving cell where it can modulate gene expression. A co-culture method was employed as an *in vitro* model in which the luciferase reporter could be validated by means of said contacts. The SGHPL5 trophoblast isolated cell line was transduced with both the LNT-Notch-JDG lentivirus, and also with the LNT-SFFV-RLuc vector, a constitutively expressed renilla construct used to normalise luciferase light units in each well of the experiment. Separately, HEK93T cells were transduced with the constitutive LNT-SFFV-Jagged-1-IRES-GFP vector. Cells were co-cultured at initial densities of 10, 30, 50, and 70% of HEK293T cells containing Jagged-1. The dose response curve indicates a significant increase in luciferase expression can be seen between each of the doses of HEK293T cells, with the highest level of significance seen when co-culturing with the maximum number of HEK293T cells at 70% (Figure 37a). Within the time-course experiment, Notch signalling was shown to be significant at 48 and 72 hours post continuous incubation with constitutively expressing Jagged-1 HEK293Ts (Figure 37b).

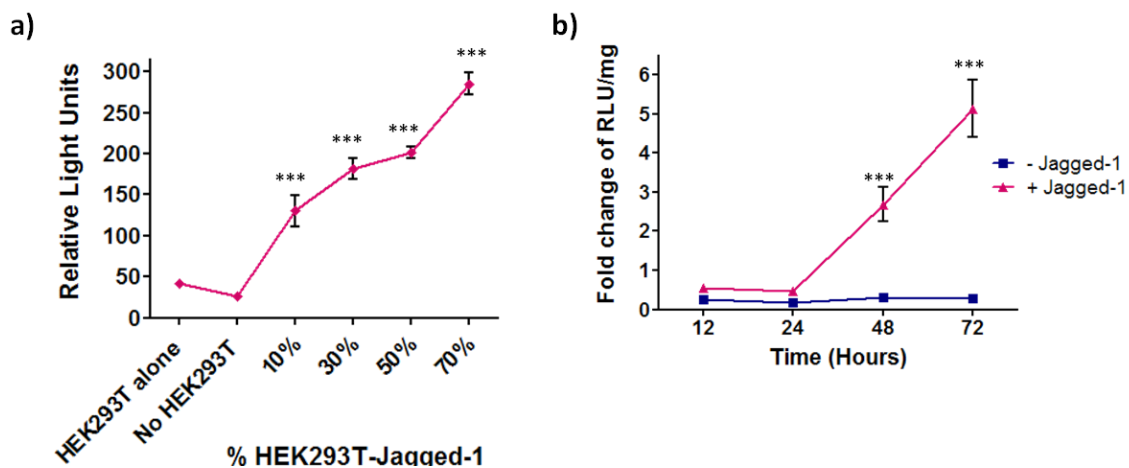


**Figure 37. *In vitro* validation of pLNT-Notch-JDG using Jagged-1 dose response curve and time course.**

a) SGHPL5 cells transduced with the Notch reporter were incubated in increasing doses of Jagged-1 overexpressing HEK293T cells and displayed dose-dependent signalling. Analysed using one-way ANOVA and Tukey post-hoc analysis b) A time course of the Notch reporter incubated with 70% Jagged-1 overexpressing HEK293T cells exhibited increasing luciferase expression over time with significance reached at 48 and 72 hours. Analysed using two-way ANOVA and Bonferonni post-hoc test. \*  $P < 0.05$ , \*\*  $P < 0.01$ , \*\*\*  $P < 0.001$ .

---

**CHAPTER FOUR**

**ANALYSIS OF SIGNALING PROFILES IN  
CHOLESTASIS USING SOMABIO**

---

## Somatotransgenic bioimaging to assess pathway activity in chronic liver diseases

The TGF- $\beta$ , NF- $\kappa$ B, WNT and Notch pathways function to activate relevant cell types required for the initiation and termination of the wound-healing response. They also have key roles in the liver's response to chronic injury through the activation of the normally quiescent progenitor cell compartment, instigating their proliferation and subsequent differentiation. Therefore, the use of somatotransgenic animals containing luciferase reporter cassettes/genes under the control of disease-specific response elements has the capacity to offer insight into the activity of these pathways during disease induction and progression within an *in vivo* context. Currently, analysis of liver disease consists of serial bleedings for analysis of serological biomarkers of liver function, particularly liver enzymes and total serum bile acids. Terminal analysis of animals for histological assessment of disease pathology also restricts temporal disease profiling within a single animal. The aim of the work described in this chapter is to present data on the *in vivo* validation of the aforementioned biosensors, before assessing the role of these pathways within a model of chronic biliary injury induced by bile duct ligation.

### 4.1 Results of reporter validations *in vivo*

#### 4.1.1 Monitoring of LPS-mediated inflammatory responses *in vivo* using a NF- $\kappa$ B reporter

Using a constitutively expressing construct, LNT-SFFV-JDG, and an NF- $\kappa$ B pathway activated biosensing construct, LNT-NF- $\kappa$ B-JDG, lentivirus containing each of these constructs was targeted for the liver in outbred CD1 and *tlr4*<sup>-/-</sup> mice. Administration of ultra-pure LPS resulted in a significant increase ( $p = 0.016$ ) in luciferase expression within the CD1 mice after 4 hours, whereas no significant effect was seen within the TLR4 knockout animals ( $p = 0.498$ ) (**Figure 38a**). Examining fold change over baseline, mice expressing the constitutively active LNT-SFFV-JDG showed no significant change in expression over time in the CD1 or the *tlr4*<sup>-/-</sup> mice (**Figure 38b**). Luciferase activity data is visualised in pseudocolour scaling format. This pseudocoloured heat map quantifies photonic output as photons/s/cm<sup>2</sup> with blue showing the least expression and red showing the highest photonic output.

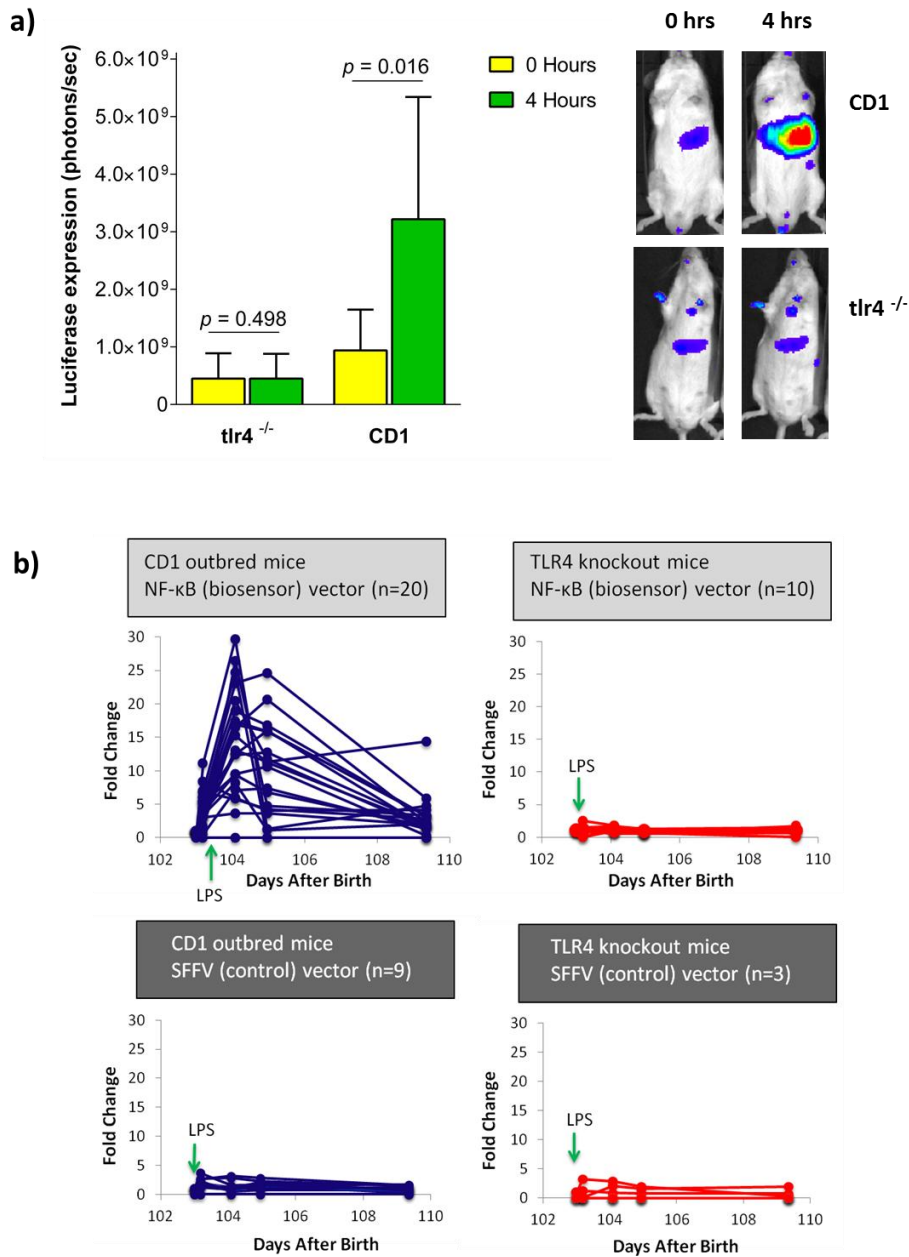


**Figure 38. Validation of NF-κB using CD1 and *tlr4*<sup>-/-</sup> mice.**

CD1 and *tlr4*<sup>-/-</sup> mice injected with LNT-NF-κB-JDG virus and imaged at 0 and 4 hours post LPS exposure. When expressed as fold change, only CD1 mice challenged with LPS showed a significant fold change in luciferase expression over baseline. b) Graphs showing outbred CD1 or *tlr4*<sup>-/-</sup> mice injected with either constitutive LNT-SFFV-JDG or LNT-NF-κB-JDG virus.

#### 4.1.2 Antagonistic abrogation of inflammatory NF-κB responses by dexamethasone

In order to show the utility of somatotropic bioluminescence imaging as a powerful tool for use in drug screening and efficacy testing, the NF-κB signalling pathway was used. This well-established model of inflammation was used in conjunction with a well-characterised anti-inflammatory steroid, dexamethasone. Animals were subjected to either LPS alone, or pre-treated with dexamethasone prior to LPS exposure. A significant NF-κB-mediated upregulation of luciferase in response to LPS was seen within 24 hours in those animals which received LPS alone, however, in stark contrast, the

animals that were pre-treated with the anti-inflammatory steroid prior to exposure were found to be protected from NF- $\kappa$ B-induced inflammation (**Figure 39a**). Pre-treatment with Dex resulted in a significant decrease in LPS-mediated response ( $p = 0.0047$ ) (**Figure 39b**).

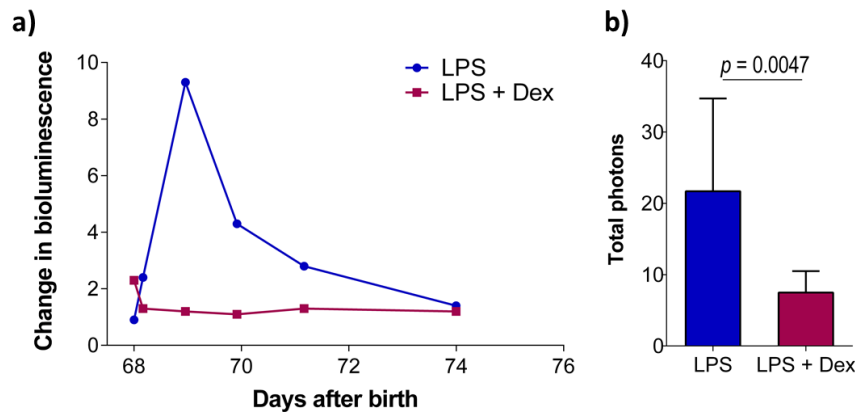


**Figure 39. Response of NF- $\kappa$ B signalling when challenged with the glucocorticoid, dexamethasone.**  
a) LNT-NF- $\kappa$ B transduced animals experience a marked increase in luciferase expression within 24 hours after receiving LPS alone, however, complete abrogation of this response was seen in those animals pre-treated with the corticosteroid, dexamethasone. b) Statistical analysis using a one-tailed t-test to compare the two groups.

#### 4.1.3 Exogenous activation of the LNT-SBE-JDG construct *in vivo* using activin A

At P0, neonatal CD1 outbred mice were injected with LNT-SBE-JDG virus. At 68 days post-birth, *in vivo* validation of this construct was performed through intravenous injection of exogenous activin A. Using this direct agonist of the SMAD 2/3 signalling pathway, there was an overall increase ( $p = 0.053$ ) in SBE-mediated luciferase expression in the animals that were given the activin A compared to those which received LPS, which is not an agonist of smad2/3 signalling. The greatest difference in photonic output was seen between the groups at 24 hours, with a t-test assuming unequal variances showing statistical significance ( $p = 0.020$ ). There was a steady decrease in expression over the following days, and a return to baseline levels 5 days post-activation.

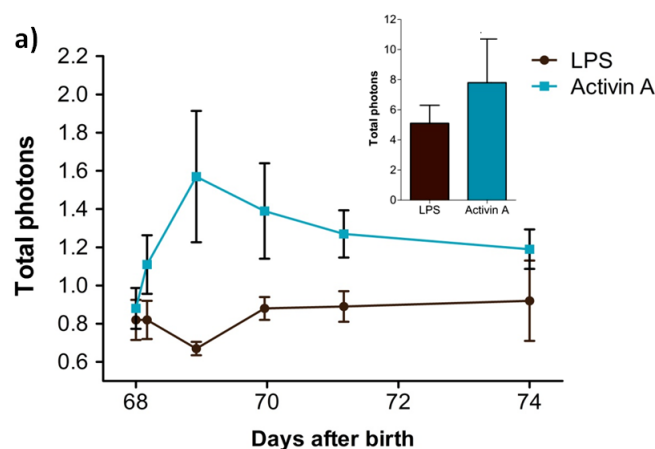


**Figure 40. Activation of pLNT-SBE-JDG *in vivo* using exogenous activin A.**  
Mice injected with LNT-SBE-JDG virus underwent either direct agonist activation using exogenously added activin a. Significant activation was obtained in activin A treated mice ( $p = 0.05$ )

## 4.2 Molecular analysis of fibrosis and virus cell-type targeting

### 4.2.1 Haematoxylin and eosin and Lilly's trichrome staining for liver morphology and fibrosis

To study signalling pathways *in vivo*, an animal model of liver fibrosis was employed. Fibrosis was induced by surgical means, with Dr. Simon Waddington performing all partial bile duct ligations. Prior to embarking on bioimaging experiments using the reporters, the development of ductular reactions and fibrosis following pBDL was confirmed.

Conventional haematoxylin and eosin (H&E) staining was performed to observe gross histological differences between the sham-operated and pBDL samples. Within the control liver sample, the large portal vein is clearly visualised, with a bile duct, containing distinctive cuboidal epithelial cells seen adjacent to the vein. Below this, the small hepatic artery is seen, completing the last part of the portal triad (**Figure 41i**). The pBDL sample showed dilation of the bile duct, the beginning of biliary hyperplasia, and the presence of ductular reactions comprised of mild mononuclear cell infiltrate and proliferating biliary cells. The periportal limiting plate, hepatocytes that usually lie adjacent to the portal tract and separate it from parenchymal hepatocytes, has been disrupted. This feature is termed piecemeal necrosis and refers to the loss of the hepatic limiting plate in response to liver damage. It is associated with lymphocytic infiltrate intruding into the adjacent parenchyma (**Figure 41ii**).

Successful pBDL results in the development of biliary fibrosis, beginning with periportal fibrosis, and progressing toward bridging fibrosis between the portal triads. Liver samples of mice 3.5 months post-pBDL were embedded, sectioned, and Lily's trichrome staining performed to detect collagen deposition, synonymous with liver fibrosis/cirrhosis following BDL surgery. This staining technique uses selective dyes of varying sizes to achieve differential staining of the tissue sections and to distinguish histological changes in the samples. The control liver showed no collagen deposition around the portal tract or within the liver parenchyma (**Figure 41iii and v**), and each of the central veins were morphologically normal. Occlusion of the bile duct is expected to result in fibrosis of the ligated lobe. Trichrome staining of the fibrosed left lobe demonstrates periportal collagen deposition in blue. Furthermore, a strong proliferative response seen as extensive biliary hyperplasia was noted by the presence of multiple biliary ductules. Portal expansion was observed with severe dilation of the bile duct and significantly increased amounts of peribiliary fibrosis seen as concentric layers of collagen deposition around the bile duct (**Figure 41iv**). Lower magnification of the liver lobe showed interlobular porto-portal bridging fibrosis along the liver septa surrounding the lobules, connecting the hepatic triads with collagenous deposits, indicative of advancing fibrosis (**Figure 41vi**).

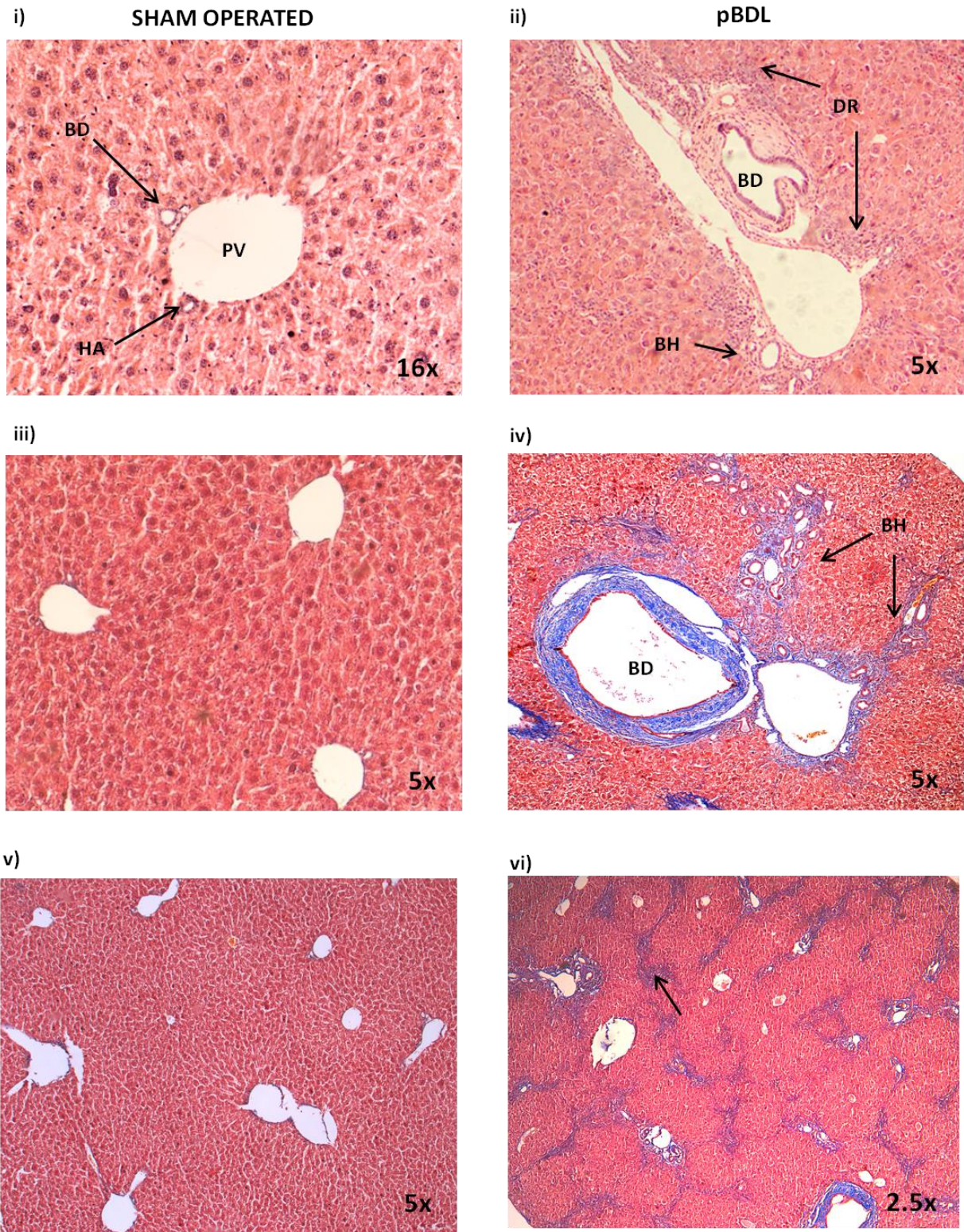
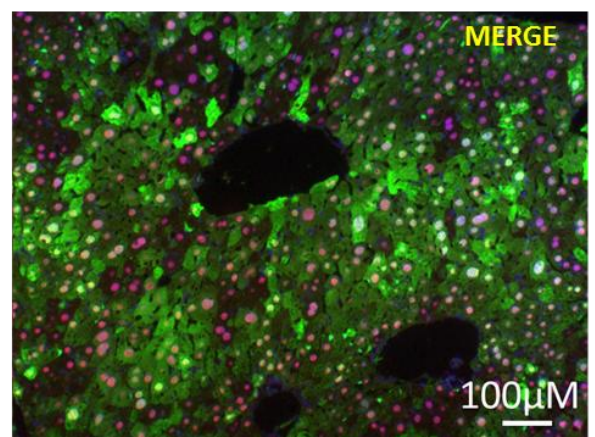
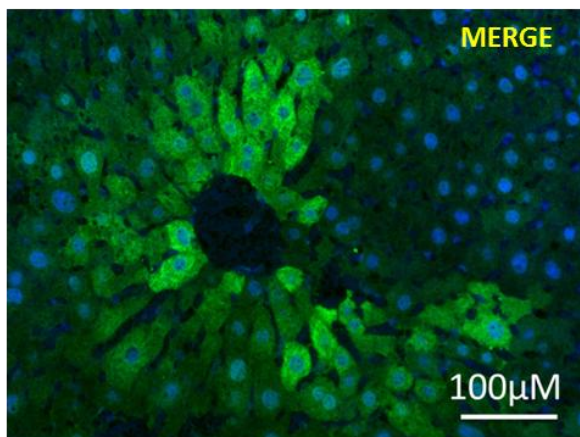
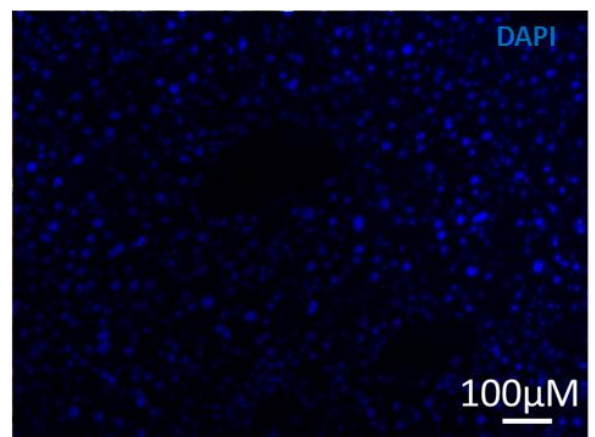
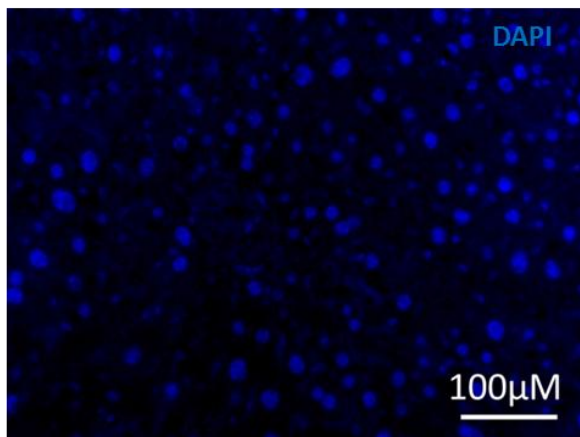
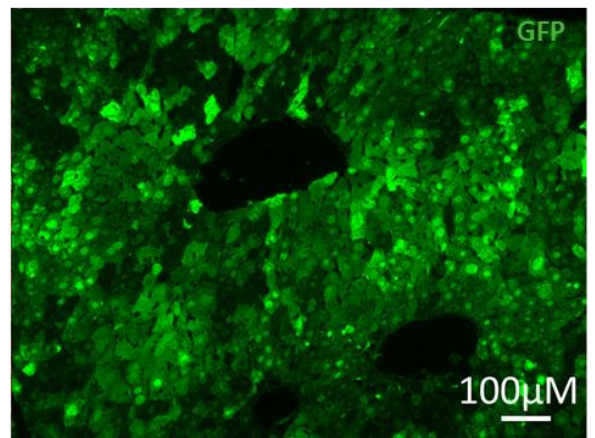
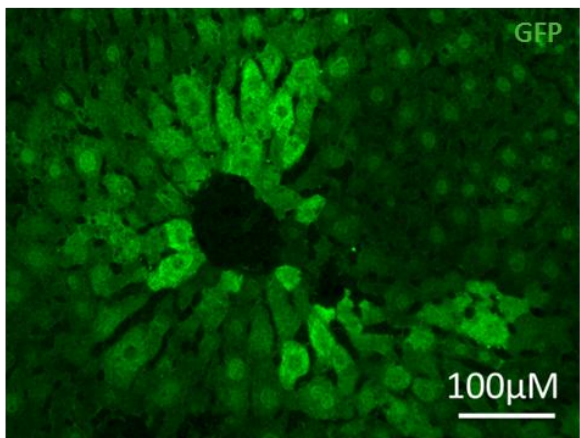
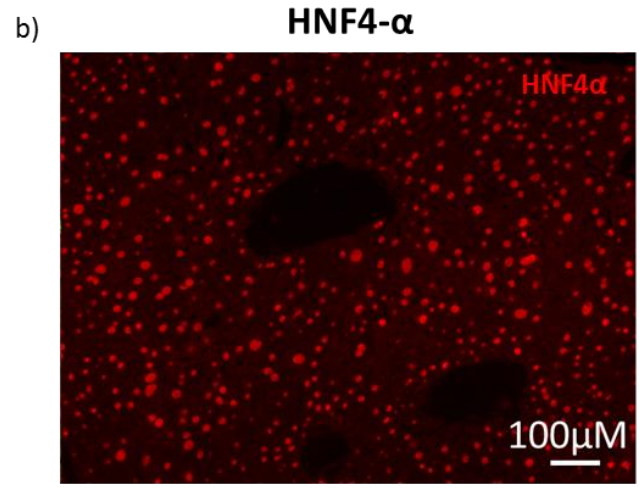
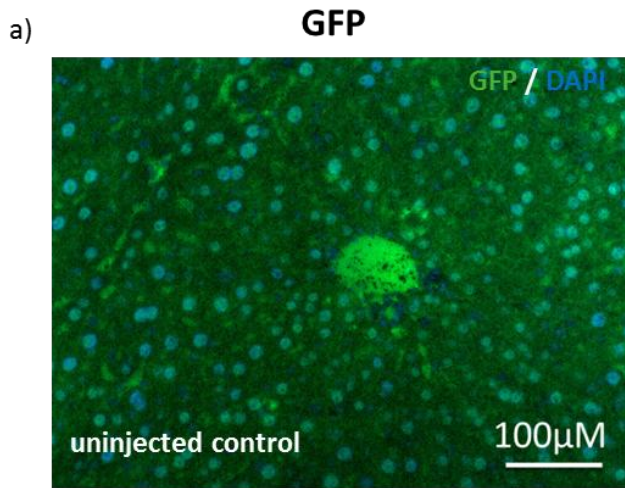


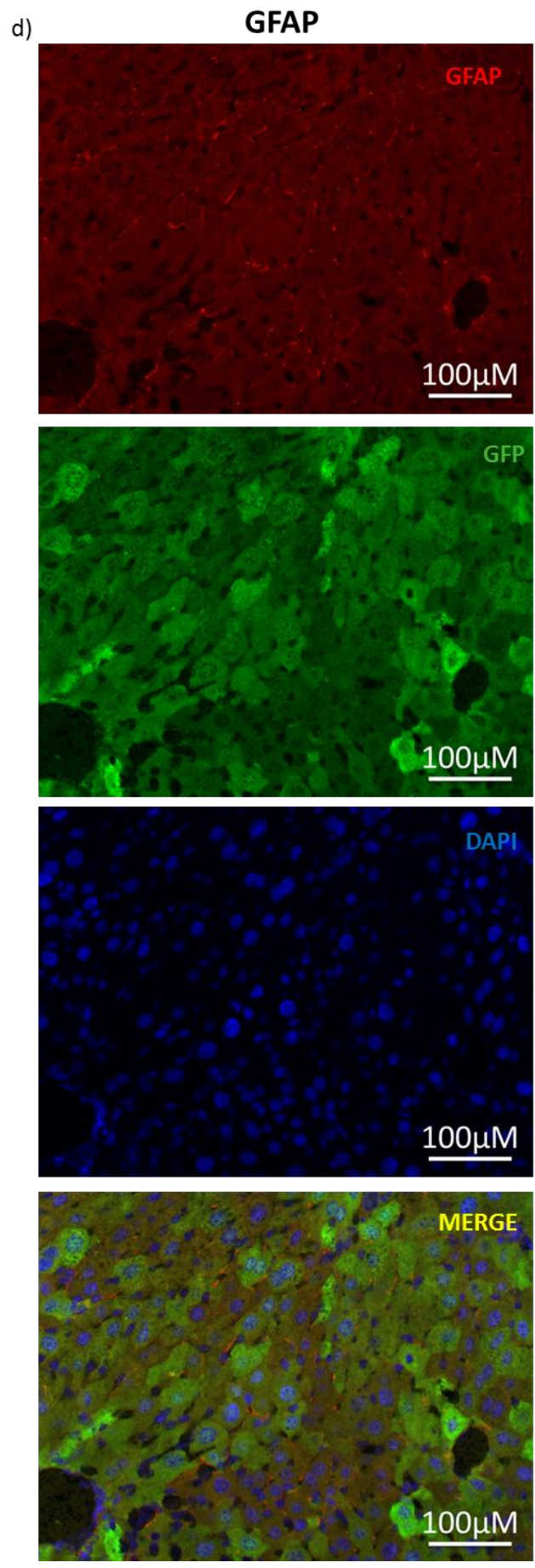
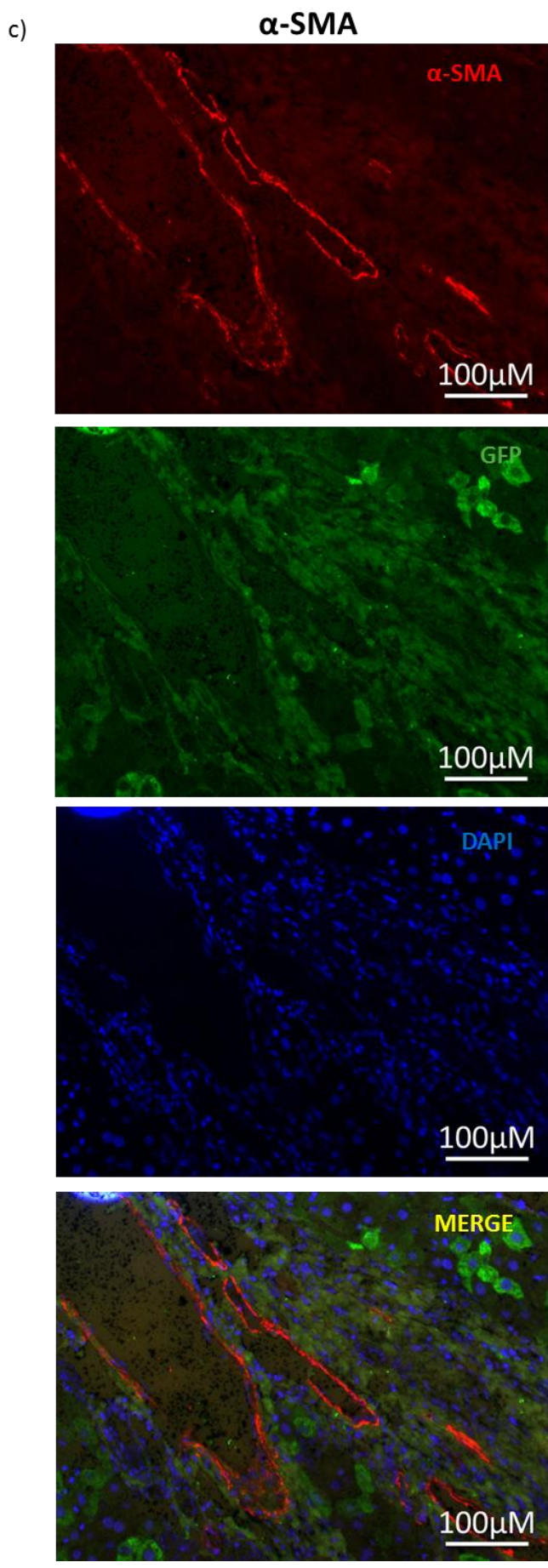
**Figure 41. H&E and trichrome staining of sham operated and pBDL livers.**

Mice livers sectioned and stained with H&E (i and ii) for histological architecture and Lilly's trichrome (iii-vi) to show the deposition of collagen (blue), nuclei (black), and cytoplasm (red). Control livers were sham operated animals while the left and right lobes were isolated from the left fibrosed lobe of a LNT-SBE-JDG injected mouse. bile duct (BD), hepatic artery (HA), portal vein (PV), biliary hyperplasia (BH), ductular reaction (DR).

#### 4.2.2 Immunohistochemical analysis of lentiviral targeting of hepatic cell types

One critical aspect of the biosensing technology is the ability to target and transduce particular organs and cell types. Immunohistochemical analysis was performed to determine the cell types being targeted in the liver when utilising VSV-g-pseudotyped lentivirus. Firstly, the levels of transduction and green background fluorescence were assessed by comparing an uninjected control to a liver that was transduced with the constitutive SFFV-JDG vector. The uninjected control showed low levels of green auto-fluorescence following 0.3% Sudan Black treatment which was used to decrease fluorescein-mediated autofluorescence known to be problematic in liver samples. The GFP-specific signal was distinct in the SFFV-JDG transduced sample and could clearly be distinguished from its uninjected counterpart (**Figure 42a**). The most prominent colocalisation was between the GFP transduced cells and the hepatocyte-specific marker HNF4 $\alpha$ . The merged image shows that a majority of the GFP positive cells contain purple nuclei produced from the dual overlay of nuclear HNF4 $\alpha$  (red) and DAPI (blue)(**Figure 42b**). Within a normal liver,  $\alpha$ -SMA is localised to the lining of the portal vein where it marks the smooth muscle of the vasculature. However, in the context of disease, it is a marker of activated myofibroblasts. In pBDL samples,  $\alpha$ -SMA was localised along the portal tracts in the stroma adjacent to the proliferating biliary cells (**Figure 42c**). Glial fibrillary acidic protein (GFAP) is also a marker of activated stellate cells. It can clearly be observed within the parenchyma adjacent to hepatocytes (**Figure 42d**). The cholangiocyte marker CK7 was seen to be expressed within the proliferating bile ducts, and GFP was limited to the region directly adjacent to this (**Figure 42e**). Pyruvate kinase isoform M2 (PKM2) is a marker of hepatic progenitor cells and stains both the cytoplasm and the nucleus where it associates with chromatin. This marker is clearly localised periportally, the region where the progenitors reside and proliferate in response to chronic cholestasis. GFP clearly does not colocalise with PKM2 as observed in the overlapping merged image, indicating a lack of progenitor cell targeting (**Figure 42f**). Confirmation of largely hepatocyte targeting of the virus was of particular importance for subsequent biosensing experiments, as the signal generated would be informative for a specific cell type and would offer an increased level of sensitivity compared to whole-organ signalling profiles.





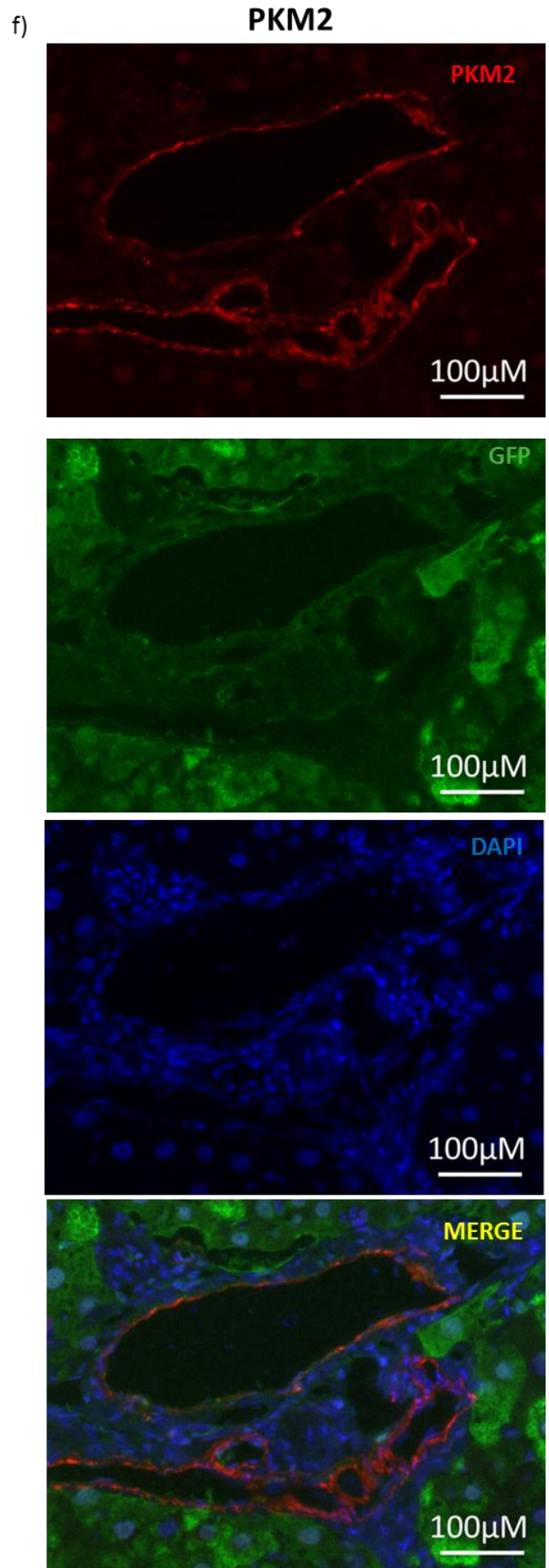
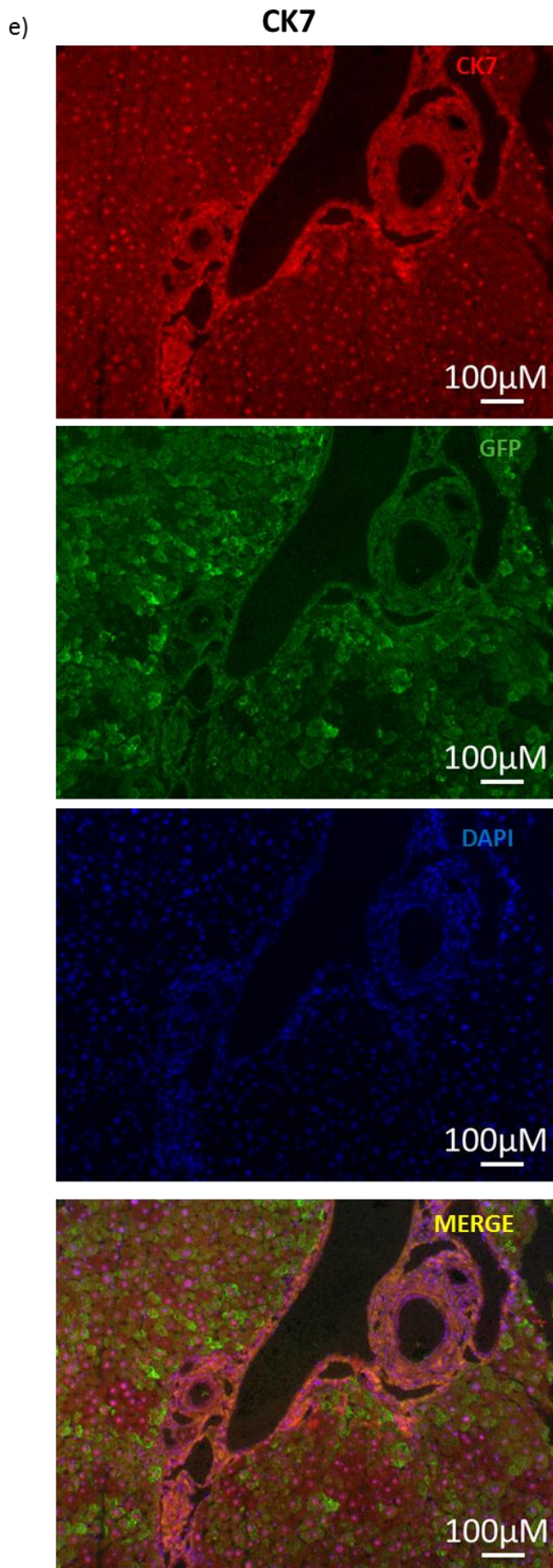


#### Figure 42. GFP colocalisation with hepatic cell types using cell-type specific markers.

Uninjected controls were used to assess background fluorescence and GFP antibody specificity. Transduction efficiency was assessed in livers injected with the constitutive SFFV-JDG virus with GFP immunofluorescence used as a marker of transduction (a). GFP was colocalised with the hepatocyte marker, HNF4 $\alpha$  (b), while it showed negative colocalisation with the activated stellate cell makers,  $\alpha$ -SMA (c) and GFAP (d), the cholangiocyte marker, CK7 (e), and the progenitor cell marker, PKM2 (f).

### 4.3 Analysis of critical pathways involved in chronic liver injury

Once each of the reporters had been successfully validated both *in vitro* and *in vivo*, their use within a biological context was assessed. The pBDL model was employed as it is a well-established model of cholestatic liver disease. Within the pBDL model, animals would express physiological levels of agonist and would require a high level of reporter sensitivity. These vectors could subsequently be developed to assess disease progression and pharmacological interventions in a host of diseases, including other types of liver disease.

#### 4.3.1 SFFV-mediated luciferase expression is unaffected by pBDL surgical procedure

Firstly, to verify that the signalling profiles obtained following pBDL were not due to the loss of signal transducing cells in response to pBDL, mice were injected with lentivirus containing the constitutively expressing LNT-SFFV-JDG vector and subsequently underwent either sham or pBDL surgery. No significant difference between the groups was noted (**Figure 43a**), indicating that deviations from basal luminescence using the biosensing reporters would be due solely to a change in luciferase signalling, and not due to the loss of cells during injury progression.

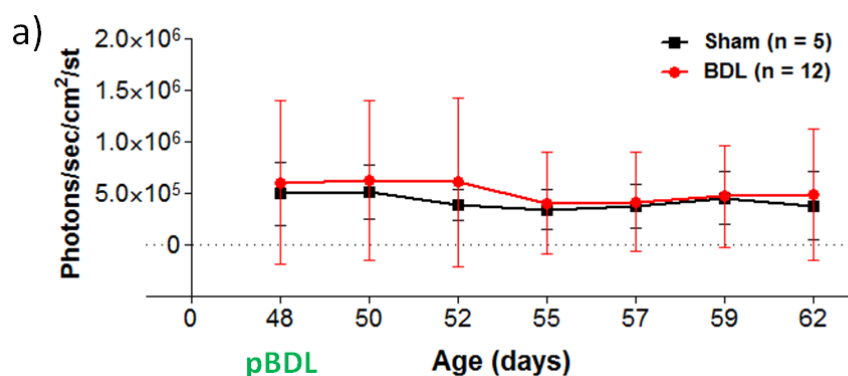


**Figure 43. Mean luminescence intensity of LNT-SFFV-JDG transduced mice with or without BDL surgery.**

Mice transduced with liver-specific LNT-SFFV-JDG virus were subjected to either BDL (red) or sham (black) surgery. Mean fluorescence intensity over baseline was plotted over time. No significant change in luciferase expression was found.

### 4.3.2 NF- $\kappa$ B activity monitoring during the acute phase of cholestasis

NF- $\kappa$ B signalling was assessed *in vivo* by injection of LNT-NF- $\kappa$ B-JDG virus into neonates. Fifty days post-birth, half of the animals underwent partial bile duct ligation surgery to induce chronic cholestasis, while the other half of the cohort underwent sham surgery, where the surgery was performed but the bile duct was not ligated. Bioimaging of the animals was assessed for 50 days during which a 33.7-fold increase in luciferase expression was seen 14 days post-surgery in the pBDL animals. Area under the curve (AUC) analysis of total photonic flux for each cohort was assessed. The mean area AUC for non-pBDL animals was 84.4 units and 621.2 units for pBDL animals. The difference in luciferase activity between the two groups was statistically significant and assessed as a t-test for the AUC analysis ( $p = 0.011$ ). Interestingly, a peak was also observed in the animals which had undergone the sham surgery, but this peak was more transient and had decreased to baseline 7 days post-surgery.

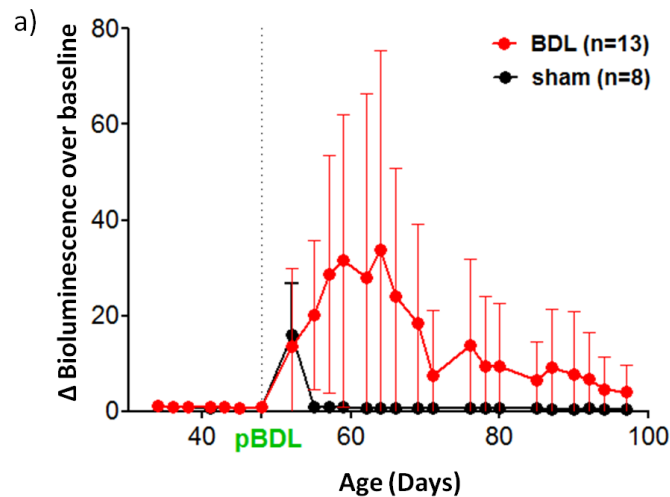


**Figure 44. NF- $\kappa$ B reporter activation in response to partial bile duct ligation model of cholestasis.** CD1 mice transduced with LNT-NF- $\kappa$ B-JDG virus underwent either pBDL (red) or sham (black) surgeries. Bioluminescent output was measured as a fold-change of the median of 3 triple time points (baseline) taken prior to disease induction. Area under the curve analysis revealed a significant increase in luciferase expression.

### 4.3.3 Smad 2/3 activation *in vivo* using fibrosis-inducing partial bile duct ligation

Another cohort of CD1 mice transduced with the LNT-SBE-JDG vector underwent pBDL or sham surgeries. At 60 days post-birth, 10 of the 21 injected mice underwent partial BDL surgery, followed by 15 imagings at several time points during the progression of chronic fibrosis (day 2, 4, 8, 11, 14, 17, 21, 24, 28, 31, 35, 38, 49, 56, 63, 71). Novel temporal TGF- $\beta$  signalling profiles were observed with the SMAD2/3 response element. Partial bile duct ligation resulted in a small, non-significant increase in light emission compared with non-operated controls (**Figure 45a**). However, a greater oscillatory amplitude was observed in pBDL mice, indicative of more dynamic TGF- $\beta$  signalling in

those animals that underwent fibrotic induction. This variation (standard deviation) was found to be significant between the two groups when analysed using a Student's T-test ( $p = 0.009$ ) (**Figure 45b**).

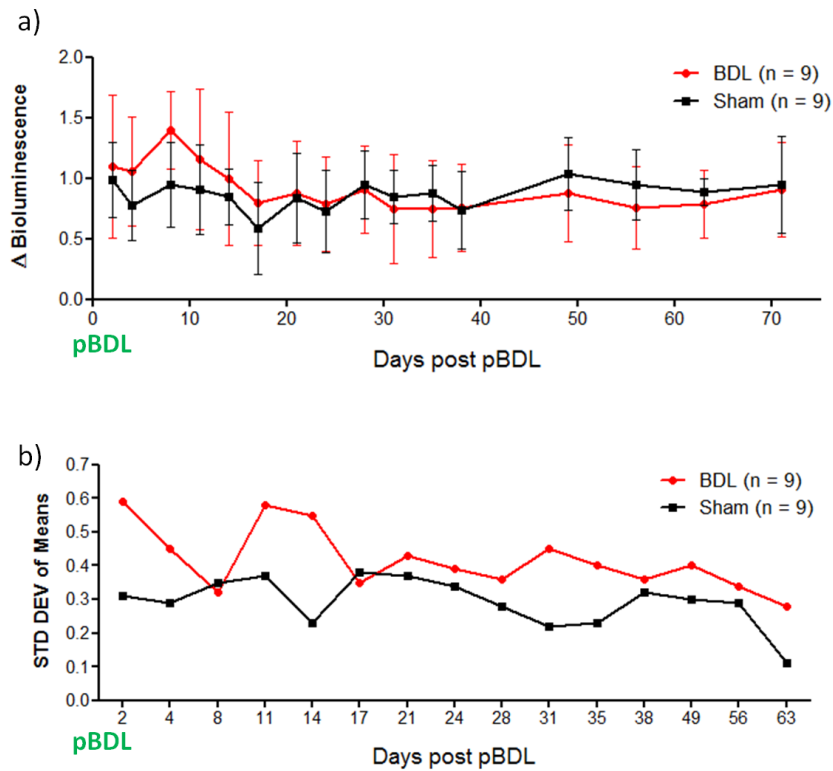


**Figure 45. Activation of pLNT-SBE-JDG *in vivo* following pBDL surgery.**

a) Mice injected with LNT-SBE-JDG virus underwent partial bile duct ligation, exacerbating fibrosis-inducing TGF- $\beta$  signalling within a biological disease model. No significant difference in means was noted. b) A difference in standard deviation was determined, indicative of the greater amplitude of luciferase signalling within the pBDL animals.

#### 4.3.4 *In vivo* assessment of GFAP expression in response to biliary injury

The activation of hepatic stellate cells results in their transdifferentiation to a myofibroblastic phenotype that expresses increased levels of glial fibrillary acidic protein (GFAP). However, immunohistochemical data indicated that the hepatic stellate cells were not be targeted by the virus, and thus would not contribute to the luciferase expression. Therefore, we determined to assess the activity of GFAP and produce a temporal profile originating specifically within hepatocytes. Neonatal mice were transduced with lentivirus containing the LNT-GFAP-JDG construct. The hepatic GFAP somatotransgenic animals were monitored for basal GFAP expression before undergoing partial bile duct ligation or sham operations 45 days post birth. From the earliest imaging time point at day 48, an increase in GFAP expression was noted ( $p = 0.06$ ). The levels of GFAP-induced luciferase expression exhibited a steady decrease over the following 3 weeks. Sham-operated animals exhibited only minimal variation for the duration of the experiment, and in contrast to NF- $\kappa$ B, did not show any signs of activation in response to the surgical procedure.

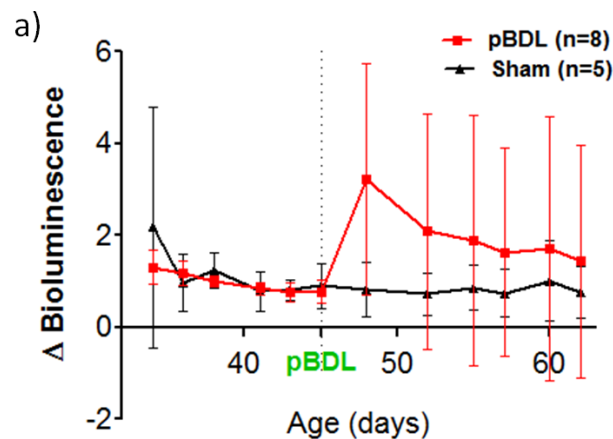


**Figure 46. GFAP activation in response to pBDL.**

CD1 mice transduced with LNT-GFAP-JDG virus underwent pBDL or sham surgeries. Animals that received a pBDL showed a fold-change increase in luciferase expression over baseline.

#### 4.3.5 *In vivo* evaluation of WNT signalling during chronic cholestasis

Using CD1 mice transduced at P0 with LNT-WNT-JDG high-titer lentivirus, partial bile duct ligation or sham surgeries were performed on 13 mice 50 days post-birth. Both sets of animals showed a decline in mean fluorescence intensity over time up to 40 days post-surgery. There was no statistically significant difference between the two cohorts at any particular time, however, from the mean graph, it appears that WNT signalling shows a trend toward being decreased within pBDL animals. The most significant point was at day 76, 24 days post BDL, with a decrease in Wnt reporter activity compared to sham operated animals ( $p = 0.094$ ) (**Figure 47a**). Terminal analysis was performed on 3 individual ligated and non-ligated bile duct livers. Gross localisation of active  $\beta$ -

catenin (non-phosphorylated) was assessed by immunohistochemistry. Interestingly, both hepatocytes and cholangiocytes expressed active  $\beta$ -catenin at the plasma membrane. The bile duct stained bright red in both samples, however, due to the biliary hyperplasia seen in bile duct ligated samples, a number of biliary ductules are stained, giving the appearance of increased  $\beta$ -catenin. Close inspection reveals that cells within the hyperplastic lesion of the biliary tree do not show nuclear accumulation of  $\beta$ -catenin. Levels of hepatocyte-associated  $\beta$ -catenin demonstrated no distinctive difference in expression levels periportal or perivenously (**Figure 47b**).

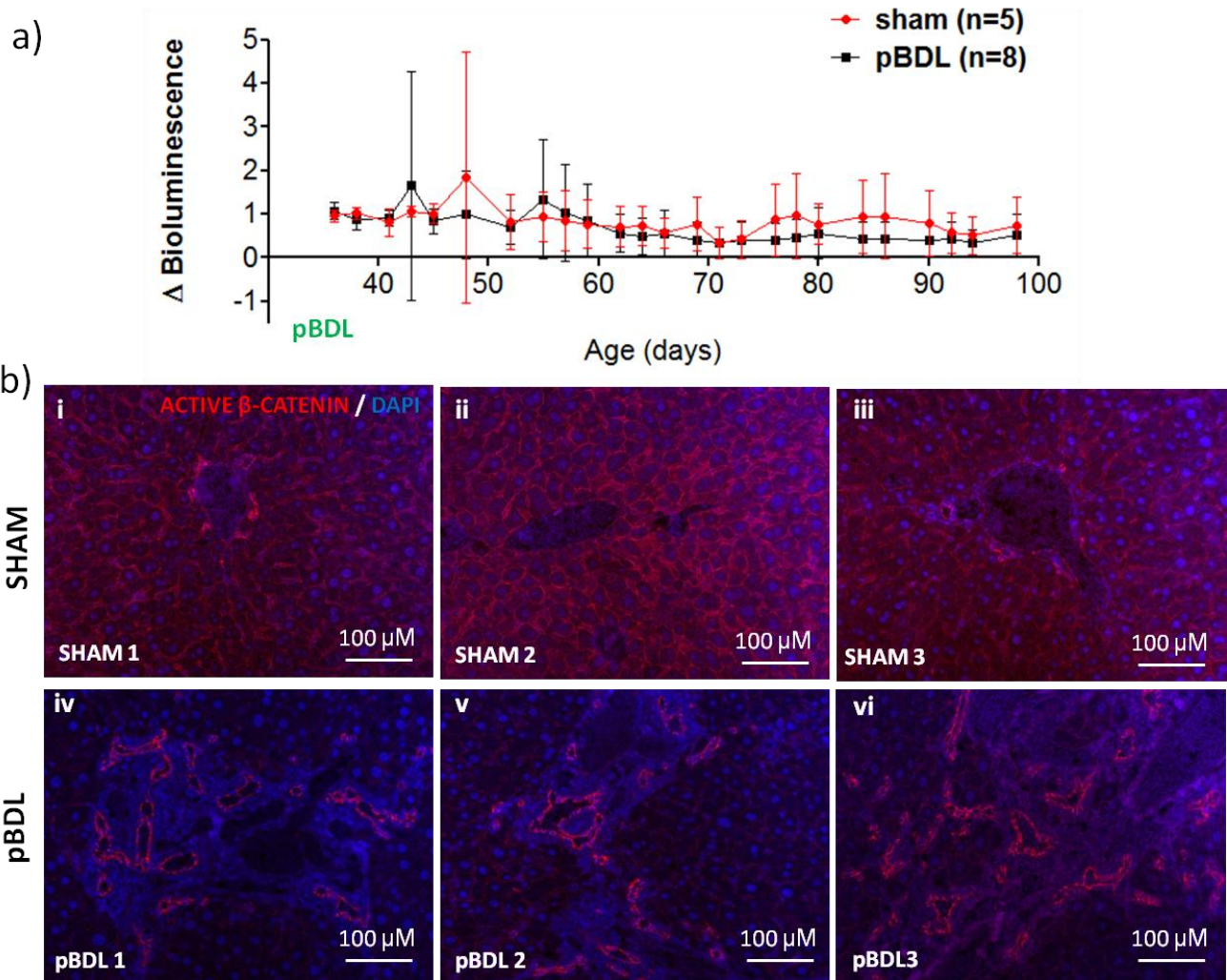


**Figure 47. Effect of pBDL on  $\beta$ -catenin signalling *in vivo*.**

a) Graph of mean fluorescence intensity of LNT-WNT-JDG transduced mice with pBDL (red) or sham (black) surgery. b) Immunofluorescence for active  $\beta$ -catenin on three individual sham and pBDL liver samples.

#### 4.3.6 *In vivo* assessment of pLNT-Notch-JDG using BDL

To elucidate the temporal profile of Notch signalling during the course of chronic biliary obstruction, the LNT-Notch-JDG virus was injected into CD1 PO neonates. At 52 days post injection, partial bile duct ligation surgery was performed on 10 mice and sham operation carried out on 5 mice followed by assessment of luciferase expression in response to chronic bile duct obstruction over time. pBDL animals showed a trend of decreased luciferase expression over time (**Figure 48a**). Histologically, no visual difference in the levels of activated Notch intracellular domain (NICD) expression levels was observed between the two groups (**Figure 48b**). NICD expression appears to be localised to the plasma membrane within the biliary epithelia, while expressing low levels of nuclear staining within the hepatocytes.

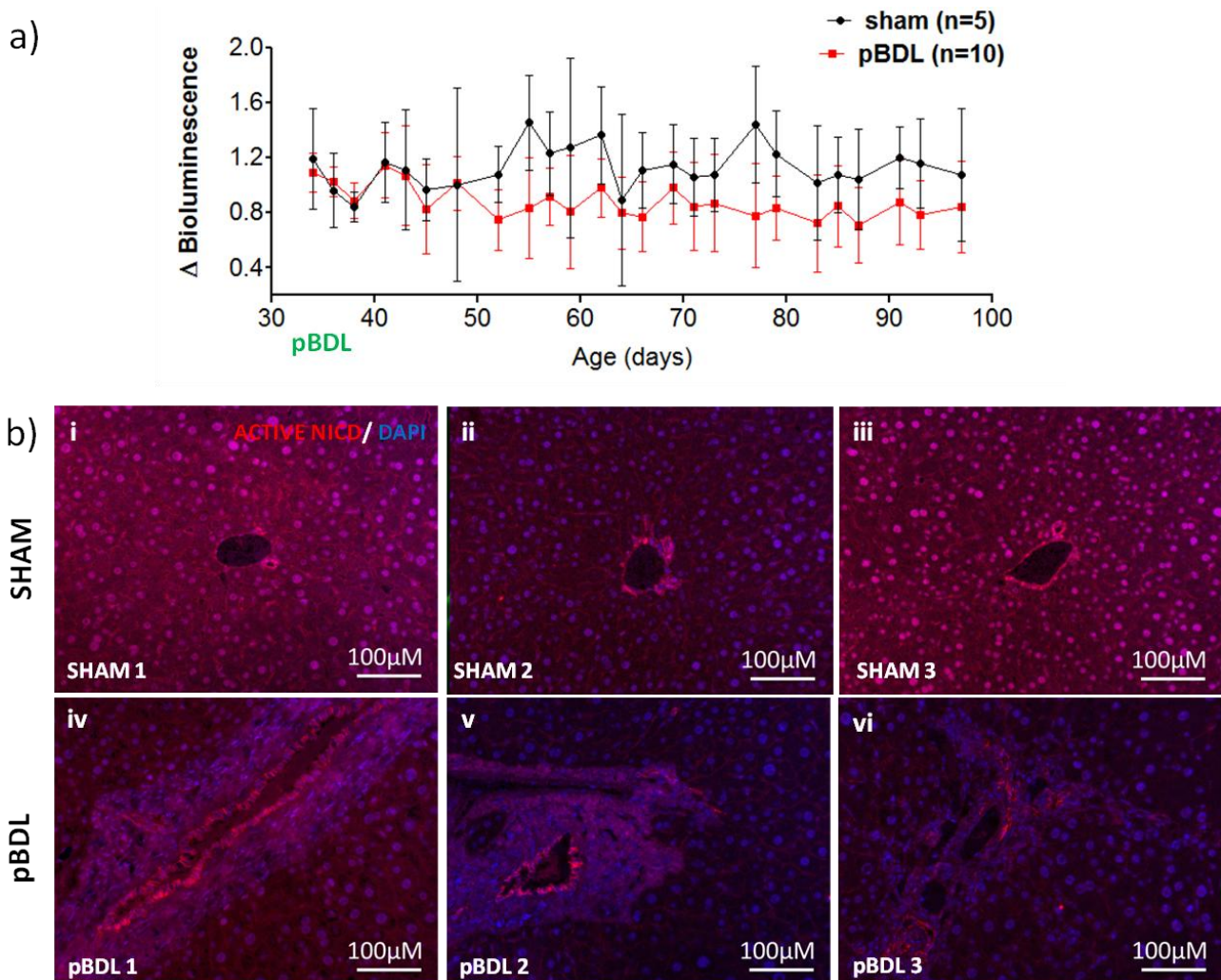


**Figure 48. Mean fluorescence intensity and immunofluorescence of LNT-Notch-JDG transduced mice with or without BDL surgery.**

a) Mice transduced with liver-specific LNT-Notch-JDG virus were subjected to either BDL (red) or sham (black) surgery. Mean fluorescence intensity over baseline was plotted over time. b) NICD-specific antibody staining in 3 individual livers from sham or pBDL operated mice.

---

**CHAPTER FIVE**

**HEPATIC PROGENITOR DIFFERENTIATION**

---

## Introduction

Following the *in vivo* interrogation of various pathways, further investigation into the role of Wnt and Notch signalling was performed *in vitro*. While the *in vivo* data demonstrated that Wnt and Notch signalling in mature hepatocytes was not affected during acute cholestatic disease, the role of these pathways within the differentiation process was subsequently interrogated using an *in vitro* model. Genetic and chemical manipulation of a progenitor cell line was predicted to give more insight into the role of these pathways as progenitor cells differentiate into cholangiocytes and hepatocytes.

Progenitor cells are the unique cells that reside within the Canal of Hering and are activated to massively increase their proliferative capacity in response to chronic injury. Their attractiveness in regenerative medicine is their ability to differentiate into either hepatocytes or cholangiocytes, dependent on the mode of injury. Expression of WNT signalling within the progenitors has been proposed to drive them toward a hepatocyte lineage, whereas increased expression of Notch signalling determines their biliary lineage. The therapeutic potential of these bipotent cells is further increased by the ability of these particular pathways to be modified, thereby harnessing a patient's own regenerative capabilities to assist hepatic regeneration. To further investigate the pathways involved in the differentiation of hepatoblasts an *in vitro* model is required. The bipotent HepaRG cell line, capable of differentiating into both cholangiocytes and hepatocytes can be used as a platform in which to study both differentiation potentials using defined media protocols. Furthermore, genetic manipulation of this cell line can give further insight into triggers which could affect each of the cellular lineages. In 2014, Dianat *et al.* published a protocol to differentiate HepaRG cells along the cholangiocyte lineage using 3 components, IL-6, sodium taurocholate, and sodium butyrate<sup>224</sup>. Their data suggest that the use of this differentiation protocol results in an enrichment of cholangiocyte-like cells from bipotent HepaRG cells. Using this novel described differentiation protocol, the aim of the subsequent experiments in this chapter was to determine whether cholangiocyte and hepatocyte populations could be enriched for using culture conditions and genetic manipulation of the HepaRG cell line. This enrichment was compared to the industry standard of hepatocyte differentiation of HepaRG cells using the addition of 2% DMSO to the culture medium.

## 5.1 Results of HepaRG differentiation through media composition and genetic modulation

### 5.1.1 Temporal reporter gene expression during alternative differentiation protocols

Progenitor HepaRG cells were transduced with lentivirus containing either LNT- $\alpha$ 1AT-NLuc, LNT-Notch-NLuc, or LNT-WNT-NLuc. To control for cell number, a second lentiviral vector was used to transduce the cells, namely LNT-SFFV-Vluc, that constitutively expresses the secreted luciferase vargula. The  $\alpha$ 1AT reporter contains a hepatocyte-specific response element and would be informative for relative levels of hepatocytes in each of the cultures. Protocol 1 was the standard

differentiation protocol for hepatocytes using 2% DMSO, while protocol 2 used the Dianat protocol that included IL-6, sodium taurocholate, and sodium butyrate in the differentiation medium. Using the dual secreted luciferase system, media was harvested and analysed every 2 days. For all reporters, both the cholangiocyte-associated Notch reporter and the hepatocyte-associated reporters showed increased levels of expression in the 3-component protocol compared to day 0. By day 4, prior to dual treatment with sodium taurocholate and sodium butyrate, all protocols showed a peak in expression for protocol 2. Using protocol 1, generally known as a hepatocyte-inducing protocol,  $\alpha$ 1AT did not show an increase in expression, but rather decreased after day 4 to a final value of 8% of the starting expression. Notch reporter activity showed a modest peak early on at day 4, but this decreased over time and also decreased to 15% of its initial value. Lastly, WNT expression mimicked  $\alpha$ 1AT expression with relatively stable expression until day 4, after which there was a rapid decrease to a quarter of its expression 2 days later at day 6, which further declined to 9% of its initial value.

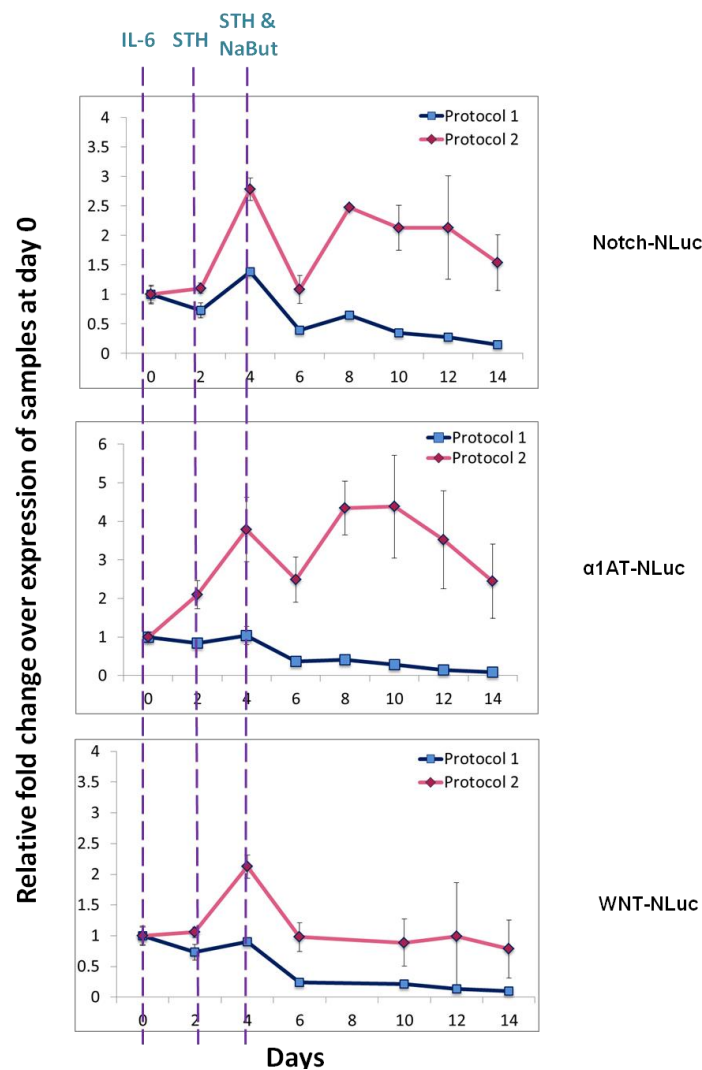


**Figure 49. Reporter gene analysis during protocol 1 and protocol 2 differentiation.**

The Notch,  $\alpha$ 1AT, and WNT reporter cell lines all showed an increase in expression levels using protocol 2 over protocol 1. All protocols exhibited a peak at day 4.

### 5.1.2 Phenotypic, qualitative, and quantitative assessment of differentiation protocols

Despite basal culture conditions of protocol 1 and protocol 2 being different, in that protocol 2 has lower levels of serum, zinc, and hydrocortisone in comparison to protocol 2, the cells appeared morphologically similar at the start of the experiment and no distinct differences could be seen. Following 2 weeks of differentiation, the cells treated with DMSO showed an elongated morphology, while the cells that had undergone protocol 2 were more densely packed and more triangular in shape. Within the second culture using protocol 2, there were some sparse collections of denser cell colonies which appeared smaller in size, presumably consisting of hepatocyte-like cells (**Figure 50**). These hepatocyte-like cell clusters were absent from the protocol 1 culture, and thus a more in-depth analysis using immunohistochemistry and qPCR was carried out (**Figure 51**).

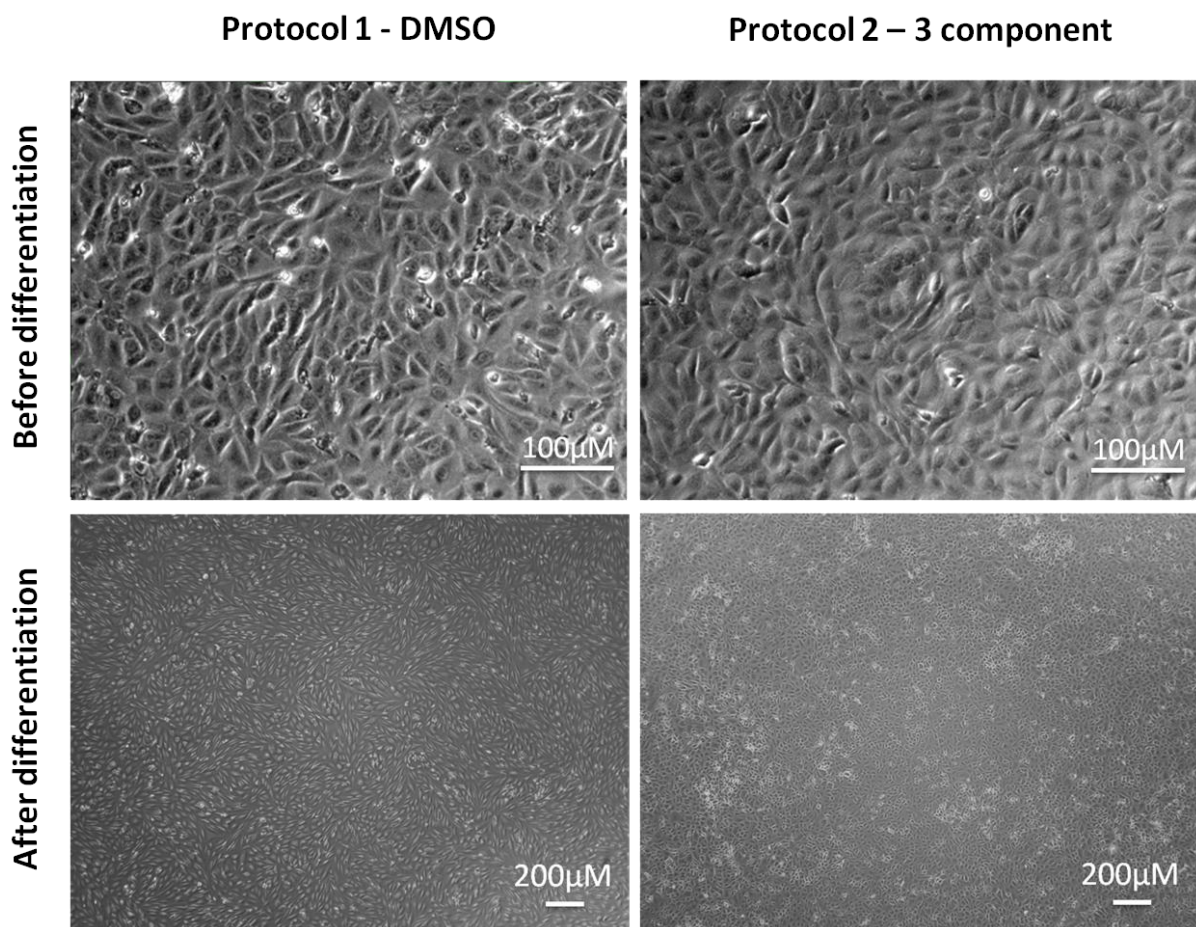


**Figure 50. Microscopic phase images of HepaRG cells using protocol 1 and 2.**

HepaRG cells were morphologically the same prior to differentiation. Following differentiation, protocol 1 resulted in morphologically distinct cells which were elongated in comparison to those which had undergone differentiation using protocol 2.

Immunohistochemical staining for the cholangiocyte marker, CK19, and the hepatocyte markers, HNF4 $\alpha$  and albumin all showed an increase in protocol 2 compared to protocol 1 (**Figure 51a**). To determine the relative amounts hepatocyte- and cholangiocyte-like cells in each of the cultures and to corroborate the data obtained from the immunohistochemical analysis, qPCR was performed for cell-

type specific markers. Albumin is a well-established marker of hepatocytes, while osteopontin and HNF-1 $\beta$  are cholangiocyte markers. The average fold change for triplicate values for protocol 1 was 22.36, 0.34, and 0.53 for albumin, osteopontin, and HNF-1 $\beta$  respectively, indicating an increase in hepatocyte marker expression and a decrease in cholangiocyte markers compared to undifferentiated HepaRG progenitor cells. The relative fold-change for the same markers using protocol 2 were 32.86, 5.20, and 2.29 indicating that both hepatocyte and cholangiocyte markers were increased utilising this protocol (**Figure 51b**).

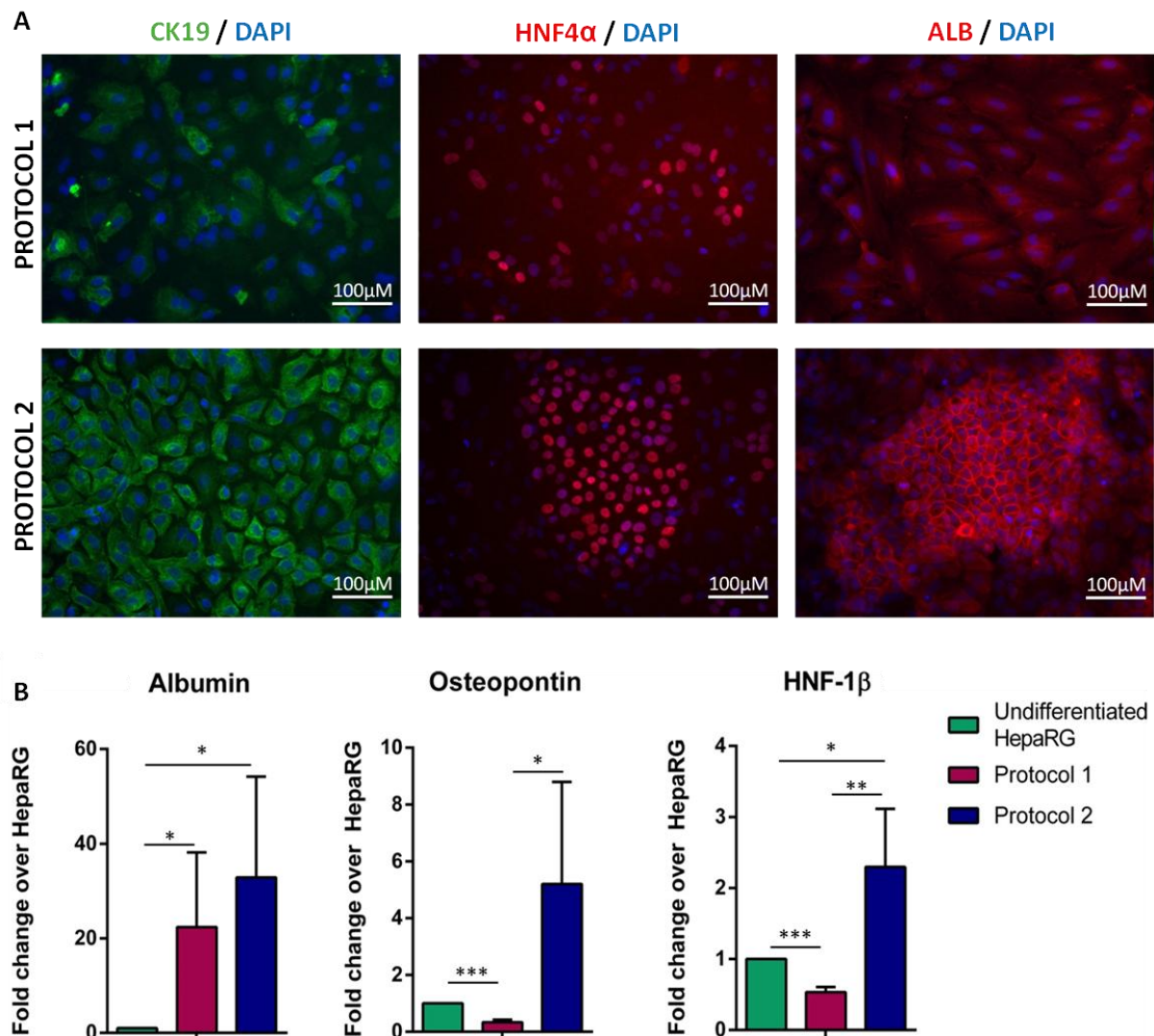


**Figure 51. Immunohistochemical and qPCR analysis of protocol 1 and protocol 2.**

a) The cholangiocyte marker CK19, and the hepatocyte markers HNF4 $\alpha$  and albumin were all comparatively higher expressed in protocol 2 than protocol 1. b) Relative expression of albumin, osteopontin and HNF-1 $\beta$  were assessed, with protocol 2 showing increased hepatocyte and cholangiocyte markers compared to protocol 1. Statistical significance determined by one-way ANOVA. \* P < 0.05, \*\* P < 0.01, \*\*\* P < 0.001.

### 5.1.3 Assessing the modulation of Notch signalling on differentiation potential

Notch signalling plays a fundamental role in the differentiation of cholangiocytes during liver development and its activation within hepatic progenitor cells via cell-to-cell interactions with stellate cells has been proposed to induce cholangiocyte differentiation. The effect of Notch modulation on

differentiation potential was assessed through Jagged-1 and Numb overexpressing HepaRG cell lines, termed HepaJag and HepaNumb respectively. Following their growth to confluence, the cells underwent differentiation protocol 1 or 2, with phase microscopy used to assess gross morphological and whole-culture differences (**Figure 52**). HepaNumb using protocol 1 yielded the least hepatocyte-like clusters, while interestingly showed the most hepatocyte clusters within protocol 2. The HepaJag culture using protocol 1 displayed increased levels of hepatocyte-like clusters when compared to its HepaNumb counterpart. A further increase in colony formation was noted when HepaJag cells underwent protocol 2 differentiation. These experiments further confirm that protocol 2, utilising IL-6, sodium taurocholate, and sodium butyrate results in more hepatocyte-like cells over the conventionally used DMSO protocol. Moreover, the cells surrounding the hepatocyte-like cells appear phenotypically more like cholangiocytes. Given the poor induction potential of protocol 1 for cholangiocytes, all further studies were conducted using protocol 2 as it is a far superior model for studying progenitor cell differentiation in response to cholestatic liver disease where the progenitor cell niche is primed for cholangiocyte differentiation and regeneration.

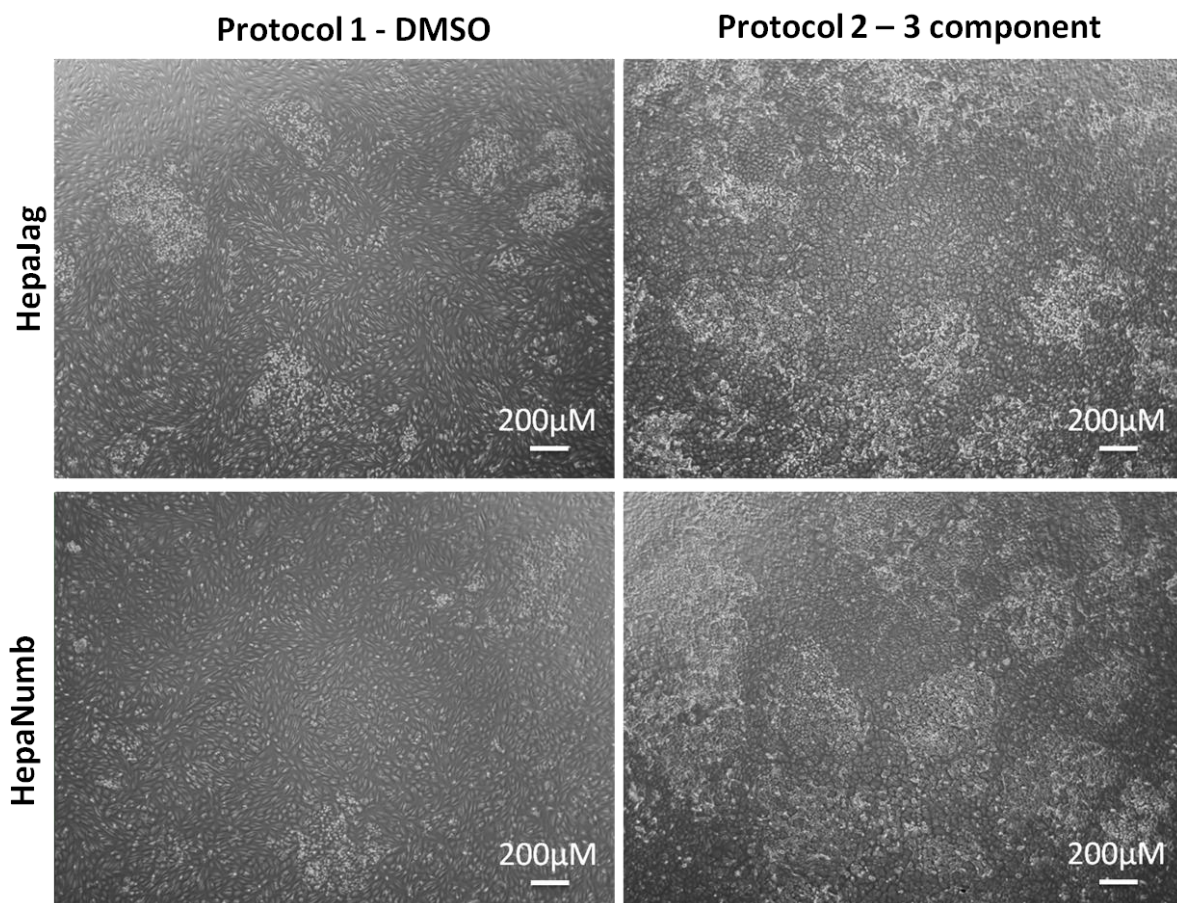


**Figure 52. Differentiation potentials of HepaJag and HepaNumb cell lines in response to variable differentiation protocols.**

Jagged-1 and Numb overexpressing HepaRG cell lines were subjected to each of the protocols. The HepaNumb cells in protocol 1 yielded the lowest hepatocyte differential potential, while the same cells in the second protocol yielded the highest potential to form hepatocyte-like cells.

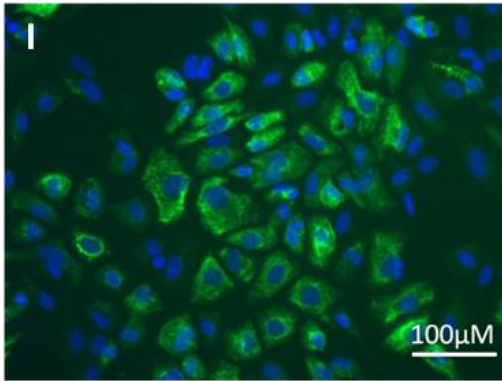
Comparison of the differentiation propensities of HepaJag (**Figure 53a**) and HepaNumb (**Figure 53b**) cell lines that had undergone protocol 2 differentiation was performed. Cells were subjected to immunohistochemistry for key markers of cholangiocytes and hepatocytes. While data presented was not quantified, a general qualitative analysis of the cultures as a whole was undertaken. Representative images are presented for each marker for each condition. HepaJag showed increased intensity staining for the cholangiocyte markers CK19 (**I**) over HepaNumb, while CK7 (**II**), a marker of more mature cholangiocytes appeared to show little difference between the cultures. This indicates that the cholangiocytes within this culture may still be immature. Conversely, HNF4 $\alpha$  (**III**) and albumin (**IV**) showed decreased levels of staining within the HepaJag compared to the HepaNumb sample which contained many more positively stained cells outside of the colony structures. Albumin expression within the HepaJag culture showed almost mutually exclusive staining of GFP and albumin, indicative of a lack of JAGGED1 expression within the albumin-expressing colony. Interestingly, SOX9 (**V**) expression was found to be highest within colony like structures in both cell lines, with lower expression seen in JAGGED1 expressing cells, as indicated by low levels of colocalisation of GFP and SOX9. The differentiation of bipotent progenitors towards hepatocytes is usually associated with an increase in *NUMB* expression, resulting in decreased accumulation of nuclear NICD. However, it appears that the hepatocyte colonies exhibited increased NICD staining (**VI**) compared to the cholangiocytes on the periphery of these colonies. Active  $\beta$ -catenin staining (**VII**) resembled that seen within the immunohistochemistry samples obtained from pBDL mice, with distinct plasma membrane staining that was significantly more intense within the hepatocyte colonies. There was also punctate nuclear staining of cells within the colonies that was not observed in the cholangiocyte cells. Lastly, acetylated  $\alpha$ -tubulin (**VIII**), a marker of primary cilia seen on cholangiocytes and not hepatocytes, did not detect ciliary structures. However, since acetylated tubulin also stains cytoskeletal acetylated tubulin and the level of acetylation differs in cell types dependent on tubulin deacetylase activity, it was intriguing to note that the cholangiocytes stained poorly for acetylated  $\alpha$ -tubulin, while the hepatocyte-like colonies exhibited intense staining. Furthermore, the colonies within the HepaJag culture displayed strong perinuclear staining, while those colonies within the HepaNumb culture displayed more dispersed cytoplasmic staining.

Overexpression of *JAGGED1* was confirmed through qPCR analysis of the downstream target, *HEY1*. HepaJag cells showed a 655.20 fold increase over undifferentiated HepaRG cells, while HepaNumb showed a fold-change of only 3.29 over undifferentiated cells. This is a decrease in expression from a fold-change of 243.04 seen in unmodified HepaRG cells which underwent protocol 2 differentiation, indicating that Numb decreases Notch signalling. Furthermore, qPCR of HepaJag cultures for the cholangiocyte markers Sox9, Osteopontin, and HNF1- $\beta$ , all showed increased levels over the HepaNumb cell line. Contrastingly, albumin was shown to be increased in the HepaNumb cell line compared to the HepaJag cell line (**Figure 53c**).

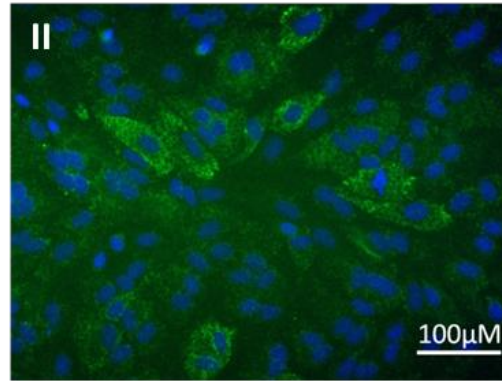
A

HepaJag differentiated using protocol 2

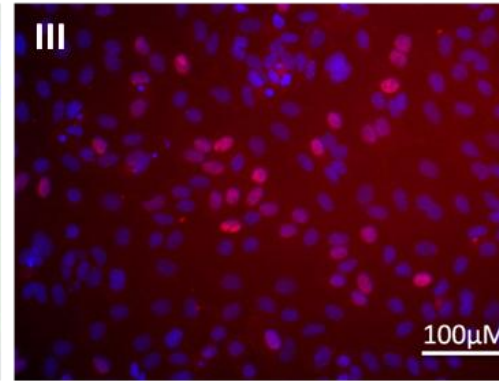
CK19 / DAPI



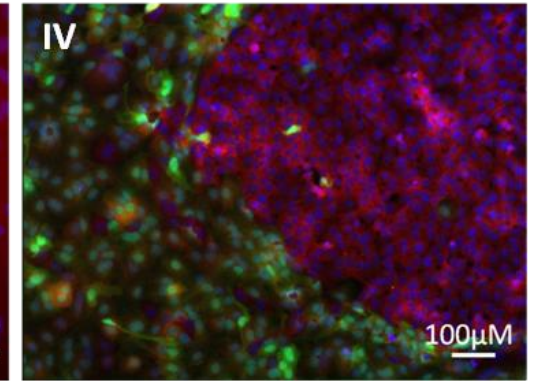
CK7 / DAPI



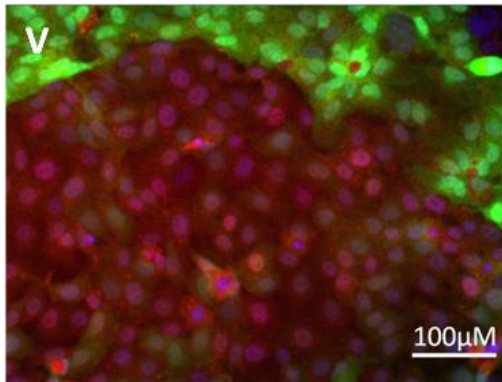
HNF4- $\alpha$  / DAPI



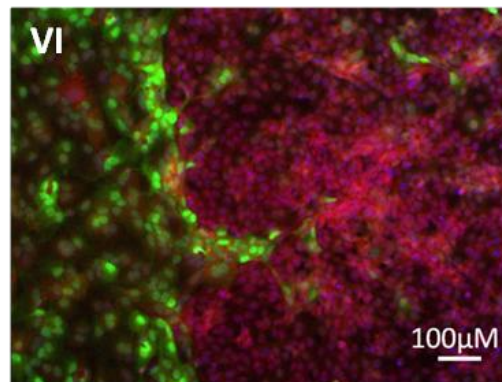
GFP / ALB / DAPI



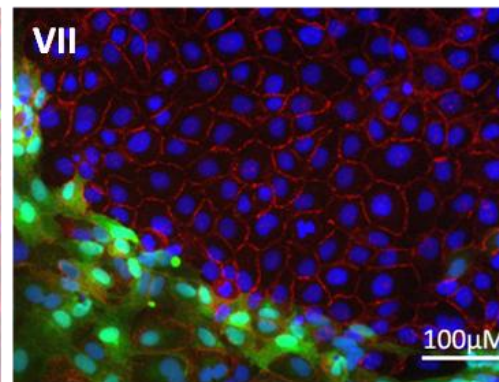
GFP / Sox9 / DAPI



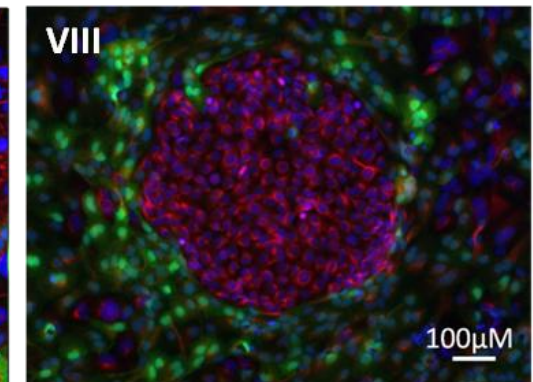
GFP / NICD / DAPI



GFP /  $\beta$ -cat / DAPI

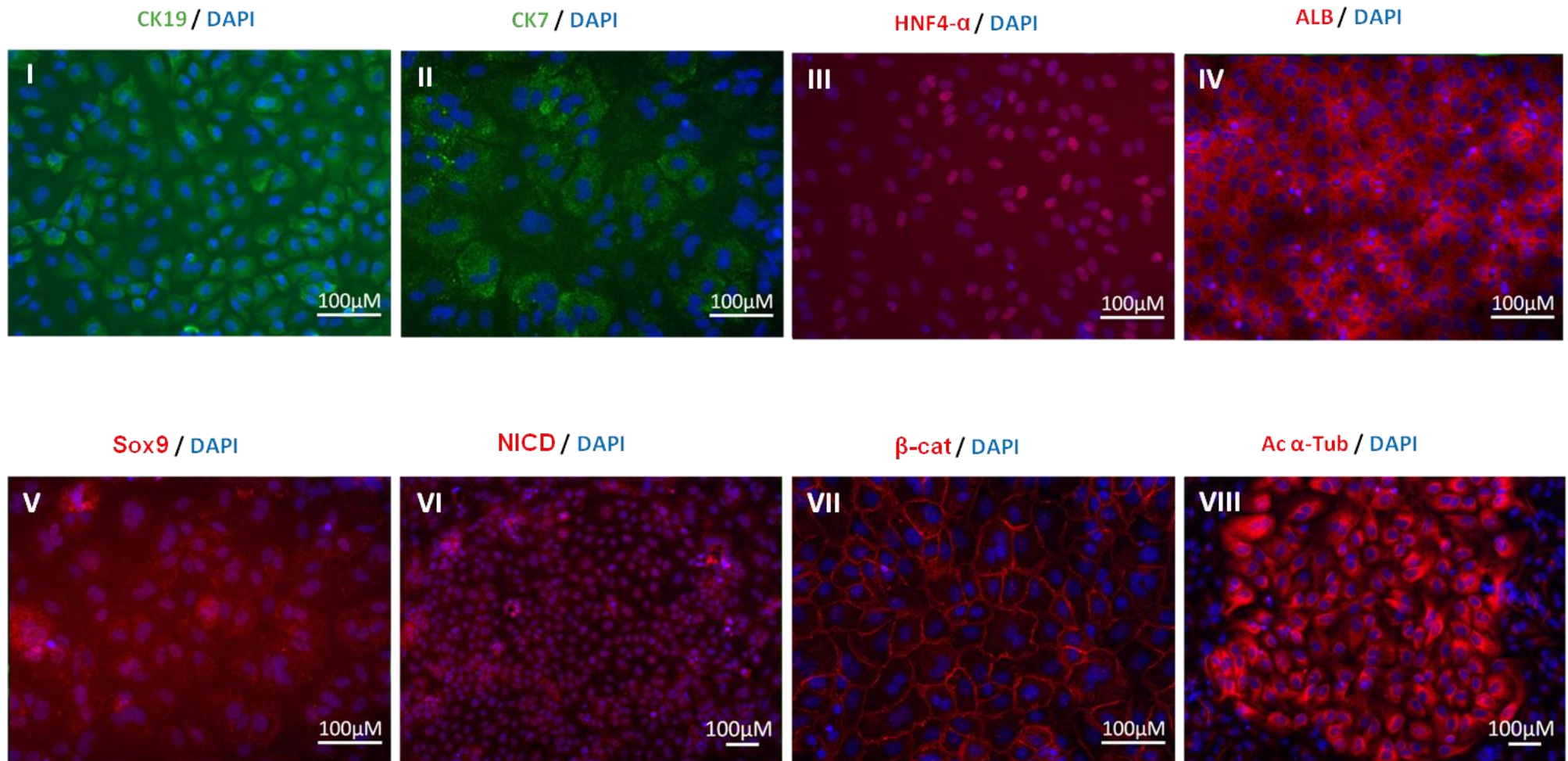


GFP / Ac  $\alpha$ -Tub / DAPI



B

HepaNumb differentiated using protocol 2



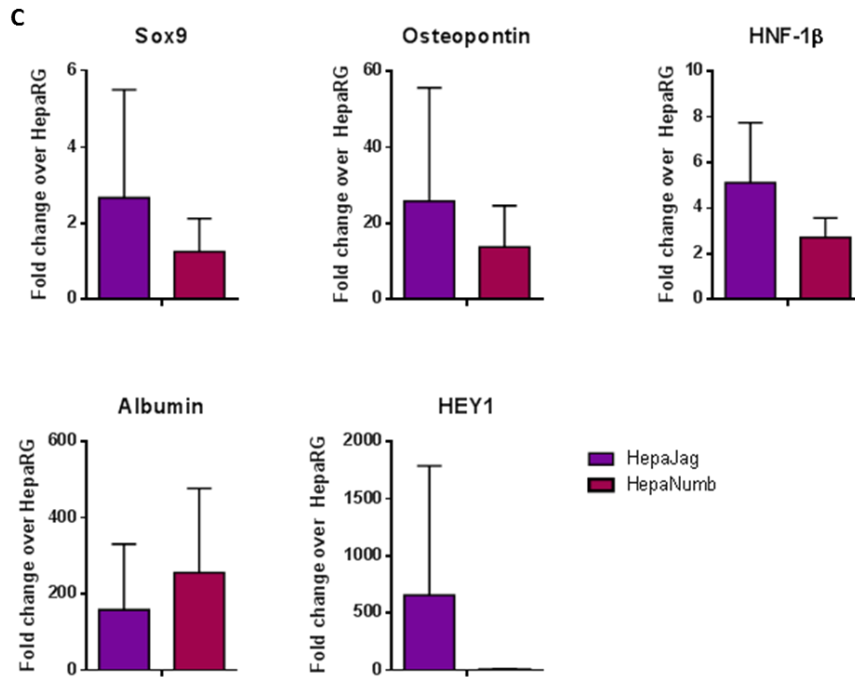


**Figure 53. Immunohistochemical and qPCR analysis of HepaJag and HepaNumb cell lines in response to protocol 1 and 2.**

a) Immunohistochemistry of HepaJag showed increase CK19 expression, while b) HepaNumb immunostaining showed increased staining for the hepatocyte markers HNF4 $\alpha$  and albumin. c) Although no points were statistically significant, qPCR analysis confirmed a trend towards increased cholangiocyte expression in Jagged overexpressing cells using Sox9, osteopontin, and HNF-1 $\beta$  markers, while HepaNumb demonstrated an increase in hepatocyte expression using albumin. HEY1 exhibited increased levels of expression in HepaJag cells. All samples expressed as fold change  $\pm$  SD over undifferentiated HepaRG cells. Statistical significance determined by two-way Anova corrected for multiple testing using Bonferroni.

---

**CHAPTER SIX**

**CRISPR/CAS9 GENOME EDITING OF SOX9**

---

## Introduction

The determination of factors which trigger hepatogenic differentiation is necessary for future development of liver cell therapies. In the previous chapter, media composition and Notch modulation were shown to definitively affect the differentiation potential of HepaRG cells, however, data increasingly suggests that Sox9 also plays a pivotal role in differentiation following hepatic injury. The role of Sox9 during embryogenesis and ductulogenesis is now well established, but its role in the process of differentiation following biliary injury is still under investigation. The use of HepaRG cells *in vitro* is used to mimic the ductular reaction in which the hepatic progenitors proliferate expansively and differentiate. Understanding the mechanistic role that a pathway contributes to a biological process is achievable through target gene validation. One of the most valuable means of validation is through disruption or overexpression of a gene within a cell culture setting or within a whole organism. This enables the elucidation of the role of a particular gene with regard to developmental processes and disease initiation, perpetuation, and resolution. Many advances in technologies have facilitated the way in which genetic manipulations are achieved. The use of overexpression vectors using transient transfection or viral delivery for long-term expression offers insight into gain-of-function roles of a gene. The use of short-interfering RNAs (siRNAs) or short hairpin RNAs (shRNAs), which reduce the expression levels of a protein through RNA interference, have also been used with much success<sup>273</sup>. The efficacy, however, is extremely variable, and levels of knockdown may not be sufficient for phenotypic or functional perturbation, and complete knockout is even less feasible. Therefore, modification of expression levels at the genomic level remains the method of choice to overcome the difficulties of gene function abolition.

Endonucleases are molecular “scissors” which have the ability to cleave DNA and cause the formation of insertions or deletion which, in the absence of suitable template DNA, results in gene disruption and knockout. Alternatively, double-stranded DNA breaks can be repaired by homology-directed repair. Site-specific nucleases can be used to cleave the DNA and permit exogenous template DNA to be substituted for genomic DNA. The latest, and undoubtedly mostly widely-used genome editing tool currently, is the CRISPR (clustered regularly interspaced short palindromic repeats)-Cas (CRISPR-associated) system. The ease of development of a targeting construct, specificity of targeting and efficiency of cleavage<sup>274</sup> has seen this technology come to considerable prominence in molecular research. Modifications of the CRISPR/Cas system are constantly being evaluated to increase the utility of this revolutionary technology for use within translational medicine<sup>275</sup>.

Given the advantages of genome editing, a CRISPR/Cas genomic knockout strategy was employed to determine the effect of *SOX9* ablation on progenitor status and differentiation potential. Given that *SOX9* is expressed in progenitors, with its expression further induced upon cholangiocyte differentiation, it is hypothesised that the knockout of this gene would further promote HepaRG cells

toward a hepatocyte phenotype, synergistically with the prior mentioned protocol 2 and HepaNumb modifications. This hypothesis was tested and is the topic of the following chapter of research.

## 6.0 Introduction to RNA-guided CRISPR/Cas9 genome editing

The CRISPR/Cas9 system forms part of the bacterial adaptive immune system based on self/non self-discrimination. CRISPR-Cas imprints genetic material into the host genome as a form of memory in the event of future invasions by phages, plasmids and other mobile genetic elements<sup>276</sup>. The system has been further modified and exploited for molecular biology use. There are three types of CRISPR/Cas systems<sup>277</sup>, with type II being the most widely used for genome editing. This system requires the formation of a secondary structure comprising the trans-activating (tracrRNA) with the pre-crRNA through complementary base pairing. This secondary structure triggers further processing of the crRNA by RNase III and silencing of foreign DNA by Cas9<sup>278</sup>. DNA targets are determined by the guide RNA (gRNA) finding regions of complementarity within the genome. The caveat to Cas9 cleavage is that a protospacer adjacent motive (PAM) sequence is required to be juxtaposed to the tracrRNA:crRNA secondary structure on the 3' end. The PAM motif is species specific, but in the case of genome editing, the *Streptococcus pyogenes* Cas9 requires an 5'-NGG-3' consensus sequence immediately following the region of complementarity to the gRNA<sup>278</sup>. The crRNA is required for target sequence recognition while the transencoded tracrRNA forms a duplex with the crRNA to form a stem loop, and in the presence of Cas9, this ribonucleoprotein complex is able to mediate specific double-stranded cleavage of the target DNA<sup>279</sup> (

**Figure 54).** Using this system, Jinek *et al.* engineered an RNA chimera vector composed of a dual tracrRNA:crRNA-guided Cas9 protein and showed that, in the presence of the Cas9 and the PAM motif, the construct could target and cleave any double-stranded DNA sequence of interest<sup>280</sup>. This RNA chimera is now routinely used to facilitate the use of the CRISPR-Cas9 system as a RNA-programmable genome editing tool.

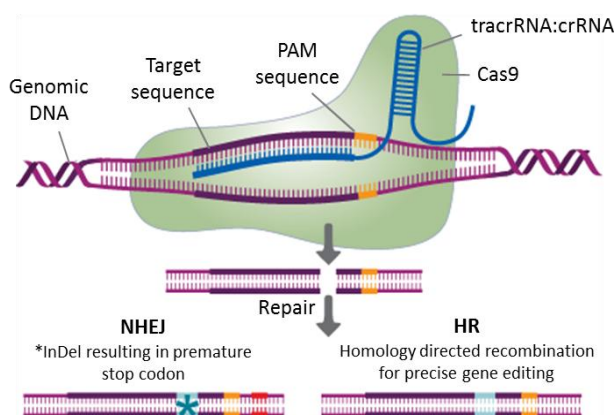


**Figure 54. Genome editing using CRISPR/Cas9.** Cas9 nuclease targeting is mediated through a 20 nucleotide guide sequence that forms part of the gRNA and binds to its complementary genomic counterpart. The remainder of the gRNA is comprised of the tracrRNA and crRNA which form a secondary structure required for crRNA processing of and activation of the Cas9 nuclease. The NGG PAM site is required for *S. pyogenes* Cas9 to recognise its target and initiate a site-specific DSB.

Upon the introduction of a double-stranded break (DSB), natural cellular repair mechanisms are activated and attempt to repair the lesion and continue transcription. In the absence of a suitable repair template, the DSB is repaired through ligation of the two cleaved ends by the error-prone system of Non-Homologous End Joining (NHEJ). Since there is an absence of template, random nucleotide bases are either inserted or deleted leading to DNA sequences which differ from the wildtype sequence. These insertions/deletions (InDels) may alter the reading frame of the target gene either through significantly altering the amino acids within the transcript, or alternatively, through the introduction of a stop codon which would cause premature transcription termination<sup>281, 282</sup>. It is these alterations to the genome that makes the CRISPR-Cas9 system such a revolutionary tool within the laboratory, as any target gene can be “knocked-out” simply through the introduction of Cas9 with a gRNA loaded with a target sequence for the gene of interest<sup>274</sup>.

## **6.1 Results of genome editing of HepaRG cells**

### **6.1.1 Cloning of guides into the px330 CRISPR/Cas9 vector**

To determine the role of *SOX9* during the differentiation two constructs were developed, one that contained the *SOX9*-specific guide, and a second which contained a guide which theoretically had no region of complementarity within the human genome. Following genome-editing, indels result in the formation of mRNA transcripts that contain a nonsense mutation resulting in the presence of a premature stop codon that would be degraded through nonsense-mediated decay. Therefore, the earlier the interruption, the increased probability of the mutation producing a non-functional protein, and to this end, the guide RNA was designed within the first bases of exon 1. The spCas9 is predicted to cut 3-4 bp upstream of the PAM sequence, and was therefore predicted to result in early termination of the *SOX9* protein.

The *Sox9* guide RNA and a negative guide RNA, with no known binding sites within the human genome, were annealed and cloned into the px330 vector upstream of the human Pol III promoter. When designing the guides, particular parameters as outlined in the seminal genome editing CRISPR/Cas paper by Cong *et al.* were adhered to in order to increase the probability of gene knockout<sup>199</sup>. To ensure that a gene is knocked out, it is preferable to design oligos corresponding to the N-terminus of the protein so that a truncated, but functional protein is not formed. Downstream of the guide was the chimeric tracrRNA:crRNA which contains the modified tracrRNA that is 85 nucleotides longer than the originally described versions has been found to have more efficient cleavage when compared to shorter tracrRNA sequences used in some other vectors<sup>283</sup>. Below is the genomic region amplified using the specified PCR primer sequences (aqua) with the guide strand

indicated (grey) adjacent to the PAM site (blue). Cas9 cleavage is expected to occur between the 3<sup>rd</sup> and 4<sup>th</sup> base from the PAM sequence, and is denoted by the ▼ symbol (**Figure 55**).

```

gtgcaagcggccactttgctcttttctccctctctctctccaattcgctccccacttgagcgggcagctgtgaactggccaccccgcttctaag
tgctcgccgtagccggccgacgcgagcttccccgggagccgctgtctccgcatccggcagccgaggggagaggagcccgctcagctcccgagccgc
cgggcttctgccttccggccaccagccccctgcgggg ▼ cccgcgatgaatctctggacccttcatgaagatgaccgacgagcaggagaaggcctgt
ccggcggccacccaccatgtccgaggactccgggctcgcctgcccgtcgggctcggctcggacaccgagaacacgcccaggagaacacgttccc
caaggcgagcccgatctgaagaaggagagcaggaggacaagtccccgtgtcatccgagggcggtcagccaggtgctcaaaggctacgactggacgtggt
gcccattccgggtgcgctcaacggctccagcaagaacaagccgacgtcaagcggccatgaacgcttcatggtgtggcgagggcgccgaggaagctgc
ggaccagtaccgcaactgcacaacggcagctcagcaagacgctgggcaagctct

```

**Figure 55. Sox9 knockout genomic location and Cas9 cleavage site.**

The guide binding site is highlighted in grey with the highlighted cccggg site corresponding to the *SmaI* restriction site. The arrow represents the predicted cleavage site of the Cas9 nuclease between the 3<sup>rd</sup> and 4<sup>th</sup> base upstream of the PAM motif, highlighted in blue. Aqua highlighting represents the primer binding sequences used for amplification of the Sox9 target sight with 274 bp upstream and 420 bp downstream of the nuclease site.

The spCas9 is flanked by nuclear localisation signals, causing nuclear import of the Cas9 protein. Lastly, the Cas9 transcript is terminated with the presence of the bovine growth hormone polyadenylation signal (bGHpA) (**Figure 56a**). Following cloning of the Sox9 and negative control guides into the px330 vector, several clones were restriction enzyme digested in order to validate whether the insert was successfully ligated into the backbone. Upon ligation of the insert into the *BbsI* restriction site, the restriction site is destroyed, but the *AgeI* restriction enzyme site approximately 1 kb upstream remains intact. Therefore, ligation of the insert is expected to yield a single band due to only digestion of one of the sites, *AgeI*, and failure of ligation will leave the *BbsI* site intact, thereby causing cleavage at both the *BbsI* and the *AgeI* sites and excising the 1 kb band. From the gel in **Figure 56b**, all 4 clones for both the Sox9 and the negative control clones contained their respective inserts, while the empty px330 backbone showed an excised band of approximately 1 kb. Sequencing validation was performed on the correct clones to ensure clone sequence integrity.

### 6.1.2 HepaRG knockout of Sox9 using CRISPR/Cas9 technology

Efficient transfection of the vectors into the target cell line was required, as the higher the transfection, the greater the probability of achieving bi-allelic knockout and the fewer clonal colonies would be required to be screened. To achieve higher transfection efficiency, electroporation of the plasmid was performed, whereby an electric field is applied to the cells to increase the permeability of the cell membrane and enhance the uptake of plasmid DNA into the cell<sup>284</sup>.

The culture was initially heterogeneous following electroporation due to the lack of antibiotic resistance or fluorescent marker genes within the px330 vector. Following nucleofection of the HepaRG cells with the px330-Sox9 and px330-ng ctrl vectors, genomic DNA was extracted from the cells. Primers flanking the guide RNA site were used to amplify the target followed by a T7

endonuclease I assay for confirmation of genome editing within the population. This assay is dependent on the formation of heteroduplexes which contain mismatches during the process of PCR product melting and slow re-annealing. These mismatches occur due to some of the DNA containing a mutation, while other fragments contain the wildtype allele. When the wildtype and mutated strands anneal, they form a base mismatch. The T7 endonuclease is a junction-resolving enzyme that recognises these mismatches and cleaves the DNA at the first, second, or third phosphodiester bond 5' to the mismatch<sup>285</sup>. Digestion of the PCR product with T7 results in multiple bands following gel electrophoresis. The presence of the additional band within the Sox9-guide transfected cells was confirmation of successful population-wide genome editing of the cells. HepaRG and negative guide PCR products showed a single band of 300 bp, while the Sox9 guide PCR product resulted in the presence of 3 bands, 300 bp, 250 bp, and 50 bp in size (**Figure 56c**). To obtain a homogenous culture, the cells were clonally amplified and genomic DNA extracted from each of the clones. PCR amplification of a larger target region was performed and should have resulted in the production of a 700 bp fragment. Clone 3, showed only a single band around 2kb in size, while all other clones contained the correct size insert of 700 bp (**Figure 56d**).

A T7 endonuclease assay was then performed on the samples in order to determine whether the clones were heterozygous for an indel. Heterozygotes would result in the formation of heteroduplexes during denaturing and re-annealing of the PCR product, whereas homozygous wildtype and homozygous mutants would only yield a single band as they would anneal perfectly, and not giving access to the T7 enzyme to cleave the annealed product. A Sox9 bi-allelic knockout cell line was desired for the differentiation protocol, and thus all heterozygote clones detected by T7EN I were discarded.

A restriction enzyme digest method of mutation analysis was employed in order to assess the presence of an indel within a particular location. The predicted Cas9 cleavage site is between the 3<sup>rd</sup> and 4<sup>th</sup> base from the PAM sequence, and corresponds to the *SmaI* recognition sequence (CCC▼GGG). Therefore, using the *SmaI* restriction site, the remaining clones underwent restriction digestion and subsequent gel electrophoresis to determine whether they contained a bi-allelic Sox9 mutation. Any mutations in the *SmaI* recognition site where the predicted cleavage site is located, would result in the abolishment of the recognition sequence, and would produce a single band on the gel. This is in contrast to the wild type amplicon which would be digested into two fragments by *SmaI*. All digests contained the same amount of DNA as measured spectrophotometrically and digested for only 1 hour to ensure that the DNA was not overdigested which result in star activity and the production of multiple bands on the gel. Using this strategy, it was found that 2 clones no longer contained the predicted *SmaI* site, and had therefore been mutated (**Figure 56e**). Furthermore, they did not show 2

alleles (3 bands on the gel, 1 for the mutant and 2 for the wildtype alleles), and were therefore predicted to be bi-allelic Sox9 knockouts.

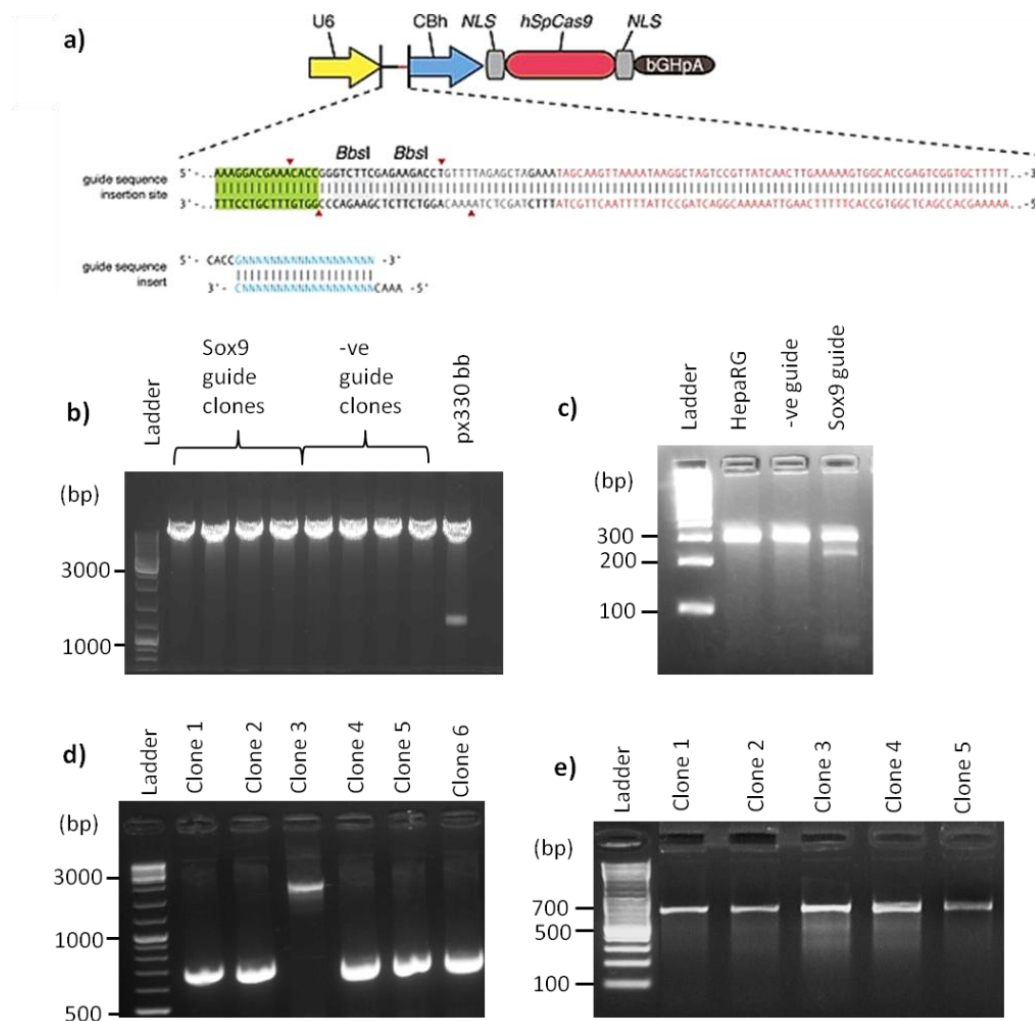


**Figure 56. Cloning and validation of the px330-Sox9 genome editing vector.**

a) *BbsI* guide-RNA cloning site in px330. b) Positive clones for Sox9 and negative guide clones in the px330 vector. c) T7EN1 assay using DNA from the HepaRG cell line and heterogeneous populations of negative and Sox9 guide nucleofected cell lines. d) PCR amplification of target region for clonally amplified populations of HepaRG Sox9 knockout clones. e) *SmaI* digest of individual clones with 3 bands indicating heterozygosity.

Sox9 DNA from clones 3 and 31 were sequenced to confirm bi-allelic mutations. Sequencing results revealed that clone 3 contained a large insertion mutation between the 3<sup>rd</sup> and 4<sup>th</sup> base upstream from the PAM site (**Figure 57a**). The misaligned sequence was analysed by BLAST and did not yield any positive hits, indicating that the inserted sequence is not from a coding region of the genome. Clone 31, interestingly, did not contain a large insertion like clone 3, but instead contained only a 6 bp deletion at the 5' end of the guide, with the sequence 5'-CCCGGG-3' (**Figure 57b**). Interestingly, the 6 bases which had been deleted corresponded exactly to the *SmaI* recognition sequence detected through failed digestion of this clone by *SmaI*.

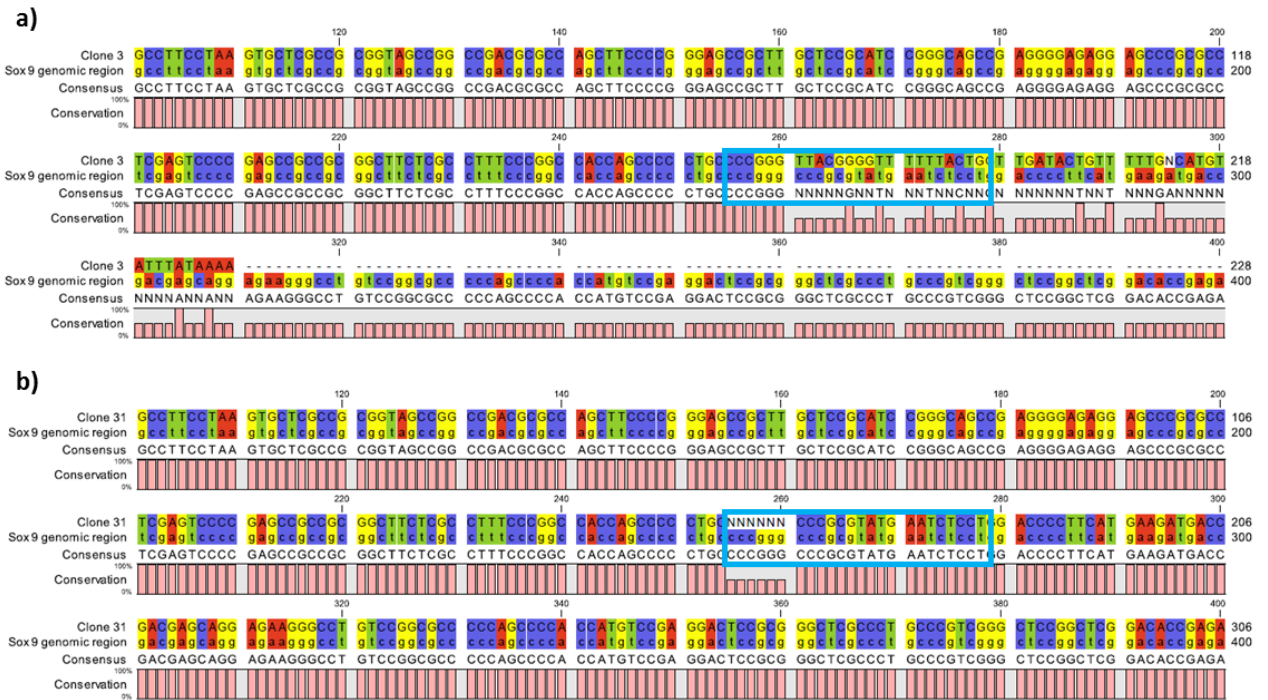


**Figure 57. Sequencing of 2 clones following CRISPR-Cas genome editing of the Sox9 locus.**

a) Sequencing of 2 individual clones containing a large insertion and b) a 6 bp deletion.

### 6.1.3 Analysis of Sox9 knockout clones

The validated clones were subsequently amplified as a homogenous HepaRG Sox9<sup>-/-</sup> cell line to be used within the 3-component differentiation protocol. A total of four Sox9 knockout clones were found. A number of phenotypic observations were made between the wildtype HepaRG cells (**Figure 58a**) and all four of the Sox9 knockout cells (**Figure 58b**) during their amplification. Firstly, the rate of proliferation was dramatically reduced compared to the wildtype cells with only a sparse number of cells seen compared to the wildtype cells which had become confluent during the same period of time. Secondly, upon proliferation, the cells displayed decreased cell-to-cell contacts, increased motility and a decreased propensity for colony formation following a series of cell divisions. Thirdly, the Sox9<sup>-/-</sup> cells appeared morphologically distinct with their elongated, spindle-like phenotype. A higher proportion of Sox9 knockout cells also contained extending processes (arrow head). Following a month of culturing, the Sox9<sup>-/-</sup> knockout cells showed growth arrest, a flattened cellular morphology, and exhibited increased cytoplasmic mass and a distinctly large nucleus (arrow), indicative of cellular senescence. Passaging of these cells resulted in the loss of the cells as they did not adhere when replated.

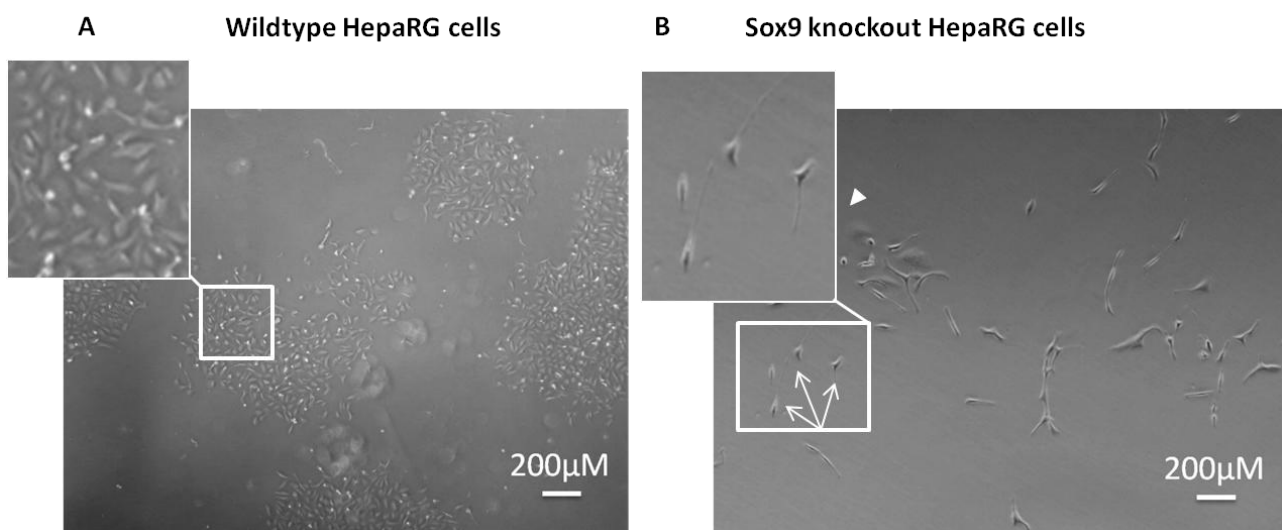


**Figure 58. Phenotypic differences in wildtype and Sox9 knockout HepaRG cells.**

a) Clonally amplified wildtype and b) Sox9 knockout cells exhibited decreased proliferation and cell-to-cell contacts and appeared phenotypically distinct to the wildtype cells at the same magnification.

---

## **CHAPTER SEVEN**

### **DISCUSSION**

---

## 7.0 Discussion

Animal models have been employed to gain insight into the evolution of pathological phenotypes. Many of these phenotypes arise due to altered signal transduction pathways at the onset and during the progression of disease. While these models provide invaluable information, there is a growing need to reduce the number of animals required for such studies by improving upon current methodologies. One innovative refinement has been the generation of whole-body reporter mice which have been generated within the last decade. Disease-mediated activation of a signalling pathway yields a quantifiable measure of luciferase activity *in vivo* to produce a temporal readout of a biological process. While this non-invasive methodology has greatly reduced the numbers of animals used by providing longitudinal imaging/data capture, the generation of these transgenic lines is immensely costly and time consuming. The research presented within this thesis illustrates the development and proof-of-concept work using somatotransgenic bioimaging. This is followed by the application of the reporters within a relevant *in vivo* liver disease model and in an *in vitro* culture system used to assess pathways implicated in chronic liver disease. The exceptionally high sensitivity of luciferase allows for the detection of small changes in gene expression. Importantly, there is no endogenous activity of the luciferase within host cells, so interference in quantification is absent, making this an ideal gene regulation reporter system. While these reporters have shown great promise for *in vivo* applications, the development of various luciferase vectors, including secreted versions for temporal *in vitro* purposes provides limitless possibilities of using such reporters within a wide range of applications.

### 7.1 Dual reporter vectors can be successfully used within *in vitro* and *in vivo* model systems

#### 7.1.1 Development of a bicistronic firefly luciferase / GFP lentiviral construct

For the purposes of this project, a bicistronic lentiviral vector containing dual reporters, namely firefly luciferase and GFP, was produced. The firefly luciferase was developed in the lab of Dr James Murray<sup>239</sup>. This engineered luciferase mutant was codon optimised for mammalian expression through base substitutions which result in synonymous mutations and thus do not alter the amino acid sequence. It also contains the non-synonymous mutations, without an accompanying loss of specific or kinetic activity relative to the wild-type version of the enzyme. These attributes make this luciferase a far more desirable candidate for both *in vitro* and *in vivo* applications. The foot-and-mouth disease virus (FMDV) 2A cleavage peptide fused to the GFP codes for a peptide that undergoes spontaneous post-translational peptide-bond cleavage, generally resulting in equimolar amounts of the transgenes upstream and downstream of the 2A sequence<sup>286</sup>. Other elements within the lentiviral cassette include the cPPT, the WPRE, and the 5' and 3' deleted LTR. The cPPT is required for positive-strand DNA synthesis following reverse transcription, and also enhances

transduction efficiency through increased nuclear import of the vector genome<sup>287</sup>, while the WPRE has been shown to enhance expression of the transgene within target cells<sup>288</sup>. The LTRs facilitate the integration of the payload area contained between them, into the host genome. The 3' LTR contains a disabling self-inactivating mutation that removed the LTR promoter activity through deletion of the TATA box, and renders the lentivector replication-incompetent<sup>289</sup>.

### 7.1.2 Validation of the pLNT-SFFV-JDG vector

Expression of the FLuc and GFP proteins was determined using 3xFLAG and GFP-specific antibodies. Results indicated that the vector expressed both transgenes *in vitro*. Using lysate from LNT-SFFV-JDG transduced HEK293T cells, it was established that 2A cleavage was 90% efficient as determined densitometrically using Western blot, which was more than adequate for the proposed work and well within the published cleavage efficiencies of 76-88% for various 2A sequences<sup>290, 291</sup>. This indicates that the bicistronic reporter cassette reliably cleaves the 2A peptide which should theoretically yield two individual proteins of equimolar quantities.

The development of novel luciferase vectors requires complete analysis of the luciferase enzymatic kinetics. Since the luciferase used has multiple modifications, it was necessary to determine the peak fluorescent output of this vector *in vitro*. The empirical peak was determined to be at 549 nm, almost the same peak wavelength expected for wild-type *Phontinus pyralis* (firefly luciferase), which has been shown to have a peak photonic emission around 560-562 nm<sup>292, 293</sup>. A 10 nm spectral shift was not predicted to be large enough to affect *in vivo* luciferase expression since the quantum yield (brightness) of the vector was exceptionally high and a significant amount of photons were being expressed above 600 nm, the region of the spectrum where the photons are not absorbed by haemoglobin, and are therefore more readily detectable from within haemoglobin-rich tissues such as the liver. Importantly, enzymatic activity was also assessed, as cleavage of the 2A sequence results in 19 residual amino acids remaining attached to the upstream protein on the carboxy terminus, while the downstream protein retains the remaining 2 amino acids on its amino terminus following cleavage<sup>294</sup>. The data confirmed that the 2A sequence did not result in any accompanying loss of enzyme activity post-cleavage. Transduction potential was visually assessed by fluorescence microscopy for the presence of GFP, while luciferase activity was detected by luciferase assay.

### 7.1.3 Development of a library of reporters using Gateway cloning

The development of a parental vector that has the capacity to quickly and efficiently generate a library of alternative vectors was a highly desirable feature. Thus, the JDG insert was directionally cloned into the pLNT-GW-MCS vector to create pLNT-GW-JDG. This vector has the ability to mediate

ligation-independent Gateway® recombination to clone transcription-factor binding response elements upstream of the dual reporter insert with a high degree of efficiency. Response elements were cloned into the pENTR shuttle plasmid containing a mouse minimal promoter that contains sequences that specify the transcriptional start site, however does not strongly recruit RNA polymerase, thus only giving basal levels of transcriptional activation. Signalling specificity and strong transcriptional activity is then conferred through the binding of specific transcription factors to their unique response elements. The rapid generation of these lentiviral reporters has immense broad-scale applicability within the biomedical sciences, as they can be used as a quantitative measure of transcription factor activity, particularly in models of inflammation, fibrosis, cancer, and metabolic processes. These signalling profiles will further contribute to our understanding of the ways that particular signalling pathways are involved in normal development and also the pathogenesis of disease.

#### **7.1.4 Dual secreted luciferase platform permits longitudinal *in vitro* analysis of signalling**

Following the successful development of the Gateway® firefly luciferase vector, the NanoLuc® (NLuc) vector was subsequently cloned. This luciferase is secreted into the media, thus allowing longitudinal studies using luminescence as the output without termination of the experiment. This mode of analysis is particularly useful in differentiation experiments where pluripotent or bipotent progenitor cells are specified toward a particular lineage through the addition of particular agonists, antagonists and/or growth factors. These differentiation experiments are typically of longer duration than most drug activation/inactivation studies. The quality of the data is also improved since the same samples can be analysed at several time points throughout the course of the experiment, thereby decreasing the amount of inter-experimental variability. The ideal vector for such temporally extended studies would contain the secreted NanoLuc that could be assayed without the need for cell lysis and also contain GFP as a visual reporter of signalling activity that could be monitored microscopically. To this end, the Gateway-NanoLuc®-2A-eGFP (pLNT-GW-NLuc2) vector (**Appendix A.vi**) was synthesised to create a parental construct into which an array of response elements could be rapidly cloned using Gateway technology.

Vargula luciferase is a naturally secreted luciferase that uses vargulin as its substrate and can be used in conjunction with NanoLuc® as the constitutive control to normalise expression. Transcription factor activity can then be determined using the biosensing NanoLuc® readout. The generation of this non-terminal luciferase assay system, and the ease with which libraries can be generated in order to obtain longitudinal readouts, is a significant development for *in vitro* bioluminescent assays, particularly with respect to differentiation experiments<sup>295</sup>.

### **7.1.5 Constitutively expressed luciferases confirm substrate specificity**

Substrate specificity of luciferases is critical for combining reporter constructs for dual quantitation either *in vitro* or *in vivo*. Validation studies confirmed that firefly luciferase was highly specific for its substrate, D-luciferin, while the other luciferases were unresponsive. Interestingly, even though renilla showed the highest fold change in luciferase activation with coelenterazine as the substrate, firefly luciferase also showed an increase in luciferase activity, but this was not significant following correction for multiple testing using the Tukey's post-hoc test. NanoLuc is known to utilise coelenterazine as a substrate, and so its photonic output in response to coelenterazine is not unexpected. However, the signal is relatively modest in comparison to other luciferases to their specific substrates. An enhanced substrate, known as furimazine, has recently been produced. This substrate is an analogue of coelenterazine and shows improved luminescent output compared to RLuc and FLuc with their respective substrates, making it an attractive alternative for luminescent-based assays<sup>248</sup>. Lastly, vargulin was tested and exhibited the greatest fold increase in the vargula luciferase sample with all other luciferases having no activity in the presence of vargulin, indicating a high degree of substrate specificity. The use of the two secreted luciferases, Vluc and NLuc, within the same well is desirable, and thus there should be minimal cross-reactivity of the NLuc vector with vargula and the Vluc vector with coelenterazine. The presented data confirms the suitability for simultaneous use of these secreted vectors within a single-well system. *In vivo* comparisons have also been conducted with Tannous and colleagues inoculating tumor cell lines expressing firefly, renilla, or vargulin luciferase into different regions of the same mouse. Following sequential (1 day apart) administration of their respective luciferins, namely D-luciferin, coelenterazine, or vargulin, only the tumor location corresponding to the paired luciferase showed an increase in luminescence<sup>296</sup>. This shows the specificity of these luciferases within an *in vivo* context and offers the potential to perform dual or even triple bioluminescence imaging analysis of cellular processes.

## **7.2 Biosensing reporters as monitors of transcription factor activity**

### **7.2.1 NF- $\kappa$ B reporter cell lines respond significantly to agonist administration *in vitro***

Coupling of genetic reporters with particular synthetic response elements facilitates the detection of pathway-specific gene activation in contrast to constitutive expression which is stimulus independent. Reporter gene expression has been increasingly used to determine the impact of relative expression levels on the phenotype of an organism or culture assay. To this end, the NF- $\kappa$ B-JDG vector was used within the proof-of-concept *in vitro* assay of the biosensing reporters using the hepatic Huh7 cell line. This cell line is a human hepatoma-derived cell line, and has been used extensively to study many hepatic processes and pathways, including mechanisms of HCV infection and replication, xenobiotic responses, and the effects of potential therapies<sup>297</sup>. A significant proportion of hepatic insults result in an increase in inflammation, thus, the Huh7 cell line was considered a suitable model

to validate the NF- $\kappa$ B reporter using agonists that incite inflammatory responses that mimic natural *in vivo* responses. Huh7 cells were activated by ultra-pure LPS, a TLR4-specific agonist. LPS not in its ultra-pure state contains other bacterial components, such as lipopeptides, which not only stimulate TLR4, but also TLR2<sup>298</sup>, an undesirable result in the context of our experiments as this would cause NF- $\kappa$ B signaling within the *tlr4*<sup>-/-</sup> mice transduced with the vector.

Several NF- $\kappa$ B transduced cell lines showed a significant increase in luciferase expression over their inactivated counterparts in response to LPS. All cell lines were assayed at 48 hours post-activation, as this was the time of highest activation within the aforementioned time course. Huh7 cells showed significance at 48 hours with a mere 1.8 fold change, while a 4.6 fold change seen at 12 hours within the time course was not deemed significant. This is due to the number of samples that are being compared. Due to the fact that a change in expression over time was used for the time course, a two-way ANOVA was applied to determine statistical analysis. This takes into account multiple testing and corrects for it using the Bonferroni. This is in contrast to the cell line comparisons, in which a Student's t-test was performed, which does not require correction for multiple testing. A significant response was noted in HepG2, Huh7, and fibroblast cell lines. This response was specifically TLR4 mediated, as LPS failed to instigate an NF- $\kappa$ B-mediated increase in luciferase activity in *tlr4*<sup>-/-</sup> MEFs. This observation has also been published by Chow *et al.* who determined that NF- $\kappa$ B signalled specifically through TLR4<sup>299</sup>. NF- $\kappa$ B signalling has been found to be a driving force in EMT, with LPS induction resulting in an increase in expression of EMT-associated transcription factors such as SNAIL<sup>300</sup>. It has been previously shown that cholangiocytes exposed to high levels of LPS, are able to undergo EMT and contribute to the fibrogenic phenotype or even the development of hepatocellular carcinoma<sup>301</sup>. *In vitro* NF- $\kappa$ B reporters are therefore a useful tool for the continued assessments of the effects of LPS and NF- $\kappa$ B signalling on tumour cell characteristics such as invasion and survival in HCC cell lines<sup>302, 303</sup>.

### **7.2.2 Activin A induces a temporal and dose-dependent increase in Smad2/3 signalling *in vitro***

In the context of *in vivo* fibrosis, activation of the TGF- $\beta$  pathway is largely due to TGF- $\beta$ I, enhancing the transcription of fibrosis-promoting target genes, most notably collagen, fibronectin, and the protease inhibitors PAI-1 and TIMPs<sup>304</sup>. The SBE binding sequence CAGACA, also known as a CAGA box, is a TGF- $\beta$ -inducible DNA element found in the regulatory regions of fibrosis-associated genes. Using the LNT-SBE-JDG construct, a concentration of 10 ng/ml or less of activin A resulted in failure of reporter activation, while higher doses demonstrated a positive correlation with luciferase expression. Activation of the reporter was confirmed in a number of cell lines including the immortal human cell lines, HEK293T and HeLa, a human primary fibroblast cell line, and a CD1 mouse primary fibroblast cell line. All luciferase activity was normalised to total protein content. While all

cell lines were transduced with the same MOI of virus, they may not all be transduced with the same efficiency owing to cell-surface receptor availability for viral entry. All cell types were known to have intact SMAD 2/3 signalling pathways. However, it is known that there is significant variation in downstream effector abilities between signalling pathways within different cell types due to adaptor protein<sup>305</sup> and transcription factor abundance<sup>306</sup> and the regulation of gene expression via distal enhancer elements<sup>307</sup>. These factors may account for some of the variation of expression observed between cell types.

Benus *et al.* utilised TGF- $\beta$  stimulation of the SBE-Luc reporter which resulted in a 7-(HepG2) to 18-fold (A549) increase in reporter activity<sup>308</sup>. These wide-ranging effects of reporter activity between different cell lines and in response to different agonists indicates that this response element has a broad activation range and has the capacity to become activated with nanogram concentrations of agonist which is essential in a physiological context.

### **7.2.3 LiCl activates Wnt signalling and increases WNT-JDG reporter activity *in vitro***

WNT signalling is crucial in the development of the liver amongst other organs, and has increasingly been shown to be imperative in the differentiation of hepatic progenitors to hepatocytes in response to chronic liver disease. Specifically, Forbes *et al.* have shown *ex vivo* data showing that in response to hepatocyte injury, macrophages secrete the Wnt ligand, Wnt3a, initiating canonical Wnt signalling within the adjacent hepatic progenitor cells<sup>40</sup>. The use of a Wnt signalling biosensor *in vitro* and *in vivo* therefore has the potential to offer further insight into the temporal behavior of this complex pathway during the disease progression using different disease models.

LiCl is an inhibitor of GSK-3 $\beta$ , and thereby prevents the destruction of  $\beta$ -catenin via the destruction complex<sup>309</sup>. The TCF/LEF reporter was significantly activated in response to LiCl in HEK293T, NIH3T3 and HeLa cell lines. Canonical Wnt signalling is heavily activated during multiple processes during development, and thus the *in vitro* differences are expected with the embryonic human kidney HEK293T and embryonic murine fibroblast NIH3T3 cell line demonstrating the highest level of activation. The WNT pathway plays a critical role in the development of hepatocellular carcinoma. TCF/LEF-Luc expressing HepG2, Huh7, and Hep3B cell lines were used to demonstrate that omega-3 polyunsaturated fatty acids such as decosahexaenoic acid (DHA) and eicosapentaenoic acid (EPA) inhibited  $\beta$ -catenin through the activation of GSK-3 $\beta$ . This resulted in dose-dependent reduction in hepatocellular cell viability via caspase-3/9 activity<sup>310</sup>. This indicates the powerful utility of this reporter for *in vitro* drug evaluation for the treatment of human HCC.

#### 7.2.4 Jagged-1 overexpression induces Notch signalling in an *in vitro* co-culture assay

Notch signalling not only has a critical role in biliary tree development during embryogenesis, but also functions as a cell fate-determining “switch” within hepatic progenitors. The temporal kinetics of Notch signalling during *in vitro* differentiation and *in vivo* regeneration is not yet fully elucidated, and thus warrants further investigation. To this end, a Notch reporter construct containing the RBPJ $\kappa$  binding site was developed as a tool to better understand the activity profile of Notch during differentiation processes *in vitro* using the HepaRG cell line, and *in vivo* using the pBDL model of chronic cholestatic liver disease.

Using an *in vitro* co-culture model, the Notch luciferase reporter construct was validated. SGHPL5 cells are a first trimester extravillous trophoblast cell line that have been validated to ensure intact Notch signalling components, a critical factor for biosensing reporter validation studies. Inhibition of the Notch2 receptor within this cell line, using Notch2-specific blocking antibody or siRNA, results in increased migration of these cells<sup>311</sup>. Furthermore, the activity of Notch signalling within SGHPL5 cells, specifically the inhibition of proliferation through activation of RBPJ $\kappa$ , has been shown to aid in differentiation toward more mature trophoblasts within the developing human placenta<sup>312</sup>. Expression of the Notch1, Notch2 and Notch3 receptor, coupled with known biological effects of Notch signalling within this cell line made it an ideal candidate for subsequent validation studies prior to *in vivo* validation.

The transduction of HEK293T cells with a constitutively expressing JAGGED-1-IRES-GFP enabled the expression of Notch pathway ligand within the cell line since HEK293T cells express no<sup>313</sup> or very low levels<sup>314</sup> of endogenous JAGGED-1. The co-culture system exhibited a dose-dependent increase in SGHPL5 luciferase expression, which is expected as there are increased cell-to-cell contacts. This data illustrates the sensitivity of the reporter, with increasing levels of agonist showing a positive correlation on the amount of activation.

For all reporter assays presented in this thesis, a significant increase in luciferase expression was observed in response to agonist. While these and a whole range of other reporters are highly sensitive and versatile tools for the study of gene regulation, they show varying degrees of transcriptional activation and basal expression<sup>315</sup>. Taking this into account, it is important to be aware of such variation when using lentiviral reporters. Firstly, transduction of cells with lentivirus containing the transgene may result in variable levels of expression which may arise from either 1) varying number of viral integrations between cells, 2) inherent cell-to-cell variability which has been shown to have a discrepancy of protein expression of up to 15%-30%<sup>316</sup>, or 3) the genomic location of insertion which may enhance or repress expression of the transgene. With regards to the variable number of integrants, a more homogenous culture can be achieved through clonal amplification of cells followed by subsequent qPCR in order to detect the number of integrated viral copies within the clonal

population. Dual reporters can be utilized to reduce the variability that is observed due to varying transduction efficiencies of the virus between experiments. For this dual reporter approach, one reporter is driven by a biosensing response element while the second is constitutively expressed. Signal from the biosensing vector can then be normalized to the expression of the constitutively expressed reporter.

It is a well known phenomenon that transgene expression of integrated retroviruses has the capacity to be transcriptionally silenced, mainly via trans-acting factors which bind and restrict expression from the viral LTRs, or through promoter silencing<sup>317</sup>. Integrating lentiviruses, however, have been shown to have a decreased propensity for transgene silencing<sup>318, 319</sup>. Although some data has shown that silencing occurs more frequently when using vectors containing a wild-type HIV-1 LTR, silencing has been shown to be decreased by 50% when utilizing self-inactivating (SIN) vectors containing a deletion in the U3 region of the 3' LTR<sup>320</sup>. These vectors should therefore be considered as an alternative vector backbone, particularly for reporters transduced into stem cells. Another mechanism in which such silencing can be controlled is to flank the transgene with chromatin insulator elements. These elements have the ability to block interactions between enhancers and repressors from adjacent chromatin and promoters within the vector. In so doing, they are able to reduce position and methylation effects on transgene expression levels<sup>321</sup>. While most cell lines do not cause transgene silencing, it should always remain a consideration and should be controlled for inasmuch as possible through suitable vector design.

### **7.2.5 Intravenous injection of VSV-g lentivirus predominantly targets hepatocytes *in vivo***

Pseudotyping of viral vectors has been extensively used to target particular organs. VSV-g is known to be pantropic due to the highly ubiquitous receptor, LDLR, which it uses to gain entry into the cell<sup>269</sup>. Broad or cell-specific targeting of the biosensing vectors is dependent on the experimental context and will thus determine the choice of pseudotype. To give the *in vivo* bioluminescent imaging data context dependence, it is important to know the specific cell types that are targeted and are responsible for the bioluminescent output. This insight is important as it adds another layer of sensitivity to the technology by acquiring information at a cellular level as opposed to a whole-organ level. Liver samples transduced with the constitutive SFFV-JDG vector underwent colocalisation assessment using GFP as a marker of viral transduction and other cell-type specific markers of hepatocytes (HNF4 $\alpha$ ), cholangiocytes (CK7), activated myofibroblasts ( $\alpha$ -SMA and GFAP), and hepatic progenitor cells (PKM2).

Firstly, an uninjected control liver was analysed for background levels of green autofluorescence. The liver is particularly problematic with regards to autofluorescence mainly due to the high lipofuscin content within the tissue. Lipofuscins are lipid-containing granules that autofluoresce

particularly within the green emission spectrum. Background fluorescence was significantly decreased by incubation of the samples with Sudan Black stain<sup>322</sup>. The uninjected control contained only very low levels of autofluorescence, while the GFP positive sample showed high intensity GFP signal. This was particularly observed in the GFP alone, HNF4 $\alpha$ , GFAP and PKM2 samples which were retrieved with sodium citrate at pH6 as opposed to Tris buffer at pH9 which is suboptimal for the GFP antibody with higher background and lower specific signal, but was required for dual staining of  $\alpha$ -SMA and CK7. A large proportion of the cells were GFP positive, particularly around the central vein. Some hepatocytes failed to stain for GFP, adding further confidence that the green was a true signal and not merely due to autofluorescence. GFP was notably absent from regions of ductular proliferation. Confirmation of hepatocyte targeting of the reporter vector was achieved through nuclear localisation of HNF4 $\alpha$  within GFP-positive cells.

The  $\alpha$ -SMA antibody typically stains vascular smooth muscle cells of the portal vein and the hepatic artery that would also be seen within a healthy liver. However, the defining observation in cholestatic liver injury is the presence of  $\alpha$ -SMA positive myofibroblasts found surrounding the hyperplastic bile ductules with the amount of injury shown to be positively correlated to the amount of  $\alpha$ -SMA staining<sup>323</sup>. Quiescent stellate cells do not express  $\alpha$ -SMA, and only do so once they become activated and acquire a myofibroblastic phenotype. It has been suggested that peribiliary fibroblasts, and not only hepatic stellate cells, are able to transform into myofibroblasts and contribute to portal collagen accumulation in chronic cholestatic models, and will also stain positive for  $\alpha$ -SMA<sup>324</sup>. GFP staining failed to merge with the  $\alpha$ -SMA marker, indicating that quiescent stellate cells are not targeted with the VSV-g pseudotyped lentivirus within the neonate prior to disease induction and myofibroblast activation.

GFAP staining was shown to be localised to the biliary epithelia in some sections, which has also been shown by others, but is mainly localized adjacent to the hepatic plates. Mederacke *et al.* demonstrated colocalisation of GFAP and CK19, indicating that biliary cells do express GFAP<sup>325</sup>. GFP localisation with CK19 indicates that our VSV-g luciferase vector does not target the cholangiocytes, and therefore, does not contribute to their bioluminescent output. Thus, even though there is a significant biliary hyperplasia during cholestatic injury, our GFAP model exhibited an initial burst of GFAP expressivity, followed by a decline in expression over the following 3 weeks. This offers a further benefit of utilising somatotransgenic mice over many other existing GFAP-transgenic mice that may be expressing GFAP non-specifically<sup>325</sup>, and therefore limits interpretation of the data. Of specific interest is the perisinusoidal expression of GFAP, which is clearly seen and has previously been described as GFAP<sup>+</sup> activated stellate cells<sup>326</sup>. The merged image shows a distinct lack of colocalisation of GFAP with GFP, indicating that these cells are also not responsible for the

upregulation of GFAP within the pBDL liver bioimaging, as vector targeting using the GFP marker has been confirmed to be localized to HNF4<sup>+</sup> hepatocytes.

The cholangiocyte-specific marker, CK7 was used to determine if the VSV-g vector was targeting these cells. Strong CK7 staining was seen in the proliferating ductal cells lining the portal tract. These cells did not colocalise with GFP. The level of green autofluorescence within the samples was relatively high, however, a firm distinction between the GFP-positive stained hepatocytes lining the portal tract can clearly be seen.

Furthermore, there was the distinct lack of colocalisation seen between GFP and PKM2. The samples assayed originated from the left lobe of a pBDL animal in order to visualise the proliferation of the progenitor cell niche, as the proportion of progenitor cells residing within the healthy liver is minimal. The image clearly illustrates that the GFP positive cells lie on the periphery of the ductular reaction. The mass of DAPI stained cells indicate proliferating biliary cells and immune-related cells around the portal injury. The progenitor cells reside at the terminal end of the Canal of Hering where they undergo expansion and differentiation when the regenerative capacity of either the hepatocytes or cholangiocytes is severely compromised due to chronic injury. The lack of colocalisation would suggest that the progenitor cells are not being targeted within the neonates, as proliferation of the progenitor cell niche during chronic injury would give rise to clonal GFP positive cells. Instead, GFP immunohistochemistry strongly indicates that the majority of targeted GFP<sup>+</sup> cells are hepatocytes as indicated by the colocalisation of GFP with the hepatocyte marker, HNF4a.

### **7.2.6 *In vivo* NF-κB signalling following ultrapure LPS treatment is TLR4 mediated**

One of the more specific aims of developing the biosensing reporter vectors was to analyse pathways *in vivo*, both developmental and in response to disease induction, and also as a drug-efficacy platform. Following *in vitro* validation of the LNT-NF-κB-JDG vector, it was subsequently validated *in vivo*. Neonatal injection of the virus containing the LNT-NF-κB-JDG or control LNT-SFFV-JDG cassettes into CD1 or *tlr4*<sup>-/-</sup> mice via the temporal orbital vein resulted in liver-specific expression of the reporters. Four hours post-LPS administration in adult mice, the *tlr4*<sup>-/-</sup> mice failed to elicit an LPS-mediated NF-κB response, while the CD1 mice showed a significant upregulation of luciferase expression. *In vivo* fold-change values were significantly higher in CD1 biosensing mice than in *in vitro* cultures, highlighting the impact of cellular context in signalling activation. Constitutive expression using the SFFV promoter is inherently agonist independent permitting continual transcription of its associated downstream gene, which in this scenario is luciferase. This is in contrast to regulated promoters that require a specific stimulus in order for transcription to commence. Thus LPS was not expected to result in an increase in luciferase expression in CD1 or *tlr4*<sup>-/-</sup> mice when using the SFFV promoter, as the levels of expression would be continuous, irrespective of the

presence of NF- $\kappa$ B agonist. Indeed, the control SFFV-JDG-injected mice showed no biosensing activity, with levels of luciferase expression remaining stable over time.

It is important to note that the use of somatotransgenesis within this experimental model further verified the broad applicability of technology through overlaying the biosensing platform upon an already existent germline transgenic, the *tlr4*<sup>-/-</sup> mice. This introduces a new method of non-invasively obtaining more data from existing models of disease and assessing which biological pathways may be potential therapeutic targets. Moreover, organ specificity is higher when using somatotransgenic animals compared to whole-body NF- $\kappa$ B-Luc mice<sup>327-329</sup>. The luciferase within our vectors is also optimised for *in vivo* applications compared to the pGL3 luciferase from Promega used within the commercial NF- $\kappa$ B-Luc transgenic mice developed by Caliper Life Sciences.

### **7.2.7 Dexamethasone-induced abrogation of NF- $\kappa$ B signalling**

The NF- $\kappa$ B-JDG vector showed a significant response to LPS-mediated NF- $\kappa$ B signalling, indicating its utility as a surrogate marker of inflammatory responses. However, in a pharmacological context, the abrogation of such responses is of importance in the management of acute and chronic inflammatory diseases. Proof-of-concept work was performed using the conventional anti-inflammatory steroid, dexamethasone. This glucocorticoid exerts a dual-mechanistic, anti-inflammatory effect to diminish pro-inflammatory responses. The first mode of action is induced through the binding of dexamethasone to the glucocorticoid receptor. This permits functional antagonism of the GR with p65, excluding activated NF- $\kappa$ B from the nucleus and decreasing the expression of pro-inflammatory genes, particularly IL-6<sup>330</sup>. The second mode of action is through the direct binding of the activated glucocorticoid receptor to its own response element (GRRE) as a transcription factor that induces the expression of a host of anti-inflammatory mediators as well as negative regulation of other genes<sup>331</sup>. Activated GR also causes the transcriptional upregulation and synthesis of I $\kappa$ B- $\alpha$  through binding of GRRE motifs within its regulatory regions<sup>332</sup>. The upregulation of I $\kappa$ B $\alpha$  increases cytoplasmic retention of the NF- $\kappa$ B heterodimeric complex through masking of the nuclear localisation signal on p65, and maintains it in its inactive state<sup>333</sup>.

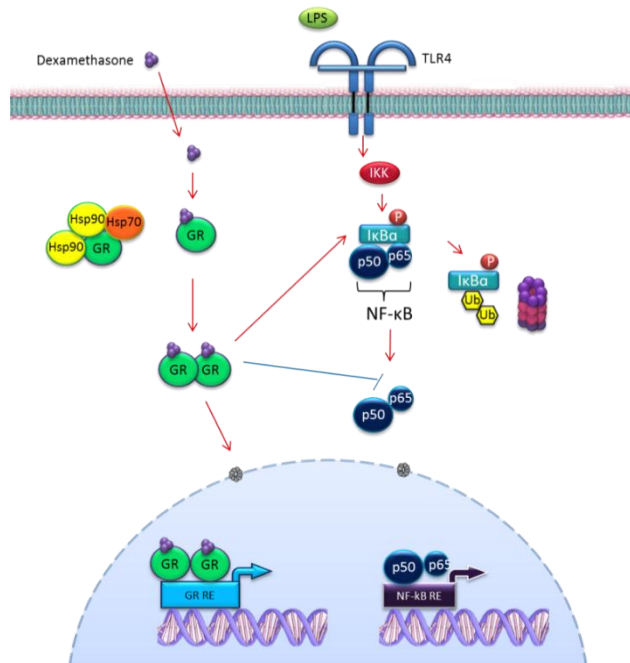


**Figure 59. Dual mechanism of anti-inflammatory activity of glucocorticoids.**

Glucocorticoids exert their anti-inflammatory effects firstly through their inhibition of the p65 subunit of activated NF-κB, and secondly through acting as a transcription factor binding to response elements of anti-inflammatory genes, as well as increasing the expression of IκBα at the transcriptional level.

The utility of NF-κB reporter mice as a platform for drug-efficacy testing was evaluated using dexamethasone to modulate NF-κB in an LPS-induced model of inflammation. The NF-κB biosensing mice exhibited a substantial decrease in luciferase output when LPS was preceded by a single dose of dexamethasone. These results validate the use of somatotransgenic bioimaging as a means of temporally analysing effects of drugs *in vivo* without the need for culling. Moreover, the same animals can be used for numerous studies as the NF-κB luminescence returns back to basal levels over time, as can be seen by day 74 post birth. A “washout” period is required to return the readings to baseline levels prior to subsequent experimentation, and is would be dependent upon the excretion and pharmacokinetics of the drug previously tested. Triple imaging for baseline luminescence should also be performed before any subsequent experiments.

Screening of compounds for anti-inflammatory activity *in vitro* is currently performed by using cell lines such THP-1, a human monocytic cell line, which secretes proinflammatory cytokines such as IL-1, IL-6, and TNF-α when challenged with LPS. Thus, various compounds can be screened within the model system to determine their potential anti-inflammatory effects<sup>334</sup>. Unfortunately, the efficacy and doses that are used *in vitro* may not necessarily be recapitulated in an *in vivo* pre-clinical scenario as the difference in biochemical environments may alter the kinetic profile of the potential anti-inflammatory drug<sup>335</sup>. To circumvent this problem, animal models such as the zebrafish have been used as an *in vivo* anti-inflammatory drug screening platform. Experiments by Yang *et al.*

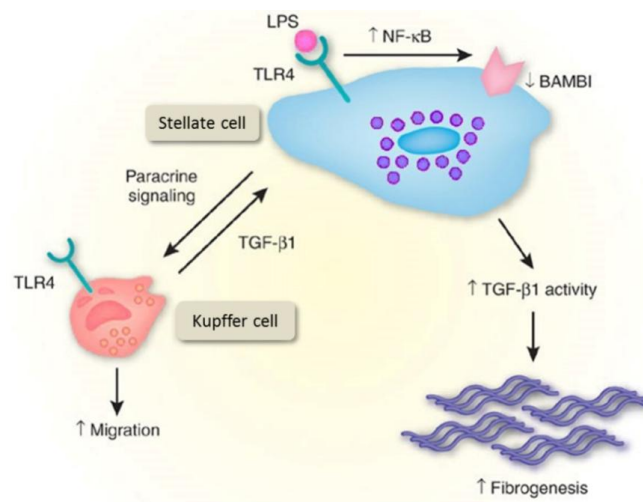
demonstrated that the administration of LPS followed by a dose of anti-inflammatory compounds such as chlorogenic acid, or the well-established corticosteroid, dexamethasone, resulted in a decreased inflammatory phenotype, such as the reduction of macrophage and neutrophil recruitment<sup>336</sup>. Although this model clearly and significantly illustrates the efficacy of chlorogenic acid against endotoxin-induced inflammation, the number of animals required was in the region of 34 to 300 animals per experiment with the mortality experiment requiring 6 groups each containing 50 animals. From an NC3Rs perspective, there is scope for improved and refined methodologies in order to reduce the numbers of animals required to determine drug efficacy, particularly within longitudinal studies.

Larger animals such as mice have also been utilised for *in vivo* anti-inflammatory screening. Several transgenic lines containing luciferase reporter genes have been described, including those using the inducible nitric-oxide synthase. The iNOS-luc transgenic mouse is used as a model for rheumatoid arthritis, septic shock, contact hypersensitivity autoimmune diseases, and myocardial ischemia. Administration of the known iNOS inhibitors, epigallocatechin-3-gallate,  $\alpha$ -phenyl-N-tert-butyl nitrene, ebselen, and dexamethasone all exhibited a decrease in iNOS induction when challenged with IFN- $\gamma$  and LPS<sup>337</sup>. The LPS-mediated induction of the iNOS reporter is quite variable, and though undesirable, may be unavoidable due to the fact that the bioluminescent transgenic founders that were screened for luciferase activity showed varying induction of the reporter, and thus offspring arising from different mating pairs showed variability. The use of somatotransgenesis overcomes this problem by having tissue-restricted expression while also being more cost-effective as generation of somatic transgenic animals is not reliant upon backcrossing in order to obtain the transgenic reporter colony.

### **7.2.8 Activin A induces upregulation of SBE-mediated luciferase expression *in vivo***

Just as activin A was used for *in vitro* validation of the SBE-JDG construct, it was important to validate the construct *in vivo* using an exogenous agonist, prior to using it within the pBDL disease model. Somatotransgenic mice transduced with SBE-JDG-containing lentivirus demonstrated a TGF- $\beta$ -mediated increase in luciferase expression that remained above basal levels for 6 days following activin A administration. LPS stimulation showed a minor decrease in luciferase expression 2 days post administration, but did not show any deviation from baseline for any subsequent time points. LPS has been shown to antagonise TGF- $\beta$  signalling through decreased expression of TGF- $\beta$  receptors, T $\beta$ RI and T $\beta$ RII, and concurrently the expression of SMAD2 within rat primary microglia<sup>338</sup>. Other studies show contradictory data showing that within the liver LPS-mediated activation of TLR4 is able to downregulate the TGF- $\beta$  pseudoreceptor, BAMBI<sup>121</sup>. This pseudoreceptor lacks the intracellular kinase domain required for TGF- $\beta$  signal transduction, and the

interaction of BAMBI with type I receptors inhibits the formation of receptor complexes required for normal signalling, and in this way acts as a negative regulator of TGF- $\beta$  signalling<sup>339</sup>. The downregulation of BAMBI with activation of TLR4 subsequently was shown to enhance TGF- $\beta$  signalling through increased sensitisation of the hepatic stellate cells to TGF- $\beta$  signalling<sup>121</sup>. More in-depth mechanistic data has recently been published using chromatin immunoprecipitation analysis. This demonstrated that the NF- $\kappa$ B p50:p50 homodimer, in conjunction with a histone deacetylase, associated with transcriptional silencing, was bound to the promoter region of BAMBI, resulting in its transcriptional repression in hepatic stellate cells<sup>340</sup>. The observed decrease in TGF- $\beta$  signalling in response to LPS during the initial phases, may therefore be a cell-specific response.



<http://www.nature.com/nm/journal/v13/n11/images/nm1107-1281-F1.jpg>

**Figure 60. NF- $\kappa$ B-mediated enhancement of TGF- $\beta$  signalling in HSCs via BAMBI downregulation.** LPS signals through TLR4 to increase NF- $\kappa$ B signalling. P50 homodimers subsequently bind to the BAMBI promoter, resulting in increased TGF- $\beta$  signalling within the HSCs through sensitisation of the TGF $\beta$ IR.

### 7.2.9 Increases in NF- $\kappa$ B signalling are observed during the acute phases of pBDL

Following confirmation of fibrosis development and the presence of reactive ductular reactions within mice subjected to pBDL, analysis of signalling pathway activity in response to chronic cholestasis was undertaken. pBDL was performed through occlusion of the common bile duct between the left/median and the right/caudate lobes, inducing fibrosis largely only in the left and median lobes. This was the preferred method of fibrosis induction as total bile duct ligation is highly associated with severe hepatic injury and accompanying mortality. More importantly, indicators of cholestasis are present within this model without the tissue-damage associated with total occlusion of the bile duct<sup>205</sup>, making this a more NC3Rs acceptable model of acute cholestasis. Using mice that had been transduced with viruses containing reporter under the control of an NF- $\kappa$ B response element, pBDL resulted in a significant increase in an acute NF- $\kappa$ B-mediated response seen as a transient peak in luciferase expression at day 14 post surgery, before returning almost to baseline over the subsequent 7

weeks. The sham-operated animals also exhibited a transient increase in expression, albeit for only 4 days, before decreasing to baseline, indicative of a degree of “sham effect” immediately following the surgical procedure.

*In vivo* experiments have shown that particular bile acids have the capacity to activate NF- $\kappa$ B signalling in cultured hepatocytes<sup>341</sup>. This has implications for cholestatic diseases where chronic retention of cytotoxic bile acids causes oxidative stress and apoptosis of hepatocytes. The increase in bile acids induces proapoptotic signals within the hepatocytes through the activation of Fas signalling. Specific bile salts such as taurochenodeoxycholate have the capacity to activate survival-inducing phosphatidylinositol 3 kinase (PI3K) signalling and downstream NF- $\kappa$ B signalling<sup>341</sup>, thus responding as an adaptive mechanism to prevent hepatotoxicity while permitting the hepatocytes to function in spite of the development of cholestasis. This is consistent with other studies which determined that a reduction of hepatocyte apoptosis during regeneration occurs with the administration of TNF- $\alpha$ <sup>342</sup>, which causes the loss of I $\kappa$ B $\alpha$ , resulting in the activation of NF- $\kappa$ B<sup>110</sup>.

To determine the role of NF- $\kappa$ B during the acute phase of cholestatic liver disease, Miyoshi *et al.* induced cholestasis in mice by means of common bile duct ligation. Terminal analysis of liver disease was performed by culling of the animals, liver sample extraction, and molecular analysis. Electrophoretic mobility gel shift assay of nuclear extracts and immunohistochemistry of livers 3 days post-BDL exhibited increased levels of nuclear NF- $\kappa$ B localisation within hepatocytes. Furthermore, the same authors demonstrated increased liver injury in response to the administration of an adenovirus containing inhibitor of kappa B (I $\kappa$ B), proposing that NF- $\kappa$ B functions to reduce the extent of liver injury following acute biliary injury<sup>343</sup>. This study confirms the data collated in our NF- $\kappa$ B somatotransgenic model with a dramatic increase in NF- $\kappa$ B signalling during the initial phases of cholestatic induction. Comparative assessment of the number of animals used, however, shows that 6-12 animals were used in the control and the treated groups within their experiment, with data obtained being restricted to a single time point. This is in contrast to the 13 BDL and 8 sham NF- $\kappa$ B biosensing animals used in order to assess NF- $\kappa$ B signalling over a series of 25 time points during chronic injury within our model. The guidelines given by the NC3Rs recommends that fewer animals should be used to obtain the same amount of data, or that the same number of animals should be used in order to obtain more information compared to conventional methodologies. Somatotransgenic bioimaging is therefore the preferred method of transcription factor activity interrogation.

In contrast to the beneficial role of NF- $\kappa$ B signalling during the initial hepatic “wound-healing” response, maladaptive continuous activation of NF- $\kappa$ B promotes chronic inflammation, and is strongly linked to the development of fibrosis, subsequent cirrhosis, and hepatocellular carcinoma<sup>344</sup>. This has been shown using the chemical compounds, pyrrolidine dithiocarbamate and sulfasalazine, potent NF- $\kappa$ B inhibitors. Both compounds exerted a therapeutic effect on BDL-mediated liver

damage in Sprague-Dawley rats terminally assessed 10 days post-BDL<sup>345</sup>. However, the long term inactivation of components of the NF- $\kappa$ B pathway, such as TGF- $\beta$ -activated kinase (TAK1), an upstream modulator of NF- $\kappa$ B activity, results in the spontaneous development of pathological injury, including fibrosis and carcinogenesis<sup>346</sup>. A second study, observing NF- $\kappa$ B signalling during a chronic state of obstruction confirms the signalling profile seen within the somatotransgenic animals, but utilising classical technologies involving termination of the animals. Lin *et al.* quantitated the levels of the NF- $\kappa$ B downstream targets, TNF- $\alpha$  and IL-6, in rat hepatic macrophages following BDL, and showed they were increased during the initial 2 weeks, followed by signal attenuation by the third week. As further confirmation of the sensitivity of somatotransgenic bioimaging, data from the same authors noted increased NF- $\kappa$ B binding activity within Kupffer cells using a gel mobility shift assay, with NF- $\kappa$ B binding enhanced by 2.9-fold in the first week, 4.2-fold in the second week and 1.9-fold by the third week<sup>347</sup>. An increase was noted not only in the BDL-induced animals, but also within the sham-operated animals with a 2.6-fold increase in NF- $\kappa$ B binding over non-operated controls. This effect was also seen using our biosensing platform with the sham-operated animals exhibiting a transient 16-fold increase in NF- $\kappa$ B signalling, highlighting the improved sensitivity of the bioluminescent imaging over alternative molecular techniques. This “sham-effect” is most likely due to the inflammation caused by the surgical procedure.

NF- $\kappa$ B is a key modulator of hepatic homeostasis and the regulation of disease progression through its role during inflammation, cell death, and wound healing. It is therefore critical from a therapeutic perspective to fully understand the signalling profile of NF- $\kappa$ B and other pathways involved in the fibrotic response, as therapeutic intervention may be required at defined time-points. Ideally, NF- $\kappa$ B signalling should allow initial phases of inflammation to aid in the healing response, while therapy should prevent signalling from continuing indefinitely and permitting exacerbation of the original injury. Furthermore, the targeting of biosensing vectors to specific cell types through differential pseudotyping and the use of alternative viruses has the potential to be invaluable in understanding NF- $\kappa$ B signalling profiles in specific cell types that could prove useful for molecular targeting of therapeutic interventions for chronic liver disease.

#### **7.2.10 Novel Smad2/3 expression profiles are observed using SBE somatotransgenic animals**

In order for somatotransgenic bioimaging to successfully be used in disease modelling applications, the biosensors should be responsive to physiological concentrations of agonists and antagonists within a biological model. Interestingly, the levels of TGF- $\beta$  signaling in LNT-SBE-JDG transduced mice did not increase over time, but rather showed an oscillatory signalling output. Significant differences in luminescence, however, were not found at any one particular time point. Assessment of luminescence shows inherent variation even when basal levels for each animal are taken into account,

yet the experimental cohort exhibited a significant increase in the amount of variation over the control group. This difference in variation means that the amplitude of the luminescent output for the pBDL group was greater in the positive and negative direction than for the sham-operated group. This variation was statistically significant, and when averaged across all animals, showed a novel temporal TGF- $\beta$  signalling profile that would not have been seen using serial culling methodologies. The fluctuation of TGF- $\beta$ -mediated luciferase expression is most likely due to the liver's propensity for re-equilibration following disruption of normal homeostasis. Whole-body SBE-Luc transgenic mice have been developed in order to study the temporal and spatial patterns of Smad2/3-dependent pathway signalling *in vivo*. These animals were utilised to show TGF- $\beta$  signalling in response to kainic acid model of neuronal degradation and inflammation of the CNS. The usefulness of bioluminescent imaging as a drug platform was further shown with the amelioration of TGF- $\beta$  signalling using a glutamate receptor antagonist, MK-801<sup>348</sup>. The time and resources required for generation of these whole-body transgenics, however, limits its broader applicability and encourages the use of more continual imaging methodologies.

#### **7.2.11 Induction of cholestatic liver injury results in a significant increase in GFAP expression**

Within the normal liver, quiescent hepatic stellate cells are vitamin A-storing cells that play a fundamental role in the regulation of retinoid homeostasis<sup>349</sup>. There have been publications indicating that GFAP is a marker of quiescent HSCs, and that liver injury downregulates the expression of GFAP within these cells<sup>350</sup>, however, the majority of publications have shown GFAP as a marker of activated HSCs<sup>351, 352</sup>. Upon hepatic injury, these cells have the capacity to transdifferentiate into more mesenchymal, ECM-producing myofibroblasts that are known to express both  $\alpha$ -SMA and GFAP upon activation. A whole-body transgenic GFAP reporter mouse has been generated, with *ex vivo* GFAP expression shown to be highest in the brain, with detectible luciferase expression also seen in the heart. The lung, muscle, and kidney exhibited undetectable levels of luciferase<sup>353</sup>. Therefore, targeting of the liver with high specificity using our lentiviral reporters was performed in order to determine whether the use of our novel biosensing platform would perform better due to the enhanced luciferase and lack of background signal arising from the remainder of the animal.

Bioluminescent imaging was used as a quantitative measure of GFAP expression during the acute response of cholestasis, and as far as is known, is the first known GFAP reporter mouse used to non-invasively monitor its activation in a temporal manner. The sharp increase in luciferase expression within 3 days following surgery was expected as terminal molecular assessments have shown that stellate cells become activated by day 3 of injury, with persistent upregulated  $\alpha$ -SMA expression seen for the duration of the experiment until day 21 using the CDE model of chronic cholestatic injury<sup>354</sup>. Since stellate cells that undergo activation to myofibroblasts secrete an array of modulatory molecules

that have a role in inflammation and fibrosis during liver disease, their inhibition has been suggested as a therapeutic target. A murine model depleted of hepatic stellate cells has been developed by Puche *et al.* in order to determine the contributions of hepatic stellate cells in response to acute liver damage. In this model, the GFAP promoter was used to selectively express the herpes simplex virus-thymidine kinase (HSV-Tk), making the stellate cells susceptible to death through administration of the antiviral agent, ganciclovir, specifically during proliferation. In response to bile duct ligation, these mice showed marked attenuation of liver fibrosis, while displaying an increase in IL-10 expression<sup>355</sup>. Although the mechanism of fibrotic attenuation is not yet fully elucidated, it is hypothesised that this cytokine plays a significant role. The treatment of Sprague-Dawley rats with IL-10 has been shown to suppress the growth factors, TGF- $\beta$ 1, EGF, and HGF within hepatic stellate cells in response to chronic CCl<sub>4</sub> liver injury and has anti-inflammatory and anti-fibrogenic activity<sup>356</sup>. Others have debated the use of GFAP as a marker solely of stellate cells, and have instead found its expression within cholangiocytes in untreated mice and in both cholangiocytes and oval cells in response to CDE-induced liver damage<sup>352</sup>. Exposure of the liver to the hepatotoxicant, thioacetamide also induces bile duct proliferation, and showed colocalisation of GFAP with CK19-positive ductular cells<sup>351</sup>. This has further been confirmed by others using an alternative GFAP-driven transgenic mouse in response to BDL<sup>325</sup>. So although HSCs are the most prominent cell type within the liver to express GFAP in response to hepatic injury, it appears that it is by no means the only cell type to do so.

Within my current work, colocalisation assessment has shown that VSV-g pseudotyped lentivirus does not target hepatic stellate cells or cholangiocytes, but rather hepatocytes and possibly Kupffer cells. Previous sections of rat liver were negatively stained for GFAP in hepatocytes, however, these were in normal liver samples without any injury induction<sup>357</sup>. Other studies have also noted that GFAP is absent in endothelial cells, hepatocytes, and Kupffer cells<sup>326</sup>, making the bioimaging results even more intriguing. Furthermore, it is known that VSV-g pseudotyped lentivirus has a propensity for targeting Kupffer cells within the liver when administered via portal vein injection<sup>358</sup>. The F4/80 antibody, the most common marker of Kupffer cells, however failed to stain the liver samples in various conditions, and requires further optimisation and investigation. Kupffer cells cannot be disregarded as the GFAP biosensing cells until colocalisation studies are performed. Thus, the bioimaging results offer an interesting insight into the expression profile of GFAP in response to fibrosis that is not stellate or biliary cell mediated. There is a possibility that *in vivo* luciferase expression may be upregulated within hepatocytes by the truncated GFAP promoter, but that post-translational regulatory mechanisms may be involved in the stability of the protein, causing a loss of protein expression. This would account for the loss of GFAP expression within the hepatocytes within immunohistochemical samples, even though virus-targeted hepatocytes are showing a significant increase in GFAP-mediated luciferase expression at the transcriptional level. The data

indicates that GFAP within hepatocytes or possibly Kupffer cells may have a role to play within the acute phase of cholestasis, and requires further interrogation within the BDL model of fibrosis. GFAP somatotransgenic animals offer a new platform with which to study cell-type specific GFAP activity in various models of liver disease, while also being used as a platform for inhibition assays for anti-fibrotic therapy.

### **7.3 The role of WNT signalling in cholestatic liver disease**

#### **7.3.1 Hepatic $\beta$ -catenin localisation is not changed *in vivo* during BDL**

The role of Wnt signalling within the progenitor cell niche has been characterised, with nuclear  $\beta$ -catenin accumulation occurring within the progenitors to direct their hepatocytic fate in response to chronic damage. However, since my data has clearly demonstrated that there is no colocalisation of GFP with the liver progenitor marker, PKM2, the contribution of Wnt signalling output from these cells will not confound the data generated when assessing the role of Wnt signalling in hepatocytes in response to chronic biliary injury.

pBDL mice did not show a significant decrease in TCF/LEF-mediated luciferase expression compared to sham-operated animals. The overall median fold change of bioluminescence did not deviate from the basal levels, however, there was a high degree of variation seen at days 43 (pBDL) and 48 (sham), but in both cases, this was due to the signalling of a single animal, which increased the standard deviation. Liver enzymatic zonation is  $\beta$ -catenin dependent, with nuclear  $\beta$ -catenin shown to be expressed within 1-2 cell layers adjacent to the perivenous zone<sup>359, 360</sup>. Following immunohistochemical staining, however, this perivenous  $\beta$ -catenin boundary was not observed in my samples. Immunohistochemistry of sham 1 and 3 shows periportal sections with strong staining of the bile ducts, however, this staining was not nuclear and therefore not indicative of activated canonical Wnt signalling. Sham 2 clearly shows the central vein without any enhanced nuclear  $\beta$ -catenin staining within cells limited to the region surrounding this region. Strong plasma membrane staining was observed in hepatocytes and cholangiocytes. It is known that  $\beta$ -catenin is a component of adherens junctions. It is here that it binds to the cytoplasmic tails of various different cadherins, most notably E-cadherin which it tightly interacts with<sup>361</sup>. It has been hypothesised that seeing as there are many mutations within the cadherins within epithelial tumours, that this perhaps releases  $\beta$ -catenin from the adherens junctions and allows it to become part of the cytoplasmic Wnt signalling pathway. This permits  $\beta$ -catenin to interact with Tcf transcription factors and activate downstream Wnt target genes implicated in oncogenesis<sup>362</sup>, a comorbidity often featured in chronic forms of liver disease.

During the initial phases of regeneration, the Wnt/ $\beta$ -catenin signalling pathway has a fundamental role in ensuring proper G<sub>1</sub> to S transition of hepatocytes through expression of cyclin-D1, a Wnt target<sup>363</sup>. However, the hyperactivation of  $\beta$ -catenin through mutations in Axin<sup>364</sup> and Dishevelled<sup>365</sup> have been

associated with the development of hepatocellular carcinoma, a risk factor in cholestatic liver disease. The Wnt ligands Wnt3, 4, and 5a have been found to be overexpressed in hepatocellular carcinoma<sup>366</sup>. Yang *et al.* determined, through a series of cell-type specific knockouts of genes involved in Wnt secretion, that hepatocytes are not the source of Wnts secreted for canonical Wnt signalling. Rather, they produce Wnt5a, a Wnt protein involved in the termination of  $\beta$ -catenin signalling following late liver regeneration in a partial hepatectomy model. Wnt5a thus acts as a negative regulator of  $\beta$ -catenin and hepatocyte proliferation<sup>367</sup>. Chronic biliary damage also results in low levels of hepatocyte loss due to bile acid-induced hepatotoxicity, requiring regenerative intervention. It is very likely that the luminescent data obtained from the Wnt analysis during the development of cholestasis is signalling from the most abundantly transduced cells, namely the hepatocytes. Data from somatotransgenic animals indicate that Wnt signalling within targeted hepatocytes generally remains lower within the latter period of injury, and this may be due to the ensuing Wnt5a signalling in animals undergoing hepatocyte regeneration.

## **7.4 The role of Notch signalling in cholestatic liver disease**

### **7.4.1 Notch signalling displays a trend in decreased expression during acute phase of pBDL**

*In vivo* monitoring of hepatic Notch reporter activity during chronic cholestasis was assessed. The hypothesis is that an increase in Notch signalling would be seen through activation of Notch in two cell types in particular, the progenitor cells and hepatocytes. Firstly, during chronic cholestatic injury resident hepatic stellate cells would become activated, causing their transdifferentiation. These myofibroblasts express Jagged-1 ligand, and their subsequent interactions with the Notch receptor on the progenitors would be expected to increase Notch signalling<sup>40</sup>. Secondly, within a culture setting, Jagged-1 was found to be mitogenic for hepatocytes, with siRNA knockdown of either Notch or Jagged-1 resulting in a decrease in hepatocyte proliferation<sup>368</sup>. The activated Notch receptor, NICD, acts as a transcription factor that mediates the expression of several genes involved in cellular proliferation and cell cycle regulation, including Cyclin D1 and CDK2<sup>369</sup>. BDL is known to induce Fas-mediated hepatocyte apoptosis through the accumulation of toxic bile salts<sup>370</sup>, therefore, Notch-induced mitogenic signals within hepatocytes would be expected to increase hepatocyte proliferation during the regenerative process.

*In vivo* bioluminescence data using the pBDL model indicated a significant decrease in overall hepatic Notch reporter activity at several time points compared to the sham operated animals when each of the time points were analysed individually (t-tests without correction for multiple testing), however this failed to reach significance when analysed over time. This trend towards decreased expression was noted during the very early stages of disease and continued for the duration of the experiment. This result was unexpected as alternative liver disease models have definitively indicated increases in

Notch expression following injury in both hepatocytes and cholangiocytes dependent upon the injury type. Within the partial hepatectomy model, Notch and Jagged are known to be upregulated within hepatocytes for up to 4 days, and initial nuclear accumulation of NICD has been observed within 15 minutes following partial hepatectomy, with downstream target expression of HES1 seen within 30-60 minutes<sup>368</sup>. Köhler *et al.* demonstrated that increased nuclear accumulation of activated NICD began 5-15 minutes following partial hepatectomy, with non-significant fluctuations of NICD seen between the control and operated group at times between 30 minutes and 7 days post hepatectomy, in acute injury<sup>368</sup>. The Notch signalling components, Jagged-1 and Notch3, and the downstream target, *Hes1*, have been noted to be significantly upregulated in response to chronic, fibrosis-inducing CCl<sub>4</sub> treatment<sup>371</sup>. DDC-induced biliary injury mirrors these results with an increase in periportal Notch signalling components and downstream targets, *Hes* and *Hey*<sup>40</sup>.

Neonatal mice containing immature hepatocytes remain responsive to Notch signalling and have the capacity to switch fates and become BECs upon ectopic Notch pathway activation<sup>372</sup>. Notch signalling is switched off within hepatocytes or is present at very low levels in order to resist transdifferentiation toward a biliary phenotype. Aberrant function of the Notch pathway results in pathogenesis, with a number of malignancies associated with its activation<sup>373</sup>. Experiments have indicated that Notch-mediated conversion of hepatocytes to BECs is able to induce intrahepatic cholangiocarcinoma, with the intensity of Notch signalling within the hepatocytes showing a positive correlation with malignancy and disease progression<sup>374</sup>.

Immunohistochemistry revealed no differences in pBDL versus sham groups, with both groups staining intensely for NICD within the biliary epithelia. This result is unexpected as immunohistochemical evidence from previous studies have indicated that the Notch receptor is found within biliary epithelial cells, hepatocytes, and endothelial cells, while its ligand, Jagged-1, is expressed within biliary epithelial cells and hepatocytes<sup>368</sup>. Since it is known that these cell types express the required receptors for signal transduction, it was hypothesized that the levels of Notch-mediated luciferase expression would increase from the signal-producing hepatocytes in response to mitogenic signals, but this was not found to be the case. One possibility for a reduction in signaling may be the increased expression of the Notch antagonist, Numb, which has the ability to decrease downstream Notch signaling. Further interrogation into the effects of exogenous and genetic factors was subsequently assessed within the bipotent HepaRG cell line. This permitted the manipulation of Notch signaling components and the subsequent assessment of these modifications upon the differentiation potential used as a model of *in vivo* regeneration.

## **7.5 Modulation of media composition and Notch signalling results in differential capacities of hepatic progenitors to differentiate into hepatocytes and cholangiocytes *in vitro***

### **7.5.1 Notch, WNT, and $\alpha$ 1AT reporters show increased activity in response to protocol 2**

Treatment of HepaRG cells with 1.7-2.0% DMSO is the standard protocol to programme the cells to undergo hepatocyte differentiation in order to perform functional assays<sup>222, 375, 226</sup>. The seeding of HepaRG cells at a low cell density enables maintenance of their bipotent progenitor phenotype and aids in their rapid proliferation. Cells grown to confluence undergo spontaneous differentiation, albeit with low hepatocyte functionality. An alternative protocol in order to stimulate the presence of cholangiocytes from HepaRG cells has also been described through the addition of 3 components, namely IL-6, sodium taurocholate hydrate, and sodium butyrate<sup>224</sup>. The difference between these two protocols on cell-type differentiation was assessed.

Using lentiviral transduction of the Notch, WNT, and  $\alpha$ 1AT reporters, the relative contribution of each of the cell types can be compared between the two protocols. As already stated, Notch pathway activation is associated with progenitors destined for a biliary lineage, while Wnt pathway activation is associated with the hepatic lineage according to Boulter *et al*<sup>40</sup>. In contrast to the data describing  $\beta$ -catenin signalling as a driver of hepatocyte differentiation, Cerec *et al.* describe an early and transient expression of active  $\beta$ -catenin during biliary differentiation within HepaRG cells<sup>226</sup>, highlighting the temporal complexity of this signalling pathway in hepatic differentiation. Such a peak was also noted on day 4 of differentiation using protocol 2, followed by a reduction of WNT activation for the duration of the experiment.

The alpha-1 antitrypsin ( $\alpha$ 1AT) promoter element is hepatocyte-specific within this context. The promoter drives expression of the human alpha-1 antitrypsin gene which encodes a serine protease inhibitor, and is the prototypic member of the serpin superfamily. Its role is to protect tissues from the enzymes of inflammatory cells, particularly neutrophil elastase released from leukocytes, which functions to eliminate bacterial infection while concurrently causing host tissue destruction<sup>376</sup>. Hepatocyte-specificity is conferred through the presence of a distal non-specific control element, and a proximal hepatocyte-specific response element containing HNF1 and HNF4 response elements, proteins which are both enriched within hepatocytes<sup>377</sup>. Thus, the reporter vector contains the hepatocyte-specific 5' cis-acting element specifically designed for cell-specific expression<sup>378</sup> and has been utilised to assess hepatocyte differentiation.

Comparison of pathway activation during the process of differentiation resulted in a significant increase of the biliary-associated Notch pathway, and interestingly also the  $\alpha$ 1AT and WNT hepatocyte-associated pathways under protocol 2 conditions. This indicates that both cell types are being enriched for within this culture and are expressing these pathways as they terminally

differentiate. This preliminary data prompted a more comprehensive investigation of the culture using alternative molecular techniques.

### 7.5.2 Verification of increased hepatic and biliary markers using protocol 2

Immunohistochemical staining of the cultures clearly indicated that the cholangiocyte marker, CK19, and the hepatocyte markers HNF4 $\alpha$  and albumin were increased in protocol 2 cultures. Furthermore, the cultures contained clusters of small, binucleated cells that resembled primary hepatocytes. It is these colonies that stained intensely for HNF4 $\alpha$  and albumin and were surrounded by HNF4 $\alpha$ <sup>-</sup> cells. The CK19<sup>+</sup> cells surrounded these clusters and possessed a flattened morphology. Protocol 1 samples stained weakly for all of the markers, indicating a decrease in their lineage specification. Moreover, these cultures contained no colony-forming structures.

Using qPCR, quantitative validation further verified the relative abundance of hepatocyte and cholangiocyte cells within protocol 2. Since protocol 1 is a hepatocyte-specifying protocol, it is not surprising that the smallest difference is seen in albumin expression, even so, protocol 2 outperformed protocol 1 in producing cells expressing hepatic markers.

Protocol 2 was established by Dianat *et al.* to largely induce cholangiocyte differentiation. Given the constituents of the medium and the role that they play within a physiological context, it is not that surprising that the results presented here were found to enrich both cholangiocytes and hepatocytes. Day 0 indicates the day that the pleiotropic cytokine, IL-6, was added to the cells in protocol 2. IL-6 is known to be an initiator of quiescent cell re-entry into the cell cycle during the acute phase response during regeneration. IL-6<sup>-/-</sup> mice show a reduced ability to undergo hepatocyte regeneration following partial hepatectomy<sup>379, 380</sup>. This was further corroborated by Ezure *et al.* who used IL-6<sup>-/-</sup> mice, in conjunction with bile duct ligation, to confirm the reduced ability to sustain compensatory liver mass even though the rate of apoptosis was shown to be the same between WT and IL-6<sup>-/-</sup> animals. The lack of IL-6 was also associated with increased mortality rates discovered to be due to the decrease in gp130/STAT3 cell signalling<sup>381</sup>. These *in vivo* models highlight the integral role that IL-6 has in hepatocyte response to liver damage. Hepatocytes require IL-6 for their proliferation, and it is therefore not surprising that the addition of IL-6 to the medium would enhance hepatocyte differentiation potential. IL-6 is also crucial in the regenerative process of cholangiocytes. *In situ* analysis of human biliary disease samples exhibited increased IL-6 within the biliary cells and damaged ductules, particularly those originating from patients afflicted with primary biliary cirrhosis<sup>382</sup>. Moreover, corroborative *in vitro* data has demonstrated that primary intrahepatic BECs express IL-6 and secrete it within the culture medium, presumably to enhance their own proliferation<sup>382</sup>. Other studies, have shown that *SOX9* expression was downregulated following the treatment with IL-6, however this was in articular chondrocytes and the effects may be cell-type

specific<sup>383</sup>. The decrease in *SOX9* expression in response to IL-6 would thus be expected to increase the differentiation of cells toward a hepatocyte cell fate as opposed to a cholangiocyte one.

On day 2, sodium taurocholate hydrate, the sodium salt of taurocholic acid, was added to the media. *In vivo* cholic acid is synthesised from cholesterol to form bile taurocholic acid within the hepatocytes. It subsequently undergoes biotransformations by microorganisms in the intestinal lumen during enterohepatic circulation to form a number of secondary bile acids. These secondary bile acids are reabsorbed by the liver, and are subsequently conjugated to either glycine or taurine within the hepatocytes before being secreted back into the bile ducts<sup>384</sup>. Thus, during normal bile synthesis, both hepatocytes and cholangiocytes are immersed in a pool of bile acids, with the unconjugated form of taurocholic acid, namely cholic acid, being one of the most abundant<sup>385</sup>.

Lastly, on day 4 and subsequently every second day, sodium taurocholate hydrate and sodium butyrate were added to the media. According to Dianat *et al*, the addition of sodium butyrate was for the prevention of spontaneous differentiation of the HepaRG cells down along the hepatocyte lineage<sup>224</sup>. Sodium butyrate functions as a histone deacetylase (HDAC) inhibitor. Histone acetylation is an epigenetic modification that is associated with a more relaxed DNA conformation surrounding the nucleosomes, thus assisting in increased levels of gene expression<sup>386</sup>. Studies have shown enhanced differentiation potential of cells in response to HDAC inhibitor treatment. The effect of HDAC inhibitors on hepatic progenitor differentiation has been assessed through isolation of rat hepatic progenitor cells following chronically induced cholestatic disease and *in vitro* culturing and treatment with sodium butyrate. Subsequent Western blot and gross morphological assessment revealed a substantial increase in albumin expression, decreased nucleus:cytoplasmic ratio, and a 50% increase in the percentage of binucleated cells, indicative of hepatocyte-like cells<sup>387</sup>. Thus, sodium butyrate may function to retain the epigenetic signature of cells already primed to become hepatocytes through treatment of IL-6 and sodium taurocholate.

Methods of increasing the level of these cells from hepatic progenitors is immensely useful as a tool for disease modelling and drug testing as primary cells have a finite lifespan and are challenging to obtain. Instead specific populations of cells can be isolated using cell-type specific markers and using FACS analysis, thereby offering an unlimited supply of cells for research and therapeutic investigations.

### **7.5.3 *JAGGED-1* overexpression increases cholangiocyte differentiation while *Numb* overexpression results in increased hepatocyte differentiation using protocol 2**

Since Notch signalling is integral in cell-type specific differentiation, this pathway was an intriguing candidate for genetic modulation. To this end, constitutive Notch pathway activation was achieved

through overexpression of *JAGGED-1*, while its expression was inhibited using overexpression of *Numb*, a downstream target of Wnt signalling. A constitutive pLNT-SFFV-*Numb* vector was initially used to create HepaNumb cells that were hypothesised to generate an increased number of hepatocyte-like cells. Alternatively, a pCMV-Jagged-IRES-GFP vector was also used to generate HepaJag cells. Importantly, the expression of the CMV promoter is known to be silenced within hepatocytes through the action of methyltransferases and acetylases<sup>388</sup>, and therefore, the expression of Jagged and its associated GFP marker gene would thus be limited to cells fated to become cholangiocytes. Cells which were already primed to become hepatocytes would thus naturally silence the CMV promoter, thus restricting the expression of JAG1 to cells which had the capacity to differentiate to cholangiocytes only.

HepaJag cells exposed to protocol 2 appeared visually more abundant in CK19 and CK7 expression than HepaNumb cells, indicative of an increased proportion of cholangiocytes within the culture. The culture, however, was not homogenous with *Numb* overexpression correlating with an increase in cells positively stained for hepatocyte markers within the culture. HNF4 $\alpha$  and albumin were seen at lower levels in HepaJag than in the HepaNumb cells, in which over 50% of the cells were HNF4 $\alpha$ <sup>+</sup> and albumin staining was significantly more intense. *SOX9* is a downstream target of Notch signalling and one of the earliest markers of biliary fate determination from hepatoblasts<sup>90</sup>. It is interesting then that the cells that do not express JAGGED1 and are within the hepatocyte colony stain higher for *SOX9* than the cells outside. This is in contrast to other studies which have shown that knockdown of expression using a *SOX9*-specific shRNA results in the hepatogenic differentiation of human liver progenitor cells. The same publication, however, reciprocally revealed that in human samples, *SOX9* expression, specifically within the hepatocytes of diseased livers, including biliary atresia, were significantly increased<sup>389</sup>. These results indicate the need for further investigative analysis into the role of *SOX9* within hepatocytes during the regenerative process, as it may have an alternative expression profile than during development. NICD expression was also unexpectedly higher within the hepatocyte colonies within both HepaJag and HepaNumb cultures, and perplexingly in the cells that were shown to be GFP/JAGGED1 negative. This is in contrast to the mostly widely published paper regarding Notch signalling in progenitor cell differentiation towards the cholangiocyte fate by Boulter *et al*<sup>40</sup>. As expected, expression of  $\beta$ -catenin was only found within the hepatocyte clusters of both cell lines. However, this expression was mainly localised to the plasma membranes of hepatocyte-like cells, with only low levels of punctate nucleolar staining also seen within the colonies. This suggests that  $\beta$ -catenin is not active within these hepatocyte clusters following 2 weeks of HepaRG differentiation.

The marker acetylated  $\alpha$ -tubulin is ordinarily used as a marker of primary cilia, which are localised to cholangiocytes and function as osmo-, mechano-, and chemosensory regulators of bile acid levels<sup>390</sup>.

<sup>391</sup>. Terminally differentiated hepatocytes lack primary cilia and therefore this marker is proposed to be cholangiocyte-specific<sup>392</sup>. Interestingly, and in stark contrast to that seen by Dianat *et al.*, primary cilia could not be detected on either hepatocytes or cholangiocytes. This may be due to the lack of maturity of the cholangiocytes which would require subsequent culturing or due to the low resolution of the microscope compared to confocal microscopy which would make the cilia more difficult to visualise. The hypothesis that the cholangiocytes are still immature at 2 weeks following induction is based upon the concomitant low levels of CK7 seen within the culture. This cytokeratin is associated with later biliary development in humans, while CK19 is present at low levels in hepatoblasts and increases within duct cells during development<sup>393, 394</sup>. Intense staining of microtubules, centrioles, and mitotic spindles within the hepatocytes, however, were clearly visualised. The centrioles and spindles play a critical role within mitosis, while the cytoskeleton has a mechanistic role in a number of cellular processes including intracellular protein trafficking<sup>395</sup>. Post-translational modification of the microtubules has been termed the “tubulin code”<sup>396</sup>. This code is known to be modulated within alcoholic liver disease, with  $\alpha$ -tubulin being highly susceptible to post-translational modification, specifically via acetylation, due to the presence of reactive oxygen species and other reactive metabolites<sup>397</sup>. The cellular consequence of altered microtubule formation has the potential to disrupt the binding of microtubule-associated proteins and enhance steatosis<sup>395</sup>.

Cytoskeletal staining was mostly perinuclear within the HepaJag cells, while the staining was more dispersed within the entirety of the cytoplasm within the HepaNumb cells, indicative of enhanced acetylation of the tubulin in the HepaNumb cells. The acetylated tubulin staining of the HepaNumb cells was similar to cells treated with the histone deacetylase 6 inhibitor, trichostatin A (TSA), which results in the acetylation and increased stability of the microtubules, while reducing membrane trafficking<sup>398</sup>. The surrounding cholangiocytes within both cultures exhibited only modest staining. The direct contrast seen within the two different cell types warrants further investigation of the role of acetylation within the differentiation of the HepaRG cells, with the Notch modulated cells intriguingly hinting that the activation or inhibition of this signalling pathway might be involved in the altered acetylation status and possibly the stabilisation of the microtubules within these cells<sup>399</sup>. Modulation of acetylation status has been proposed as a possible therapeutic strategy for liver disease, and thus future in-depth analysis within Notch-modulated HepaRG cells might prove to be a useful tool to assess the role of altered microtubule polymerisation within hepatocytes.

Utilising qPCR, expression of the Notch downstream target, significant *HEY1* expression was confirmed in HepaJag cells. Although *HEY1* expression increased in HepaNumb cells compared to progenitors, this was lower than unmodified cells that had undergone differentiation using protocol 2, confirming Numbs repressive effect upon Notch signalling.

*SOX9* expression is low within progenitors and is shown to be upregulated in HepaJag cells. The forced overexpression of Notch signalling in HepaJag cells also led to an increase in cholangiocyte markers and a decrease in hepatocyte markers compared to HepaNumb. This confirms that Notch signalling is increased in HepaRG cells during protocol 2 differentiation. Furthermore, the expression of *JAGGED-1* in conjunction with protocol 2 results in a synergistic increase in cholangiocyte-specific markers.

HepaJag cells that underwent protocol 2 differentiation resulted in an unexpected increase in albumin expression (158.69-fold over HepaRG) when compared to differentiated HepaRG cells alone (32.86-fold over HepaRG). This may initially seem counter-intuitive; however, it has been shown by Köhler *et al.* that the addition of recombinant JAGGED-1 to primary hepatocytes induces DNA synthesis<sup>368</sup>. Furthermore, the same authors showed that both *Notch-1* and *Jagged-1* peaked within 15 minutes and remained upregulated for up to four days within hepatocytes following partial hepatectomy<sup>368</sup>. This indicates its involvement in the natural regenerative response during the early stages of acute hepatic injury<sup>368</sup>. There is a possibility that some of the cells within the culture are already “primed” to become hepatocytes as HepaRG cells have the capability to spontaneously differentiate upon confluence, albeit with significantly lower hepatocyte functional activity. Thus, the presence of JAGGED-1 may increase the proliferation of those cells which had already begun to differentiate into hepatocytes. Interestingly, YFP lineage-labelled hepatocytes that underwent forced expression of NICD over 6 weeks in an *in vivo* model triggered hepatocyte to cholangiocyte reprogramming. This reprogramming only occurred in a subset of hepatocytes, indicating that the forced expression of Notch signalling is not enough for cells to develop into biliary epithelia<sup>400</sup>. It has also been demonstrated that HepaRG cells, differentiated *in vitro* and subsequently transplanted into uPA/SCID mice, are able to undergo transdifferentiation via reversion to a bipotent progenitor phenotype, particularly upon induction of biliary injury<sup>226</sup>. Thus this Notch modulated culture system may be a useful model to elucidate the effect of Notch signalling on other signalling pathways during hepatic reprogramming events and gain more insight into what other factors are involved in the subset of Notch-expressing hepatocytes.

Overexpression of *Numb* in HepaNumb cells resulted in a further increase in albumin expression compared to both HepaRG (255.90-fold) and HepaJag (1.61-fold) cells. Data from a 2014 publication has noted that inhibition of Notch signalling utilising Notch2-specific siRNA and also the  $\gamma$ -secretase inhibitor L-685,458 promoted hepatic differentiation from isolated hepatoblasts from E14.5 livers. This was followed by a decrease in HNF-1 $\beta$  expression. The converse experiment looking at Notch upregulation resulted in an increase in HNF-1 $\beta$  expression, accompanied with a downregulation of the hepatocyte-specific markers HNF-1 $\alpha$ , HNF4 $\alpha$  and c/EBP $\alpha$ . This data strongly implicates HNF-1 $\beta$  in hepatoblast lineage specification through altering of liver-enriched transcription factors involved in

the core signalling network<sup>401</sup>. There was a moderate increase of HNF-1 $\beta$  expression in HepaJag (5.10-fold over HepaRG) compared to HepaNumb (2.72-fold over HepaRG). This lack of HNF-1 $\beta$  upregulation within the HepaNumb cell line may therefore also be a contributing factor to the increase in hepatocyte-like cells within the culture. This data confirms that *Numb* overexpression in conjunction with protocol 2 resulted in a synergistic increase in hepatocyte-specific markers. Thus, Notch modulation can be exploited as a means to enrich for hepatocyte or cholangiocyte lineages using HepaRG progenitor cells. In conclusion, protocol 2 is able to generate both BECs and hepatocytes, however, both have been shown to be immature as indicated by the low levels of CK7 seen in BECs and high SOX9 staining observed in hepatocytes. The overexpression of *JAGGED-1* within the culture results in the most mature phenotype of both cell types and indicates that Notch signalling plays a critical role in the maturation of hepatic parenchymal cell types.

## **7.6 HepaRG knockout of Sox9 using CRISPR/Cas9 technology**

### **7.6.1 Sox9 site-specific genome editing using a cas9-expressing vector**

HepaRG cells were selected to be genome edited, as these bipotent hepatic progenitors are expected to express SOX9 as progenitor cells and also as cholangiocytes, indicating that it may be required for the progenitors to differentiate into cholangiocytes. Knockout of SOX9 was therefore hypothesised to induce differentiation toward the hepatocyte lineage, which could potentially be enhanced by protocol 2 and *Numb* overexpression to produce a more homogenous culture of hepatocytes.

### **7.6.2 Bi-allelic Sox9 knockout results in a mesenchymal phenotype that is non-viable**

Unfortunately, following serial passaging of genome-edited HepaRG cells, a number of phenotypic features became apparent including a decrease in proliferative potential. The decrease in proliferation followed by a senescence-appearing phenotype is believed to be attributed to the inhibition of the G1 to S progression within the cell cycle. This has previously been validated in primary cells devoid of SOX9<sup>402</sup>. Building on this, Bellido *et al.* illustrated that a decrease in *SOX9* expression resulted in an increase in the cycle-cycle regulator, p21. Taken together, this would indicate that the enlarged, flattened Sox9<sup>-/-</sup> cells had indeed undergone senescence. Ideally, the senescence phenotype would have been confirmed at the molecular level using the cell cycle inhibitors, p16<sup>INK4a</sup> and p21<sup>CIP1</sup>, as they have been shown to also be upregulated during growth arrest. The p21 tumour suppressor has also been known to be upregulated in response to several growth factors and cytokines that are involved in the process of liver regeneration and differentiation particularly by mediating the anti-apoptotic effects of IL-6-type cytokines like OSM<sup>403</sup>. The knockout data strongly suggests that SOX9 may indirectly have a role in cell-cycle regulation, and may account for the non-viability of cells which do not express it.

Furthermore, prior to senescence, Sox9<sup>-/-</sup> cells appeared more elongated (spindle-shaped), mesenchymal-like, and more motile compared to the more polarised stationary epithelial cells. This would suggest that epithelial to mesenchymal transition (EMT) had taken place. This data is also in line with other studies which have shown that the loss of SOX9 *in vivo* is associated with increased risk of cholangiocarcinoma and poorer prognosis. EMT is a common feature of cancers, with an increase in mobility associated with metastasis<sup>404</sup>.

Recently, Paganelli *et al.* assessed the role of Sox9 expression during the differentiation process, and the impact of its altered expression. Firstly, they noted that hepatic differentiation within liver mesenchymal stem/progenitor cells resulted in approximately 70% decrease in SOX9 mRNA expression. This information is critical for subsequent experiments, as it appears that only 30% SOX9 expression is required for cell viability, as the authors do not note any senescence phenotype within their progenitor cells. Secondly, they revealed that the blunting of SOX9 expression, using a shRNA-containing lentivirus, caused an increase in the hepatic marker, tryptophan 2,3 dioxygenase (TDO), while subsequently downregulating the expression of CK19 within differentiated progenitor cells. A number of alternative early hepatic markers, however, did not show an increase in expression<sup>389</sup>. The same authors detected an increase in hepatic SOX9 expression within human disease liver samples. Cancers overexpressing SOX9 have shown to have increased proliferation coupled with inhibition of senescence. The proposed mechanism behind these traits is the ability of SOX9 to bind to the promoter of *Bmi1*, a polycomb protein which acts to suppress the tumour suppressor, *Ink4a/Arf*<sup>402</sup> giving the reciprocal phenotype compared to SOX9 knockout. Thus, further investigation into its role in differentiation and disease could lead to novel drug targeting strategies to regulate its expression in hyperplastic scenarios.

Since there is a proposed connection between downregulated SOX9 and an increase in hepatocyte differentiation, it would be interesting to determine whether the combination of HepaNumb expressing, SOX9-downregulated cells differentiated via the 3-component protocol would yield a further synergistic upregulation of hepatocyte markers. A reduction in SOX9 expression could be achieved either through the stable expression of a SOX9 shRNA or through the generation of a heterozygous CRISPR knockout. It is predicted that this trio of modifications would result in an increased proportion of hepatocyte colonies arising from the HepaRG progenitor cells.

## 7.7 Conclusions

The development of the described methodologies has a broad scope of applicability for models of disease. The generation of biosensing, reporter animals that are able to undergo longitudinal assessment of transcription factor activity in response to disease induction or drug intervention has significant implications for the number of animals currently being utilised within research.

Furthermore, the data shows that this novel platform is able to generate more data per animal when used in conjunction with existing germline transgenics. The specificity of transduction decreases confounding background luciferase expression, and is conferred through targeted viral delivery methods and viral vector pseudotyping. The use of this technology specifically within the context of hepatic fibrosis has highlighted the temporal activation of NF- $\kappa$ B during the acute phase of the disease, with activation of myofibroblasts mirroring this signalling profile when using the GFAP reporter. The signalling profile of SMAD signalling was distinct, with a cyclical expression profile exhibited, in particular with increased intensity during the acute phase followed by a stabilisation of expression subsequent to the initial injury. While Notch and Wnt signalling have recently been shown to be critical in the differentiation of hepatic progenitors during hepatic or biliary injury, our data largely targets hepatocytes, and indicated that the role of Notch and Wnt signalling within hepatocytes did not contribute to disease progression or regeneration as they did not show significant upregulation of luciferase in response to pBDL. Further work is required in order to specifically target the cholangiocytes with Wnt and Notch biosensing reporters to monitor responses during progenitor cell differentiation during cholestasis. This model could further be used to analyse the use of Numb as a potential gene therapy for cholestatic liver disease through its inhibition of the biliary cell-inducing Notch pathway.

Furthermore, this data builds upon the work developed by Dianat *et al.* who were the first to describe the addition of 3 components to HepaRG media in order to specifically enrich the culture for functional cholangiocytes. The data presented in this body of work increases our understanding of the role of Notch signalling within the hepatic progenitors in order to guide their differentiation down a particular path. It was shown that the overexpression of *JAGGED*, in conjunction with the Dianat differentiation protocol, resulted in improved yields of cholangiocyte cells within the culture, while the overexpression of Numb in this culture media was found to decrease cholangiocyte markers while enhancing the presence of hepatocyte-like colonies. Thus, modulation of the Notch signalling pathway within HepaRG cells is a useful development in order to enhance for a particular cell type arising from the bipotent progenitors. This has implications in functional studies as current cell lines do not adequately recapitulate the functionality of primary hepatocytes in culture.

---

**CHAPTER EIGHT**

**MATERIALS AND METHODS**

---

## 8.0 Materials and Methods

### 8.1 Cloning of the constitutive SFFV- and GW-JDG parental vectors

Overlap-extension PCR was employed to generate a bicistronic cassette consisting of the 3xFLAG with the luciferase and 2A-eGFP as depicted in **Figure 61**.

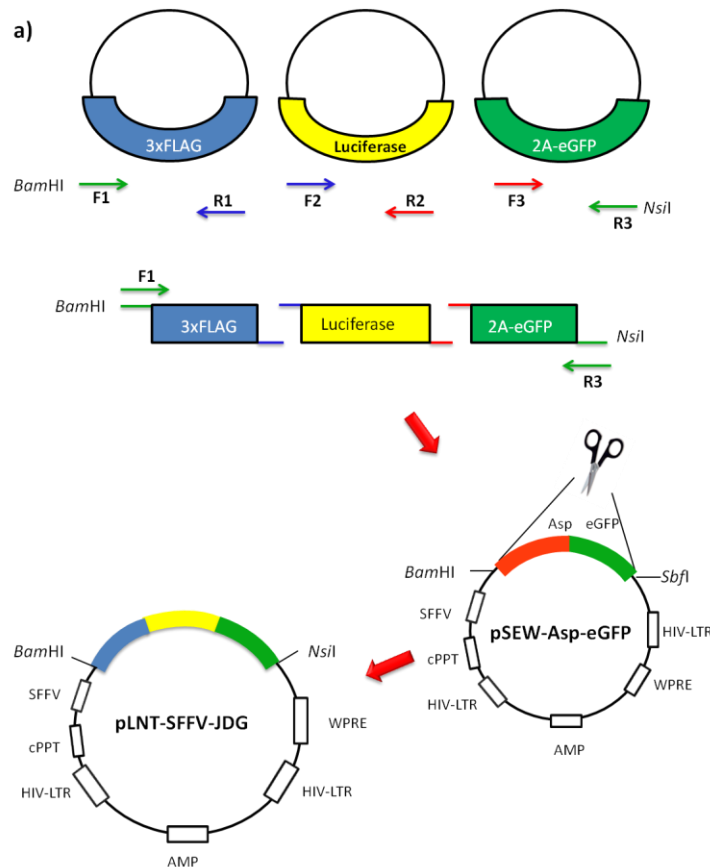


**Figure 61. Overlap extension concept and cloning of pLNT-SFFV-JDG.**

Diagram depicting primer pairs used during primary amplification of 3xFLAG, firefly luciferase, and eGFP amplicons, and secondary PCR primers used in subsequent fusion PCR. Final fused product (*Bam*HI / *Sbf*I) was cloned into the pSEW-Asp-eGFP (*Bam*HI / *Nsi*I) to yield the constitutively expressed reporter construct, pLNT-SFFV-JDG vector.

#### 8.1.1 Primary PCR reagents and cycling parameters

Using three plasmid vectors as template, 3xFLAG, FLuc, and 2A-eGFP were each separately amplified with gene-specific primers as partially overlapping fragments. Primer F1 was engineered to contain a *Bam*HI restriction site, while primer R3 contained an *Nsi*I site (also highlighted in red). Primer pairs are listed in

**Table 3** and reaction parameters in (**Table 4**).

**Table 3. Primers used to generate primary products for 3xFLAG-FLuc-2A-eGFP construction.**

Primer	Sequence (5' --> 3')
<b>3xFLAG (F1)</b>	CTGGGGCCACGAG <b>▼ GATCC</b> GCCACCATGGACTACAAAGACCATGACGGTGATTATAAGATC
<b>3xFLAG (R1)</b>	TTCTTGGCGTCCTCCATGCTGCCGCCGCCGCTCTTG
<b>Fluc (F2)</b>	GCAGCATGGAGGACGCCAAGAACATCAAGAAGGG
<b>Fluc (R2)</b>	CTGCGCGGATCTTGCCGCCCTTCTTGCC
<b>2A-eGFP (F3)</b>	AAGGGCGGCAAGATCCGCGCAGAGGGCCGGGGCTCAT
<b>2A-eGFP (R3)</b>	GTCAGCTGGGCA <b>ATGCA ▲</b> TACTAGTTTGTGAGTCAAACCTAGAGCCTGGACCA

Note: Restriction enzyme sites highlighted in red

**Table 4. Reaction parameters to generate primary products for 3xFLAG-FLuc-2A-eGFP construction.**

Reagent and Concentration	Volume
Phusion buffer HF (5X)	10.0 µl
Forward primer (25 µM)	1.0 µl
Reverse primer (25 µM)	1.0 µl
dNTPs (10mM)	1.0 µl
Phusion® polymerase (1U)	0.5 µl
DNA (200 ng/µl)	1.0 µl
dH <sub>2</sub> O	35.5 µl
<b>Final Volume</b>	<b>50 µl</b>

PCR amplification of target DNA was achieved by an initial denaturation 98°C for 30 seconds followed by 40 cycles of 98°C for 35 seconds, 65°C for 40 seconds, 72°C for 1 minute 42 seconds. There was a final elongation step of 72°C for 10 minutes.

### 8.1.2 Secondary PCR to create the 3XFLAG-FLuc-2A-eGFP bicistronic cassette

Initially, primary PCR fragments were gel purified using the QIAquick Gel Extraction Kit (Qiagen). Excised gel slices were dissolved in guanidine thiocyanate-containing Buffer QG before being applied to a silica membrane column. The column was centrifuged at 13,000 rpm for 1 minute before undergoing a series of ethanol washes in Buffer PE. DNA was eluted in 30 µl dH<sub>2</sub>O. The products of gel extraction were assembled through overlap-extension secondary PCR using all three primary PCR products as template and 3xFLAG (F1) and 2A-eGFP (R3) primers for amplification as shown in (Table 5). PCR amplification was achieved as follows: an initial denaturation step at 98°C for 2 minutes was followed by 35 cycles of 98°C for 40 seconds, 65°C for 40 seconds, 72°C for 2 minute 30 seconds. There was a final elongation of 72°C for 10 minutes.

**Table 5. Reagents and concentrations for secondary overlap-extension PCR.**

Reagent and Concentration	Volume
Phusion buffer HF (5X)	10.0 $\mu$ l
Forward primer (25 $\mu$ M)	1.0 $\mu$ l
Reverse primer (25 $\mu$ M)	1.0 $\mu$ l
dNTPs (10mM)	1.0 $\mu$ l
Phusion <sup>®</sup> polymerase (1U)	0.5 $\mu$ l
Template DNA (3xFLAG)	1.0 $\mu$ l
Template DNA (Fluc)	1.0 $\mu$ l
Template DNA (2A-eGFP)	1.0 $\mu$ l
dH <sub>2</sub> O	33.5 $\mu$ l
<b>Final Volume</b>	<b>50 <math>\mu</math>l</b>

### 8.1.3 Restriction digest and ligation to produce pLNT-SFFV-JDG

The triple-template DNA amplicon formed from the secondary PCR consists of 3xFLAG-FLuc-2A-eGFP, and this bicistronic cassette shall hereinafter be termed JDG. In order to clone the JDG insert into a 2<sup>nd</sup> generation lentiviral expression vector, the amplicon was further purified using the QIAquick PCR Purification Kit (Qiagen) as per manufacturer's instructions. Briefly, the PCR reaction was resuspended in 5 PCR volumes of buffer PB. The solution was loaded onto the silica membrane-containing column and briefly centrifuged before undergoing an ethanol wash with buffer PE. Residual ethanol was removed through the addition of a second centrifuge step, followed by elution of purified PCR product in 30  $\mu$ l of dH<sub>2</sub>O. Purified DNA subsequently underwent restriction enzyme digestion to form DNA overhangs. The JDG amplicon was double-digested with *Bam*HI / *Nsi*I (NEB) restriction enzymes and ligated into pSEW-Asp-eGFP (**Appendix A.i**) which was *Bam*HI / *Sbf*I (NEB) digested to remove the *Aspergillus*-IRES-eGFP bicistronic cassette, leaving the lentiviral backbone containing the constitutive SFFV promoter intact. Since only the four-base overhang needs to be complementary, and not the whole restriction recognition sequence, it is possible to ligate a molecule that has been digested with *Nsi*I (ATGCA▼T), which has an overhang sequence of TGCA, with *Sbf*I, whose recognition sequence is CCTGCA▼GG and also creates an overhang sequence of TGCA following digestion. The reactions are detailed in **Table 6**. All restriction digests were carried out at 37°C for 4 hours.

**Table 6. Restriction enzyme digests of JDG insert and pSEW-Asp-eGFP backbone.**

Reagent	Insert digestion Volumes	Vector Backbone digestion Volumes
dH <sub>2</sub> O	-	69.0 µl
Buffer 3 (NEB)	10.0 µl	10.0 µl
BSA (100x) (NEB)	1.0 µl	1.0 µl
<i>Bam</i> HI	5.0 µl	5.0 µl
<i>Nsi</i> I	5.0 µl	-
<i>Sbf</i> I	-	5.0 µl
Insert	79.0 µl (12.0 µg)	-
Backbone - pSEW-Asp-GFP	-	10.0 µl (5.0 µg)
<b>TOTAL</b>	100.0 µl	100.0 µl

Both vector and insert were subjected to gel electrophoresis at 90 V/cm<sup>2</sup> for 30 minutes on a 1% agarose gel containing 5 µl / 100 ml GelRed (1X) to isolate and purify the DNA. The DNA products were gel extracted using the QIAquick gel extraction kit and subsequently ligated using a Quick Ligation Kit (NEB) both as per manufacturer's instructions. The pLNT-SEW lentiviral backbone and JDG PCR product insert were ligated using the volumes of vector, insert, and ligation reagents as noted in **Table 7** with the reaction performed at room temperature for 5 minutes.

**Table 7. Reagents and volumes for quick ligation of pLNT-SFFV-JDG.**

Reagent	Volume
dH <sub>2</sub> O	2.0 µl
Buffer (2x)	10.0 µl
Digested vector (pSEW-Asp-eGFP)	1.5 µl
Digested insert (JDG)	5.0 µl
Quick ligase	1.5 µl
<b>TOTAL</b>	20 µl

#### 8.1.4 Transformation and positive clone selection of pLNT-SFFV-JDG

Using 5 µl of the ligation reaction, Stb13 competent cells were transformed by incubating the DNA with the competent cells on ice for 20 minutes. This was followed by a 30 second heat-shock at 42°C and rapid cooling on ice for 2 minutes. 250 µl pre-warmed super optimal broth with catabolite repression (SOC) media was added to the competent cells and allowed to recover for 1 hour at 37°C in the shaking incubator at 220 rpm. The transformation reaction was plated onto Luria broth (LB)-containing agar plates supplemented with 100 µg/ml carbenicillin (Sigma), a more stable analogue of ampicillin, to select for plasmid-containing clones and incubated overnight at 37°C. Colonies were selected and placed in 5 ml of LB broth containing carbenicillin (100 µg/ml) overnight. Plasmid DNA was isolated using the QIAprep Spin Miniprep Kit (Qiagen). The overnight culture was

pelleted to remove the LB broth before being resuspended in 250 µl buffer P1. Bacterial alkaline lysis was carried out using 250 µl buffer P2 for 5 minutes after which 350 µl buffer P3 was used to neutralise and stop the lysis reaction. Following 10 minutes of centrifugation at 13,000 rpm to precipitate the cellular debris the supernatant was transferred to a silicon membrane column. Following binding of the DNA to the column using 500 µl Buffer PB followed by centrifugation, the column was washed with 750 µl buffer PE before the DNA was eluted in water. Purified plasmid DNA was used in a restriction digestion to determine the presence of a positive clone. A double digest was set up using *Mlu*I and *Nhe*I restriction enzymes incubated for 1 hour at 37°C with the reagents and volumes as outlined in (Table 8).

**Table 8. Restriction digest reagents and volumes for the detection of positive recombinant clones.**

Reagent	Volume
dH <sub>2</sub> O	13.0 µl
Buffer 2 (NEB)	2.0 µl
BSA (10x) (NEB)	2.0 µl
<i>Mlu</i> I	1.0 µl
<i>Nhe</i> I	1.0 µl
Clone Plasmid DNA (0.5 µg)	1.0 µl
<b>TOTAL</b>	<b>20.0 µl</b>

The products of restriction digestion were analysed by agarose gel electrophoresis. Using 4 µl of loading dye to the 20 µl restriction digest reaction, the samples were loaded onto a 1% agarose gel containing 1x GelRed. The samples were electrophoresed at 120 V/cm<sup>2</sup> for 40 minutes in Tris-acetate-EDTA (TAE) buffer. Positive clones were sequenced (Source Bioscience), with predicted sequence of the inserts available in **Appendix B**, and the novel bicistronic vector, hereon termed pLNT-SFFV-JDG, available in map format in **Appendix A.ii**.

### 8.1.5 Cloning to create the parental pLNT-GW-JDG vector

Using pLNT-SFFV-JDG vector as template, the JDG insert was excised using a *Bam*HI and *Mlu*I double digest and subcloned into the pZsGreen-C1 vector (Clontech) (**Appendix A.iii**) digested with the same enzymes. This construct was termed pZsGreen-JDG, and was used as a subcloning vector before the insert could be cloned into its final lentiviral vector. pZsGreen-JDG was double digested with *Sall* / *Mlu*I restriction enzymes and cloned, using quick ligase as per manufacturer's protocol, into pLNT-Gateway-MCS (**Appendix A.iv**) using the compatible *Xho*I / *Mlu*I sites. This produced a novel destination vector with which to recombine pENTR clones into. *Sall* (G▼TCGAC) and *Xho*I (C▼TCGAG) generate the same sequence overhangs after digestion, also known as compatible

cohesive ends (underlined), and can therefore be ligated together. The parental vector, pLNT-GW-MCS (a kind gift from Dr Steven Howe, UCL), is a second generation lentiviral vector containing a multiple cloning site downstream of the Gateway reading frame C cassette. This facilitates cloning of transgenes, in this case JDG, downstream of the Gateway cassette into which specific promoters or transcription factor activated response elements can be recombined in order to drive expression of the downstream transgene. Restriction enzyme reactions were carried out at 37°C for 4 hours. The Gateway cassette contains dual resistance genes, namely *ccdB* toxicity and chloramphenicol resistance genes. The *ccdB* toxicity gene encodes a cytotoxic protein which acts as a potent poison of DNA-topoisomerase II complexes. Ligation reactions were transformed into *ccdB*-resistant DB3.1 competent cells (Invitrogen) and selected for using ampicillin (100 µg/ml) (Sigma). Clones were grown overnight in LB broth containing ampicillin (100 µg/ml) and plasmid isolated and purified using the QIAprep spin mini-prep kit as per manufacturer's instructions. Positive-clone selection was performed by *Sbf*I / *Mlu*I double digestion for 1 hour at 37°C. A single colony showing the predicted DNA bands after restriction digestion and gel electrophoresis on a 1% agarose gel was selected and further amplified overnight in LB broth at 37°C. Plasmid was isolated and purified using the QIAprep midi-prep kit (Qiagen) as per manufacturer's instructions. The resultant pLNT-GW-JDG (**Appendix A.v**) lentiviral cassette has a Gateway cloning acceptor site upstream of the FLuc-2A-eGFP JDG bicistronic reporter cassette.

## 8.2 Cloning of pLNT-GW-NanoLuc®-2A-eGFP and pLNT-SFFV-VLuc

In order to analyse multiple pathways *in vitro* and *in vivo* simultaneously, alternative luciferases, each with particular substrate specificity, can be utilised. In order to construct such vectors, the luciferases, NanoLuc®, as well as the 2A-eGFP fragments were initially amplified in a primary PCR. The template for the secreted NanoLuc® was the pNL1.3 vector (Promega), while the 2A-eGFP fragment was amplified from the pLNT-SFFV-JDG vector which is previously described. The primers were engineered with *Xho*I (C▼TCGAG) and *Mlu*I (A▼CGCGT) restriction sites flanking the primers. The PCR primers have overlapping sequences to allow subsequent annealing and extension of the fragments in subsequent secondary or overlap-extension PCRs which would yield a fused product. Primer sequences and primary PCR parameters were set out as in **Table 9a**. PCR amplification of target DNA was achieved by an initial denaturation of 98°C for 30 seconds followed by 45 cycles of 98°C for 10 seconds, 57°C for 30 seconds, 72°C for 45 seconds and a final elongation step of 72°C for 5 minutes. Using overlap extension PCR as per **Table 9b**, NanoLuc was fused to 2A-eGFP to yield NLuc2. PCR cycling parameters were: initial denaturation 98°C for 2 minutes followed by 35 cycles of 98°C for 40 seconds, 65°C for 40 seconds, 72°C for 2 minutes with a final elongation step of 72°C for 10 minutes. Secondary PCR amplicons were column purified as previously described and double-digested with *Xho*I / *Mlu*I, heat inactivated, and directionally cloned into the pLNT-GW-MCS

vector digested with the same enzymes. The vector and insert were ligated using the NEB Quick Ligase kit as per manufacturer's instructions using a 3:1 molar ratio of insert:backbone. Confirmation of correct clones was carried out using a *XhoI* / *MluI* restriction digest to excise the NLuc2 bicistronic insert. The resultant plasmid contained the NLuc2 dual luminescent/fluorescent cassette downstream of the Gateway® cassette. The plasmid map is listed in **Appendix A.vi**.

The constitutively expressing vargula plasmid was developed by amplifying vargula from the pCMV-Cypridina vector (ThermoFisher Scientific) using primers designed to contain a *BamHI* (G▼GATCC) and a *NotI* (GC▼GGCCGC) restriction site on the primers. Following PCR amplification as outlined in **Table 9a**, the PCR product was cleaned using the Qiagen PCR purification kit before being digested with *BamHI* / *NotI* and ligated into pENTR-1A digested with the same enzymes. Correct clones were selected by performing a *BamHI* / *NotI* digest on clones. A clone containing the correct insert was used in the Gateway® recombination reaction into the pLNT-SFFV-GW vector. Screening for a positive clone was performed by using *BamHI* / *NotI* restriction enzymes. The map of pLNT-SFFV-Vluc can be found in **Appendix A.vii**. PCR amplification of target DNA was achieved by an initial denaturation of 98°C for 30 seconds followed by 45 cycles of 98°C for 10 seconds, 57°C for 20 seconds, 72°C for 30 seconds. There was a final elongation step of 72°C for 5 minutes. All primers used to develop both the pLNT-GW-NLuc2 and pLNT-SFFV-Vluc vectors are given in (**Table 10**) with the relevant restriction sites highlighted in red and the site of cleavage shown by the ▼ symbol.

**Table 9. Primary and Secondary PCR for the generation of NLuc-2A-GFP and VLuc.**

Reagent	Volume
Standard Q5 buffer (5x)	10 µl
dNTPs (10 mM)	1.0 µl
Forward primer (10 µM)	0.5 µl
Reverse primer (10 µM)	0.5 µl
Q5 high-fidelity polymerase	0.5 µl
dH <sub>2</sub> O	36.5 µl
pNL1.3 (Sec Nluc) or pCMV-Cypridina DNA template (100 ng)	1.0 µl
TOTAL	50 µl

Reagent	Volume
Buffer HF (5x)	5.0 µl
GC Enhancer	5.0 µl
dNTPs (10 mM)	1.0 µl
Forward primer (10 µM)	1.0 µl
Reverse primer (10 µM)	1.0 µl
Phusion polymerase	0.5 µl
DNA	0.5 µl of each 1° PCR product
dH <sub>2</sub> O	33.5 µl
TOTAL	30 µl

**Table 10. Primers oligonucleotides for amplification of NanoLuc®, 2A-eGFP and vargula.**

Primer	Sequence
Nluc Forward	CACAC ▼ TCGAGGCCACCATGAACTCCTTCTCCACAAGCG
Nluc Reverse	CAATGAGCCCCGGCCCTCTGCGCGCGCCAGAATGCGTTCGCACAGCCGCCAGCCGGTCAC
2A-eGFP Forward	CTGGCGGCTGTGCGAACGCATTCTGGCGCGCGCAGAGGGCCGGGGCTCATTGCTGACCTGTGGAG/
2A-eGFP Reverse	GATGACGCG ▼ TTTACTTGTACAGCTCGTCCATGCCG
Vluc Forward	TATCG ▼ GATCCGCCACCATGAAGACCCTGATC
Vluc Reverse	GAGTGC ▼ GGCCGCTCACTTGCACCTCGTC

### 8.3 Recombination reactions to produce lentiviral reporters.

The sub-cloning plasmid pENTR-1A (**Appendix A.viii**) contains Gateway® directional homologous recombination arms flanking the chloramphenicol and *ccdB* bacterial toxicity gene with multiple cloning restriction sites on either side. First, the chloramphenicol/*ccdB* expression cassette was removed by performing an *EcoRI* restriction enzyme digest to remove the cassette, followed by religation of the *EcoRI* sites using quick ligase. We will forthwith describe this as “empty” pENTR. Next, overlapping oligonucleotides were designed to encode the adenoviral E1A minimal promoter (MP) sequence with flanking *XhoI* restriction sites at the termini as shown in **Table 11**. The E1A oligos were initially placed at a concentration of 5 µM in a buffer solution (NEB buffer 4) and heated to 75°C for 10 minutes, followed by slow cooling to allow the oligos to hybridise. Once annealed, the oligos were subjected to *XhoI* restriction enzyme digestion, isolated by gel electrophoresis and column purified. The E1A minimal promoter sequence was then ligated into the *XhoI* site in empty pENTR vector, the resultant cloning vector was called pENTR-MP. Subsequently, all transcription factor binding elements were cloned into the pENTR-MP vector by Aldevron using the *BamHI* / *EcoRI* restriction enzyme sites.

Once the Gateway and pENTR vectors were cloned, a recombination reaction was performed using the Gateway® LR Clonase™ Enzyme Mix (Invitrogen) which contains the recombination proteins, integrase and excisionase. The site-specific recombination reaction occurs between regions of sequence homology, e.g. the *attL* sites found flanking the transgene (in this case the response elements with MP) within the pENTR vector and the *attR* sites found flanking the Gateway cassette in the destination vector. Non-recombinants are dually selected against. Bacteria transformed with the non-recombined parental vector containing *ccdB* are killed due to its cytotoxicity in *ccdB*-sensitive, *Stb13* competent cells. Non-recombined pENTR vectors are selected against through antibiotic selection, as the pENTR vectors contain kanamycin resistance, while the destination vector contains the ampicillin resistance gene. Theoretically this should lead to the growth of bacteria transformed

only with recombinants on the ampicillin agar plates. All LR recombination reactions were performed as per the Invitrogen Gateway cloning manual.

**Table 11. Sequence of adenoviral E1A minimal promoter oligos.**

Primer	Sequence (5' --> 3')
Minimal promoter (Forward)	C▼TCGAGGGGCTATAAAAGGGGGTGGGGGCGCGTTCGTCCTCACTCTCTCC▼TCGAG
Minimal promoter (Reverse)	GAGCT▲CCCCGATATTTCCCCACCCCGCGCAAGCAGGAGTGAGAGAAGG GAGCT▲C

## 8.4 Validation of the pLNT-SFFV-JDG vector

### 8.4.1 Fluorescence-Activated Cell Sorting for 3xFLAG tag and eGFP

HEK293T cells transfected with pLNT-SFFV-JDG were washed with PBS (Sigma), trypsinised with trypsin-EDTA (Sigma), and centrifuged for 5 minutes at 400x g. Supernatant was removed and cells resuspended in PBS. To each tube, 250 µl Cytotfix (BD Biosciences) was added and incubated at 4°C for 20 minutes. Subsequently, 2 ml Perm/Wash permeabilisation buffer (BD Biosciences) was added followed by centrifugation at 400x g for 5 minutes. The supernatant was decanted and the pellet resuspended in residual buffer. To this, 1 µl primary anti-FLAG M2 (Sigma) antibody was added, vortexed, and incubated at 4°C for 15 minutes. Following incubation with the primary antibody, 2 µl of the secondary APC goat anti-mouse Ig antibody was added, the cells briefly vortexed, and subsequently incubated at 4°C for 15 minutes. A further 3 ml Perm/Wash was added and the cells centrifuged at 400x g for 5 minutes. The pellet was resuspended in 500 µl PBS. The CyAn ADP was used for flow cytometry with Summit v4.0 used for data capture. For GFP FACS, samples were trypsinised, washed twice in PBS, and flow cytometry performed using the FACS Calibur Flow Cytometer with data capture performed using Cell Quest, and data analysis carried out using the FlowJo v7.6.4 software.

### 8.4.2 Western blot for 3xFLAG and eGFP

Growth medium was removed and cells were subsequently washed twice in PBS pre-warmed to 37°C. Cells were resuspended in 300 µl 2x Laemmli sample buffer (Sigma) for 5 minutes and homogenised by being passed through a 21G syringe approximately 10 times. Samples were centrifuged at 13,000x g for 2 minutes and the soluble protein containing supernatant separated from the insoluble debris pellet by aspiration. From each sample, 12 µg of total protein quantified by Bradford assay was diluted in 300 µl Laemmli sample buffer (2x) for 5 minutes. Samples were boiled for 10 minutes at

100°C and centrifuged at 13,000x g for 5 minutes to remove any contaminating insoluble debris. Protein was separated by polyacrylamide gel electrophoresis. Protein samples were loaded in up to 20 µl volumes or 10 µl Novex Sharp Pre-stained Protein Standard (Life Technologies) in 1x MOPS buffer (Life Technologies) onto a 10% NuPAGE Novex gel (Life Technologies). Samples were subjected to electrophoresis for 75 minutes at 150 Volts. After electrophoresis, the protein containing gel, filter paper (Millipore), and PVDF transfer membrane (Millipore) were equilibrated in 1x transfer buffer (2.4g tris, 9g glycine, and 20 ml methanol) and protein transfer to the PVDF membrane performed at 15 volts for 30 minutes. The transfer membrane was incubated at 4°C overnight in blocking solution containing 5 % w/v non-fat powdered milk in 1x PBS and 0.1% Tween-20 (PBS-TWEEN). Blocking solution was discarded and the membrane incubated for a further 3 hours at room temperature in 10 ml PBS-TWEEN containing 5% w/v non-fat powdered milk, 1.0 µl (1:10,000) mouse anti-β-actin antibody (Sigma) as the loading control, and a primary antibody; either 10µl (1:1,000) rabbit anti-3xFLAG antibody (Sigma) or 1.0 µl (1:10,000) rabbit anti-GFP antibody (Abcam). The membrane was briefly washed 3 times for 10 minutes in PBS-TWEEN at room temperature. The wash solution was discarded and the secondary goat anti-rabbit and goat anti-mouse fluorophore-containing antibodies were each diluted (1:10,000) in PBS-TWEEN containing 5% w/v non-fat powdered milk and incubated in foil on the shaker for 1 hour at room temperature. The membrane was briefly washed three times for 10 minutes in PBS-TWEEN on the shaker. A brief final wash was performed using PBS only. Fluorescent imaging of the membrane was carried out using the Odyssey Infrared Imaging System (Li-Cor Biosciences) as per manufacturer's instructions. The green channel (800 nm) was used for sample detection, and red channel (680 nm) for β-actin loading control detection.

### **8.5 Bradford assay for total protein quantification**

This colourimetric assay is based on the binding of the acidic dye, Coomassie Brilliant Blue G-250, in response to varying concentrations of protein followed by spectrophotometric reading<sup>405</sup>. Growth medium was removed and cells were subsequently washed once in PBS pre-warmed to 37°C. Cells were subjected to lysis using 300 µl per well of a 12-well plate (ie. 3.8 cm<sup>2</sup>) luciferase lysis buffer (10 mM Tris phosphate pH 8.0, 1mM EDTA pH8.0, 0.65% NP40, 150 mM NaCl) was added. The cell lysis supernatant was subjected to centrifugation for 1 minute at 13,000x g to precipitate cell debris. Five microliters of the soluble fraction of cell lysate was aliquoted into wells of a 96-well plate and 195 µl diluted (1:5) Protein Assay Dye Reagent (Biorad) was added. Samples were incubated for 5 minutes at room temperature, and the absorbance read at 595 nm using the Promega Glomax (Promega) as per manufacturer's instructions.

## 8.6 Luciferase assay for the assessment of luciferase reporter activity

Approximately  $5 \times 10^5$  cells were lysed in 300  $\mu$ l luciferase lysis buffer (0.65% NP40, 10 mM Tris (pH 8.0), 1 mM EDTA (pH 8.0), 150 mM NaCl) and the soluble fraction of the supernatant clarified by centrifugation at 13,000x g for 1 minute. Using 20  $\mu$ l of cell extract, each sample was plated in triplicate in an opaque, white, 96-well microplate. To this, 20  $\mu$ l assay buffer (25 mM Tris phosphate pH 7.8, 1 mM DTT, 1 mM EDTA, 1% Triton X-100, 8 mM  $MgCl_2$ , 3 ml glycerol, 1.25 mM rATP, 0.5% BSA)(All purchased from Sigma) was added. Luciferin substrate (Gold Biotechnology) was injected into each well at a final concentration of 1.5 mM. Luminescence output was measured using the POLARstar Omega microplate reader (BMG Labtech) and analysis performed using MARS data analysis software (BMG Labtech). Relative photonic light units were normalised relative to total protein as determined by Bradford assay.

## 8.7 General cell culture

HEK293T, HeLa, HepG2, Huh7, NIH3T3, MEFs and HDF cells were cultured in Dulbecco's Modified Eagle's Media (Sigma) supplemented with 10% fetal bovine serum (FBS) (Gibco), 1% penicillin/streptomycin (Sigma), 2 mM L-glutamine (Gibco) and 1x non-essential amino acids (Gibco). Primary mouse embryonic fibroblasts (MEFs) and human dermal fibroblasts (HDFs) were plated at around 60-70% confluence onto tissue culture plastic pre-coated with 0.1% gelatine and incubated at 37°C for 1 hour.

HepaRG cells were cultured in William's E medium containing Glutamax and sodium pyruvate (Invitrogen) supplemented with 10% FBS (Gibco), 1% pen/strep (Sigma), 1x non-essential amino acids, 4  $\mu$ g/ml human recombinant insulin zinc solution (Gibco), and 50  $\mu$ M hydrocortisone (Sigma). Cells were plated onto plates pre-coated with 50  $\mu$ g/ml collagen I (Santa Cruz Biotechnology) solubilised in 0.02N acetic acid (Sigma) and incubated at room temperature for 1 hour.

SGHPL5 cells were cultured in Ham's F-10 medium (Sigma) supplemented with 10% FBS, and 1% pen/strep.

All cell lines were incubated at 5%  $CO_2$  humidified atmosphere at 37°C.

## 8.8 Isolation and culturing of CD1 and *tlr4*<sup>-/-</sup> MEFs

Pregnant mice were terminally anaesthetised using isofluorane approximately 14 days post-coitum. The abdominal cavity was doused with 70% ethanol to ensure sterile conditions prior to surgery. The uterine horns containing the embryos were immediately placed in sterile PBS on ice. Subsequent procedures were performed in a sterile hood and on ice inasmuch as possible. The head and soft

organs were removed and the remaining carcass was washed in two changes of ice-cold PBS. The cleaned carcass was subsequently minced as finely as possible using scissors and a clean, sharp scalpel. To each embryo in a 50 ml Falcon tube, 4 ml of trypsin/EDTA (0.25%) was added and incubated at 37°C for 5 minutes. This was mixed by pipetting of the fragments using a P1000, and leaving the trypsin to digest material for a further 5 minutes. After incubation, 20 mls of mEF media (DMEM + 10% FBS + Glutamine + Pen/Strep + NEAA) was added to each tube and subsequently centrifuged for 5 minutes at 1200 rpm. The trypsin-containing supernatant was removed as much as possible, the pellet resuspended in 15 mls of mEF media, and plated on 0.1% gelatine-coated flasks, at a density of 1 embryo per T175 flask. These were incubated at 37°C and 5% CO<sub>2</sub> overnight before the media was removed, two washes performed using PBS, and fresh mEF media added. Cells were allowed to proliferate to 90% confluence before being trypsinised and frozen down at P1, or split for subsequent experiments.

### **8.9 Lentivirus production and titering**

Cells were seeded at approximately  $2 \times 10^7$  cells per T175 cm<sup>2</sup> flask and incubated at 37°C, 5% CO<sub>2</sub> overnight to achieve up to 90% confluence. Per flask, 50 µg transgene vector, 17.5 µg pMD.G2 VSV-g envelope vector, and 32.5 µg pCMVΔ8.74 gag-pol packaging vector were incubated for 5 minutes at room temperature in 6ml OptiMEM (Gibco). To this, another 6 ml OptiMEM containing 1 µl polyethylenimine (PEI) (10mM)(Sigma) was added and incubated for a further 20 minutes at room temperature. Medium was removed from cells, washed with PBS and 12 mls of PEI/DNA/OptiMEM solution was added and the cells incubated at 37°C, 5% CO<sub>2</sub> for 3 hours. After incubation, PEI/DNA/OptiMEM solution was removed and the cells supplemented with complete DMEM containing 1% Penicillin / Streptomycin and 10% FCS. After 24 hours, the medium was changed and the cells supplemented with fresh complete medium. The 48 hour supernatant was collected and filtered through a 0.45 µm PVDF filter (Nalgene), and the pellet resuspended in 50 µl OptiMEM per 12 ml viral supernatant and stored at 4°C overnight. This was repeated for the 72 hour supernatant, and the two high-titer supernatants pooled and stored at -80°C. All viruses were titered using a p24 antigen enzyme-linked immunosorbent assay (ELISA) (Zeptomatrix) as per manufacturer's protocol. Using samples diluted in water to 10<sup>-6</sup> for *in vitro* preps, and 10<sup>-7</sup> for the highly concentrated *in vivo* preps, the samples were incubated overnight in order to be captured by the p24 antibody on the plate. The captured antigen was subsequently incubated with anti-HIV-1 antibody conjugated to biotin. After washing, a Streptavidin-Peroxidase solution was added to each well. After the addition of the substrate, the absorbance of the samples, in conjunction with the standard curve of known p24 concentrations, was measured at 450 nm using the Glomax®-Multi+ microplate reader (Promega). The resultant optical density of the sample is proportional to the concentration of bound HIV p24 antigen within each sample, and through generation of an equation for the standard curve, the

concentration of the unknown samples were determined to produce a viral titer expressed as viral particles/ml (vp/ml).

### 8.10 Reporter assays

Cells transduced with reporter lentivirus at a multiplicity of infection (MOI) of between 5-10 were plated at a density of  $2 \times 10^5$  cells per well of a 12-well plate. Within 24 hours after plating, the cells were activated with their respective ligand/inhibitor as per (**Table 12**).

**Table 12. Table of reporters, agonists, and activation parameters.**

Response Element	Agonist / Inhibitor	Conc.	Activation Duration	Activation Media	Maintenance Media
NF- $\kappa$ B	Ultra-pure LPS (InvivoGen)	0.1 mg/ml	4 hours	OptiMem	Complete DMEM
SBE	Activin A (Peprotech)	100 ng/ml	duration	Complete DMEM	Complete DMEM
WNT	Lithium Chloride (LiCl) (Sigma)	50 mM	24 hours	Complete DMEM	Complete DMEM
Notch	Jagged-1	70% Jag-1 cells	duration	1:1 Complete DMEM and Ham's F10	1:1 Complete DMEM and Ham's F10

### 8.11 Development of the px330-Sox9 knockout CRISPR-Cas9 vector

#### 8.11.1 Cloning of the Sox9 guide-RNA into the px330 backbone

The px330 backbone was used to clone in the guide RNA into the *BbsI* restriction site (restriction half-site highlighted in red within the oligo (**Table 13**). This vector also contains the Cas9 nuclease downstream of a constitutive chicken  $\beta$ -actin promoter. Oligos containing *BbsI* restriction half sites (bold red) were designed using the free online software CHOPCHOP<sup>406</sup> and were targeted toward the human Sox9 gene, while the negative control was a guide that had no target within the human genome. The guides and the PCR primers used for subsequent amplification and validation of the target region are given in **Table 13**. Target guides were designed to target exons only, lie directly upstream of an NGG PAM motif, be 20 bp in length, begin with a G for optimal U6-driven expression, and were designed to have zero predicted off-targets. Lyophilised oligos were resuspended in distilled H<sub>2</sub>O to a concentration of 100  $\mu$ M. Each of the oligos was phosphorylated using T4 polynucleotide kinase (NEB) by incubation for 1 hour at 37°C and heat inactivated for 20 minutes at 65°C (**Table 14**). Complementary phosphorylated oligos were mixed in a 1:1 ratio (10  $\mu$ l each) and heated for 10 minutes at 75°C. The oligos were annealed by slow cooling to room temperature by turning the heating block off.

**Table 13. Oligos used to develop guide RNAs and amplify Sox9 target region.**

Oligo	Sequence
Sox9 top strand guide	5' <b>CACC</b> GGAGATTCATACGCGGGCCC 3'
Sox9 bottom strand guide	5' <b>AAAC</b> GGGCCCCGCGTATGAATCTCC 3'
-ve control top strand guide	5' <b>CACC</b> GCACTACCAGAGCTAACTCA 3'
-ve control bottom strand guide	5' <b>AAAC</b> TGAGTTAGCTCTGGTAGTGC 3'
Sox9 amplicon for T7EN assay (forward)	5' GTGCAAGCGCCCCACTTTTGCTCTTTTCCTCCCC 3'
Sox9 amplicon for T7EN assay (reverse)	5' AGAGCTTGCCAGCGTCTTGCTGAGCTCGGCGTTGTGCAAGTGC 3'

**Table 14. Phosphorylation reaction using T4 polynucleotide kinase.**

Reagent	Volume ( $\mu$ l)
Stock oligo (100 $\mu$ M)	2 $\mu$ l
ATP	2 $\mu$ l
T4 polynucleotide kinase buffer	2 $\mu$ l
T4 polynucleotide kinase	0.5 $\mu$ l
H <sub>2</sub> O	13.5 $\mu$ l
<b>Final Volume</b>	<b>20 <math>\mu</math>l</b>

### 8.11.2 Ligation of phosphorylated, annealed oligos into *Bbs*I digested px330

Each of the phosphorylated, annealed oligos was diluted 25-fold for a final concentration of 200 nM. Ligation was performed using 50 ng of linearised (*Bbs*I digested) px330 with 5  $\mu$ l diluted, double-stranded oligo. This was ligated using NEB Quick Ligase before being transformed in Stbl3 competent cells. A negative control containing 5  $\mu$ l of H<sub>2</sub>O instead of the annealed oligos was added in order to determine the background ligation potential. Following this, 4 clones from the px330-Sox9, 4 clones from the px330-neg, and 1 from the negative control plate were amplified overnight in 5ml LB broth containing 100  $\mu$ g/ml carbenicillin. The plasmid DNA from these clones was isolated using the Qiagen Mini-pep kit as previously described, and the samples double digested with *Bbs*I/*Age*I to determine whether the oligo had annealed into the px330 backbone.

### 8.11.3 Nucleofection of genome editing plasmids and clonal amplification of HepaRG cells

To obtain expression of the px330-Sox9 and px330-neg-ctrl vectors within the cells, progenitor HepaRG cells were electroporated using the Amaxa nucleofector kit (Lonza). Firstly, the HepaRG cells were trypsinised and resuspended in media. Cells were centrifuged for 5 minutes at 1200 rpm and the pellet resuspended in 3 mls of media before cells were counted 3 times using a haemocytometer. Using the average of the 3 numbers around  $4-5 \times 10^5$  cells were re-centrifuged for 5 minutes at 1200 rpm and the supernatant removed. To 100  $\mu$ l buffer, containing the supplied

supplement, 8 µg of DNA was added, the cells resuspended in the buffer/supplement/DNA mix, and transferred to an Amaxa electrode vessel. This vessel was placed into the Amaxa nucleofector and the T-028 program voltage applied. Electroporated cells were transferred to pre-coated collagen plates and the media replaced the following day. After 3 days, the cells were plated in a 96-well plate at a seeding density of 0.5 cells/well in order to give a greater chance of obtaining a single cell per well. Two weeks after plating, the wells were assessed for the formation of single colonies, while those which had multiple colonies were marked and disregarded for future work. Single clonal cell lines were transferred to a 6-well plate for DNA isolation and validation of genome editing.

#### 8.11.4 Genomic DNA isolation from clonally amplified cells and PCR of Sox9 target region.

Cells were trypsinised from the 6-well plate and resuspended in media, centrifuged for 5 minutes at 300 g and the supernatant removed. Cells were washed in PBS and centrifuged for a second time. DNA was isolated using a genomic DNA isolation kit (Sigma), according to manufacturer’s instructions but briefly described below. One deviation to this protocol was elution of the DNA in H<sub>2</sub>O instead of the supplied elution buffer. The protocol utilises enzymatic digestion with proteinase K at 70°C for 10 minutes to release the DNA. The column is prepared by adding a buffer solution followed by a single centrifugation. To the cell lysate, 200 µl ethanol (100%) was added, vortexed thoroughly to ensure homogeneity, and loaded onto the column. The column was centrifuged, the flow-through removed, and the DNA subsequently bound to the column with binding buffer which is also subsequently centrifuged through. The DNA is washed twice with buffer containing ethanol, centrifuged twice to remove any residual buffer, and eluted in 30 µl of RNase/DNase-free water. All DNA samples were quantified and made up to a final concentration of 100 ng/µl.

The genomic region containing the genome edited target site was amplified using PCR. The PCR was set up as per **Table 15**. PCR amplification parameters were an initial denaturation of 98°C for 30 seconds followed by 30 cycles of 98°C for 10 seconds, 58°C for 20 seconds, 72°C for 30 seconds, with a final elongation step of 72°C for 3 minutes.

**Table 15. PCR reaction for amplification of Sox9 genomic region containing CRISPR/Cas9 target site.**

Reagent and Concentration	Volume
Forward Sox9 primer (10 µM)	1.25 µl
Reverse Sox9 primer (10 µM)	1.25 µl
Q5 Hot-start polymerase Master Mix (2x)	12.5 µl
Template genomic DNA (50 ng total DNA per reaction)	0.5 µl
dH <sub>2</sub> O	9 µl
<b>Final Volume</b>	<b>25 µl</b>

### 8.11.5 *Sma*I digest and T7 endonuclease I assay to determine occurrence of genome editing

The PCR product that was visualised on the agarose gel was excised, and subsequently gel extracted. The gel extracted product was digested by *Sma*I restriction enzyme, in order to see whether the original site found within Sox9 had been mutated. The digest was performed using 1 unit of *Sma*I enzyme, and incubated at 25°C for 1 hour before being electrophoresed and examined for the presence or absence of the *Sma*I site in the Sox9 amplified product.

It was desirable to obtain a mono-allelic Sox9 knockout cell line. Therefore, in order to remove colonies from the screening procedure that were bi-allelic for any mutation, a T7 endonuclease I assay was performed. This protocol relies on the denaturation and slow annealing of DNA producing heteroduplexes where the mutation forms a mismatch with the wildtype base. The T7 endonuclease recognises this mismatch and is able to cleave the product, resulting in 2 digested products. Perfectly annealed products will yield only a single, undigested band. The T7 endonuclease I assay was initially set up as in **Table 16** in order to denature and hybridise the DNA:

**Table 16. T7 endonuclease assay hybridisation mix.**

Reagent and Concentration	Volume
NEB buffer 2	2.0 µl
Gel extracted Sox9 PCR product (200 ng)	variable µl
dH <sub>2</sub> O	variable µl
<b>Final Volume</b>	<b>19 µl</b>

The hybridisation reaction was performed in the Eppendorf PCR cyclor

- 5 min, 95°C
- ramp down to 85°C at -2°C/sec
- ramp down to 25°C at -0.1°C/sec
- hold at 4°C

To the hybridised mix, 1 µl (10U) T7 endonuclease I was added and incubate at 37°C for 15 minutes. The reaction was stopped by adding 2 µl of 0.25 M EDTA and was electrophoresed immediately on a 1.5% agarose gel.

### 8.11.6 Clonal amplification and knockout validation using PCR and restriction digestion

Nucleofected cells were trypsinised for 1 minute, and resuspended in 5 mls of complete HepaRG media. These cells were centrifuged for 5 minutes at 300 g and the media containing trypsin was

removed. The cell pellet was resuspended in 5 mls of complete HepaRG media and the cells counted using a haemocytometer. Cell counting was performed three times. Cells were subsequently resuspended in complete HepaRG media so that each well of a 96-well plate contained 100 µl of media with a cell density of 0.5 cells per well in order to improve the chances of obtaining a single cell and subsequently a single clonal colony of cells per well. The clones were grown for three weeks, after which the wells were assessed for the formation of single colonies. The wells containing single colonies were trypsinised and the cells further grown up in a 6-well plate format.

#### **8.11.7 Sequencing of Sox9 homozygous knockout clones**

Clones that showed either the introduction of large insertions or deletions in the amplified PCR product, were mono-allelic for the T7 endonuclease I assay, or those which showed a mutation in the *SmaI* restriction site, were sequenced by Source Bioscience in order to confirm and characterise the type of mutation. Sequencing was performed using a 1:2 dilution of the gel-extracted product and the Sox9 genomic DNA forward PCR primer was used to prime the DNA during the sequencing reaction.

#### **8.12 Tissue fixation, embedding, and sectioning**

Mice were anaesthetised with isoflurane as per the code of practice for the humane killing of animals under schedule 1 of the Animals (Scientific Procedures) Act 1986. The livers were perfused with PBS to remove haemoglobin from the livers. Livers were immediately removed, sliced into 5-10mm sections, and placed in formalin for 48 hours at 4°C. For long-term storage, liver sections were removed from formalin and stored in 70% ethanol and kept refrigerated at 4°C until embedding. All animal procedures were carried out by Dr Simon Waddington and Mr Dany Perocheau at the UCL animal facility under the appropriate UK Home Office Project Licence.

Prior to embedding, perfusion-fixed tissues were dehydrated by serial washes through a graded series of 80%, 90% and 2x 100% ethanol baths each for one hour. Following dehydration, samples were incubated overnight in HistoClear (National Diagnostics) at room temperature.

Tissues were suspended in 60°C preheated Fibrowax (VWR), and subjected to 575 in/Hg pressure. This process was repeated three times to remove residual HistoClear. Tissues were subsequently transferred to a metal dish, filled with Fibrowax, an embedding cassette placed on top, and additional wax added to the top of the cassette and allowed to solidify overnight. Paraffin-embedded samples were sectioned into 5 µm sections using a Leica RM2255 microtome, and placed onto positively-charged 3-aminopropyltriethoxysilane (APES)(Sigma)-coated slides. Slides were prepared by immersion in 0.85% APES solution for 5 seconds, 2 washes in acetone (Sigma) for 5 seconds each, followed by 2 washes of distilled water. Slides were allowed to dry at 37°C overnight before use.

### **8.13 Hematoxylin and eosin staining**

Histological sections were rehydrated by clearing twice in Histoclear for 10 minutes each, followed by 5 minutes in absolute industrial methylated spirits (IMS), 3 minutes each in 90%, 70%, and 50% IMS, followed by a final bath for 5 minutes in distilled water. Sections were placed in Weigert's haematoxylin for 5 minutes and then rinsed in running water. Differentiation, or selective removal of excessive staining through controlled leaching in an acid alcohol solution, was performed by incubating the slides in acid alcohol (70% EtOH with 0.5% HCl) for approximately 10 minutes in order to achieve the desired degree of staining. Sections were once again rinsed in water and subsequently stained in eosin for 5 minutes. Sections were then dehydrated by rapidly passing through 70%, 90% and 100% alcohol for 2-3 seconds followed by a final 100% alcohol bath for 5 minutes. Sections were incubated in 2 final baths of Histoclear for 10 minutes each and allowed to dry before mounting with Histomount (Sigma).

### **8.14 Lilley's trichrome staining**

Since the histological dyes are aqueous in nature, it is important that the slides are gradually hydrated and the clearing agent, Histoclear, is removed so that the dyes can bind affectively. Sections are brought to water by passing the slides through descending concentrations of alcohol solutions with a final wash in water. Histological sections were subsequently incubated in Weigert's haematoxylin for 5 minutes and rinsed in running water and then distilled water. Slides were placed in working strength picric acid solution for 10 minutes, washed in distilled water, and stained in Xylidine Red solution (Sigma) for 1 minute before being rinsed again in distilled water. Differentiation was performed using a 1% phosphomolybdic acid bath for 10 minutes. Collagen staining was achieved by subsequently staining slides in Aniline Blue solution (Sigma) for 1 minute before being placed in fresh 1% phosphomolybdic acid for 2 minutes and 1% acetic acid for 3 minutes prior to rapid dehydration of samples in 95% and 2x 100% alcohol. Slides were left to dry before being cleared in 2 baths of Histoclear for 10 minutes each. After drying, sections were mounted using Histomount and analysed for fibrosis.

### **8.15 Immunohistochemistry of liver sections**

Tissue sections mounted on APES-coated glass slides were bathed twice in Histoclear for 10 minutes each, and brought to water by immersing in absolute industrial methylated spirits (IMS) for 5 minutes, followed by 3 minutes each in 90%, 70%, and 50% IMS, followed by a final bath for 5 minutes in distilled water. Antigen retrieval was performed by heat-induced antigen retrieval in 10 mM citrate buffer (pH6.0) (Sigma) or 10 mM Tris HCL (Sigma) as indicated for 40 or 10 minutes respectively and then allowed to cool for a further 20 minutes. Samples were incubated for 10 minutes in TBS

containing 0.3% Triton X-100 (TBS-T) followed by blocking in TBS-T + 15% normal goat serum (NGS) (Vector Laboratories) for 1 hour at room temperature. Primary antibody was diluted in TBS-T/10% NGS overnight at 4°C. Slides were rinsed thrice for 5 minutes each time in TBS followed by incubation in secondary antibody diluted in TBS-T/10% NGS for 1 hour at room temperature. Once again the samples were washed thrice for 5 minutes in TBS before removal of background fluorescence using 0.3% Sudan Black B (VWR) made up in 70% ethanol for 15 minutes at room temperature. Sections were rinsed thrice with TBS for 5 minutes each followed by a final jet wash with TBS. Sections were mounted using Fluorescence Mounting Medium (Dako). Staining parameters given in **Table 17**.

**Table 17. Primary and secondary antibodies used for immunohistochemistry.**

<b>Antibody</b>	<b>Antigen retrieval</b>	<b>Dilution</b>
chicken $\alpha$ GFP (New England Biolabs (ab13970))	10 mM Na Citrate (pH6.0)	1:300
mouse $\alpha$ HNF-4 $\alpha$ (Perseus proteomics (PP-H415-00))	10 mM Na Citrate (pH6.0)	1:200
rabbit $\alpha$ -SMA (Dako (M0851))	10 mM Tris HCL (pH10)	1:100
rabbit $\alpha$ -GFAP (Dako (Z0334))	10 mM Na Citrate (pH6.0)	1:200
mouse $\alpha$ CK7 (Dako (M7018))	10 mM Tris HCL (pH10)	1:500
rabbit $\alpha$ PKM2 (Life Technologies (PA5-23034))	10 mM Na Citrate (pH6.0)	1:200
goat $\alpha$ -rabbit Alexafluor (Life Technologies (A-11011))		1:500
goat $\alpha$ -mouse Alexafluor (Life Technologies (A-11031))		1:500
goat $\alpha$ -chicken Northern Lights (R&D Systems (NL018))		1:400
4',6-diamidino-2-phenylindole (DAPI)(Sigma Aldrich (D9542))		1:1000

### **8.16 Hepatocyte and cholangiocyte differentiation utilising the HepaRG cell line**

HepaRG cells were seeded at low density and maintained in William's E medium containing hydrocortisone and insulin as detailed in the general cell culture methods section 2.6. Cells were passaged every 3-4 days onto collagen-coated plates to maintain low confluence for 2 weeks in order to encourage the growth of hepatic progenitors. For hepatocyte maturation, the HepaRG hepatoblasts (HepaRG-HB) cells were allowed to grow to confluence after which the culture was supplemented with 1.2% DMSO (Sigma) to induce hepatocyte differentiation and maturation (protocol 1) to produce HepaHep cells. In order to differentiate cells into cholangiocytes, termed HepaChol (protocol 2), confluent HepaRG-HB cells were treated with IL-6 (10 ng/ml) (R&D Systems) for 2 days, followed by 2 days of sodium taurocholate hydrate (10 nM) (Sigma) treatment, and a further 8 days of sodium taurocholate hydrate (10 nM) (Sigma) and sodium butyrate (1.8  $\mu$ M) (Sigma) treatment.

## 8.17 Generation and differentiation of Numb and Jagged overexpressing HepaRG lines

HepaRG cells were seeded at low density. The following day, the cells were transduced with either high-titer pLNT-SFFV-Numb or pLNT-CMV-Jagged-IRES-GFP virus at an MOI of 20. The cells were cultured for a week before any experiments in order for the virus to integrate and for stable basal levels of the proteins to be achieved. Following stable expression of the proteins, both cell lines were differentiated down both the hepatocyte and the cholangiocyte lineages following the above protocol. Samples were subsequently stained by immunocytochemistry or lysed for RNA extraction.

### 8.17.1 Immunocytochemistry of modified and unmodified differentiated HepaRG cells

At the end of the HepaRG differentiation experiments using protocol 1 or 2, media was removed from cells and cells washed three times in PBS. Cells were fixed by incubation in 4% paraformaldehyde (PFA) (Sigma) for 20 minutes followed by three washes in PBS to remove any residual PFA. Blocking buffer (PBS, 0.3% Triton X-100, 1% BSA) was added to the cells and incubated for one hour at room temperature to reduce non-specific binding of the primary antibody. Primary antibody resuspended in blocking buffer was added to the cells and incubated overnight at 4°C. Primary antibody was removed and the cells washed three times in PBS for 5 minutes. Fluorophore-conjugated secondary antibody resuspended in blocking buffer was incubated on the cells for 1 hour at room temperature. This was followed by three washes in PBS. Cells were incubated in 1x 4',6-diamidino-2-phenylindole (DAPI)(Sigma) in PBS for 10 minutes before being washed again three times in PBS for 5 minutes each time. Cells were kept in PBS for fluorescent imaging using an Olympus microscope and analysed using Cell F imaging software. Primary and secondary antibody dilutions and additional information are given in **Table 18**.

**Table 18. Primary and secondary antibody information used for immunocytochemistry.**

<b>Antibody</b>	<b>Supplier</b>	<b>Dilution</b>
mouse $\alpha$ CK19 (cholangiocyte)	Dako (M0888)	1:200
mouse $\alpha$ CK7 (cholangiocytes)	Sigma (4465P)	1:200
mouse $\alpha$ HNF-4 $\alpha$ (hepatocytes)	Perseus (PP-H1415-00)	1:200
mouse $\alpha$ ALB (hepatocytes)	R&D Systems (MAB1455)	1:200
goat $\alpha$ Sox9 (progenitors and cholangiocytes)	R&D Systems (AF3075)	1:500
rabbit $\alpha$ -activated Notch (NICD)	Abcam (ab8925)	1:200
rabbit $\alpha$ Non-phospho (active) $\beta$ -catenin	New England Biolabs (8814S)	1:200
rabbit $\alpha$ Acetylated tubulin	Cell Signaling (5335S)	1:200
rabbit $\alpha$ -goat Alexafluor	Life Technologies (A11079)	1:500
goat $\alpha$ -rabbit Alexafluor	Life Technologies (A11011)	1:500
goat $\alpha$ -mouse Alexafluor	Life Technologies (A11031)	1:500
4',6-diamidino-2-phenylindole (DAPI)(Blue)	Sigma Adrich (D9542)	1:1000

## 8.17.2 qPCR for expression of markers of progenitors, hepatocytes, and cholangiocytes

### 8.17.2.1 RNA extraction

Confluent wells of a 12-well plate were washed twice with PBS to remove any media. Buffer RLT (350  $\mu$ l) was added directly to the monolayer of cells. The cells were scraped using a P1000 tip in order to completely resuspend and lyse the cells in the lysis buffer. The lysate was loaded directly onto a QIAshredder spin column and centrifuged for 2 minutes on full speed. To the homogenised lysate, 350  $\mu$ l ethanol (70%) was added and pipetted repeatedly to mix well. The sample was subsequently loaded onto an RNeasy spin column and centrifuged for 15s at 13,000 rpm. The flow-through was discarded and 350  $\mu$ l Buffer RW1 added to the column. Once again the column was centrifuged for 15 seconds at 13,000 rpm and the flow-through discarded. The sample was DNase treated on-column using 10  $\mu$ l of RQ11 DNase (Promega) in DNase buffer to a total volume of 70  $\mu$ l. This was incubated for 20 minutes at room temperature (20-30°C). Another 350  $\mu$ l of RW1 was added to the column and centrifuged for 15 seconds at 13,000 rpm and the flow-through discarded. Next, 500  $\mu$ l Buffer RPE was added to the RNeasy spin column, centrifuged at 13,000 rpm for 15 seconds and the flow-through discarded. This wash step was repeated a second time and centrifuged at 13,000 for 2 minutes. The column was placed in a new 2ml collection tube and centrifuged at full speed for 1 minute to remove any residual wash buffer. The column was transferred to a new Eppendorf tube and 30  $\mu$ l dH<sub>2</sub>O added directly to the spin column membrane. This was incubated at room temperature for 5 minutes before being centrifuged at full-speed for 30 seconds. The RNA samples were quantified using the NanoDrop™ and placed at -80°C for long-term storage.

### 8.17.2.2 First-Strand cDNA synthesis

In order to denature RNA secondary structure, the RNA (up to 1  $\mu$ g) was incubated with 0.5 $\mu$ g Random Primers at 70°C for 5 minutes and immediately cooled on ice to prevent the reformation of any secondary structures. The following reagents were subsequently added as per **Table 19**, and incubated at 37°C for 1 hour. A control containing dH<sub>2</sub>O instead of reverse transcriptase was also set up and is designated the No RT control. cDNA was kept at -20°C for long-term storage.

**Table 19. First-strand cDNA synthesis reaction.**

Reagent and Concentration	Volume
M-MLV 5x Reaction Buffer	5.0 $\mu$ l
dNTPs (10 $\mu$ M)	5.0 $\mu$ l
RNA (up to 1 $\mu$ g)	variable
Random primer (0.5 $\mu$ g/ $\mu$ l)	1.0 $\mu$ l
M-MLV reverse transcriptase (200 units)	1.0 $\mu$ l
Recombinant Rnasin® Ribonuclease inhibitor	0.5 $\mu$ l
H <sub>2</sub> O	variable

### 8.17.2.3 qPCR to quantitate hepatocytes and cholangiocytes from differentiation protocols

cDNA samples were diluted 1:7 and subsequently used as the template in the qPCR reactions. The reactions were as per **Table 20** and **Table 21**, with cycling parameters as per **Table 22** for Sox9, OPN, HNF-1 $\beta$  and  $\beta$ -actin **Table 23** for Hey1 and  $\beta$ -actin. The relative expression levels were calculated using the Pfaffl method which incorporated the varying primer efficiencies using the equation of the standard curve. All primer sequences are given in **Table 24**.

**Table 20. qPCR reaction for Sox9, OPN, HNF-1 $\beta$ , and Hey1.**

Reagent and Concentration	Volume
SybrMaster Mix (2x)	5.0 $\mu$ l
Forward primer (10 $\mu$ M)	0.55 $\mu$ l
Reverse primer (10 $\mu$ M)	0.55 $\mu$ l
cDNA	2.0 $\mu$ l
H <sub>2</sub> O	1.9 $\mu$ l
<b>Final Volume</b>	<b>10 <math>\mu</math>l</b>

**Table 21. qPCR reaction for ALB and  $\beta$ -actin.**

Reagent and Concentration	Volume
Sybr Select Master Mix (2x)	5.0 $\mu$ l
Forward primer (10 $\mu$ M)	0.38 $\mu$ l
Reverse primer (10 $\mu$ M)	0.38 $\mu$ l
cDNA	2.0 $\mu$ l
H <sub>2</sub> O	2.25 $\mu$ l
<b>Final Volume</b>	<b>10 <math>\mu</math>l</b>

**Table 22. Cycling parameters for qPCR using Sybr Select qPCR mix.**

Temperature	Time	
50°C	2 minutes	1x
95°C	2 minutes	1x
95°C	3 seconds	40 x
59°C	30 seconds	
65°C to 95°C in 0.5°C increments (Melt curve)	5 seconds	1x

**Table 23. Cycling parameters for qPCR using Sybr® greenER™ qPCR mix Sybr Select qPCR mix.**

Temperature	Time	Cycles
95°C	3 minutes	1x
95°C	3 seconds	40x
60°C	20 seconds	
72°C	1 second	
65°C to 95°C in 0.5°C increments (Melt curve)	5 seconds	1x

**Table 24. Primers used in differentiation experiment qPCR reactions.**

Marker	Primer	Sequence (5' → 3')	Amplicon Size
progenitors / cholangiocytes	Sox9 forward	GACTTCCGCGACGTGGAC	99 bp
progenitors / cholangiocytes	Sox9 reverse	GTTGGGCGGCAGGTA CTG	
cholangiocytes	OPN forward	CTCAGGCCAGTTGCAGCC	81 bp
cholangiocytes	OPN reverse	CAAAAGCAAATCACTGCAATTCTC	
cholangiocytes	HNF-1β forward	TGTACACCTGGTACGTCA GAAA	140 bp
cholangiocytes	HNF-1β reverse	ATGGCTCTGTTGACTGAACTCT	
hepatocytes	ALB forward	TGCAACTCTTCGTGAAACCTATG	135 bp
hepatocytes	ALB reverse	ACATCAACCTCTGGTCTCACC	
Notch signalling	HEY1 forward	CGGCAGGAGGGAAAGGTT	61 bp
Notch signalling	HEY1 reverse	CCCAA ACTCCGATAGTCCATAGC	
Housekeeping gene	β-actin forward	CGGGACCTGACTGACTACC	292 bp
Housekeeping gene	β-actin reverse	TGAAGGTAGTTTCGTGGATGC	

### 8.17.3 Notch, Wnt and α1AT reporter expression during differentiation

HepaRG cells were transduced at an MOI of 10 for each of the reporter constructs prior to plating in a 12-well plate. The reporters used were LNT-Notch-NLuc2, LNT-Wnt-NLuc2, and LNT-α1AT-NLuc2. The α1AT reporter contains the promoter element of the gene coding for alpha-1 antitrypsin (α1AT), a hepatocyte-specific marker. In conjunction with the secreted Nanoluc vectors, the cells were transduced at an MOI of 1 using the constitutively expression LNT-SFFV-Vluc vector in order to compensate for cell number during the experiment. Cells were grown to confluence in a monolayer prior to the start of differentiation. Differentiation was performed using the cholangiocyte and the hepatocyte differentiation protocols as per section 7.16. At the start of the experiment, and every second day thereafter, media was removed and assayed for Nanoluc activity using coelenterazine at a final concentration of 1 μM, and vargula activity using vargulin at a final concentration of 10 nM. Activity of Nanoluc was normalised to the activity of Vargula. Data for each reporter was plotted at each time point for the duration of the differentiation experiment.

## 8.18 Statistical analysis

Statistical analysis on *in vitro* data was performed using an unpaired student's t-test with a p-value of <0.05 considered significant for single time-points. Time course experiments were analysed using two-way ANOVA with repeated measures with Bonferroni post-hoc test used for significance. Dose-response experiments were analysed using one-way ANOVA with Tukey's multiple comparison test for significance. Analysis of the different constitutive luciferases was performed using one-way ANOVA with Tukey's post-hoc test. All data are expressed as mean values  $\pm$  SEM, with each sample being measured in triplicate.

## 8.19 *In vivo* work

### 8.19.1 Animals

All mice used for *in vivo* experiments were outbred CD1 mice (Charles River). Mice were time mated 3 weeks prior to the expected neonatal injection date. Neonatal (P0) CD1 mice were anaesthetised on ice before being injected either intracranially (5  $\mu$ l), intravenously (20  $\mu$ l), subcutaneously (10  $\mu$ l), intranasally (20  $\mu$ l), or ventral subcutaneously (5  $\mu$ l) followed by imaging. All animal work was compliant with the rules and regulations set out by the United Kingdom Home Office.

### 8.19.2 Bioluminescence imaging

Induction of anaesthesia was achieved using 4% isoflurane (Abbott Laboratories) in 100% oxygen, before being injected intraperitoneally with 300  $\mu$ l D-luciferin (Gold Biotechnology) at a concentration of 15 mg/ml, a dose of approximately 150 mg/kg. The mice were connected to an anaesthesia system in a warmed light-proof detection chamber within in the IVIS *in vivo* imaging system (Perkin Elmer). Imaging was performed 5 minutes post D-luciferin administration using a cooled charge-coupled device (CCCD) camera with image acquisition performed using a 24 cm field-of-view for greyscale photographic images. Luminescent images were subsequently acquired using a binning factor of 4, with an aperture of f/1.2 and expressed as photons per second per cm<sup>2</sup> per steradian. An overlay of the two images was generated using Living Image software (Perkin Elmer) to create a pseudo-coloured image to depict fluorescent intensities over each animal. Regions of interest (ROIs) were manually defined using a standard area for each organ. Prior to agonist-mediated activation or surgical induction of disease, each of the animals was imaged three times in order to ascertain a robust median baseline measurement of bioluminescent imaging which could then be used to express subsequent data points as a fold-change over this baseline value.

### **8.19.3 *In vivo* reporter analysis**

Activation experiments and bile duct ligations were performed by Dr. Simon Waddington (University College London). D-luciferin administration and bioluminescent image data capture were performed by Dr. Suzanne Buckley and Mr Dany Perocheau.

#### **8.19.3.1 NF- $\kappa$ B activation using LPS**

LPS was given intraperitoneally at the time of D-luciferin administration at a dose of 30  $\mu$ g per mouse. Animals were imaged at T = 0 and T = 4 hours post-LPS.

#### **8.19.3.2 Dexamethasone-mediated abrogation of NF- $\kappa$ B signalling.**

Dexamethasone at a dose of 18 mg/kg was administered 2 hours prior to and concomitantly with LPS and luciferin.

#### **8.19.3.3 Bile duct ligation model of cholestasis.**

Firstly, animals were anaesthetised with isoflurane. Abdominal fur was removed with an electric shaver and antiseptic applied to the skin. An abdominal longitudinal incision, ventral to the xiphisternum, was made and the peritoneal cavity opened. The liver was lifted out and the bile duct exposed. A suture was placed around the common hepatic duct downstream of the median and left liver lobes, leaving the right and caudate lobe free from ligation. The liver was replaced into the abdominal cavity before closure of the peritoneum and cutis plus fascia. The operation area was sterilised with antiseptic and the mice administered with 50  $\mu$ l morphine (6.67 mg/ml) and 100  $\mu$ l bupivacaine hydrochloride (2 mg/kg) for systemic post-operative analgesia.

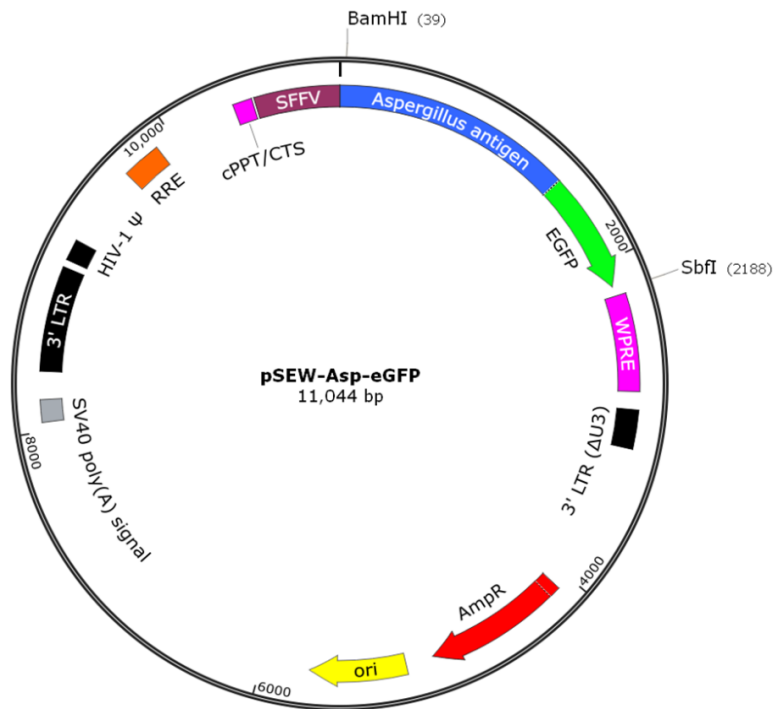
### **8.19.4 Statistical analysis of *in vivo* experiment results**

Analysis of variance (ANOVA) test for significance was used for *in vivo* experimental data with Newman-Keuls post-hoc multiple comparison test.

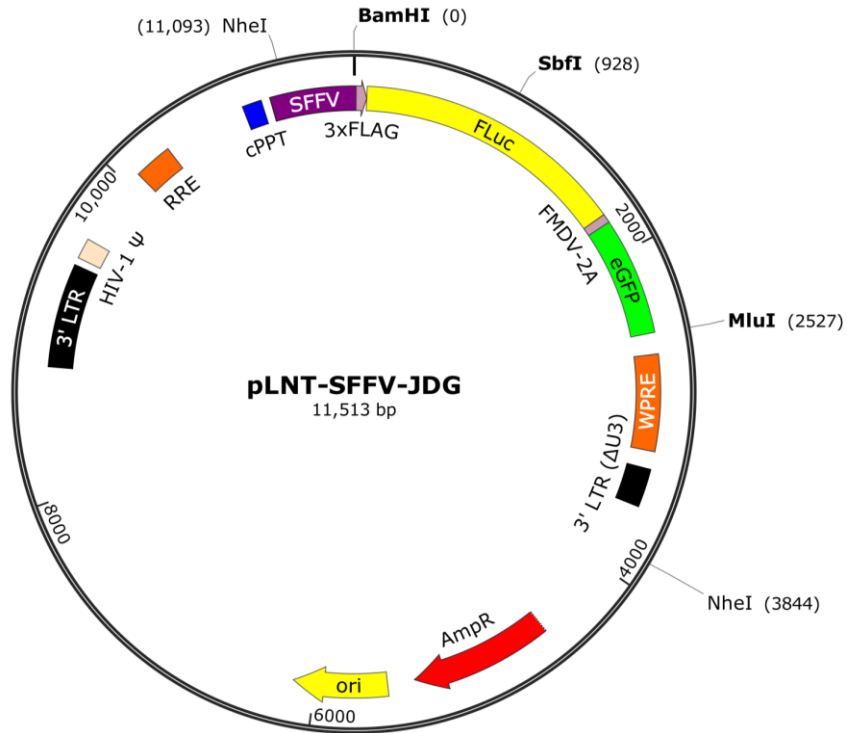
# APPENDICES

## Appendix A – Plasmid Maps

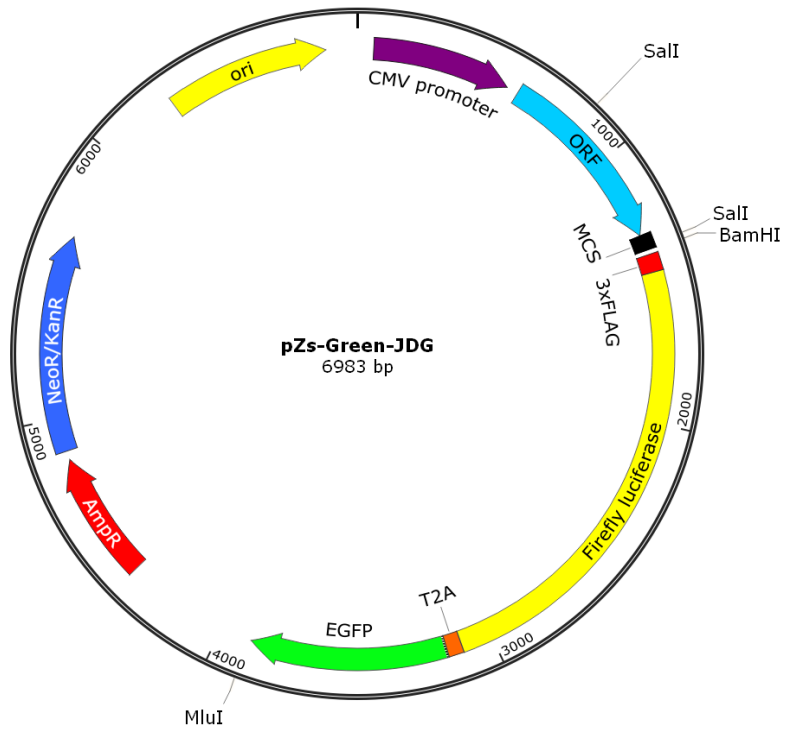
### Appendix A.i Plasmid map of pSEW-Asp-eGFP



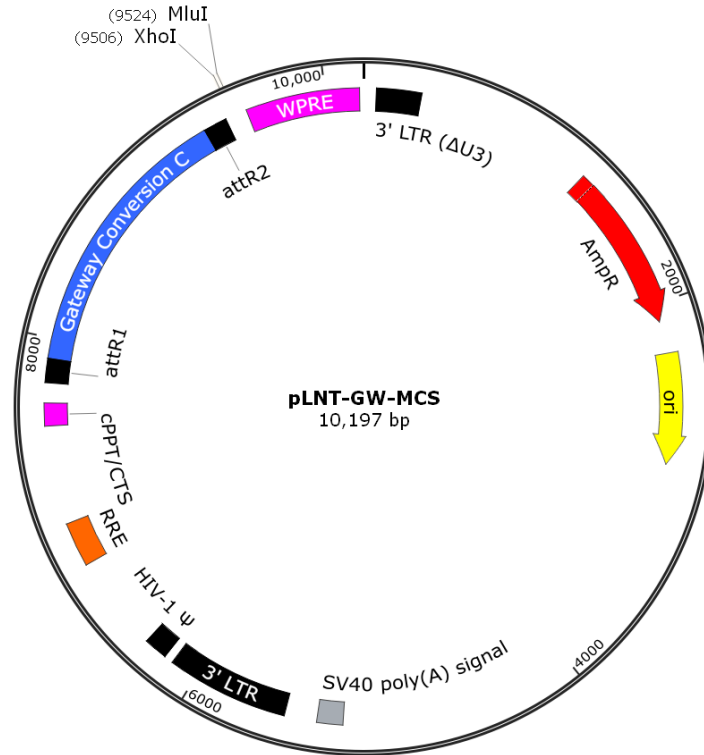
**Appendix A.ii Plasmid map of pLNT-SFFV-JDG**



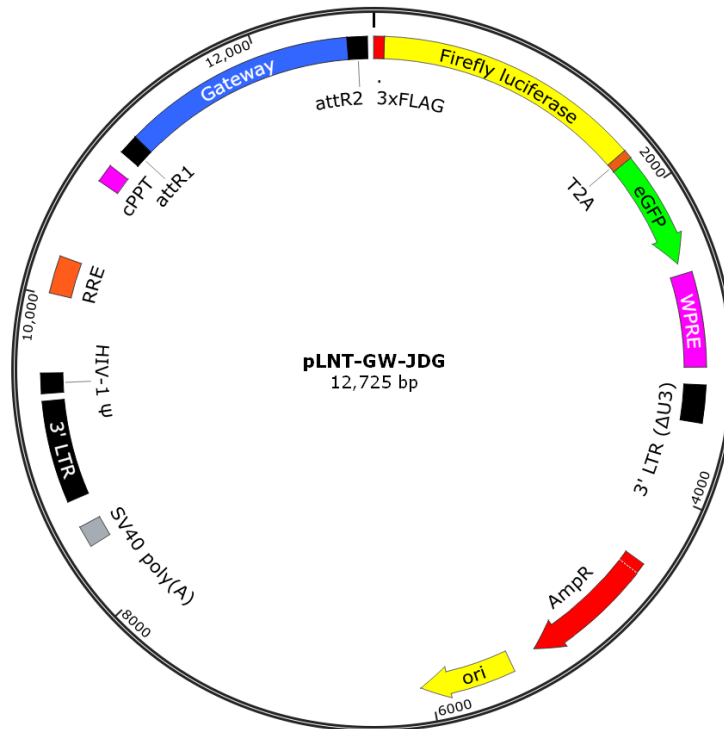
**Appendix A.iii Plasmid map of pZs-Green-JDG**



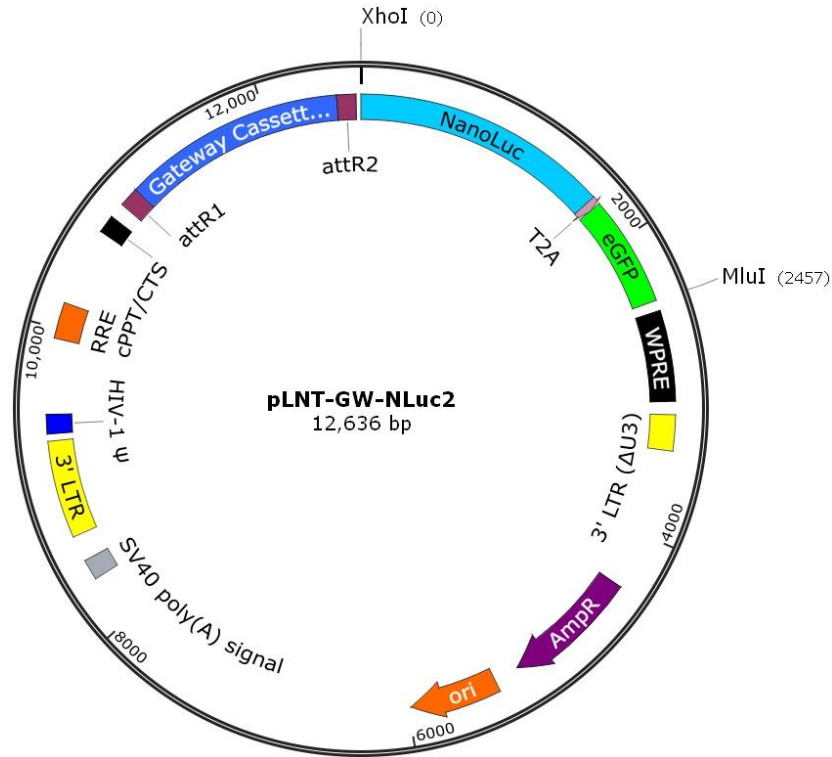
### Appendix A.iv Plasmid map of pLNT-GW-MCS



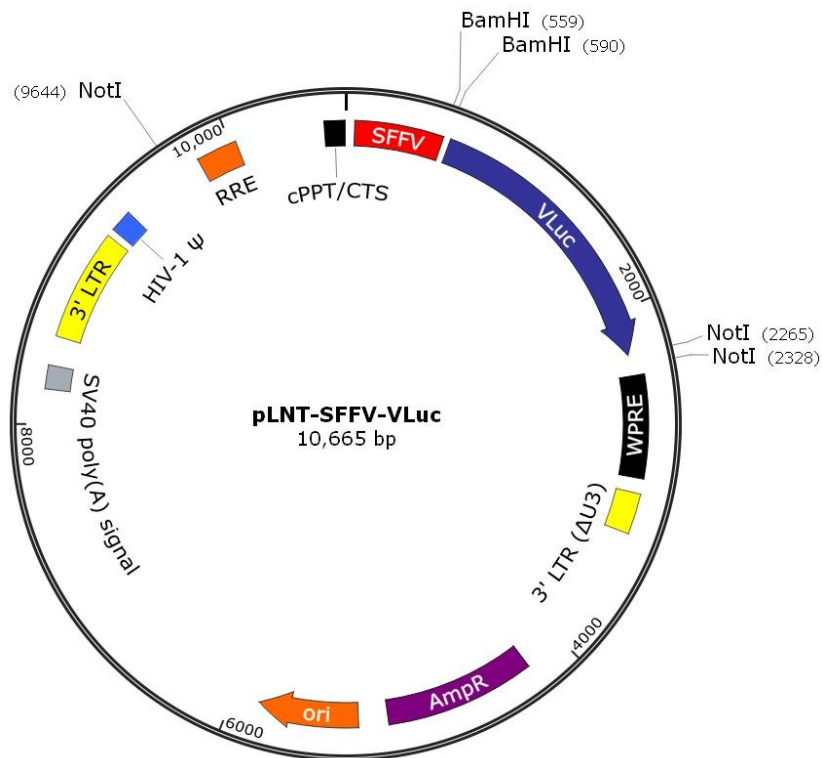
### Appendix A.v Plasmid map of pLNT-GW-JDG



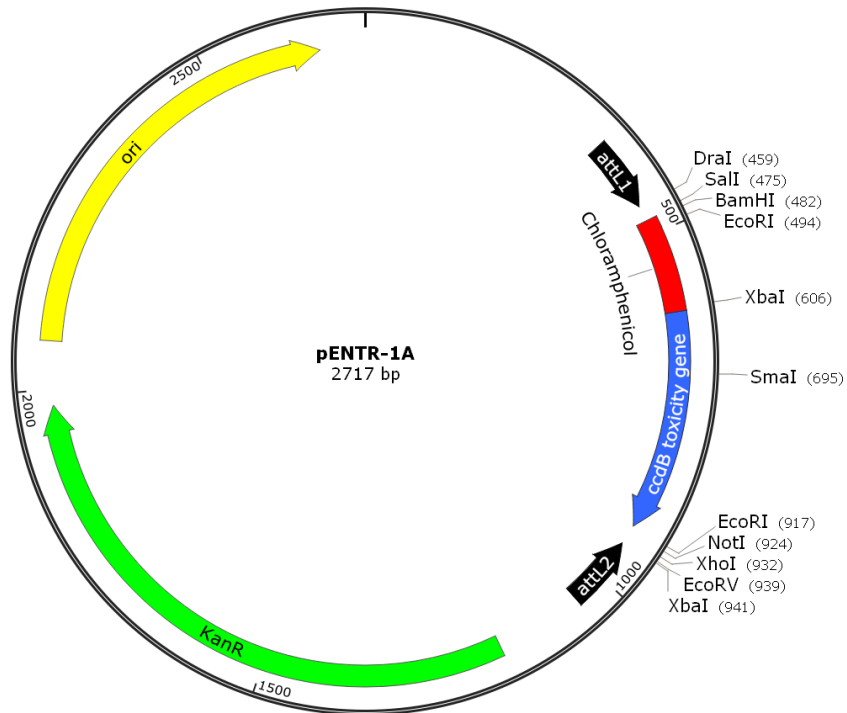
**Appendix A.vi Plasmid map of pLNT-GW-NLuc2**



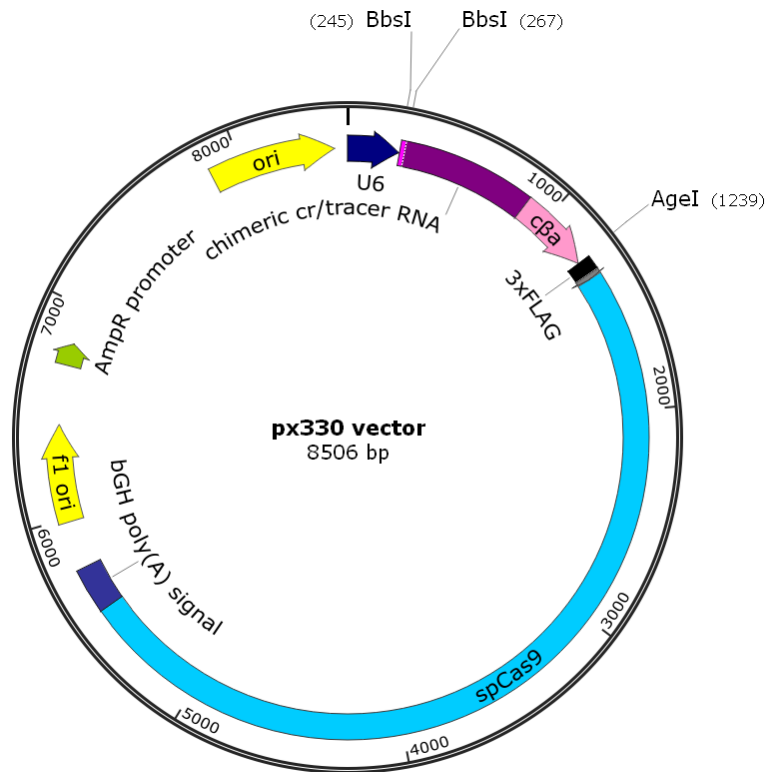
**Appendix A.vii Plasmid map of pLNT-SFFV-VLuc**



**Appendix A.viii Plasmid map of pENTR-1A**



**Appendix A.ix Plasmid map of px330 with *BbsI* restriction sites for target sequence cloning**





## Appendix C – Home Office Animals (Scientific Procedures) Act 1986 Project Licence



No. PPL 70/8030

### ANIMALS (SCIENTIFIC PROCEDURES) ACT 1986

#### PROJECT LICENCE

to carry out a programme of scientific procedures  
on living animals

In pursuance of the powers vested in him by the above Act, the  
Secretary of State hereby licences

Dr S N Waddington  
Gene Transfer Technology Group  
University College London  
86-96 Chencies Mews  
London  
WC1E 6HX

to carry out the programme of work specified in the Schedule subject to the restrictions and provisions contained in the Act and subject also to the limitations and conditions contained in this licence and to such other conditions as the Secretary of State may from time to time prescribe.

Under this project licence number PPL 70/8030 the Secretary of State grants authority only for the work specified on the Schedule. The procedures and animal types which may be used and the place or places at which the work may be carried out are specified in the Schedule. Authority is granted only for the severity limits attached to individual procedures specified in Part E of the schedule.

The Secretary of State has determined that a retrospective assessment of this licence is not required in accordance with Section 5B of the Act.

This licence, unless earlier revoked, shall be in force until 25 February 2019.

Home Office  
2 Marsham Street  
London SW1P 4DF

For the Secretary  
of State



25 February 2014

NB. This licence does not authorise the project licence holder or any other person to carry out procedures on any animals unless he/she holds a personal licence issued under the Act which authorises him/her to carry out those procedures on the animals of those types.

## Appendix D – Turnitin Plagiarism report

JuliettePhDthesis29032016Turnitin.pdf

### ORIGINALITY REPORT

<b>9</b> %	<b>4</b> %	<b>5</b> %	<b>4</b> %
SIMILARITY INDEX	INTERNET SOURCES	PUBLICATIONS	STUDENT PAPERS

### PRIMARY SOURCES

<b>1</b>	Submitted to Imperial College of Science, Technology and Medicine Student Paper	1%
<b>2</b>	Submitted to Higher Education Commission Pakistan Student Paper	1%
<b>3</b>	"Abstracts", Molecular Therapy, 2015. Publication	<1%
<b>4</b>	Buckley, Suzanne M. K., Juliette M. K. M. Delhove, Dany P. Perocheau, Rajvinder Karda, Ahad A. Rahim, Steven J. Howe, Natalie J. Ward, Mark A. Birrell, Maria G. Belvisi, Patrick Arbuthnot, Mark R. Johnson, Simon N. Waddington, and Tristan R. McKay. "In vivo bioimaging with tissue-specific transcription factor activated luciferase reporters", Scientific Reports, 2015. Publication	<1%
<b>5</b>	Submitted to National University of Singapore Student Paper	<1%
<b>6</b>	Mohd Shaufi, Mohd Asrore Sieo, Chin Chin	

The full copy of the Turnitin report can be found on the accompanying CD.

# REFERENCES

1. Takiya, C.M., Paredes, B.D., Guintanilha, L. (2013). Liver resident stem cell. Resident stem cells and regenerative therapy, ed. Goldenberg RC, de Carvalho AC, 177-203.
2. Banerjee, A. (2005). The Liver. In *Clinical Physiology: An Examination Primer*, Ashis Banerjee, ed.: Cambridge University Press), pp. 334-343.
3. Bouwens, L., Knook, D.L., Wisse, E. (1986). Local proliferation and extrahepatic recruitment of liver macrophages (Kupffer cells) in partial-body irradiated rats. *J. Leukoc. Biol.* 39, 687-697.
4. Mencin, A., Kluwe, J., Schwabe, R.F. (2009). Toll-like receptors as targets in chronic liver diseases. *Gut* 58, 704-720.
5. Hautekeete, M.L., Geerts, A. (1997). The hepatic stellate (Ito) cell: its role in human liver disease. *Virchows Arch.* 430, 195-207.
6. Kordes, C., Sawitza, I., Muller-Marbach, A., Ale-Agha, N., Keitel, V., Klonowski-Stumpe, H., Haussinger, D. (2007). CD133+ hepatic stellate cells are progenitor cells. *Biochem. Biophys. Res. Commun.* 352, 410-417.
7. Kordes, C., Sawitza, I., Gotze, S., Haussinger, D. (2012). Stellate cells from rat pancreas are stem cells and can contribute to liver regeneration. *PLoS One* 7, e51878.
8. Hohenester, S., Wenniger, L.M., Paulusma, C.C., van Vliet, S.J., Jefferson, D.M., Elferink, R.P., Beuers, U. (2012). A biliary HCO<sub>3</sub><sup>-</sup> umbrella constitutes a protective mechanism against bile acid-induced injury in human cholangiocytes. *Hepatology* 55, 173-183.
9. Kang, L., Mars, W.M., Michalopoulos, G.K. (2012). Signals and cells involved in regulating liver regeneration. *Cells* 1, 1261-1292.
10. Tso, P., McGill, J. (2003). The Physiology of the Liver. In *Medical Physiology*, R.A. Rhoades, G.A. Tanner, eds. (Baltimore: Lippincott Williams and Wilkins), pp. 514-525.
11. Behari, J. (2010). The Wnt/ $\beta$ -catenin signaling pathway in liver biology and disease.
12. Boldt, J. (2010). Use of albumin: an update. *British Journal of Anaesthesia* 104, 276-284.
13. Mold, C., Gewurz, H., Du Clos, T.W. (1999). Regulation of complement activation by C-reactive protein. *Immunopharmacology* 42, 23-30.
14. Rochette, L., Gudjoncik, A., Guenancia, C., Zeller, M., Cottin, Y., Vergely, C. (2014). The iron-regulatory hormone hepcidin: A possible therapeutic target? *Pharmacol. Ther.*
15. Anderson, E.R., Shah, Y.M. (2013). Iron homeostasis in the liver. *Comprehensive Physiology*.
16. Hofmann, A.F. (1999). Bile Acids: The Good, the Bad, and the Ugly. *News Physiol. Sci.* 14, 24-29.
17. Khurana, I. (2005). Red Blood Cells and Anaemias. In *Textbook of Medical Physiology*, Anonymous (India: Elsevier), pp. 156-162.
18. Cui, Y., Konig, J., Leier, I., Buchholz, U., Keppler, D. (2001). Hepatic uptake of bilirubin and its conjugates by the human organic anion transporter SLC21A6. *J. Biol. Chem.* 276, 9626-9630.
19. Maines, M.D. (1988). Heme oxygenase: function, multiplicity, regulatory mechanisms, and clinical applications. *FASEB J.* 2, 2557-2568.
20. Wang, X., Chowdhury, J.R., Chowdhury, N.R. (2006). Bilirubin metabolism: applied physiology. *Current Paediatrics* 16, 70-74.
21. Boyer, J.L. (2013). Bile Formation and Secretion. In *Comprehensive Physiology*, Anonymous : John Wiley & Sons, Inc.).
22. Ganong, W.F., Barrett, K.E. (2005). *Review of Medical Physiology: McGraw-Hill Medical* ^ eNew York New York).

23. Gafvelin, G., Jornvall, H., Mutt, V. (1990). Processing of prosecretin: isolation of a secretin precursor from porcine intestine. *Proc. Natl. Acad. Sci. U. S. A.* 87, 6781-6785.
24. Alpini, G., Glaser, S., Robertson, W., Rodgers, R.E., Phinizy, J.L., Lasater, J., LeSage, G.D. (1997). Large but not small intrahepatic bile ducts are involved in secretin-regulated ductal bile secretion. *Am. J. Physiol.* 272, G1064-74.
25. Lenzen, R., Alpini, G., Tavoloni, N. (1992). Secretin stimulates bile ductular secretory activity through the cAMP system. *Am. J. Physiol.* 263, G527-32.
26. Alvaro, D., Mennone, A., Boyer, J.L. (1997). Role of kinases and phosphatases in the regulation of fluid secretion and Cl<sup>-</sup>/HCO<sub>3</sub><sup>-</sup> exchange in cholangiocytes. *Am. J. Physiol.* 273, G303-13.
27. Pall, H., Zielenski, J., Jonas, M.M., DaSilva, D.A., Potvin, K.M., Yuan, X., Huang, Q., Freedman, S.D. (2007). Primary sclerosing cholangitis in childhood is associated with abnormalities in cystic fibrosis-mediated chloride channel function. *J. Pediatr.* 151, 255-259.
28. Allen, A., Flemstrom, G. (2005). Gastroduodenal mucus bicarbonate barrier: protection against acid and pepsin. *Am. J. Physiol. Cell. Physiol.* 288, C1-19.
29. Melamed, P., Melamed, F. (2014). Chronic metabolic acidosis destroys pancreas. *JOP* 15, 552-560.
30. Liddle, R.A. (1995). Regulation of cholecystokinin secretion by intraluminal releasing factors. *Am. J. Physiol.* 269, G319-27.
31. Park, K. (2011). TGF-beta Family Signaling in Embryonic Stem Cells. *International Journal of Stem Cells* 4, 18-23.
32. Yamashita, H., ten Dijke, P., Franzen, P., Miyazono, K., Heldin, C.H. (1994). Formation of hetero-oligomeric complexes of type I and type II receptors for transforming growth factor-beta. *J. Biol. Chem.* 269, 20172-20178.
33. Nakao, A., Imamura, T., Souchelnytskyi, S., Kawabata, M., Ishisaki, A., Oeda, E., Tamaki, K., Hanai, J., Heldin, C.H., Miyazono, K. et al. (1997). TGF-beta receptor-mediated signalling through Smad2, Smad3 and Smad4. *EMBO J.* 16, 5353-5362.
34. Shi, Y., Massague, J. (2003). Mechanisms of TGF-beta signaling from cell membrane to the nucleus. *Cell* 113, 685-700.
35. Nusslein-Volhard, C., Wieschaus, E., Kluding, H. (1984). Mutations affecting the pattern of the larval cuticle in *Drosophila melanogaster*. *Wilhelm Roux's archives of developmental biology* 193, 267-282.
36. Reya, T., Clevers, H. (2005). Wnt signalling in stem cells and cancer. *Nature* 434, 843-850.
37. Wallingford, J.B., Rowning, B.A., Vogeli, K.M., Rothbacher, U., Fraser, S.E., Harland, R.M. (2000). Dishevelled controls cell polarity during *Xenopus* gastrulation. *Nature* 405, 81-85.
38. Itoh, K., Krupnik, V.E., Sokol, S.Y. (1998). Axis determination in *Xenopus* involves biochemical interactions of axin, glycogen synthase kinase 3 and beta-catenin. *Current Biology* 8, 591-594.
39. Moon, R.T., Brown, J.D., Torres, M. (1997). WNTs modulate cell fate and behavior during vertebrate development. *Trends in Genetics* 13, 157-162.
40. Boulter, L., Govaere, O., Bird, T.G., Radulescu, S., Ramachandran, P., Pellicoro, A., Ridgway, R.A., Seo, S.S., Spee, B., Van Rooijen, N. et al. (2012). Macrophage-derived Wnt opposes Notch signaling to specify hepatic progenitor cell fate in chronic liver disease. *Nat. Med.* 18, 572-579.
41. Bhanot, P., Brink, M., Samos, C.H., Hsieh, J.C., Wang, Y., Macke, J.P., Andrew, D., Nathans, J., Nusse, R. (1996). A new member of the frizzled family from *Drosophila* functions as a Wingless receptor. *Nature* 382, 225-230.
42. Li, Y., Bu, G. (2005). LRP5/6 in Wnt signaling and tumorigenesis. *Future Oncol.* 1, 673-681.
43. Orford, K., Crockett, C., Jensen, J.P., Weissman, A.M., Byers, S.W. (1997). Serine phosphorylation-regulated ubiquitination and degradation of beta-catenin. *J. Biol. Chem.* 272, 24735-24738.
44. Roose, J., Molenaar, M., Peterson, J., Hurenkamp, J., Brantjes, H., Moerer, P., van de Wetering, M., Destree, O., Clevers, H. (1998). The *Xenopus* Wnt effector XTcf-3 interacts with Groucho-related transcriptional repressors. *Nature* 395, 608-612.

45. Chen, G., Courey, A.J. (2000). Groucho/TLE family proteins and transcriptional repression. *Gene* 249, 1-16.
46. Mao, J., Wang, J., Liu, B., Pan, W., Farr, G.H., 3rd, Flynn, C., Yuan, H., Takada, S., Kimelman, D., Li, L. et al. (2001). Low-density lipoprotein receptor-related protein-5 binds to Axin and regulates the canonical Wnt signaling pathway. *Mol. Cell* 7, 801-809.
47. Zeng, X., Tamai, K., Doble, B., Li, S., Huang, H., Habas, R., Okamura, H., Woodgett, J., He, X. (2005). A dual-kinase mechanism for Wnt co-receptor phosphorylation and activation. *Nature* 438, 873-877.
48. Wong, H.C., Bourdelas, A., Krauss, A., Lee, H.J., Shao, Y., Wu, D., Mlodzik, M., Shi, D.L., Zheng, J. (2003). Direct binding of the PDZ domain of Dishevelled to a conserved internal sequence in the C-terminal region of Frizzled. *Mol. Cell* 12, 1251-1260.
49. Yamamoto, H., Kishida, S., Kishida, M., Ikeda, S., Takada, S., Kikuchi, A. (1999). Phosphorylation of axin, a Wnt signal negative regulator, by glycogen synthase kinase-3 $\beta$  regulates its stability. *J. Biol. Chem.* 274, 10681-10684.
50. Komiya, Y., Habas, R. (2008). Wnt signal transduction pathways. *Organogenesis* 4, 68-75.
51. Daniels, D.L., Weis, W.I. (2005). Beta-catenin directly displaces Groucho/TLE repressors from Tcf/Lef in Wnt-mediated transcription activation. *Nat. Struct. Mol. Biol.* 12, 364-371.
52. Tian, X., Liu, Z., Niu, B., Zhang, J., Tan, T.K., Lee, S.R., Zhao, Y., Harris, D.C., Zheng, G. (2011). E-cadherin/beta-catenin complex and the epithelial barrier. *J. Biomed. Biotechnol.* 2011, 567305.
53. Yeh, T., Krauland, L., Singh, V., Zou, B., Devaraj, P., Stolz, D.B., Franks, J., Monga, S.P., Sasatomi, E., Behari, J. (2010). Liver-specific  $\beta$ -catenin knockout mice have bile canalicular abnormalities, bile secretory defect, and intrahepatic cholestasis. *Hepatology* 52, 1410-1419.
54. Matsui, T., Kinoshita, T., Morikawa, Y., Tohya, K., Katsuki, M., Ito, Y., Kamiya, A., Miyajima, A. (2002). K-Ras mediates cytokine-induced formation of E-cadherin-based adherens junctions during liver development. *EMBO J.* 21, 1021-1030.
55. Monga, S.P., Mars, W.M., Padiaditakis, P., Bell, A., Mule, K., Bowen, W.C., Wang, X., Zarnegar, R., Michalopoulos, G.K. (2002). Hepatocyte growth factor induces Wnt-independent nuclear translocation of beta-catenin after Met-beta-catenin dissociation in hepatocytes. *Cancer Res.* 62, 2064-2071.
56. Glinka, A., Wu, W., Delius, H., Monaghan, A.P., Blumenstock, C., Niehrs, C. (1998). Dickkopf-1 is a member of a new family of secreted proteins and functions in head induction. *Nature* 391, 357-362.
57. Hoang, B.H., Thomas, J.T., Abdul-Karim, F.W., Correia, K.M., Conlon, R.A., Luyten, F.P., Ballock, R.T. (1998). Expression pattern of two Frizzled-related genes, Frzb-1 and Sfrp-1, during mouse embryogenesis suggests a role for modulating action of Wnt family members. *Developmental Dynamics* 212, 364-372.
58. Wang, S., Krinks, M., Lin, K., Luyten, F.P., Moos, M., Jr. Frzb, a Secreted Protein Expressed in the Spemann Organizer, Binds and Inhibits Wnt-8. *Cell* 88, 757-766.
59. Hsieh, J., Kodjabachian, L., Rebbert, M.L., Rattner, A., Smallwood, P.M., Samos, C.H., Nusse, R., Dawid, I.B., Nathans, J. (1999). A new secreted protein that binds to Wnt proteins and inhibits their activities. *Nature* 398, 431-436.
60. Itasaki, N., Jones, C.M., Mercurio, S., Rowe, A., Domingos, P.M., Smith, J.C., Krumlauf, R. (2003). Wise, a context-dependent activator and inhibitor of Wnt signalling. *Development* 130, 4295-4305.
61. Artavanis-Tsakonas, S., Rand, M.D., Lake, R.J. (1999). Notch signaling: cell fate control and signal integration in development. *Science* 284, 770-776.
62. Sato, C., Zhao, G., Ilagan, M.X. (2012). An overview of notch signaling in adult tissue renewal and maintenance. *Curr. Alzheimer Res.* 9, 227-240.
63. Imayoshi, I., Kageyama, R. (2011). The role of Notch signaling in adult neurogenesis. *Mol. Neurobiol.* 44, 7-12.
64. Takeuchi, H., Haltiwanger, R.S. (2010). Role of glycosylation of Notch in development. *Semin. Cell Dev. Biol.* 21, 638-645.
65. Wu, J., Bresnick, E.H. (2007). Bare rudiments of notch signaling: how receptor levels are regulated. *Trends Biochem. Sci.* 32, 477-485.

66. Logeat, F., Bessia, C., Brou, C., LeBail, O., Jarriault, S., Seidah, N.G., Israel, A. (1998). The Notch1 receptor is cleaved constitutively by a furin-like convertase. *Proc. Natl. Acad. Sci. U. S. A.* 95, 8108-8112.
67. Gordon, W.R., Roy, M., Vardar-Ulu, D., Garfinkel, M., Mansour, M.R., Aster, J.C., Blacklow, S.C. (2009). Structure of the Notch1-negative regulatory region: implications for normal activation and pathogenic signaling in T-ALL. *Blood* 113, 4381-4390.
68. Brou, C., Logeat, F., Gupta, N., Bessia, C., LeBail, O., Doedens, J.R., Cumano, A., Roux, P., Black, R.A., Israel, A. (2000). A novel proteolytic cleavage involved in Notch signaling: the role of the disintegrin-metalloprotease TACE. *Mol. Cell* 5, 207-216.
69. De Strooper, B., Annaert, W., Cupers, P., Saftig, P., Craessaerts, K., Mumm, J.S., Schroeter, E.H., Schrijvers, V., Wolfe, M.S., Ray, W.J. et al. (1999). A presenilin-1-dependent gamma-secretase-like protease mediates release of Notch intracellular domain. *Nature* 398, 518-522.
70. Kadesch, T. (2004). Notch signaling: the demise of elegant simplicity. *Curr. Opin. Genet. Dev.* 14, 506-512.
71. Nam, Y., Sliz, P., Song, L., Aster, J.C., Blacklow, S.C. (2006). Structural basis for cooperativity in recruitment of MAML coactivators to Notch transcription complexes. *Cell* 124, 973-983.
72. Fryer, C.J., White, J.B., Jones, K.A. (2004). Mastermind recruits CycC:CDK8 to phosphorylate the Notch ICD and coordinate activation with turnover. *Mol. Cell* 16, 509-520.
73. Liu, J., Sato, C., Cerletti, M., Wagers, A. (2010). Chapter Twelve - Notch Signaling in the Regulation of Stem Cell Self-Renewal and Differentiation. *Curr. Top. Dev. Biol.* 92, 367-409.
74. Iso, T., Kedes, L., Hamamori, Y. (2003). HES and HERP families: Multiple effectors of the notch signaling pathway. *J. Cell. Physiol.* 194, 237-255.
75. Berdnik, D., Torok, T., Gonzalez-Gaitan, M., Knoblich, J.A. (2002). The endocytic protein alpha-Adaptin is required for numb-mediated asymmetric cell division in *Drosophila*. *Dev. Cell.* 3, 221-231.
76. McGill, M.A., McGlade, C.J. (2003). Mammalian numb proteins promote Notch1 receptor ubiquitination and degradation of the Notch1 intracellular domain. *J. Biol. Chem.* 278, 23196-23203.
77. Serls, A.E., Doherty, S., Parvatiyar, P., Wells, J.M., Deutsch, G.H. (2005). Different thresholds of fibroblast growth factors pattern the ventral foregut into liver and lung. *Development* 132, 35-47.
78. McLin, V.A., Rankin, S.A., Zorn, A.M. (2007). Repression of Wnt/beta-catenin signaling in the anterior endoderm is essential for liver and pancreas development. *Development* 134, 2207-2217.
79. Jung, J., Zheng, M., Goldfarb, M., Zaret, K.S. (1999). Initiation of mammalian liver development from endoderm by fibroblast growth factors. *Science* 284, 1998-2003.
80. Gualdi, R., Bossard, P., Zheng, M., Hamada, Y., Coleman, J.R., Zaret, K.S. (1996). Hepatic specification of the gut endoderm in vitro: cell signaling and transcriptional control. *Genes Dev.* 10, 1670-1682.
81. Duncan, S.A., Manova, K., Chen, W.S., Hoodless, P., Weinstein, D.C., Bachvarova, R.F., Darnell, J.E., Jr. (1994). Expression of transcription factor HNF-4 in the extraembryonic endoderm, gut, and nephrogenic tissue of the developing mouse embryo: HNF-4 is a marker for primary endoderm in the implanting blastocyst. *Proc. Natl. Acad. Sci. U. S. A.* 91, 7598-7602.
82. Shiojiri, N., Sugiyama, Y. (2004). Immunolocalization of extracellular matrix components and integrins during mouse liver development. *Hepatology* 40, 346-355.
83. Tremblay, K.D., Zaret, K.S. (2005). Distinct populations of endoderm cells converge to generate the embryonic liver bud and ventral foregut tissues. *Dev. Biol.* 280, 87-99.
84. Bort, R., Signore, M., Tremblay, K., Martinez Barbera, J.P., Zaret, K.S. (2006). Hex homeobox gene controls the transition of the endoderm to a pseudostratified, cell emergent epithelium for liver bud development. *Dev. Biol.* 290, 44-56.
85. Margagliotti, S., Clotman, F., Pierreux, C.E., Lemoine, P., Rousseau, G.G., Henriot, P., Lemaigre, F.P. (2008). Role of metalloproteinases at the onset of liver development. *Dev. Growth Differ.* 50, 331-338.
86. Zorn, A.M. (2008). Liver development. In *StemBook*, Anonymous (Cambridge (MA): Aaron M. Zorn).

87. Hunter, M.P., Wilson, C.M., Jiang, X., Cong, R., Vasavada, H., Kaestner, K.H., Bogue, C.W. (2007). The homeobox gene *Hhex* is essential for proper hepatoblast differentiation and bile duct morphogenesis. *Dev. Biol.* 308, 355-367.
88. Clotman, F., Lannoy, V.J., Reber, M., Cereghini, S., Cassiman, D., Jacquemin, P., Roskams, T., Rousseau, G.G., Lemaigre, F.P. (2002). The onecut transcription factor *HNF6* is required for normal development of the biliary tract. *Development* 129, 1819-1828.
89. Coffinier, C., Gresh, L., Fiette, L., Tronche, F., Schutz, G., Babinet, C., Pontoglio, M., Yaniv, M., Barra, J. (2002). Bile system morphogenesis defects and liver dysfunction upon targeted deletion of *HNF1beta*. *Development* 129, 1829-1838.
90. Antoniou, A., Raynaud, P., Cordi, S., Zong, Y., Tronche, F., Stanger, B.Z., Jacquemin, P., Pierreux, C.E., Clotman, F., Lemaigre, F.P. (2009). Intrahepatic bile ducts develop according to a new mode of tubulogenesis regulated by the transcription factor *SOX9*. *Gastroenterology* 136, 2325-2333.
91. Fabris, L., Cadamuro, M., Libbrecht, L., Raynaud, P., Spirli, C., Fiorotto, R., Okolicsanyi, L., Lemaigre, F., Strazzabosco, M., Roskams, T. (2008). Epithelial expression of angiogenic growth factors modulate arterial vasculogenesis in human liver development. *Hepatology* 47, 719-728.
92. Shiojiri, N., Katayama, H. (1987). Secondary joining of the bile ducts during the hepatogenesis of the mouse embryo. *Anat. Embryol. (Berl)* 177, 153-163.
93. Tan, X., Apte, U., Micsenyi, A., Kotsagrelis, E., Luo, J., Ranganathan, S., Monga, D.K., Bell, A., Michalopoulos, G.K., Monga, S.P. (2005). Epidermal growth factor receptor: a novel target of the *Wnt*/ $\beta$ -catenin pathway in liver. *Gastroenterology* 129, 285-302.
94. Michalopoulos, G.K., Bowen, W.C., Mule, K., Luo, J. (2003). HGF-, EGF-, and dexamethasone-induced gene expression patterns during formation of tissue in hepatic organoid cultures. *Gene Expr.* 11, 55-75.
95. Monga, S.P., Monga, H.K., Tan, X., Mulé, K., Padiaditakis, P., Michalopoulos, G.K. (2003).  $\beta$ -catenin antisense studies in embryonic liver cultures: role in proliferation, apoptosis, and lineage specification. *Gastroenterology* 124, 202-216.
96. Hussain, S.Z., Sneddon, T., Tan, X., Micsenyi, A., Michalopoulos, G.K., Monga, S.P. (2004). *Wnt* impacts growth and differentiation in ex vivo liver development. *Exp. Cell Res.* 292, 157-169.
97. Tan, X., Yuan, Y., Zeng, G., Apte, U., Thompson, M.D., Cieply, B., Stolz, D.B., Michalopoulos, G.K., Kaestner, K.H., Monga, S.P. (2008).  $\beta$ -Catenin deletion in hepatoblasts disrupts hepatic morphogenesis and survival during mouse development. *Hepatology* 47, 1667-1679.
98. Clotman, F., Jacquemin, P., Plumb-Rudewicz, N., Pierreux, C.E., Van der Smissen, P., Dietz, H.C., Courtoy, P.J., Rousseau, G.G., Lemaigre, F.P. (2005). Control of liver cell fate decision by a gradient of *TGF $\beta$*  signaling modulated by *Onecut* transcription factors. *Genes & Development* 19, 1849-1854.
99. Tanimizu, N., Miyajima, A. (2004). *Notch* signaling controls hepatoblast differentiation by altering the expression of liver-enriched transcription factors. *J. Cell. Sci.* 117, 3165-3174.
100. Suzuki, A., Sekiya, S., Buscher, D., Izipisua Belmonte, J.C., Taniguchi, H. (2008). *Tbx3* controls the fate of hepatic progenitor cells in liver development by suppressing *p19ARF* expression. *Development* 135, 1589-1595.
101. Shiojiri, N., Takeshita, K., Yamasaki, H., Iwata, T. (2004). Suppression of *C/EBP  $\alpha$*  expression in biliary cell differentiation from hepatoblasts during mouse liver development. *J. Hepatol.* 41, 790-798.
102. Yamasaki, H., Sada, A., Iwata, T., Niwa, T., Tomizawa, M., Xanthopoulos, K.G., Koike, T., Shiojiri, N. (2006). Suppression of *C/EBP $\alpha$*  expression in periportal hepatoblasts may stimulate biliary cell differentiation through increased *Hnf6* and *Hnf1b* expression. *Development* 133, 4233-4243.
103. Ader, T., Norel, R., Levoci, L., Rogler, L.E. (2006). Transcriptional profiling implicates *TGF $\beta$* /*BMP* and *Notch* signaling pathways in ductular differentiation of fetal murine hepatoblasts. *Mech. Dev.* 123, 177-194.
104. Roelandt, P., Antoniou, A., Libbrecht, L., Van Steenberghe, W., Laleman, W., Verslype, C., Van der Merwe, S., Nevens, F., De Vos, R., Fischer, E. et al. (2012). *HNF1B* deficiency causes ciliary defects in human cholangiocytes. *Hepatology* 56, 1178-1181.
105. Raynaud, P., Carpentier, R., Antoniou, A., Lemaigre, F.P. (2011). Biliary differentiation and bile duct morphogenesis in development and disease. *Int. J. Biochem. Cell Biol.* 43, 245-256.

106. Kodama, Y., Hijikata, M., Kageyama, R., Shimotohno, K., Chiba, T. (2004). The role of notch signaling in the development of intrahepatic bile ducts. *Gastroenterology* 127, 1775-1786.
107. Blachier, M., Leleu, H., Peck-Radosavljevic, M., Valla, D., Roudot-Thoraval, F. (2013). The burden of liver disease in Europe: a review of available epidemiological data. *J. Hepatol.* 58, 593-608.
108. Bogdanos, D.P., Gao, B., Gershwin, M.E. (2013). Liver Immunology. *Comprehensive Physiology* 3, 567-598.
109. Ahmad-Nejad, P., Häcker, H., Rutz, M., Bauer, S., Vabulas, R.M., Wagner, H. (2002). Bacterial CpG-DNA and lipopolysaccharides activate Toll-like receptors at distinct cellular compartments. *Eur. J. Immunol.* 32, 1958-1968.
110. Beg, A.A., Finco, T.S., Nantermet, P.V., Baldwin, A.S., Jr. (1993). Tumor necrosis factor and interleukin-1 lead to phosphorylation and loss of I kappa B alpha: a mechanism for NF-kappa B activation. *Mol. Cell. Biol.* 13, 3301-3310.
111. Muriel, P. (2009). NF-kappaB in liver diseases: a target for drug therapy. *J. Appl. Toxicol.* 29, 91-100.
112. Hacker, H., Karin, M. (2006). Regulation and function of IKK and IKK-related kinases. *Sci. STKE* 2006, re13.
113. Knolle, P., Schlaak, J., Uhrig, A., Kempf, P., Meyer zum Buschenfelde, K.H., Gerken, G. (1995). Human Kupffer cells secrete IL-10 in response to lipopolysaccharide (LPS) challenge. *J. Hepatol.* 22, 226-229.
114. Racanelli, V., Rehermann, B. (2006). The liver as an immunological organ. *Hepatology* 43, S54-62.
115. Shao, B., Lu, M., Katz, S.C., Varley, A.W., Hardwick, J., Rogers, T.E., Ojogun, N., Rockey, D.C., Dematteo, R.P., Munford, R.S. (2007). A host lipase detoxifies bacterial lipopolysaccharides in the liver and spleen. *J. Biol. Chem.* 282, 13726-13735.
116. Thomson, A.W., Knolle, P.A. (2010). Antigen-presenting cell function in the tolerogenic liver environment. *Nat. Rev. Immunol.* 10, 753-766.
117. Decker, K. (1990). Biologically active products of stimulated liver macrophages (Kupffer cells). *Eur. J. Biochem.* 192, 245-261.
118. Tran-Thi, T.A., Phillips, J., Falk, H., Decker, K. (1985). Toxicity of D-galactosamine for rat hepatocytes in monolayer culture. *Exp. Mol. Pathol.* 42, 89-116.
119. Schümann, J., Wolf, D., Pahl, A., Brune, K., Papadopoulos, T., van Rooijen, N., Tiegs, G. (2000). Importance of Kupffer cells for T-cell-dependent liver injury in mice. *The American journal of pathology* 157, 1671-1683.
120. Marra, F., DeFranco, R., Grappone, C., Milani, S., Pastacaldi, S., Pinzani, M., Romanelli, R.G., Laffi, G., Gentilini, P. (1998). Increased expression of monocyte chemoattractant protein-1 during active hepatic fibrogenesis: correlation with monocyte infiltration. *Am. J. Pathol.* 152, 423-430.
121. Seki, E., De Minicis, S., Österreicher, C.H., Kluwe, J., Osawa, Y., Brenner, D.A., Schwabe, R.F. (2007). TLR4 enhances TGF- $\beta$  signaling and hepatic fibrosis. *Nat. Med.* 13, 1324-1332.
122. Wynn, T.A., Barron, L. (2010). Macrophages: master regulators of inflammation and fibrosis. *Semin. Liver Dis.* 30, 245-257.
123. Selzner, N., Selzner, M., Odermatt, B., Tian, Y., van Rooijen, N., Clavien, P. (2003). ICAM-1 triggers liver regeneration through leukocyte recruitment and Kupffer cell-dependent release of TNF- $\alpha$ /IL-6 in mice. *Gastroenterology* 124, 692-700.
124. Husztko, E., Lazar, G., Parducz, A. (1980). Electron microscopic study of Kupffer-cell phagocytosis blockade induced by gadolinium chloride. *Br. J. Exp. Pathol.* 61, 624-630.
125. Muriel, P., Escobar, Y. (2003). Kupffer cells are responsible for liver cirrhosis induced by carbon tetrachloride. *Journal of Applied Toxicology* 23, 103-108.
126. Iredale, J.P. (2007). Models of liver fibrosis: exploring the dynamic nature of inflammation and repair in a solid organ. *J. Clin. Invest.* 117, 539-548.
127. Dooley, S., ten Dijke, P. (2012). TGF-beta in progression of liver disease. *Cell Tissue Res.* 347, 245-256.
128. Maher, J.J., Bissell, D.M., Friedman, S.L., Roll, F.J. (1988). Collagen measured in primary cultures of normal rat hepatocytes derives from lipocytes within the monolayer. *J. Clin. Invest.* 82, 450-459.

129. Li, D., Friedman, S.L. (1999). Liver fibrogenesis and the role of hepatic stellate cells: new insights and prospects for therapy. *J. Gastroenterol. Hepatol.* 14, 618-633.
130. Friedman, S.L. (2000). Molecular regulation of hepatic fibrosis, an integrated cellular response to tissue injury. *J. Biol. Chem.* 275, 2247-2250.
131. Ghosh, A.K., Vaughan, D.E. (2012). PAI-1 in tissue fibrosis. *J. Cell. Physiol.* 227, 493-507.
132. Lyons, R.M., Gentry, L.E., Purchio, A.F., Moses, H.L. (1990). Mechanism of activation of latent recombinant transforming growth factor beta 1 by plasmin. *J. Cell Biol.* 110, 1361-1367.
133. Huang, X., Kawakatsu, H. (1999). The integrin alpha v beta 6 binds and activates latent TGF beta 1: a mechanism for 4 5 6 regulating pulmonary inflammation and fibrosis. *Cell* 96, 319-328.
134. Sheppard, D. (2005). Integrin-mediated activation of latent transforming growth factor  $\beta$ . *Cancer Metastasis Rev.* 24, 395-402.
135. Taipale, J., Koli, K., Keski-Oja, J. (1992). Release of transforming growth factor-beta 1 from the pericellular matrix of cultured fibroblasts and fibrosarcoma cells by plasmin and thrombin. *J. Biol. Chem.* 267, 25378-25384.
136. Li, M.O., Flavell, R.A. (2008). TGF- $\beta$ : a master of all T cell trades. *Cell* 134, 392-404.
137. Fallowfield, J.A., Mizuno, M., Kendall, T.J., Constandinou, C.M., Benyon, R.C., Duffield, J.S., Iredale, J.P. (2007). Scar-associated macrophages are a major source of hepatic matrix metalloproteinase-13 and facilitate the resolution of murine hepatic fibrosis. *J. Immunol.* 178, 5288-5295.
138. Fischer, R., Cariers, A., Reinehr, R., Haussinger, D. (2002). Caspase 9-dependent killing of hepatic stellate cells by activated Kupffer cells. *Gastroenterology* 123, 845-861.
139. Apte, U., Gkretsi, V., Bowen, W.C., Mars, W.M., Luo, J.H., Donthamsetty, S., Orr, A., Monga, S.P., Wu, C., Michalopoulos, G.K. (2009). Enhanced liver regeneration following changes induced by hepatocyte-specific genetic ablation of integrin-linked kinase. *Hepatology* 50, 844-851.
140. Katoonizadeh, A., Poustchi, H., Malekzadeh, R. (2014). Hepatic progenitor cells in liver regeneration: current advances and clinical perspectives. *Liver International*, n/a-n/a.
141. Zhou, H., Rogler, L.E., Teperman, L., Morgan, G., Rogler, C.E. (2007). Identification of hepatocytic and bile ductular cell lineages and candidate stem cells in bipolar ductular reactions in cirrhotic human liver. *Hepatology* 45, 716-724.
142. Gouw, A.S., Clouston, A.D., Theise, N.D. (2011). Ductular reactions in human liver: diversity at the interface. *Hepatology* 54, 1853-1863.
143. Wagner, T., Wirth, J., Meyer, J., Zabel, B., Held, M., Zimmer, J., Pasantes, J., Bricarelli, F.D., Keutel, J., Hustert, E. et al. (1994). Autosomal sex reversal and campomelic dysplasia are caused by mutations in and around the SRY-related gene SOX9. *Cell* 79, 1111-1120.
144. Furuyama, K., Kawaguchi, Y., Akiyama, H., Horiguchi, M., Kodama, S., Kuhara, T., Hosokawa, S., Elbahrawy, A., Soeda, T., Koizumi, M. et al. (2011). Continuous cell supply from a Sox9-expressing progenitor zone in adult liver, exocrine pancreas and intestine. *Nat. Genet.* 43, 34-41.
145. Hanley, K.P., Oakley, F., Sugden, S., Wilson, D.I., Mann, D.A., Hanley, N.A. (2008). Ectopic SOX9 mediates extracellular matrix deposition characteristic of organ fibrosis. *J. Biol. Chem.* 283, 14063-14071.
146. Pritchett, J., Harvey, E., Athwal, V., Berry, A., Rowe, C., Oakley, F., Moles, A., Mann, D.A., Bobola, N., Sharrocks, A.D. et al. (2012). Osteopontin is a novel downstream target of SOX9 with diagnostic implications for progression of liver fibrosis in humans. *Hepatology* 56, 1108-1116.
147. Uede, T. (2011). Osteopontin, intrinsic tissue regulator of intractable inflammatory diseases. *Pathol. Int.* 61, 265-280.
148. Nagoshi, S. (2014). Osteopontin: Versatile modulator of liver diseases. *Hepatol. Res.* 44, 22-30.
149. De Minicis, S., Seki, E., Uchinami, H., Kluwe, J., Zhang, Y., Brenner, D.A., Schwabe, R.F. (2007). Gene expression profiles during hepatic stellate cell activation in culture and in vivo. *Gastroenterology* 132, 1937-1946.

150. Yang, M., Ramachandran, A., Yan, H.M., Woolbright, B.L., Copple, B.L., Fickert, P., Trauner, M., Jaeschke, H. (2014). Osteopontin is an initial mediator of inflammation and liver injury during obstructive cholestasis after bile duct ligation in mice. *Toxicol. Lett.* 224, 186-195.
151. Wang, X., Lopategi, A., Ge, X., Lu, Y., Kitamura, N., Urtasun, R., Leung, T.M., Fiel, M.I., Nieto, N. (2014). Osteopontin induces ductular reaction contributing to liver fibrosis. *Gut*.
152. Coombes, J.D., Swiderska-Syn, M., Dolle, L., Reid, D., Eksteen, B., Claridge, L., Briones-Orta, M.A., Shetty, S., Oo, Y.H., Riva, A. et al. (2014). Osteopontin neutralisation abrogates the liver progenitor cell response and fibrogenesis in mice. *Gut*.
153. Spee, B., Carpino, G., Schotanus, B.A., Katoonizadeh, A., Vander Borght, S., Gaudio, E., Roskams, T. (2010). Characterisation of the liver progenitor cell niche in liver diseases: potential involvement of Wnt and Notch signalling. *Gut* 59, 247-257.
154. Al-Suleiman, A.M., Bu-sobaih, J. (2006). Acute fulminant cholestatic jaundice in sickle cell disease. *Ann. Saudi Med.* 26, 138-140.
155. Thapa, B.R., Walia, A. (2007). Liver function tests and their interpretation. *Indian J. Pediatr.* 74, 663-671.
156. Roche, S.P., Kobos, R. (2004). Jaundice in the adult patient. *Am. Fam. Physician* 69, 299-308.
157. Venigalla, S., Gourley, G.R. (2004). Neonatal cholestasis. 28, 348-355.
158. Fevery, J., Blanckaert, N., Heirwegh, K.P., Preaux, A.M., Berthelot, P. (1977). Unconjugated bilirubin and an increased proportion of bilirubin monoconjugates in the bile of patients with Gilbert's syndrome and Crigler-Najjar disease. *J. Clin. Invest.* 60, 970-979.
159. Poupon, R.E., Lindor, K.D., Pares, A., Chazouilleres, O., Poupon, R., Heathcote, E.J. (2003). Combined analysis of the effect of treatment with ursodeoxycholic acid on histologic progression in primary biliary cirrhosis. *J. Hepatol.* 39, 12-16.
160. Paumgartner, G., Beuers, U. (2002). Ursodeoxycholic acid in cholestatic liver disease: mechanisms of action and therapeutic use revisited. *Hepatology* 36, 525-531.
161. Sokol, R.J. (1994). Fat-soluble vitamins and their importance in patients with cholestatic liver diseases. *Gastroenterol. Clin. North Am.* 23, 673-705.
162. Barbatis, C., Grases, P., Shepherd, H.A., Chapman, R.W., Trowell, J., Jewell, D.P., McGee, J.O. (1985). Histological features of sclerosing cholangitis in patients with chronic ulcerative colitis. *J. Clin. Pathol.* 38, 778-783.
163. Kaplan, M.M., Gershwin, M.E. (2005). Primary Biliary Cirrhosis. *N. Engl. J. Med.* 353, 1261-1273.
164. Alvaro, D., Invernizzi, P., Onori, P., Franchitto, A., De Santis, A., Crosignani, A., Sferra, R., Ginanni-Corradini, S., Grazia Mancino, M., Maggioni, M. et al. (2004). Estrogen receptors in cholangiocytes and the progression of primary biliary cirrhosis. *J. Hepatol.* 41, 905-912.
165. Walker, J., Doniach, D., Roitt, I., Sherlock, S. (1965). Serological tests in diagnosis of primary biliary cirrhosis. *The Lancet* 285, 827-831.
166. You, Z., Wang, Q., Bian, Z., Liu, Y., Han, X., Peng, Y., Shen, L., Chen, X., Qiu, D., Selmi, C. et al. (2012). The immunopathology of liver granulomas in primary biliary cirrhosis. *J. Autoimmun.* 39, 216-221.
167. Nakanuma, Y., Harada, K. (1993). Florid duct lesion in primary biliary cirrhosis shows highly proliferative activities. *J. Hepatol.* 19, 216-221.
168. Bowlus, C.L., Gershwin, M.E. (2014). The diagnosis of primary biliary cirrhosis. *Autoimmunity Reviews* 13, 441-444.
169. Mack, C.L., Feldman, A.G., Sokol, R.J. (2012). Clues to the etiology of bile duct injury in biliary atresia. *Semin. Liver Dis.* 32, 307-316.
170. Kelly, D.A., Davenport, M. (2007). Current management of biliary atresia. *Arch. Dis. Child.* 92, 1132-1135.
171. Tyler, K.L., Sokol, R.J., Oberhaus, S.M., Le, M., Karrer, F.M., Narkewicz, M.R., Tyson, R.W., Murphy, J.R., Low, R., Brown, W.R. (1998). Detection of reovirus RNA in hepatobiliary tissues from patients with extrahepatic biliary atresia and choledochal cysts. *Hepatology* 27, 1475-1482.

172. Riepenhoff-Talty, M., Gouvea, V., Evans, M.J., Svensson, L., Hoffenberg, E., Sokol, R.J., Uhnoo, I., Greenberg, S.J., Schakel, K., Zhaori, G. et al. (1996). Detection of group C rotavirus in infants with extrahepatic biliary atresia. *J. Infect. Dis.* 174, 8-15.
173. Domiati-Saad, R., Dawson, D.B., Margraf, L.R., Finegold, M.J., Weinberg, A.G., Rogers, B.B. (2000). Cytomegalovirus and human herpesvirus 6, but not human papillomavirus, are present in neonatal giant cell hepatitis and extrahepatic biliary atresia. *Pediatric and Developmental Pathology* 3, 367-373.
174. Fischler, B., Ehrnst, A., Forsgren, M., Örvell, C., Nemeth, A. (1998). The viral association of neonatal cholestasis in Sweden: a possible link between cytomegalovirus infection and extrahepatic biliary atresia. *J. Pediatr. Gastroenterol. Nutr.* 27, 57-64.
175. Drut, R., Drut, R.M., Gómez, M.A., Rúa, E.C., Lojo, M.M. (1998). Presence of human papillomavirus in extrahepatic biliary atresia. *J. Pediatr. Gastroenterol. Nutr.* 27, 530-535.
176. Mahjoub, F., Shahsiah, R., Ardalani, F.A., Iravanloo, G., Sani, M.N., Zarei, A., Monajemzadeh, M., Farahmand, F., Mamishi, S. (2008). Detection of Epstein Barr Virus by Chromogenic In Situ Hybridization in cases of extra-hepatic biliary atresia. *Diagn Pathol* 3, 19.
177. Garcia-Barcelo, M.M., Yeung, M.Y., Miao, X.P., Tang, C.S., Cheng, G., So, M.T., Ngan, E.S., Lui, V.C., Chen, Y., Liu, X.L. et al. (2010). Genome-wide association study identifies a susceptibility locus for biliary atresia on 10q24.2. *Hum. Mol. Genet.* 19, 2917-2925.
178. Donaldson, P.T., Clare, M., Constantini, P.K., Hadzic, N., Mieli-Vergani, G., Howard, E., Kelley, D. (2002). HLA and cytokine gene polymorphisms in biliary atresia. *Liver* 22, 213-219.
179. Shih, H.H., Lin, T.M., Chuang, J.H., Eng, H.L., Juo, S.H., Huang, F.C., Chen, C.L., Chen, H.L. (2005). Promoter polymorphism of the CD14 endotoxin receptor gene is associated with biliary atresia and idiopathic neonatal cholestasis. *Pediatrics* 116, 437-441.
180. Bezerra, J.A. (2005). Potential etiologies of biliary atresia. *Pediatr. Transplant.* 9, 646-651.
181. Mack, C.L. (2007). The pathogenesis of biliary atresia: evidence for a virus-induced autoimmune disease. *Semin. Liver Dis.* 27, 233-242.
182. Fabris, L., Cadamuro, M., Guido, M., Spirli, C., Fiorotto, R., Colledan, M., Torre, G., Alberti, D., Sonzogni, A., Okolicsanyi, L. et al. (2007). Analysis of liver repair mechanisms in Alagille syndrome and biliary atresia reveals a role for notch signaling. *Am. J. Pathol.* 171, 641-653.
183. Krantz, I.D., Piccoli, D.A., Spinner, N.B. (1999). Clinical and molecular genetics of Alagille syndrome. *Curr. Opin. Pediatr.* 11, 558-564.
184. Piccoli, D.A., Spinner, N.B. (2001). Alagille syndrome and the Jagged1 gene. *Semin. Liver Dis.* 21, 525-534.
185. Oda, T., Elkahoul, A.G., Pike, B.L., Okajima, K., Krantz, I.D., Genin, A., Piccoli, D.A., Meltzer, P.S., Spinner, N.B., Collins, F.S. et al. (1997). Mutations in the human Jagged1 gene are responsible for Alagille syndrome. *Nat. Genet.* 16, 235-242.
186. Li, L., Krantz, I.D., Deng, Y., Genin, A., Banta, A.B., Collins, C.C., Qi, M., Trask, B.J., Kuo, W.L., Cochran, J. et al. (1997). Alagille syndrome is caused by mutations in human Jagged1, which encodes a ligand for Notch1. *Nat. Genet.* 16, 243-251.
187. McDaniell, R., Warthen, D.M., Sanchez-Lara, P.A., Pai, A., Krantz, I.D., Piccoli, D.A., Spinner, N.B. (2006). NOTCH2 mutations cause Alagille syndrome, a heterogeneous disorder of the notch signaling pathway. *Am. J. Hum. Genet.* 79, 169-173.
188. Roskams, T.A., Theise, N.D., Balabaud, C., Bhagat, G., Bhathal, P.S., Bioulac-Sage, P., Brunt, E.M., Crawford, J.M., Crosby, H.A., Desmet, V. et al. (2004). Nomenclature of the finer branches of the biliary tree: canals, ductules, and ductular reactions in human livers. *Hepatology* 39, 1739-1745.
189. Ward, J.F. (1995). Radiation mutagenesis: the initial DNA lesions responsible. *Radiat. Res.* 142, 362-368.
190. Mandell, J., Koch, W.K., Nidess, R., Preminger, G.M., McFarland, E. (1983). Congenital polycystic kidney disease. Genetically transmitted infantile polycystic kidney disease in C57BL/6J mice. *The American Journal of Pathology* 113, 112-114.
191. Fickert, P., Ståhlger, U., Fuchsbichler, A., Moustafa, T., Marschall, H., Weiglein, A.H., Tsybrovskyy, O., Jaeschke, H., Zatloukal, K., Denk, H. et al. (2007). A New Xenobiotic-Induced Mouse Model of Sclerosing Cholangitis and Biliary Fibrosis. *The American Journal of Pathology* 171, 525-536.

192. Becker, B.A., Plaa, G.L. (1965). The nature of alpha-naphthylisothiocyanate-induced cholestasis. *Toxicol. Appl. Pharmacol.* 7, 680-685.
193. Connolly, A.K., Price, S.C., Connelly, J.C., Hinton, R.H. (1988). Early changes in bile duct lining cells and hepatocytes in rats treated with  $\alpha$ -naphthylisothiocyanate. *Toxicol. Appl. Pharmacol.* 93, 208-219.
194. Paques, F., Duchateau, P. (2007). Meganucleases and DNA double-strand break-induced recombination: perspectives for gene therapy. *Curr. Gene Ther.* 7, 49-66.
195. Le Provost, F., Lillico, S., Passet, B., Young, R., Whitelaw, B., Vilotte, J.L. (2010). Zinc finger nuclease technology heralds a new era in mammalian transgenesis. *Trends Biotechnol.* 28, 134-141.
196. Carroll, D. (2011). Genome engineering with zinc-finger nucleases. *Genetics* 188, 773-782.
197. Li, T., Huang, S., Jiang, W.Z., Wright, D., Spalding, M.H., Weeks, D.P., Yang, B. (2011). TAL nucleases (TALNs): hybrid proteins composed of TAL effectors and FokI DNA-cleavage domain. *Nucleic Acids Res.* 39, 359-372.
198. Christian, M., Cermak, T., Doyle, E.L., Schmidt, C., Zhang, F., Hummel, A., Bogdanove, A.J., Voytas, D.F. (2010). Targeting DNA double-strand breaks with TAL effector nucleases. *Genetics* 186, 757-761.
199. Cong, L., Zhang, F. (2015). Genome Engineering Using CRISPR-Cas9 System. *Methods Mol. Biol.* 1239, 197-217.
200. Hayashi, H., Sakai, T. (2011). Animal models for the study of liver fibrosis: new insights from knockout mouse models. *Am. J. Physiol. Gastrointest. Liver Physiol.* 300, G729-38.
201. Oertelt, S., Lian, Z.X., Cheng, C.M., Chuang, Y.H., Padgett, K.A., He, X.S., Ridgway, W.M., Ansari, A.A., Coppel, R.L., Li, M.O. et al. (2006). Anti-mitochondrial antibodies and primary biliary cirrhosis in TGF-beta receptor II dominant-negative mice. *J. Immunol.* 177, 1655-1660.
202. Wakabayashi, K., Lian, Z., Moritoki, Y., Lan, R.Y., Tsuneyama, K., Chuang, Y., Yang, G., Ridgway, W., Ueno, Y., Ansari, A.A. (2006). IL-2 receptor  $\alpha^{-/-}$  mice and the development of primary biliary cirrhosis. *Hepatology* 44, 1240-1249.
203. Mauad, T.H., van Nieuwkerk, C.M., Dingemans, K.P., Smit, J.J., Schinkel, A.H., Notenboom, R.G., van den Bergh Weerman, M.A., Verkruijsen, R.P., Groen, A.K., Oude Elferink, R.P. (1994). Mice with homozygous disruption of the *mdr2* P-glycoprotein gene. A novel animal model for studies of nonsuppurative inflammatory cholangitis and hepatocarcinogenesis. *Am. J. Pathol.* 145, 1237-1245.
204. Kountouras, J., Billing, B.H., Scheuer, P.J. (1984). Prolonged bile duct obstruction: a new experimental model for cirrhosis in the rat. *Br. J. Exp. Pathol.* 65, 305-311.
205. Heinrich, S., Georgiev, P., Weber, A., Vergopoulos, A., Graf, R., Clavien, P.A. (2011). Partial bile duct ligation in mice: a novel model of acute cholestasis. *Surgery* 149, 445-451.
206. Osawa, Y., Seki, E., Adachi, M., Taura, K., Kodama, Y., Siegmund, S.V., Schwabe, R.F., Brenner, D.A. (2006). Systemic mediators induce fibrogenic effects in normal liver after partial bile duct ligation. *Liver Int.* 26, 1138-1147.
207. Tannuri, A.C., Coelho, M.C., de Oliveira Goncalves, J., Santos, M.M., Ferraz da Silva, L.F., Bendit, I., Tannuri, U. (2012). Effects of selective bile duct ligation on liver parenchyma in young animals: histologic and molecular evaluations. *J. Pediatr. Surg.* 47, 513-522.
208. Aller, M.A., Arias, J.L., Garcia-Dominguez, J., Arias, J.I., Duran, M., Arias, J. (2008). Experimental obstructive cholestasis: the wound-like inflammatory liver response. *Fibrogenesis Tissue Repair* 1, 6-1536-1-6.
209. Hossini, A.M., Megges, M., Prigione, A., Lichtner, B., Toliat, M.R., Wruck, W., Schroter, F., Nuernberg, P., Kroll, H., Makrantonaki, E. et al. (2015). Induced pluripotent stem cell-derived neuronal cells from a sporadic Alzheimer's disease donor as a model for investigating AD-associated gene regulatory networks. *BMC Genomics* 16, 84.
210. Anadon, A., Martinez, M.A., Castellano, V., Martinez-Larranaga, M.R. (2014). The role of in vitro methods as alternatives to animals in toxicity testing. *Expert Opin. Drug Metab. Toxicol.* 10, 67-79.
211. Costa, A., Sarmiento, B., Seabra, V. (2014). An evaluation of the latest in vitro tools for drug metabolism studies. *Expert Opin. Drug Metab. Toxicol.* 10, 103-119.

212. Lee, J.H., Park, H.J., Jang, I.K., Kim, H.E., Lee, D.H., Park, J.K., Lee, S.K., Yoon, H.H. (2014). In vitro differentiation of human liver-derived stem cells with mesenchymal characteristics into immature hepatocyte-like cells. *Transplant. Proc.* 46, 1633-1637.
213. Osakada, F., Jin, Z.B., Hirami, Y., Ikeda, H., Danjyo, T., Watanabe, K., Sasai, Y., Takahashi, M. (2009). In vitro differentiation of retinal cells from human pluripotent stem cells by small-molecule induction. *J. Cell. Sci.* 122, 3169-3179.
214. Dye, B.R., Hill, D.R., Ferguson, M.A., Tsai, Y.H., Nagy, M.S., Dyal, R., Wells, J.M., Mayhew, C.N., Nattiv, R., Klein, O.D. et al. (2015). In vitro generation of human pluripotent stem cell derived lung organoids. *Elife* 4, 10.7554/eLife.05098.
215. Brandon, E.F., Raap, C.D., Meijerman, I., Beijnen, J.H., Schellens, J.H. (2003). An update on in vitro test methods in human hepatic drug biotransformation research: pros and cons. *Toxicol. Appl. Pharmacol.* 189, 233-246.
216. Wilkening, S., Stahl, F., Bader, A. (2003). Comparison of primary human hepatocytes and hepatoma cell line Hepg2 with regard to their biotransformation properties. *Drug Metab. Dispos.* 31, 1035-1042.
217. Guo, L., Dial, S., Shi, L., Branham, W., Liu, J., Fang, J.L., Green, B., Deng, H., Kaput, J., Ning, B. (2011). Similarities and differences in the expression of drug-metabolizing enzymes between human hepatic cell lines and primary human hepatocytes. *Drug Metab. Dispos.* 39, 528-538.
218. Gripon, P., Rumin, S., Urban, S., Le Seyec, J., Glaise, D., Cannie, I., Guyomard, C., Lucas, J., Trepo, C., Guguen-Guillouzo, C. (2002). Infection of a human hepatoma cell line by hepatitis B virus. *Proc. Natl. Acad. Sci. U. S. A.* 99, 15655-15660.
219. Nibourg, G.A.A., Chamuleau, R.A.F.M., van der Hoeven, T., V., Maas, M.A.W., Ruiter, A.F.C., Lamers, W.H., Oude Elferink, R., P.J., van Gulik, T., M., Hoekstra, R. (2012). Liver Progenitor Cell Line HepaRG Differentiated in a Bioartificial Liver Effectively Supplies Liver Support to Rats with Acute Liver Failure. *PLoS ONE* 7, e38778.
220. Hu, D., Wu, C., Li, Z., Liu, Y., Fan, X., Wang, Q., Ding, R. Characterizing the mechanism of thiazolidinedione-induced hepatotoxicity: An in vitro model in mitochondria. *Toxicol. Appl. Pharmacol.*
221. Laurent, V., Glaise, D., Nabel, T., Gilot, D., Corlu, A., Loyer, P. (2013). Highly Efficient SiRNA and Gene Transfer into Hepatocyte-Like HepaRG Cells and Primary Human Hepatocytes: New Means for Drug Metabolism and Toxicity Studies. In , I.R. Phillips, E.A. Shephard, P.R. Ortiz de Montellano, eds.: Humana Press), pp. 295-314.
222. Guillouzo, A., Corlu, A., Aninat, C., Glaise, D., Morel, F., Guguen-Guillouzo, C. (2007). The human hepatoma HepaRG cells: A highly differentiated model for studies of liver metabolism and toxicity of xenobiotics. *Chem. Biol. Interact.* 168, 66-73.
223. Bouezzedine, F., Fardel, O., Gripon, P. (2015). Interleukin 6 inhibits HBV entry through NTCP down regulation. *Virology* 481, 34-42.
224. Dianat, N., Dubois-Pot-Schneider, H., Steichen, C., Desterke, C., Leclerc, P., Raveux, A., Combettes, L., Weber, A., Corlu, A., Dubart-Kupferschmitt, A. (2014). Generation of functional cholangiocyte-like cells from human pluripotent stem cells and HepaRG cells. *Hepatology* 60, 700-714.
225. Antherieu, S., Chesne, C., Li, R., Camus, S., Lahoz, A., Picazo, L., Turpeinen, M., Tolonen, A., Uusitalo, J., Guguen-Guillouzo, C. et al. (2010). Stable expression, activity, and inducibility of cytochromes P450 in differentiated HepaRG cells. *Drug Metab. Dispos.* 38, 516-525.
226. Cerec, V., Glaise, D., Garnier, D., Morosan, S., Turlin, B., Drenou, B., Gripon, P., Kremsdorf, D., Guguen-Guillouzo, C., Corlu, A. (2007). Transdifferentiation of hepatocyte-like cells from the human hepatoma HepaRG cell line through bipotent progenitor. *Hepatology* 45, 957-967.
227. de Wet, J.R., Wood, K.V., Helinski, D.R., DeLuca, M. (1985). Cloning of firefly luciferase cDNA and the expression of active luciferase in *Escherichia coli*. *Proc. Natl. Acad. Sci. U. S. A.* 82, 7870-7873.
228. Kocher, B., Piwnicka-Worms, D. (2013). Illuminating cancer systems with genetically engineered mouse models and coupled luciferase reporters in vivo. *Cancer. Discov.* 3, 616-629.
229. Roura, S., Gálvez-Montón, C., Bayes-Genis, A. (2013). Bioluminescence imaging: a shining future for cardiac regeneration. *J. Cell. Mol. Med.* 17, 693-703.
230. Hochgrafe, K., Mandelkow, E.M. (2013). Making the brain glow: in vivo bioluminescence imaging to study neurodegeneration. *Mol. Neurobiol.* 47, 868-882.

231. Andreu, N., Zelmer, A., Wiles, S. (2011). Noninvasive biophotonic imaging for studies of infectious disease. *FEMS Microbiol. Rev.* 35, 360-394.
232. de Almeida, P.E., van Rappard, J.R., Wu, J.C. (2011). In vivo bioluminescence for tracking cell fate and function. *Am. J. Physiol. Heart Circ. Physiol.* 301, H663-71.
233. Branchini, B.R., Ablamsky, D.M., Davis, A.L., Southworth, T.L., Butler, B., Fan, F., Jathoul, A.P., Pule, M.A. (2010). Red-emitting luciferases for bioluminescence reporter and imaging applications. *Anal. Biochem.* 396, 290-297.
234. Wilson, T., Hastings, J.W. (1998). Bioluminescence. *Annu. Rev. Cell Dev. Biol.* 14, 197-230.
235. Prescher, J.A., Contag, C.H. (2010). Guided by the light: visualizing biomolecular processes in living animals with bioluminescence. *Curr. Opin. Chem. Biol.* 14, 80-89.
236. Lipshutz, G.S., Gruber, C.A., Cao, Y., Hardy, J., Contag, C.H., Gaensler, K.M. (2001). In utero delivery of adeno-associated viral vectors: intraperitoneal gene transfer produces long-term expression. *Mol. Ther.* 3, 284-292.
237. Rice, B.W., Cable, M.D., Nelson, M.B. (2001). In vivo imaging of light-emitting probes. *J. Biomed. Opt.* 6, 432-440.
238. Shabalina, S.A., Spiridonov, N.A., Kashina, A. (2013). Sounds of silence: synonymous nucleotides as a key to biological regulation and complexity. *Nucleic Acids Res.* 41, 2073-2094.
239. Law, G.H., Gandelman, O.A., Tisi, L.C., Lowe, C.R., Murray, J.A. (2006). Mutagenesis of solvent-exposed amino acids in *Photinus pyralis* luciferase improves thermostability and pH-tolerance. *Biochem. J.* 397, 305-312.
240. Lorenz, W.W., McCann, R.O., Longiaru, M., Cormier, M.J. (1991). Isolation and expression of a cDNA encoding *Renilla reniformis* luciferase. *Proc. Natl. Acad. Sci. U. S. A.* 88, 4438-4442.
241. Venisnik, K.M., Olafsen, T., Loening, A.M., Iyer, M., Gambhir, S.S., Wu, A.M. (2006). Bifunctional antibody-*Renilla* luciferase fusion protein for in vivo optical detection of tumors. *Protein Eng. Des. Sel.* 19, 453-460.
242. Colin, M., Moritz, S., Schneider, H., Capeau, J., Coutelle, C., Brahimi-Horn, M.C. (2000). Haemoglobin interferes with the ex vivo luciferase luminescence assay: consequence for detection of luciferase reporter gene expression in vivo. *Gene Ther.* 7, 1333-1336.
243. Contag, C.H., Contag, P.R., Mullins, J.I., Spilman, S.D., Stevenson, D.K., Benaron, D.A. (1995). Photonic detection of bacterial pathogens in living hosts. *Mol. Microbiol.* 18, 593-603.
244. Tromberg, B.J., Shah, N., Lanning, R., Cerussi, A., Espinoza, J., Pham, T., Svaasand, L., Butler, J. (2000). Non-invasive in vivo characterization of breast tumors using photon migration spectroscopy. *Neoplasia* 2, 26-40.
245. Loening, A.M., Wu, A.M., Gambhir, S.S. (2007). Red-shifted *Renilla reniformis* luciferase variants for imaging in living subjects. *Nat. Methods* 4, 641-643.
246. Morin, J.G. (2011). Based on a review of the data, use of the term 'cypridinid' solves the *Cypridina/Vargula* dilemma for naming the constituents of the luminescent system of ostracods in the family Cypridinidae. *Luminescence* 26, 1-4.
247. Thompson, E.M., Nagata, S., Tsuji, F.I. (1990). *Vargula hilgendorffii* luciferase: a secreted reporter enzyme for monitoring gene expression in mammalian cells. *Gene* 96, 257-262.
248. Hall, M.P., Unch, J., Binkowski, B.F., Valley, M.P., Butler, B.L., Wood, M.G., Otto, P., Zimmerman, K., Vidugiris, G., Machleidt, T. et al. (2012). Engineered luciferase reporter from a deep sea shrimp utilizing a novel imidazopyrazinone substrate. *ACS Chem. Biol.* 7, 1848-1857.
249. Russell, W.M., Burch, R.L. (2009). Prefatory Note. *Altern. Lab. Anim.* 37, 267-268.
250. Goldberg, A.M., Zurlo, J., Rudacille, D. (1996). The Three Rs and Biomedical Research. *Science* 272, 1403-1403.
251. Biesmans, S., Acton, P.D., Cotto, C., Langlois, X., Ver Donck, L., Bouwknecht, J.A., Aelvoet, S., Hellings, N., Meert, T.F., Nuydens, R. (2015). Effect of stress and peripheral immune activation on astrocyte activation in transgenic bioluminescent Gfap-luc mice. *Glia* 63, 1126-1137.

252. Kudishevich, E., Jung, B., Kim, J. (2011). Transgenic mice expressing luciferase under a 4.5 kb tyrosine hydroxylase promoter. *Cureus* 3.
253. Sergeeva, I.A., Hooijkaas, I.B., Van Der Made, I., Jong, W.M., Creemers, E.E., Christoffels, V.M. (2014). A transgenic mouse model for the simultaneous monitoring of ANF and BNP gene activity during heart development and disease. *Cardiovasc. Res.* 101, 78-86.
254. Contag, P.R. (2008). Bioluminescence imaging to evaluate infections and host response in vivo. *Methods Mol. Biol.* 415, 101-118.
255. Zhang, N., Ahsan, M.H., Purchio, A.F., West, D.B. (2005). Serum amyloid A-luciferase transgenic mice: response to sepsis, acute arthritis, and contact hypersensitivity and the effects of proteasome inhibition. *J. Immunol.* 174, 8125-8134.
256. Lin, A.H., Luo, J., Mondschein, L.H., ten Dijke, P., Vivien, D., Contag, C.H., Wyss-Coray, T. (2005). Global analysis of Smad2/3-dependent TGF-beta signaling in living mice reveals prominent tissue-specific responses to injury. *J. Immunol.* 175, 547-554.
257. de Heredia, L.L., Gengatharan, A., Foster, J., Mather, S., Magoulas, C. (2011). Bioluminescence imaging of the brain response to acute inflammation in living C/EBP reporter mice. *Neurosci. Lett.* 497, 134-138.
258. Contag, C.H., Spilman, S.D., Contag, P.R., Oshiro, M., Eames, B., Dennery, P., Stevenson, D.K., Benaron, D.A. (1997). Visualizing gene expression in living mammals using a bioluminescent reporter. *Photochem. Photobiol.* 66, 523-531.
259. Ittner, L.M., Gotz, J. (2007). Pronuclear injection for the production of transgenic mice. *Nat. Protoc.* 2, 1206-1215.
260. Naldini, L., Blomer, U., Gallay, P., Ory, D., Mulligan, R., Gage, F.H., Verma, I.M., Trono, D. (1996). In vivo gene delivery and stable transduction of nondividing cells by a lentiviral vector. *Science* 272, 263-267.
261. Buckley, S.M., Howe, S.J., Sheard, V., Ward, N.J., Coutelle, C., Thrasher, A.J., Waddington, S.N., McKay, T.R. (2008). Lentiviral transduction of the murine lung provides efficient pseudotype and developmental stage-dependent cell-specific transgene expression. *Gene Ther.* 15, 1167-1175.
262. Rahim, A.A., Wong, A.M., Howe, S.J., Buckley, S.M., Acosta-Saltos, A.D., Elston, K.E., Ward, N.J., Philpott, N.J., Cooper, J.D., Anderson, P.N. et al. (2009). Efficient gene delivery to the adult and fetal CNS using pseudotyped non-integrating lentiviral vectors. *Gene Ther.* 16, 509-520.
263. Kafri, T., Blomer, U., Peterson, D.A., Gage, F.H., Verma, I.M. (1997). Sustained expression of genes delivered directly into liver and muscle by lentiviral vectors. *Nat. Genet.* 17, 314-317.
264. Waddington, S.N., Mitrophanous, K.A., Ellard, F.M., Buckley, S.M., Nivsarkar, M., Lawrence, L., Cook, H.T., Al-Allaf, F., Bigger, B., Kingsman, S.M. et al. (2003). Long-term transgene expression by administration of a lentivirus-based vector to the fetal circulation of immuno-competent mice. *Gene Ther.* 10, 1234-1240.
265. Thomas, C.E., Ehrhardt, A., Kay, M.A. (2003). Progress and problems with the use of viral vectors for gene therapy. *Nat. Rev. Genet.* 4, 346-358.
266. Harel, J., Rassart, E., Jolicoeur, P. (1981). Cell cycle dependence of synthesis of unintegrated viral DNA in mouse cells newly infected with murine leukemia virus. *Virology* 110, 202-207.
267. Naldini, L. (1998). Lentiviruses as gene transfer agents for delivery to non-dividing cells. *Curr. Opin. Biotechnol.* 9, 457-463.
268. Cronin, J., Zhang, X.Y., Reiser, J. (2005). Altering the tropism of lentiviral vectors through pseudotyping. *Curr. Gene Ther.* 5, 387-398.
269. Finkelshtein, D., Werman, A., Novick, D., Barak, S., Rubinstein, M. (2013). LDL receptor and its family members serve as the cellular receptors for vesicular stomatitis virus. *Proc. Natl. Acad. Sci. U. S. A.* 110, 7306-7311.
270. Fumoto, S., Kawakami, S., Hashida, M., Nishida, K. (2013). Targeted Gene Delivery: Importance of Administration Routes. In *Novel Gene Therapy Approaches*, D.G. Ming Wei, ed. (Croatia: InTech), pp. 11-404.
271. Yamada, K., Morozumi, H., Okamoto, T. (1995). LTR-directed homologous recombination of full-length HIV-1 provirus clone in recA(-) bacteria. *Arch. Virol.* 140, 1007-1014.

272. Bernard, P., Couturier, M. (1992). Cell killing by the F plasmid CcdB protein involves poisoning of DNA-topoisomerase II complexes. *J. Mol. Biol.* 226, 735-745.
273. Rao, D.D., Vorhies, J.S., Senzer, N., Nemunaitis, J. (2009). siRNA vs. shRNA: similarities and differences. *Adv. Drug Deliv. Rev.* 61, 746-759.
274. Ran, F.A., Hsu, P.D., Wright, J., Agarwala, V., Scott, D.A., Zhang, F. (2013). Genome engineering using the CRISPR-Cas9 system. *Nat. Protocols* 8, 2281-2308.
275. Zetsche, B., Gootenberg, J.S., Abudayyeh, O.O., Slaymaker, I.M., Makarova, K.S., Essletzbichler, P., Volz, S.E., Joung, J., van der Oost, J., Regev, A. (2015). Cpf1 is a single RNA-guided endonuclease of a class 2 CRISPR-Cas system. *Cell* 163, 759-771.
276. Fineran, P.C., Charpentier, E. (2012). Memory of viral infections by CRISPR-Cas adaptive immune systems: acquisition of new information. *Virology* 434, 202-209.
277. Makarova, K.S., Haft, D.H., Barrangou, R., Brouns, S.J., Charpentier, E., Horvath, P., Moineau, S., Mojica, F.J., Wolf, Y.I., Yakunin, A.F. et al. (2011). Evolution and classification of the CRISPR-Cas systems. *Nat. Rev. Microbiol.* 9, 467-477.
278. Deltcheva, E., Chylinski, K., Sharma, C.M., Gonzales, K., Chao, Y., Pirzada, Z.A., Eckert, M.R., Vogel, J., Charpentier, E. (2011). CRISPR RNA maturation by trans-encoded small RNA and host factor RNase III. *Nature* 471, 602-607.
279. Gasiunas, G., Barrangou, R., Horvath, P., Siksnys, V. (2012). Cas9-crRNA ribonucleoprotein complex mediates specific DNA cleavage for adaptive immunity in bacteria. *Proc. Natl. Acad. Sci. U. S. A.* 109, E2579-86.
280. Jinek, M., Chylinski, K., Fonfara, I., Hauer, M., Doudna, J.A., Charpentier, E. (2012). A programmable dual-RNA-guided DNA endonuclease in adaptive bacterial immunity. *Science* 337, 816-821.
281. Pfeiffer, P., Thode, S., Hancke, J., Vielmetter, W. (1994). Mechanisms of overlap formation in nonhomologous DNA end joining. *Mol. Cell. Biol.* 14, 888-895.
282. Roth, D.B., Porter, T.N., Wilson, J.H. (1985). Mechanisms of nonhomologous recombination in mammalian cells. *Mol. Cell. Biol.* 5, 2599-2607.
283. Hsu, P.D., Scott, D.A., Weinstein, J.A., Ran, F.A., Konermann, S., Agarwala, V., Li, Y., Fine, E.J., Wu, X., Shalem, O. (2013). DNA targeting specificity of RNA-guided Cas9 nucleases. *Nat. Biotechnol.* 31, 827-832.
284. Neumann, E., Schaefer-Ridder, M., Wang, Y., Hofschneider, P.H. (1982). Gene transfer into mouse lyoma cells by electroporation in high electric fields. *EMBO J.* 1, 841-845.
285. White, M.F., Giraud-Panis, M.E., Pöhler, J.R.G., Lilley, D.M. (1997). Recognition and manipulation of branched DNA structure by junction-resolving enzymes. *J. Mol. Biol.* 269, 647-664.
286. Ibrahim, A., Vande Velde, G., Reumers, V., Toelen, J., Thiry, I., Vandeputte, C., Vets, S., Deroose, C., Bormans, G., Baekelandt, V. et al. (2009). Highly efficient multicistronic lentiviral vectors with peptide 2A sequences. *Hum. Gene Ther.* 20, 845-860.
287. Van Maele, B., De Rijck, J., De Clercq, E., Debyser, Z. (2003). Impact of the central polypurine tract on the kinetics of human immunodeficiency virus type 1 vector transduction. *J. Virol.* 77, 4685-4694.
288. Zufferey, R., Donello, J.E., Trono, D., Hope, T.J. (1999). Woodchuck hepatitis virus posttranscriptional regulatory element enhances expression of transgenes delivered by retroviral vectors. *J. Virol.* 73, 2886-2892.
289. Zufferey, R., Dull, T., Mandel, R.J., Bukovsky, A., Quiroz, D., Naldini, L., Trono, D. (1998). Self-inactivating lentivirus vector for safe and efficient in vivo gene delivery. *J. Virol.* 72, 9873-9880.
290. Ryan, M.D., Drew, J. (1994). Foot-and-mouth disease virus 2A oligopeptide mediated cleavage of an artificial polyprotein. *EMBO J.* 13, 928-933.
291. de Felipe, P., Hughes, L.E., Ryan, M.D., Brown, J.D. (2003). Co-translational, intraribosomal cleavage of polypeptides by the foot-and-mouth disease virus 2A peptide. *J. Biol. Chem.* 278, 11441-11448.
292. Kajiyama, N., Nakano, E. (1991). Isolation and characterization of mutants of firefly luciferase which produce different colors of light. *Protein Eng.* 4, 691-693.

293. Rice, B.W., Cable, M.D., Nelson, M.B. (2001). In vivo imaging of light-emitting probes. *J. Biomed. Opt.* 6, 432-440.
294. Rothwell, D.G., Crossley, R., Bridgeman, J.S., Sheard, V., Zhang, Y., Sharp, T.V., Hawkins, R.E., Gilham, D.E., McKay, T.R. (2010). Functional expression of secreted proteins from a bicistronic retroviral cassette based on foot-and-mouth disease virus 2A can be position dependent. *Hum. Gene Ther.* 21, 1631-1637.
295. Hawkins, K., Joy, S., Delhove, J.K.M., Kotiadis, V., Fernandez, E., Fitzpatrick, L., Whiteford, J., King, P., Bolanos, J., Duchon, M. et al. NRF2 Orchestrates the Metabolic Shift during Induced Pluripotent Stem Cell Reprogramming. *Cell Reports*.
296. Maguire, C.A., Bovenberg, M.S., Crommentuijn, M.H., Niers, J.M., Kerami, M., Teng, J., Sena-Esteves, M., Badr, C.E., Tannous, B.A. (2013). Triple bioluminescence imaging for in vivo monitoring of cellular processes. *Molecular Therapy—Nucleic Acids* 2, e99.
297. Krelle, A.C., Okoli, A.S., Mendz, G.L. (2013). Huh-7 Human Liver Cancer Cells: A Model System to Understand Hepatocellular Carcinoma and Therapy.
298. Hirschfeld, M., Ma, Y., Weis, J.H., Vogel, S.N., Weis, J.J. (2000). Cutting edge: repurification of lipopolysaccharide eliminates signaling through both human and murine toll-like receptor 2. *J. Immunol.* 165, 618-622.
299. Chow, J.C., Young, D.W., Golenbock, D.T., Christ, W.J., Gusovsky, F. (1999). Toll-like receptor-4 mediates lipopolysaccharide-induced signal transduction. *J. Biol. Chem.* 274, 10689-10692.
300. Jing, Y.Y., Han, Z.P., Sun, K., Zhang, S.S., Hou, J., Liu, Y., Li, R., Gao, L., Zhao, X., Zhao, Q.D. et al. (2012). Toll-like receptor 4 signaling promotes epithelial-mesenchymal transition in human hepatocellular carcinoma induced by lipopolysaccharide. *BMC Med.* 10, 98-7015-10-98.
301. Zhao, L., Yang, R., Cheng, L., Wang, M., Jiang, Y., Wang, S. (2011). LPS-induced epithelial-mesenchymal transition of intrahepatic biliary epithelial cells. *J. Surg. Res.* 171, 819-825.
302. Harmey, J.H., Bucana, C.D., Lu, W., Byrne, A.M., McDonnell, S., Lynch, C., Bouchier-Hayes, D., Dong, Z. (2002). Lipopolysaccharide-induced metastatic growth is associated with increased angiogenesis, vascular permeability and tumor cell invasion. *International journal of cancer* 101, 415-422.
303. Liu, X., Liang, J., Li, G. (2010). Lipopolysaccharide promotes adhesion and invasion of hepatoma cell lines HepG2 and HepG2. *2.15. Mol. Biol. Rep.* 37, 2235-2239.
304. Verrecchia, F., Mauviel, A., Farge, D. (2006). Transforming growth factor- $\beta$  signaling through the Smad proteins: role in systemic sclerosis. *Autoimmunity reviews* 5, 563-569.
305. van Boxel-Dezaire, A.H., Rani, M.R., Stark, G.R. (2006). Complex modulation of cell type-specific signaling in response to type I interferons. *Immunity* 25, 361-372.
306. Schaefer, M.H., Yang, J.S., Serrano, L., Kiel, C. (2014). Protein conservation and variation suggest mechanisms of cell type-specific modulation of signaling pathways. *PLoS Comput. Biol.* 10, e1003659.
307. Heinz, S., Romanoski, C.E., Benner, C., Glass, C.K. (2015). The selection and function of cell type-specific enhancers. *Nat. Rev. Mol. Cell Biol.* 16, 144-154.
308. Benus, G.F., Wierenga, A.T., de Gorter, D.J., Schuringa, J.J., van Bennekum, A.M., Drenth-Diephuis, L., Vellenga, E., Eggen, B.J. (2005). Inhibition of the transforming growth factor beta (TGFbeta) pathway by interleukin-1beta is mediated through TGFbeta-activated kinase 1 phosphorylation of SMAD3. *Mol. Biol. Cell* 16, 3501-3510.
309. Klein, P.S., Melton, D.A. (1996). A molecular mechanism for the effect of lithium on development. *Proc. Natl. Acad. Sci. U. S. A.* 93, 8455-8459.
310. Lim, K., Han, C., Dai, Y., Shen, M., Wu, T. (2009). Omega-3 polyunsaturated fatty acids inhibit hepatocellular carcinoma cell growth through blocking beta-catenin and cyclooxygenase-2. *Mol. Cancer. Ther.* 8, 3046-3055.
311. Plessl, K., Haider, S., Fiala, C., Pollheimer, J., Knöfler, M. (2015). Expression pattern and function of Notch2 in different subtypes of first trimester cytotrophoblast. *Placenta* 36, 365-371.
312. Velicky, P., Haider, S., Otti, G.R., Fiala, C., Pollheimer, J., Knofler, M. (2014). Notch-dependent RBPJkappa inhibits proliferation of human cytotrophoblasts and their differentiation into extravillous trophoblasts. *Mol. Hum. Reprod.* 20, 756-766.

313. Lin, L., Mernaugh, R., Yi, F., Blum, D., Carbone, D.P., Dang, T.P. (2010). Targeting specific regions of the Notch3 ligand-binding domain induces apoptosis and inhibits tumor growth in lung cancer. *Cancer Res.* 70, 632-638.
314. Hansson, E.M., Lanner, F., Das, D., Mutvei, A., Marklund, U., Ericson, J., Farnebo, F., Stumm, G., Stenmark, H., Andersson, E.R. et al. (2010). Control of Notch-ligand endocytosis by ligand-receptor interaction. *J. Cell. Sci.* 123, 2931-2942.
315. Buckley, S.M., Delhove, J.M., Perocheau, D.P., Karda, R., Rahim, A.A., Howe, S.J., Ward, N.J., Arbuthnot, P., Johnson, M.R., Waddington, S.N. et al. (2015). In vivo bioimaging with tissue-specific transcription factor activated luciferase reporter. *Scientific Reports*.
316. Sigal, A., Milo, R., Cohen, A., Geva-Zatorsky, N., Klein, Y., Liron, Y., Rosenfeld, N., Danon, T., Perzov, N., Alon, U. (2006). Variability and memory of protein levels in human cells. *Nature* 444, 643-646.
317. Cherry, S.R., Biniszkiwicz, D., van Parijs, L., Baltimore, D., Jaenisch, R. (2000). Retroviral expression in embryonic stem cells and hematopoietic stem cells. *Mol. Cell. Biol.* 20, 7419-7426.
318. Ellis, J. (2005). Silencing and variegation of gammaretrovirus and lentivirus vectors. *Hum. Gene Ther.* 16, 1241-1246.
319. Pfeifer, A., Ikawa, M., Dayn, Y., Verma, I.M. (2002). Transgenesis by lentiviral vectors: lack of gene silencing in mammalian embryonic stem cells and preimplantation embryos. *Proc. Natl. Acad. Sci. U. S. A.* 99, 2140-2145.
320. Pannell, D., Osborne, C.S., Yao, S., Sukonnik, T., Pasceri, P., Karaiskakis, A., Okano, M., Li, E., Lipshitz, H.D., Ellis, J. (2000). Retrovirus vector silencing is de novo methylase independent and marked by a repressive histone code. *EMBO J.* 19, 5884-5894.
321. Pikaart, M.J., Recillas-Targa, F., Felsenfeld, G. (1998). Loss of transcriptional activity of a transgene is accompanied by DNA methylation and histone deacetylation and is prevented by insulators. *Genes Dev.* 12, 2852-2862.
322. Schnell, S.A., Staines, W.A., Wessendorf, M.W. (1999). Reduction of lipofuscin-like autofluorescence in fluorescently labeled tissue. *J. Histochem. Cytochem.* 47, 719-730.
323. Ramm, G.A., Carr, S.C., Bridle, K.R., Li, L., Britton, R.S., Crawford, D.H., Vogler, C.A., Bacon, B.R., Tracy, T.F. (2000). Morphology of liver repair following cholestatic liver injury: resolution of ductal hyperplasia, matrix deposition and regression of myofibroblasts. *Liver* 20, 387-396.
324. Beaussier, M., Wendum, D., Schiffer, E., Dumont, S., Rey, C., Lienhart, A., Housset, C. (2007). Prominent contribution of portal mesenchymal cells to liver fibrosis in ischemic and obstructive cholestatic injuries. *Laboratory investigation* 87, 292-303.
325. Mederacke, I., Hsu, C.C., Troeger, J.S., Huebener, P., Mu, X., Dapito, D.H., Pradere, J., Schwabe, R.F. (2013). Fate tracing reveals hepatic stellate cells as dominant contributors to liver fibrosis independent of its aetiology. *Nature communications* 4.
326. Neubauer, K., Knittel, T., Aurisch, S., Fellmer, P., Ramadori, G. (1996). Glial fibrillary acidic protein-a cell type specific marker for Ito cells in vivo and in vitro. *J. Hepatol.* 24, 719-730.
327. Vykhovanets, E.V., Shukla, S., MacLennan, G.T., Resnick, M.I., Carlsen, H., Blomhoff, R., Gupta, S. (2008). Molecular imaging of NF-kappaB in prostate tissue after systemic administration of IL-1 $\beta$ . *Prostate* 68, 34-41.
328. Tukhvatulin, A., Logunov, D., Gitlin, I., Shmarov, M., Kudan, P., Adzhieva, A., Moroz, A., Kostyukova, N., Burdelya, L., Naroditsky, B. (2011). A in vitro and in vivo study of the ability of NOD1 ligands to activate the transcriptional factor NF-kB. *Acta naturae* 3, 77.
329. Carlsen, H., Moskaug, J.O., Fromm, S.H., Blomhoff, R. (2002). In vivo imaging of NF-kappa B activity. *J. Immunol.* 168, 1441-1446.
330. Ray, A., Prefontaine, K.E. (1994). Physical association and functional antagonism between the p65 subunit of transcription factor NF-kappa B and the glucocorticoid receptor. *Proc. Natl. Acad. Sci. U. S. A.* 91, 752-756.
331. Barnes, P.J., Adcock, I.M. (2009). Glucocorticoid resistance in inflammatory diseases. *The Lancet* 373, 1905-1917.
332. Auphan, N., DiDonato, J.A., Rosette, C., Helmberg, A., Karin, M. (1995). Immunosuppression by glucocorticoids: inhibition of NF-kappaB activity through induction of I-kappaB synthesis. *Science* 270, 286.
333. Jacobs, M.D., Harrison, S.C. (1998). Structure of an I $\kappa$ B $\alpha$ /NF- $\kappa$ B complex. *Cell* 95, 749-758.

334. Singh, U., Tabibian, J., Venugopal, S.K., Devaraj, S., Jialal, I. (2005). Development of an in vitro screening assay to test the antiinflammatory properties of dietary supplements and pharmacologic agents. *Clin. Chem.* 51, 2252-2256.
335. Wienkers, L.C., Heath, T.G. (2005). Predicting in vivo drug interactions from in vitro drug discovery data. *Nature reviews Drug discovery* 4, 825-833.
336. Yang, L., Wang, G., Yang, L., Huang, Z., Zhang, W., Yu, L. (2014). Endotoxin molecule lipopolysaccharide-induced zebrafish inflammation model: a novel screening method for anti-inflammatory drugs. *Molecules* 19, 2390-2409.
337. Zhang, N., Weber, A., Li, B., Lyons, R., Contag, P.R., Purchio, A.F., West, D.B. (2003). An inducible nitric oxide synthase-luciferase reporter system for in vivo testing of anti-inflammatory compounds in transgenic mice. *J. Immunol.* 170, 6307-6319.
338. Mitchell, K., Shah, J.P., Tsytsikova, L.V., Campbell, A.M., Afram, K., Symes, A.J. (2014). LPS antagonism of TGF- $\beta$  signaling results in prolonged survival and activation of rat primary microglia. *J. Neurochem.* 129, 155-168.
339. Onichtchouk, D., Chen, Y., Dosch, R., Gawantka, V., Delius, H., Massague, J., Niehrs, C. (1999). Silencing of TGF- $\beta$  signalling by the pseudoreceptor BAMBI. *Nature* 401, 480-485.
340. Liu, C., Chen, X., Yang, L., Kisseleva, T., Brenner, D.A., Seki, E. (2014). Transcriptional repression of the transforming growth factor beta (TGF-beta) Pseudoreceptor BMP and activin membrane-bound inhibitor (BAMBI) by Nuclear Factor kappaB (NF-kappaB) p50 enhances TGF-beta signaling in hepatic stellate cells. *J. Biol. Chem.* 289, 7082-7091.
341. Takikawa, Y., Miyoshi, H., Rust, C., Roberts, P., Siegel, R., Mandal, P.K., Millikan, R.E., Gores, G.J. (2001). The bile acid-activated phosphatidylinositol 3-kinase pathway inhibits Fas apoptosis upstream of bid in rodent hepatocytes. *Gastroenterology* 120, 1810-1817.
342. Iimuro, Y., Nishiura, T., Hellerbrand, C., Behrns, K.E., Schoonhoven, R., Grisham, J.W., Brenner, D.A. (1998). NFkappaB prevents apoptosis and liver dysfunction during liver regeneration. *J. Clin. Invest.* 101, 802-811.
343. Miyoshi, H., Rust, C., Guicciardi, M.E., Gores, G.J. (2001). NF- $\kappa$ B is activated in cholestasis and functions to reduce liver injury. *The American journal of pathology* 158, 967-975.
344. Luedde, T., Schwabe, R.F. (2011). NF- $\kappa$ B in the liver—linking injury, fibrosis and hepatocellular carcinoma. *Nature Reviews Gastroenterology and Hepatology* 8, 108-118.
345. Demirbilek, S., Akın, M., Gürünlüoğlu, K., Aydın, N.E., Emre, M.H., Taş, E., Aksoy, R.T., Ay, S. (2006). The NF- $\kappa$ B inhibitors attenuate hepatic injury in bile duct ligated rats. *Pediatr. Surg. Int.* 22, 655-663.
346. Inokuchi, S., Aoyama, T., Miura, K., Osterreicher, C.H., Kodama, Y., Miyai, K., Akira, S., Brenner, D.A., Seki, E. (2010). Disruption of TAK1 in hepatocytes causes hepatic injury, inflammation, fibrosis, and carcinogenesis. *Proc. Natl. Acad. Sci. U. S. A.* 107, 844-849.
347. Lin, M., Rippe, R.A., Niemela, O., Brittenham, G., Tsukamoto, H. (1997). Role of iron in NF-kappa B activation and cytokine gene expression by rat hepatic macrophages. *Am. J. Physiol.* 272, G1355-64.
348. Luo, J., Lin, A.H., Masliah, E., Wyss-Coray, T. (2006). Bioluminescence imaging of Smad signaling in living mice shows correlation with excitotoxic neurodegeneration. *Proc. Natl. Acad. Sci. U. S. A.* 103, 18326-18331.
349. Blomhoff, R., Blomhoff, H.K. (2006). Overview of retinoid metabolism and function. *J. Neurobiol.* 66, 606-630.
350. Yang, L., Jung, Y., Omenetti, A., Witek, R.P., Choi, S., Vandongen, H.M., Huang, J., Alpini, G.D., Diehl, A.M. (2008). Fate-Mapping Evidence That Hepatic Stellate Cells Are Epithelial Progenitors in Adult Mouse Livers. *Stem Cells* 26, 2104-2113.
351. Tennakoon, A.H., Izawa, T., Wijesundera, K.K., Katou-Ichikawa, C., Tanaka, M., Golbar, H.M., Kuwamura, M., Yamate, J. (2015). Analysis of glial fibrillary acidic protein (GFAP)-expressing ductular cells in a rat liver cirrhosis model induced by repeated injections of thioacetamide (TAA). *Exp. Mol. Pathol.* 98, 476-485.
352. Ueberham, E., Bottger, J., Ueberham, U., Grosche, J., Gebhardt, R. (2010). Response of sinusoidal mouse liver cells to choline-deficient ethionine-supplemented diet. *Comp Hepatol* 9.
353. Cho, W., Hagemann, T.L., Johnson, D.A., Johnson, J.A., Messing, A. (2009). Dual transgenic reporter mice as a tool for monitoring expression of glial fibrillary acidic protein. *J. Neurochem.* 110, 343-351.

354. Van Hul, N.K., Abarca-Quinones, J., Sempoux, C., Horsmans, Y., Leclercq, I.A. (2009). Relation between liver progenitor cell expansion and extracellular matrix deposition in a CDE-induced murine model of chronic liver injury. *Hepatology* 49, 1625-1635.
355. Puche, J.E., Lee, Y.A., Jiao, J., Aloman, C., Fiel, M.I., Muñoz, U., Kraus, T., Lee, T., Yee, H.F., Friedman, S.L. (2013). A novel murine model to deplete hepatic stellate cells uncovers their role in amplifying liver damage in mice. *Hepatology* 57, 339-350.
356. Shi, M.N., Zheng, W.D., Zhang, L.J., Chen, Z.X., Wang, X.Z. (2005). Effect of IL-10 on the expression of HSC growth factors in hepatic fibrosis rat. *World J. Gastroenterol.* 11, 4788-4793.
357. Gard, A.L., White, F.P., Dutton, G.R. (1985). Extra-neural glial fibrillary acidic protein (GFAP) immunoreactivity in perisinusoidal stellate cells of rat liver. *J. Neuroimmunol.* 8, 359-375.
358. van Til, N.P., Markusic, D.M., van der Rijt, R., Kunne, C., Hiralall, J.K., Vreeling, H., Frederiks, W.M., Oude-Elferink, R.P., Seppen, J. (2005). Kupffer cells and not liver sinusoidal endothelial cells prevent lentiviral transduction of hepatocytes. *Molecular Therapy* 11, 26-34.
359. Burke, Z.D., Reed, K.R., Phesse, T.J., Sansom, O.J., Clarke, A.R., Tosh, D. (2009). Liver zonation occurs through a  $\beta$ -catenin-dependent, c-Myc-independent mechanism. *Gastroenterology* 136, 2316-2324. e3.
360. Benhamouche, S., Decaens, T., Godard, C., Chambrey, R., Rickman, D.S., Moinard, C., Vasseur-Cognet, M., Kuo, C.J., Kahn, A., Perret, C. et al. (2006). Apc Tumor Suppressor Gene Is the “Zonation-Keeper” of Mouse Liver. *Developmental Cell* 10, 759-770.
361. Peifer, M., McCreath, P.D., Green, K.J., Wieschaus, E., Gumbiner, B.M. (1992). The vertebrate adhesive junction proteins beta-catenin and plakoglobin and the Drosophila segment polarity gene armadillo form a multigene family with similar properties. *J. Cell Biol.* 118, 681-691.
362. Christofori, G., Semb, H. (1999). The role of the cell-adhesion molecule E-cadherin as a tumour-suppressor gene. *Trends Biochem. Sci.* 24, 73-76.
363. Sekine, S., Gutiérrez, P.J., Yu-Ang Lan, B., Feng, S., Hebrok, M. (2007). Liver-specific loss of  $\beta$ -catenin results in delayed hepatocyte proliferation after partial hepatectomy. *Hepatology* 45, 361-368.
364. Ishizaki, Y., Ikeda, S., Fujimori, M., Shimizu, Y., Kurihara, T., Itamoto, T., Kikuchi, A., Okajima, M., Asahara, T. (2004). Immunohistochemical analysis and mutational analyses of  $\beta$ -catenin, axin family and APC genes in hepatocellular carcinomas. *Int. J. Oncol.* 24, 1077-1083.
365. Chan, D.W., Chan, C., Yam, J.W., Ching, Y., Ng, I.O. (2006). Prickle-1 negatively regulates Wnt/ $\beta$ -catenin pathway by promoting Dishevelled ubiquitination/degradation in liver cancer. *Gastroenterology* 131, 1218-1227.
366. Bengochea, A., De Souza, M., Lefrancois, L., Le Roux, E., Galy, O., Chemin, I., Kim, M., Wands, J., Trepo, C., Hainaut, P. (2008). Common dysregulation of Wnt/Frizzled receptor elements in human hepatocellular carcinoma. *Br. J. Cancer* 99, 143-150.
367. Yang, J., Cusimano, A., Monga, J.K., Preziosi, M.E., Pullara, F., Calero, G., Lang, R., Yamaguchi, T.P., Nejak-Bowen, K.N., Monga, S.P. (2015). WNT5A Inhibits Hepatocyte Proliferation and Concludes  $\beta$ -Catenin Signaling in Liver Regeneration. *The American journal of pathology* 185, 2194-2205.
368. Köhler, C., Bell, A.W., Bowen, W.C., Monga, S.P., Fleig, W., Michalopoulos, G.K. (2004). Expression of Notch-1 and its ligand Jagged-1 in rat liver during liver regeneration. *Hepatology* 39, 1056-1065.
369. Ronchini, C., Capobianco, A.J. (2001). Induction of cyclin D1 transcription and CDK2 activity by Notch(ic): implication for cell cycle disruption in transformation by Notch(ic). *Mol. Cell. Biol.* 21, 5925-5934.
370. Miyoshi, H., Rust, C., Roberts, P.J., Burgart, L.J., Gores, G.J. (1999). Hepatocyte apoptosis after bile duct ligation in the mouse involves Fas. *Gastroenterology* 117, 669-677.
371. Chen, Y., Zheng, S., Qi, D., Zheng, S., Guo, J., Zhang, S., Weng, Z. (2012). Inhibition of Notch signaling by a  $\gamma$ -secretase inhibitor attenuates hepatic fibrosis in rats.
372. Zong, Y., Panikkar, A., Xu, J., Antoniou, A., Raynaud, P., Lemaigre, F., Stanger, B.Z. (2009). Notch signaling controls liver development by regulating biliary differentiation. *Development* 136, 1727-1739.

373. Villanueva, A., Alsinet, C., Yanger, K., Hoshida, Y., Zong, Y., Toffanin, S., Rodriguez-Carunchio, L., Solé, M., Thung, S., Stanger, B.Z. (2012). Notch signaling is activated in human hepatocellular carcinoma and induces tumor formation in mice. *Gastroenterology* 143, 1660-1669. e7.
374. Sekiya, S., Suzuki, A. (2012). Intrahepatic cholangiocarcinoma can arise from Notch-mediated conversion of hepatocytes. *J. Clin. Invest.* 122, 3914-3918.
375. Ferreira, A., Rodrigues, M., Silvestre, S., Falcão, A., Alves, G. (2014). HepaRG cell line as an in vitro model for screening drug–drug interactions mediated by metabolic induction: Amiodarone used as a model substance. *Toxicology in Vitro* 28, 1531-1535.
376. Carrell, R.W. (1986). alpha 1-Antitrypsin: molecular pathology, leukocytes, and tissue damage. *J. Clin. Invest.* 78, 1427-1431.
377. Kramer, M.G., Barajas, M., Razquin, N., Berraondo, P., Rodrigo, M., Wu, C., Qian, C., Fortes, P., Prieto, J. (2003). In vitro and in vivo comparative study of chimeric liver-specific promoters. *Molecular Therapy* 7, 375-385.
378. De Simone, V., Ciliberto, G., Hardon, E., Paonessa, G., Palla, F., Lundberg, L., Cortese, R. (1987). Cis- and trans-acting elements responsible for the cell-specific expression of the human alpha 1-antitrypsin gene. *EMBO J.* 6, 2759-2766.
379. Cressman, D.E., Greenbaum, L.E., DeAngelis, R.A., Ciliberto, G., Furth, E.E., Poli, V., Taub, R. (1996). Liver failure and defective hepatocyte regeneration in interleukin-6-deficient mice. *Science* 274, 1379-1383.
380. Blindenbacher, A., Wang, X., Langer, I., Savino, R., Terracciano, L., Heim, M.H. (2003). Interleukin 6 is important for survival after partial hepatectomy in mice. *Hepatology* 38, 674-682.
381. Ezure, T., Sakamoto, T., Tsuji, H., Lunz, J.G., Murase, N., Fung, J.J., Demetris, A.J. (2000). The development and compensation of biliary cirrhosis in interleukin-6-deficient mice. *The American journal of pathology* 156, 1627-1639.
382. Yasoshima, M., Kono, N., Sugawara, H., Katayanagi, K., Harada, K., Nakanuma, Y. (1998). Increased expression of interleukin-6 and tumor necrosis factor-alpha in pathologic biliary epithelial cells: in situ and culture study. *Lab. Invest.* 78, 89-100.
383. Legendre, F., Dudhia, J., Pujol, J.P., Bogdanowicz, P. (2003). JAK/STAT but not ERK1/ERK2 pathway mediates interleukin (IL)-6/soluble IL-6R down-regulation of Type II collagen, aggrecan core, and link protein transcription in articular chondrocytes. Association with a down-regulation of SOX9 expression. *J. Biol. Chem.* 278, 2903-2912.
384. Floch, M. (2002). Bile salts, intestinal microflora and enterohepatic circulation. *Digestive and Liver Disease* 34, S54-S57.
385. Bhardwaj, U., Bhardwaj, R. *Biochemistry for Nurses: Pearson Education India*).
386. Candido, E.P.M., Reeves, R., Davie, J.R. (1978). Sodium butyrate inhibits histone deacetylation in cultured cells. *Cell* 14, 105-113.
387. Wang, P., Jia, J.D., Tang, S.Z., Yan, Z.Y., You, H., Cong, M., Wang, B.E., Chen, L., An, W. (2004). Sodium butyrate induces rat hepatic oval cells differentiating into mature hepatocytes in vitro. *Zhonghua Gan Zang Bing Za Zhi* 12, 718-721.
388. Oertel, M., Rosencrantz, R., Chen, Y., Thota, P.N., Sandhu, J.S., Dabeva, M.D., Pacchia, A.L., Adelson, M.E., Dougherty, J.P., Shafritz, D.A. (2003). Repopulation of rat liver by fetal hepatoblasts and adult hepatocytes transduced ex vivo with lentiviral vectors. *Hepatology* 37, 994-1005.
389. Paganelli, M., Nyabi, O., Sid, B., Evraerts, J., El Malmi, I., Heremans, Y., Dollé, L., Benton, C., Calderon, P., van Grunsven, L. (2014). Downregulation of Sox9 expression associates with hepatogenic differentiation of human liver mesenchymal stem/progenitor cells. *Stem cells and development* 23, 1377-1391.
390. De La Iglesia, F., Porta, E. (1967). Ciliated biliary epithelial cells in the livers of non-human primates. *Experientia* 23, 49-51.
391. Masyuk, A.I., Masyuk, T.V., LaRusso, N.F. (2008). Cholangiocyte primary cilia in liver health and disease. *Developmental Dynamics* 237, 2007-2012.
392. Seeley, E.S., Nachury, M.V. (2010). The perennial organelle: assembly and disassembly of the primary cilium. *J. Cell. Sci.* 123, 511-518.
393. Desmet, V., van Eyken, P., Sciote, R. (1990). Cytokeratins for probing cell lineage relationships in developing liver. *Hepatology* 12, 1249-1251.

394. Stosiek, P., Kasper, M., Karsten, U. (1990). Expression of cytokeratin 19 during human liver organogenesis. *Liver* 10, 59-63.
395. Groebner, J.L., Tuma, P.L. (2015). The Altered Hepatic Tubulin Code in Alcoholic Liver Disease. *Biomolecules* 5, 2140-2159.
396. Verhey, K.J., Gaertig, J. (2007). The tubulin code. *Cell Cycle* 6, 2152-2160.
397. Kannarkat, G.T., Tuma, D.J., Tuma, P.L. (2006). Microtubules are more stable and more highly acetylated in ethanol-treated hepatic cells. *J. Hepatol.* 44, 963-970.
398. Joseph, R.A., Shepard, B.D., Kannarkat, G.T., Rutledge, T.M., Tuma, D.J., Tuma, P.L. (2008). Microtubule acetylation and stability may explain alcohol-induced alterations in hepatic protein trafficking. *Hepatology* 47, 1745-1753.
399. Piperno, G., LeDizet, M., Chang, X.J. (1987). Microtubules containing acetylated alpha-tubulin in mammalian cells in culture. *J. Cell Biol.* 104, 289-302.
400. Yanger, K., Zong, Y., Maggs, L.R., Shapira, S.N., Maddipati, R., Aiello, N.M., Thung, S.N., Wells, R.G., Greenbaum, L.E., Stanger, B.Z. (2013). Robust cellular reprogramming occurs spontaneously during liver regeneration. *Genes Dev.* 27, 719-724.
401. Wang, T., Chen, T., Liang, H., Yan, H., Lin, N., Liu, L., Luo, H., Huang, Z., Li, N., Liu, W. (2014). Notch inhibition promotes fetal liver stem/progenitor cells differentiation into hepatocytes via the inhibition of HNF-1 $\beta$ . *Cell Tissue Res.* 357, 173-184.
402. Matheu, A., Collado, M., Wise, C., Manterola, L., Cekaite, L., Tye, A.J., Canamero, M., Bujanda, L., Schedl, A., Cheah, K.S. et al. (2012). Oncogenicity of the developmental transcription factor Sox9. *Cancer Res.* 72, 1301-1315.
403. Bellido, T., O'Brien, C.A., Roberson, P.K., Manolagas, S.C. (1998). Transcriptional Activation of the p21 WAF1, CIP1, SDI1 Gene by Interleukin-6 Type Cytokines A PREREQUISITE FOR THEIR PRO-DIFFERENTIATING AND ANTI-APOPTOTIC EFFECTS ON HUMAN OSTEOBLASTIC CELLS. *J. Biol. Chem.* 273, 21137-21144.
404. Thiery, J.P. (2002). Epithelial–mesenchymal transitions in tumour progression. *Nature Reviews Cancer* 2, 442-454.
405. Bradford, M.M. (1976). A rapid and sensitive method for the quantitation of microgram quantities of protein utilizing the principle of protein-dye binding. *Anal. Biochem.* 72, 248-254.
406. Montague, T.G., Cruz, J.M., Gagnon, J.A., Church, G.M., Valen, E. (2014). CHOPCHOP: a CRISPR/Cas9 and TALEN web tool for genome editing. *Nucleic Acids Res.* 42, W401-7.